

## Université Paris Cité

École doctorale Cerveau, Cognition, Comportement - ED 158

*Laboratoire : Neurodiderot UMR 1141*

*NeuroSpin, CEA-Saclay*

# Growing into Adolescence After Early Focal Brain Injury : Insights into Long-Term Brain Plasticity in Children after neonatal stroke *Longitudinal multimodal MRI and neuropsychology study*

Par Pierre-Yves POSTIC

Thèse de doctorat de **Neurosciences**  
Dirigée par Dr **Lucie HERTZ-PANNIER**  
Et par Dr **Mathilde CHEVIGNARD**

Présentée et soutenue **publiquement**

le 19/11/2024

Devant un jury composé de :

**Joel FLUSS**, Docteur en médecine - HDR, Hôpital pour enfants de Genève, Rapporteur

**Renaud LOPES**, Maître de conférence des universités - HDR, Centre hospitalier universitaire (CHU) de Lille, Rapporteur

**Catherine OPPENHEIM**, Professeur des universités- Praticien hospitalier, GHU Paris Psychiatrie et Neurosciences, Université Paris Cité, Examineur

**Arnaud CACHIA**, Professeur des universités, Université Paris Cité, Examineur

**Josselin HOUENOU**, Professeur des universités - Praticien hospitalier, CHU Henri Mondor, AP-HP - Université Paris-Est Créteil (UPEC), Examineur

**Frédérique LIEGEOIS**, Associate professor, University College London, Examinatrice

**Lucie HERTZ-PANNIER**, Directrice de Recherche, Commissariat à l'énergie atomique (CEA),  
Directrice de thèse

**Mathilde CHEVIGNARD**, Praticien hospitalier, HDR, Sorbonne Université, Co-directrice de thèse

**Guillaume AUZIAS**, Chargé de recherche - HDR, Membre invité

**Yann LEPRINCE**, PhD, CEA, Membre invité

# Growing into Adolescence After Early Focal Brain Injury: Insights into Long-Term Brain Plasticity in Children after neonatal stroke. Longitudinal multimodal MRI and neuropsychology study

## Abstract

This thesis explores the long-term neurodevelopmental implications of unilateral neonatal arterial ischemic stroke (NAIS) during childhood (at age 7) and adolescence (at age 16), within a prospective French cohort of children who experienced NAIS. This longitudinal prospective study aims to identify early markers of motor and cognitive outcomes by combining morphometric, microstructural (diffusion), and functional MRI markers with clinical and cognitive data.

This project required the development of methodological approaches tailored to the longitudinal study of growing and injured brains, along with comprehensive quality control at every stage.

Through a multifactorial morphometric analysis of anatomical MRI, we examined the clinical factors that may influence brain growth trajectories. The results indicate that male patients exhibit lower contralesional hemispheric brain volume compared to females at age 7, with no significant sex differences at age 16.

This suggests that puberty has little effect on these volumetric trajectories and that most of the deviations in male patients occur during early childhood. This pattern aligns with perinatal vulnerability described in other male brain development disorders, without later compensation. However, this concept of vulnerability should be nuanced, as these morphological differences do not appear to correlate with the cohort's clinical performance.

In the second part of the study, we examined functional and microstructural alterations in language hemispheric specialization and functional networks involved in mental calculation using functional MRI and diffusion MRI to test the hypothesis of a "crowding effect" (competition within a constrained neural space), particularly in the dominant hemisphere for language.

The results confirm atypical right-hemisphere language specialization in patients with lesions in the left perisylvian regions (2/3 of the subjects). This right-lateralization seems to be associated with better language and cognitive scores than bilateral language representation. Preliminary analyses of the microstructural correlates of this atypical dominance show no significant differences in the integrity of the language-related tracts between the two hemispheres, though this finding must be interpreted cautiously due to the limited sensitivity of the chosen metrics.

Finally, functional analyses suggest a typical organization of activations related to primary functions (auditory, visual, hand motor) at the group level, regardless of the side of

language dominance. However, parietal lobe activations related to calculation appear predominantly lateralized in the language-dominant hemisphere, whereas they show a more bilateral distribution in controls. These findings encourage us to temper the "crowding effect" hypothesis, but they do not allow us to reject it entirely.

This work represents a first step towards the creation of a database of markers for multimodal exploration of risk factors associated with neonatal stroke. It will contribute to deepening the understanding of early brain plasticity, helping clinicians in prognosis establishment and in the development of personalized care and early rehabilitation programs for future newborns with early brain lesions.

## Keywords

Neonatal Stroke, MRI, Functional MRI, Diffusion MRI, Morphometry, Mixed Linear Model, Sex Effects, Neurodevelopment, Brain Plasticity, Crowding Effect

# Devenir adolescent après une lésion cérébrale focale précoce (AVC néonatal) : une fenêtre sur la plasticité cérébrale à long terme chez l'enfant. Etude longitudinale en IRM avancée multimodale et en neuropsychologie

## Résumé

Cette thèse explore les implications neurodéveloppementales à long terme de l'accident vasculaire cérébral (AVC) néonatal unilatéral durant l'enfance (à 7 ans) et l'adolescence (à 16 ans), dans une cohorte prospective française d'enfants ayant subi un AVC néonatal (AVCnn). Cette étude prospective longitudinale cherche à identifier des marqueurs précoces de l'évolution motrice et cognitive en combinant des marqueurs d'IRM morphométrique, microstructurelle (diffusion) et fonctionnelle avec les données cliniques et cognitives.

Ce projet a nécessité des développements méthodologiques adaptés à l'étude longitudinale de cerveaux lésés et en croissance, ainsi qu'un contrôle qualité exhaustif à chaque étape.

À travers une analyse morphométrique multifactorielle de l'IRM anatomique, nous avons examiné les facteurs cliniques susceptibles d'influencer la trajectoire de croissance cérébrale. Les résultats montrent que la croissance cérébrale des patients masculins dans l'hémisphère contralésionnel est plus faible que chez les filles à l'âge de 7 ans, sans évolution nette des différences liées au sexe à 16 ans.

Cela suggère que la puberté a peu d'effet sur ces trajectoires volumétriques, et que la plupart des déviations chez les patients masculins se produisent pendant la petite enfance. Ce pattern semble en accord avec la vulnérabilité périnatale, décrite pour d'autres pathologies du développement du cerveau masculin, et sans compensation par la suite. Cette notion de vulnérabilité est à nuancer, car ces différences morphologiques ne semblent pas corrélées avec les performances cliniques de la cohorte.

Dans la 2ème partie du travail, nous avons étudié en IRM fonctionnelle et en IRM de diffusion les modifications fonctionnelles et microstructurelles de la spécialisation hémisphérique du langage et des réseaux fonctionnels impliqués dans le calcul mental pour tester l'hypothèse d'un effet de "surpeuplement" ou "crowding effect" (compétition dans un espace neural restreint), notamment dans l'hémisphère dominant pour le langage.

Les résultats confirment la spécialisation hémisphérique atypique droite chez les patients présentant une lésion dans les régions périsylviennes gauches (2/3 des sujets). Cette latéralisation droite semble associée à de meilleurs scores langagiers et cognitifs qu'une représentation bilatérale du langage. Les analyses préliminaires des corrélats microstructurels de cette dominance atypique ne montrent pas de différences de l'intégrité des faisceaux impliqués dans le langage entre les deux hémisphères, mais elles doivent être nuancées par manque de sensibilité des métriques choisies.

Enfin, les analyses fonctionnelles suggèrent une organisation typique des activations liées aux fonctions primaires (auditives, visuelles, motrices de la main) à l'échelle des groupes, quel que soit le côté de la dominance du langage.

En revanche, les activations liées au calcul dans le lobe pariétal semblent nettement prédominantes dans l'hémisphère dominant pour le langage, alors qu'elles ont une distribution plus bilatérale chez les contrôles. En l'état, ces résultats nous poussent à nuancer l'hypothèse du "crowding effect", mais ne permettent pas de la réfuter.

Ce travail constitue la première étape vers la création d'une base de données de marqueurs pour une exploration multimodale des facteurs de risque liés à l'AVC néonatal. Il contribuera à approfondir la compréhension de la plasticité cérébrale précoce, afin de guider les cliniciens dans l'établissement d'un pronostic et la mise en place de soins personnalisés et de programmes de rééducation précoces pour les futurs nouveau-nés atteints de lésions cérébrales précoces.

## Mots clés

AVC Néonatal, IRM, IRM fonctionnelle, IRM de diffusion, Morphométrie, Modèle Linéaire Mixte, Effets du Sexe, Neurodéveloppement, Plasticité Cérébrale, Crowding effect

# Remerciements

Je souhaiterais remercier Dr Lucie Hertz-Pannier, ma directrice de thèse, pour sa supervision, pour nos nombreux échanges, son soutien, sa patience et sa confiance. Je remercie le Dr Mathilde Chevignard, ma co-directrice de thèse, pour son soutien, sa confiance et sa présence.

Je remercie le Dr Yann Leprince, pour le temps qu'il m'a accordé, des nombreux échanges méthodologiques, le traitement d'images, les heures passées à explorer des codes sources commentés en allemand.

Je remercie Alix DeLanglais et Marguerite Fattal, les deux premières stagiaires de Master que j'ai encadré, pour leur investissement dans le projet, respectivement le prototypage des traitements d'images en IRM fonctionnelle et en IRM de diffusion.

Je remercie toutes les personnes qui ont contribué au projet, de près ou de loin, et m'ont permis à leur échelle d'arriver au niveau d'avancement où je suis sur ce projet : Emeline Peyric, Laure Drutel, respectivement sur les acquisitions en neuropsychologie et orthophonie, Helena Bounab, Flore de Laplagnolle, Noémie Palay, Ambre Cauvin, qui ont contribué à l'exploration et la synthèse des données cliniques. Hugo Costa, qui a grandement approfondi les analyses statistiques sur ces mêmes données. Sara Neumane, pour ses efforts dans la mise en place d'une base de données précise et exhaustive.

Toute l'équipe cliniques d'UNIACT, particulièrement les infirmières (Laurence, Véronique, Gaëlle) et opérateurs/opératrices IRM (Yann Chantale et Valérie), sans qui aucune inclusions ne serait possible.

Tous les membres de l'équipe InDev, particulièrement David Germanaud, pour ses apports sur les corrections de volumes cérébraux en morphométrie, Clément Poiret pour m'avoir mis le pied à l'étrier dans l'environnement numérique de Neurospin. Eliot Kerdreux pour son aide précieuse en statistique et son investissement pour la cohésion de l'équipe, Aurelie Lebrun pour nos longs échanges méthodologiques en IRM de diffusion et de soutiens mutuels, Julia Micaux pour sa gentillesse et son soutien moral. Lucas, Jérémie, Justine, Florent, Amaia, Nils, Angèle, et tous ceux que je n'ai pas cité, mais qui ont compté par leur bonne humeur, ou simplement leur présence.

J'aimerais également citer quelques chercheurs seniors, qui ont aimablement accepté de m'accorder du temps pour aborder des points parfois assez compliqués des approches que nous avons déployé dans ce projet. Le Dr Edouard Duchesnay, qui m'a apporté beaucoup en vision d'ensemble, en stat, et qui s'est toujours très investi lors de nos discussions. Le Dr Bertrand Thirion, qui a aimablement libéré du temps dans son planning pour aborder des questions statistiques en IRMf. Le Dr Mickael Dinomais et toute l'équipe d'Anger, qui ont beaucoup enrichi nos échanges. Le Dr Pauline Favre pour son aide sur R et sa disponibilité.

Enfin je souhaiterais remercier Dr Joel Fluss et Dr Renaud Lopes, qui, en tant que rapporteurs, ont consacré leur temps et leurs efforts du jury pour évaluer mon travail, ainsi que les Dr Catherine Oppenheim, Arnaud Cachia, Josselin Houenou, Frédérique Liegeois, Guillaume Auzias.

## Dédicaces

A ces amis que je me suis fait à Neurospin : Wenqi, Corentin, Pamela, Alexane, Bosco, Chloé, Cyril, sans qui NeuroSpin aurait paru plus terne, et que j'espère recroiser dans le future

A ma famille me soutenant dans ce qu'on espère ma onzième et dernière année en tant qu'étudiant

Alice, qui fait de moi une personne meilleure, qui m'a encouragé à chaque étape et qui m'a permis d'aller au bout de ce projet.

## List of abbreviations

ACT : Anatomically Constrained Tractography  
AD : Axial Diffusivity  
ADC : Apparent Diffusion coefficient  
ALE : Activation Likelihood Estimation  
ANTs : Advanced Normalization Tools  
AP : Anterior-Posterior  
APPIS : Arterial Presumed Perinatal Ischemic Stroke  
AR : AutoRegressive  
AVC : Accident Vasculaire Cérébral  
BBT : Box and Block Test  
BFMF : Bimanual Fine Motor Function  
BIDS : Brain Imaging Data Structure  
BOLD : Blood-Oxygen-Level-Dependent  
BRI : Behavior Regulation Index  
BRIEF : Behavioral Rating Inventory of Executive Function  
CAT12 : Computational Anatomy Toolbox  
CBF : Cerebral Blood Flow  
CEA : Commissariat à l'énergie atomique  
CELF : Clinical Evaluation of Language Fundamentals  
CHU : Centre Hospitalier Universitaire  
CP : Cerebral Palsy  
CSF : CerebroSpinal Fluid  
CST : Cortico-Spinal Tract  
CSVT : Cerebral sinovenous thrombosis  
CT : Cortical thickness  
DISCO : Diffeomorphic Sulcal-based COrtical technique  
DK : Desikan-Killiany  
dMRI : Diffusion Magnetic Resonance Imaging  
DTI : Diffusion Tensor Imaging  
DTVP : Developmental Test of Visual Perception  
ECLA : Evaluation des Compétences de Lecture chez l'Adulte  
EFC : Entropy Focused Criterion  
EPI : Echo Planar Imaging  
FA : Fractional Anisotropy  
FAMD : Factor Analysis for Mixed Data  
FBA : Fixel-Based Analysis  
FC : Fiber Cross-section  
FD : Fiber Density  
FDC : Fibre Density and Cross-section  
FDR : False Discovery Rate  
FOD : Fiber Orientation Distributions  
FWE : Family-Wise Error  
GEC : Global Executive Composite  
GLM : Generalized Linear Model  
GMFCS : Gross Motor Function Classification System  
GRAPPA : Generalized Autocalibrating Partially Parallel Acquisitions

GSR : Ghost to Signal Ratio  
HCP : Human Connectome Project  
HD-BET : High Definition Brain Extraction Tool  
HIP : High Intellectual Potential  
IQR : Image Quality Ratio  
IRMf : Imagerie par résonance magnétique fonctionnelle  
LI : Lateralization Index  
LMM : Linear Mixed Model  
MACS : Manual Ability Classification System  
MCA : Middle Cerebral Artery  
MD : Mean Diffusivity  
MFA : Multiple Factor Analysis  
MI : Metacognition Index  
MNI : Montreal Neurological Institute  
MPRAGE : Magnetisation Prepared Rapid Gradient Echo  
MRA : Magnetic Resonance Angiography  
MRI : Magnetic Resonance Imaging  
NAIS : Neonatal Arterial Ischemic Stroke  
NDI : Neurite Density Index  
N-EEL : Nouvelles Epreuves pour l'Evaluation du Langage  
NHS : Neonatal hemorrhagic stroke  
NODDI : Neurite Orientation Dispersion and Density Imaging  
ODI : Orientation Dispersion Index  
OHBM : Organization of Human Brain Mapping  
PA : Posterior-Anterior  
PAIS : Perinatal Arterial Ischemic Stroke  
PC : Paralysie Cérébrale  
PCA : Principal Component Analysis  
PSI : Processing Speed Index  
PVI : Periventricular venous infarction  
QC : Quality Check  
RD : Radial Diffusivity  
ROI : Regions Of Interest  
RS-fMRI : Resting-State fMRI  
SE-EPI : Spin Echo - Echo Planar Imaging  
SES : Socioeconomic Status  
SGT : Sentence Generation Task  
SIFT : Spherical-deconvolution Informed Filtering of Tractograms  
SMA : Supplementary Motor Area  
SNR : Signal-to-Noise Ratio  
SPM : Statistical Parametric Analysis  
SUIT : Spatially Unbiased Infratentorial Template  
TE : Echo Time  
TFCE : Threshold free Cluster Enhancement  
TR : Repetition Time  
tSNR : temporal Signal-to-Noise Ratio  
UCP : Unilateral Cerebral Palsy  
UMR : Unité Mixte de Recherche

UPEC : Université Paris-Est Créteil

US : Ultrasound

VBG : Virtual Brain Grafting

VCI : Verbal Comprehension Index

WAIS : Wechsler Adult Intelligence Scale

WISC : Wechsler Intelligence Scale for Children

WMI : Working Memory Index

# Table of Contents

<b>Growing into Adolescence After Early Focal Brain Injury: Insights into Long-Term Brain Plasticity in Children after neonatal stroke. Longitudinal multimodal MRI and neuropsychology study.....</b>	<b>3</b>
Abstract.....	3
Keywords.....	4
<b>Devenir adolescent après une lésion cérébrale focale précoce (AVC néonatal) : une fenêtre sur la plasticité cérébrale à long terme chez l'enfant. Etude longitudinale en IRM avancée multimodale et en neuropsychologie.....</b>	<b>5</b>
Résumé.....	5
Mots clés.....	6
<b>Remerciements.....</b>	<b>7</b>
<b>Dédicaces.....</b>	<b>8</b>
<b>List of abbreviations.....</b>	<b>9</b>
<b>Table of Contents.....</b>	<b>12</b>
<b>Chapter 1 : Context, Introduction.....</b>	<b>16</b>
1. Neonatal stroke a model of early brain focal lesion to study the post lesional plasticity of the immature brain.....	16
1.1. Neonatal Stroke Definition.....	17
1.2. Mechanisms of Arterial Occlusion and Diagnosis and infant management.....	18
1.3. Outcomes prediction.....	18
2. Literature review on MRI imaging on Perinatal and Neonatal AIS.....	20
2.1. Structural/Anatomic MRI.....	20
2.1.1. Characterization of acute or later lesion territory and extent.....	20
2.1.2. Brain growth after NAIS or APPIS.....	21
2.1.3. Brain segmentation and registration : A critical methodological challenge for studies of brains with lesions.....	21
2.2. Functional MRI.....	22
2.2.1. Sensorimotor plasticity.....	22
2.2.1.1. Activation patterns for sensorimotor function.....	22
2.2.1.2. Anatomic-clinical correlations of motor function after NAIS.....	23
2.2.2. Language function.....	23
2.2.2.1. Activation patterns for language function.....	23
2.2.2.1.1. Clinical outcomes relationship with activation pattern.....	26
2.2. IRM diffusion.....	27
2.2.1. Role and Significance.....	27
2.2.2. Clinical Correlations with ADC and DTI Metrics.....	27
2.2.3. Advanced dMRI Techniques: Fixel-Based Analysis and NODDI.....	28
2.2.4. Connectomics and Graph Theory in Perinatal Stroke.....	29
2.2.5. Future Directions and Challenges.....	29
2.3. Resting state fMRI as a future window into the development and plasticity of brain circuits after an early stroke ?.....	30
2.3.1. Principles of Resting-State fMRI (RS-fMRI).....	30
2.3.2. Importance for Perinatal Stroke.....	30
3. PhD Aim, challenge and hypothesis.....	31

3.1. Overview of the AVCnnADO Project.....	31
3.2. Focus of My Thesis Work.....	33
3.3. Structure of the Manuscript.....	33
4. The AVCnn Cohort.....	34
4.1. Cohort constitution, assessment and imaging milestones.....	34
4.1.1. Clinical characterization of the cohort at 7 years of age.....	34
4.1.2. Clinical characterization of the cohort at 16 years of age.....	35
4.1.3. Control Cohorts at both ages.....	36
4.2. Imaging protocol.....	36
4.2.1. 7 years of age session.....	36
4.2.2. 16 years of age session.....	37
5. Specific methodological considerations to the AVCnnADO image processing.....	37
5.1. Image acquisition considerations.....	37
5.2. Specificity of imaging a lesioned brain.....	38
5.3. Data processing.....	38
<b>Chapter 2 : Longitudinal Analysis of Brain Morphometry After Neonatal Stroke, Sex Differences and Developmental Changes.....</b>	<b>40</b>
1. Introduction.....	40
1.1. Clinical Relevance and rationale.....	40
1.2. Study Objectives and Hypotheses.....	41
1.3. Results overview and comments.....	41
1.4. Methodological Framework.....	42
2. Article, Supplementary Materials.....	42
3. Complementary discussion.....	72
3.1. Whole brain volume correction bias in morphometric analyses.....	72
3.2. Confirming That Sex Differences Are Specific To Patients.....	72
3.3. Methodological considerations.....	73
3.3.1. Quality Control in Scanner-Biased Longitudinal Data.....	73
3.3.2. Deformation-based Morphometry.....	74
3.3.3. Using Surface Parcellation for Volumetric Analysis.....	76
3.3.4. Exploration of cortical thickness with Threshold-Free Cluster Enhancement (TFCE).....	77
4. Final Conclusion.....	79
<b>Chapter 3 : Exploration of functional and structural brain connectivity and their relationship with clinical and language outcomes after a neonatal stroke.....</b>	<b>80</b>
1. Introduction.....	80
1.1. Main Hypothesis and experimental plan.....	80
1.2. Known functional patterns for sentence processing and calculation tasks.....	81
2. Material and Methods.....	82
2.1. Participants.....	82
2.2. Image acquisition.....	82
2.2.1. Imaging procedure.....	82
2.2.2. Functional MRI paradigms.....	82
2.3. Image preprocessing.....	83
2.3.1. Image preprocessing and Quality control.....	83

2.4. fMRI Images analysis.....	84
2.4.1. First level analysis.....	84
2.4.2. Language lateralization index in each subject.....	85
2.4.3. Correlation between LI and clinical score.....	86
2.4.4. Group analysis of functional contrast (second-level analysis).....	86
2.4.5. Creation of a Language Activation Atlas based on Group SGT contrast maps.....	86
2.4.6. Group comparisons between typical and atypical language representation..	87
2.4.7. Extraction of cluster and peaks localization.....	88
2.4.8. BOLD temporal signal extraction in clusters identified with group comparisons.....	88
2.5. Diffusion MRI images analysis.....	89
2.5.1. Fractional anisotropy (FA).....	89
2.5.2. Probabilistic Tractography.....	89
2.5.3. Language network Tractography.....	89
3. Results.....	90
3.1. Language Hemispheric specialization and its correlation with clinical outcomes and microstructure.....	90
3.1.1. Distribution of Hemispheric Language Specialization within the Cohort....	90
3.1.2. Lesion Distribution Depending on Language Lateralization.....	95
3.1.3. Correlation of Clinical Scores with Language Lateralization.....	95
3.1.4. Microstructural changes according to language lateralization.....	97
3.1.5. Discussion.....	100
3.2. Hypothesis of functional competition within the right dominant hemisphere.....	101
3.2.1. Investigation of localizer tasks per subgroup depending on language lateralization.....	101
3.2.1.1. Audio – video contrast.....	103
3.2.1.2. Left – Right contrast.....	103
3.2.1.3. Language – Calculation contrast.....	104
3.2.2. Activation pattern differences between typical and atypical hemispheric language specialization.....	104
3.2.2.1. Audio – Video contrast.....	105
3.2.2.2. Left – Right hand motor contrast.....	106
3.2.2.3. Language – Calculation contrast.....	106
3.2.3. Investigation of activation pattern differences between dominant and non-dominant hemisphere.....	107
3.2.3.1. Audio – Video contrast.....	108
3.2.3.2. Left–Right Hand Motor Activation Contrast.....	108
3.2.3.3. Language – Calculation contrast.....	109
3.2.4. Discussion.....	110
4. Conclusion.....	111
<b>Perspectives and Considerations on the Presented Studies.....</b>	<b>113</b>
1. Remarks on Morphometry studies.....	113
1.1. Strengths.....	113

1.2. Weaknesses.....	114
1.2.1. Scanner bias.....	114
1.2.2. Effect of whole brain volume.....	114
1.2.3. Generalization of this study.....	114
1.3. Perspectives.....	115
1.3.1. Normative Analysis: Addressing Generalizability and Scanner Bias.....	115
1.3.2. Normalization and parcellation methods for lesional brain in children.....	115
1.3.3. Exploring differences between cortical thickness and volume results.....	116
2. Perspectives for Functional and Structural Connectivity studies.....	116
2.1. Further investigation of homotopic language lateralization consequences.....	116
2.2. Avenues for investigating microstructural connectivity with Diffusion MRI.....	117
2.2.1. White matter tracts parcellation.....	117
2.2.2. White Matter Integrity metrics.....	117
3. Using multimodal and clinical data to extract risk factors and outcome predictors....	118
4. Outcomes of Brain Plasticity after an Early lesion.....	119
4.1. Language homotopy functional outcomes and microstructure.....	119
4.2. “Crowding Effect”.....	119
<b>Final conclusion.....</b>	<b>120</b>
<b>Bibliography.....</b>	<b>121</b>
<b>List of figures.....</b>	<b>144</b>
<b>List of Tables.....</b>	<b>147</b>
<b>Communications and Publications.....</b>	<b>165</b>
Published article.....	165
Posters presented in conferences.....	165
<b>Formations.....</b>	<b>165</b>

# Chapter 1 : Context, Introduction

## 1. Neonatal stroke a model of early brain focal lesion to study the post lesional plasticity of the immature brain

Newborns, defined as children under 28 days of age, are particularly vulnerable to strokes. The general classifications of stroke, namely hemorrhagic (caused by a bleed in the brain) versus ischemic (caused by a clot in a blood vessel in the brain), and arterial versus venous, are applicable to this age group. Specifically, cerebral arterial infarction presents with distinct mechanisms and clinical manifestations in newborns, leading to the categorization of the group of perinatal cerebral arterial infarction, or perinatal stroke.

Recent advancements in clinical research and neuroimaging have transformed the understanding of perinatal ischemic stroke. This condition is defined as “a heterogeneous condition with a brain injury due to focal cerebral arterial or venous occlusion, occurring between 20 weeks of fetal life through the 28th postnatal day” (Raju et al., 2007). Previously a poorly understood cause of cerebral palsy, perinatal ischemic stroke is now recognized as a systematically classifiable condition with specific subtypes of focal brain injuries. These conditions can be categorized based on three variables: (1) the timing of the injury (before or near birth), (2) the mechanism (ischemic or hemorrhagic; arterial or venous), and (3) the timing of symptom onset (immediately after birth or later in infancy). By integrating neuroimaging with clinical information, five distinct perinatal stroke syndromes have been identified (Dunbar & Kirton, 2018; Kirton & deVeber, 2013).

These distinct stroke subtypes involve focal injury in an otherwise healthy brain, representing an ideal model for studying developmental plasticity and outcomes following early brain injury. While they share some characteristics, they also exhibit unique features (Figure 1). Patterns of infarction may be cortical, subcortical, or combined.

Three subtypes are arterial in nature, while two involve venous occlusion :

- Neonatal Arterial Ischemic Stroke (NAIS)
- Neonatal hemorrhagic stroke (NHS)
- Arterial Presumed Perinatal Ischemic Stroke (APPIS)
- Cerebral sinovenous thrombosis (CSVt)
- Periventricular venous infarction (PVI)

Considering all perinatal stroke syndrome, prevalence is between 37 and 67 per 100,000 live births (mostly term-birth), depending on estimations, making it the most common form of childhood stroke. The risk of stroke is most acute in the week surrounding birth (Fluss et al., 2019). The outcomes often result in lifelong disabilities and contribute significantly to the global disease burden. Perinatal stroke is the leading cause of unilateral cerebral palsy, and many survivors suffer from additional neurological issues such as intellectual disabilities, developmental and behavioral disorders, and epilepsy.

Although any of the five subtypes can occur preterm, this review focuses on vascular injuries in term infants and does not cover outcomes in preterm infants. Cerebral venous thrombosis and hemorrhagic strokes in newborns share many characteristics with those in

older children and are often discussed together. However, peri- and intraventricular hemorrhages, which are specific to newborns, especially premature ones, are excluded from the definition of stroke.

Table 1 – General overview of perinatal stroke syndromes.					
Type of stroke	Birth-prevalence (37–67/100,000)	Main causes and risk factors (often plural)	Mechanism	Clinical findings	Outcome
Neonatal arterial ischemic stroke (NAIS)	- 6–17/100,000 in newborns $\geq$ 35 GA  (670/100,000 $\leq$ GA with specific findings: see text)	<b>Symptomatic cases</b> - Bacterial meningitides - Cardiac disease/procedures - ECMO  <b>Cryptogenic cases</b> - Chorioamnionitis - Perpartum asphyxia - Male sex and nulliparity	<b>Cryptogenic cases</b> - Placental cerebral embolism - Focal arteriopathy including cerebral vasculitis and (rarely) trauma	- Repeated focal seizures - In an otherwise healthy term/near term newborn	- CP: 1/3 (depending on the extend and on the localization of the infarct site) - Epilepsy: 15% - Learning/behavioural difficulties: ++ - Recurrence: exceptional
Presumed perinatal ischemic stroke (APPIS + PVI)	- 20–29/100,000	<b>APPIS</b> - Similar to NAIS  <b>PVI</b> - Preeclampsia, foetal hypotrophy	<b>APPIS</b> - Probably similar to NAIS  <b>PVI</b> - In utero ( $\leq$ 34 GA) germinal matrix haemorrhage leading to compression of the medullary veins and focal venous infarction of the periventricular white matter	<b>Delayed presentation</b> (by definition) - Most often through motor deficiency - Rarely with seizures, learning difficulties or systematic imaging	- CP: quasi systematic due to the mode of presentation - Epilepsy and learning/behavioural difficulties: higher than NAIS for APPIS and lower for PVI - Recurrence: exceptional
Perinatal haemorrhagic stroke (PHS; restricted by definition to term/near term newborns)	- 16/100,000	<b>Symptomatic (rare) cases</b> - Bleeding diathesis (thrombocytopenia) - Vascular malformation - Cardiac disease/procedures <b>Cryptogenic cases</b> - Perpartum asphyxia - Small for GA	- Primary bleeding in symptomatic cases - Haemorrhagic transformation of an ischemic injury (due to stroke or HIE) - In case of uni- or bilateral thalamic haemorrhage, suspect straight sinus thrombosis (see infra)	<b>Acute presentation</b> Similar to NAIS (seizures ++) and eventually more severe in case of intracranial hypertension <b>Delayed presentation</b> Similar to PPIS	- <b>Acute stage:</b> more severe than NAIS (mortality risk up to 25%) - <b>Long term:</b> depending on the extend and localization of the lesion and comorbid conditions (worse in symptomatic cases) - <b>Recurrence:</b> exceptional
Neonatal cerebral sinus venous thrombosis (CSVT)	- 14–12/100,000	<b>Symptomatic cases</b> - Severe neonatal condition: meningitis, dehydration, HIE ...  <b>Cryptogenic cases</b> - Gestational hypertension - Chorioamnionitis - Perpartum asphyxia	Virchow's triad	<b>Acute presentation</b> Similar to NAIS (seizures ++) <b>Discovered incidentally</b> in case of a severe disorder (e.g. meningitis) or as an incidental finding in case of systematic imaging survey (preterm, small for GA)	- <b>Long term:</b> depending on the association with parenchymal injury and comorbid conditions - Epilepsy with continuous spike and wave during sleep - <b>Recurrence:</b> exceptional

GA: gestational age; ECMO: extracorporeal membrane oxygenation; HIE: hypoxic ischemic encephalopathy; CP: cerebral palsy; APPIS: arterial presumed perinatal ischemic stroke; PVI: periventricular venous infarction; HIE: hypoxic ischemic encephalopathy.

Figure 1: Synthesis of perinatal stroke types, mechanisms, clinical findings and outcomes (Fluss et al., 2019)

## 1.1. Neonatal Stroke Definition

Neonatal Arterial Ischemic Stroke (NAIS) is the most common subtype of stroke presenting in the first week of life. Its birth prevalence in term and near-term newborns varies from 6 to 17 per 100,000 live births (Darmency-Stamboul et al., 2017). Most cases present with unilateral repetitive clonic seizures between day 1 and 3 after birth in an otherwise healthy term baby (Kirton & deVeber, 2009). Diffusion-weighted imaging confirms acute, focal brain infarction in an arterial territory. Most cases involve large artery occlusions, typically in the left middle cerebral artery (85% of cases), with combined cortical and subcortical injuries. Injuries are multifocal in 23 to 30% of cases (Kirton & deVeber, 2013).

Although the pathophysiology of NAIS is poorly understood and most cases are considered idiopathic, several studies have described potential risk factors (Li et al., 2017). Notably, males are disproportionately affected by NAIS, representing two-thirds of the NAIS population (Dunbar et al., 2020; Dunbar & Kirton, 2018). Other identified risk factors include obstetrical determinants, prepartum hypoxia, and maternal/fetal/neonatal inflammatory states. Most studies seeking to identify risk factors associated with NAIS converge on a

multifactorial origin, with a drastic risk increase when these factors are combined (Giraud et al., 2017).

## 1.2. Mechanisms of Arterial Occlusion and Diagnosis and infant management

The precise mechanism of arterial occlusion in neonatal stroke remains hypothetical. Current theories emphasize the role of the placenta. Most risk factors are determinants or markers of vascular-placental pathology, potentially leading to maternal-fetal circulation dysfunction, capillary occlusion, and placental infarction. The fetal circulation may result in a thrombus formed on these placental lesions preferentially embolizing to cerebral arteries. A less likely hypothesis involves injury to encephalic arteries during delivery (Fluss et al., 2019).

Although Ultrasound (US) imaging enables early screening in intensive care units, MRI is the modality of choice for confirming stroke diagnosis while providing useful prognostic information (Lee et al., 2017; van der Aa et al., 2014). Diffusion MRI is particularly useful at onset as it shows restricted diffusion within hours after the stroke and persists up to 10 days after the stroke. Diffusion-weighted MRI (dMRI) is the gold standard in the acute phase of neonatal arterial ischemic stroke (NAIS), enabling immediate stroke diagnosis and early prognosis. dMRI is particularly valuable for imaging early diaschisis, a phenomenon where a brain region distant from the lesion, yet anatomically connected, shows functional inhibition a few days post-stroke. This is visible through hyperintensities on dMRI and aids in early outcome prediction. It is usually recommended to perform an MR Angiography (MRA) of the neck and cerebral arteries as a complementary examination. Performing a second MRI scan, with T2 or T1 weighted images, after a few days may allow for better lesion identification.

The transfer in a dedicated Neuro-Vascular Unit of a child suspected of stroke is required to ensure precise diagnosis and rapid implementation of the appropriate support treatment. In the acute phase of neonatal infarction, maintaining neonatal homeostasis (adequate hydration, normal blood sugar and temperature levels, prevention of anemia/polycythemia) and treating convulsions are recommended. Seizures are often self-limited or controlled with antiepileptic drugs. As they rarely persist beyond the neonatal period, and given the potential neurotoxicity of antiepileptic drugs on the immature brain, the recommendation is now to shorten the duration of antiepileptic treatment. Most newborns can be discharged without medication, although practice varies widely across centers. The treatment is largely supportive unless there is a treatable medical condition or complication (Debillon et al., 2017; Fluss et al., 2019).

## 1.3. Outcomes prediction

Although rarely performed in practice, a second MRI scan several days after the event may help to precisely identify the lesional area and potential remote injuries. Most newborns show an acute infarct within the Middle Cerebral Artery (MCA) territory, but different patterns are associated with specific outcome patterns:

- Concomitant involvement of the cerebral cortex, the basal ganglia, and the posterior limb of the internal capsule is strongly associated with the development of unilateral cerebral palsy (UCP) (Boardman et al., 2005; Wagenaar et al., 2018).
- Restricted diffusion at the level of the cerebral peduncle or above, representing pre-Wallerian degeneration of the corticospinal tract (CST), strongly predicts an unfavorable motor outcome (Husson et al., 2010)
- Cerebral peduncle atrophy, reflecting established degeneration of the motor tracts, can also be identified within a few weeks and is prognostic of UCP (Dudink et al., 2009).
- Other similar network injuries remote from the infarct (also called diaschisis), are described in the thalamus, the corpus callosum, and the cerebellum (Craig, Carlson, et al., 2019; Craig, Olsen, et al., 2019; Lequin et al., 2009; Okabe et al., 2014).

Posterior circulation stroke (isolated or in association with other arterial territories) represents only 10% of NAIS in large series and is associated with a better outcome, despite frequent visual field defects. As a general rule, the larger the stroke, the higher the risk of sequelae is.

Beyond the neonatal period, continued surveillance throughout child development is needed to identify the occurrence of epilepsy and signs of motor and cognitive sequelae that may be amenable to intervention programs. Outcomes from perinatal stroke greatly vary. Despite potential increased plasticity in the developing brain, most perinatal stroke survivors have lifelong neurological morbidity, at higher rates than similar lesions acquired in later infancy or childhood (Kirton & deVeber, 2013; Sullivan et al., 2023). Due to the multifactorial nature of impairments, a multidisciplinary approach tailored to the patient's needs is required. Recent rather-homogeneous cohorts have provided valuable data regarding short- and medium-term outcomes (Chabrier et al., 2016; Darmency-Stamboul et al., 2017; Dunbar & Kirton, 2018; Wagenaar et al., 2018; Westmacott et al., 2010).

The epilepsy rate is consistent in children, around 14% when estimated in recent homogeneous cohorts. Epilepsy tends to cluster with cerebral palsy (CP), poor academic performance, and cognitive impairment (Wagenaar et al., 2018).

The primary motor complication is the development of UCP, previously named infantile cerebral hemiplegia. Virtually all children with presumed perinatal cerebral infarction develop this type of sequela, as motor impairment is the usual telltale sign of such incidents. The rate of CP is close to 30%, with the majority of affected children being classified as GMFCS (Gross Motor Function Classification System) grade I or II (all children walk independently) (Chabrier et al., 2016; Wagenaar et al., 2018). The upper limb is more affected, and motor outcome is the more predictable outcome, as noted previously. Poorer motor outcomes generally occur when the lesion extends to the CST (Dinomais et al., 2015; Ecury-Goossen et al., 2016; Husson et al., 2010; Wagenaar et al., 2018), and the sensorimotor system shows limited plasticity due to its early maturation (Fluss et al., 2019).

Because speech and other higher cognitive functions emerge later in childhood, children with perinatal stroke are considered to grow into their deficits when specific developmental stages are reached. Long-term neuropsychological studies are currently defining the evolution and spectrum of these higher-order deficits. Regardless of the side

and extent of the lesion, preserved speech ability is the rule, although the trajectory of early oral language milestones can be slightly delayed (Chabrier et al., 2016; Trauner et al., 2013; Wagenaar et al., 2018). More subtle deficits might emerge in school years where sophisticated linguistic abilities need to be mastered (Reilly et al., 2013). Functional MRI studies have indeed shown that early injury to the language network in the dominant hemisphere can be at least partially, if not completely, compensated by a contralateral homotopic reorganization (Martin et al., 2023). Right-hemispheric language reorganization after unilateral left hemispheric lesion appears particularly efficient in the neonatal (Lidzba et al., 2017).

Three prospective studies have investigated the global cognitive outcomes at school age following NAIS. Ricci et al. found that children had global intelligence scores within the normal range. reported that NAIS preschoolers were comparable to controls, though cognitive deficits, especially in non-verbal reasoning, might appear later. In the French AVCnn cohort, while most children retained their intellectual abilities, a notable subset exhibited low academic performance, which was strongly linked to language skills (Chabrier et al., 2016; Ricci et al., 2008; Westmacott et al., 2010).

The lack of finer and reproducible long term studies impairs our comprehensive understanding of outcomes after NAIS (Kirton & deVeber, 2009). until adolescence and adulthood. Recent reviews and meta-analyses report a lack of homogeneous case reporting and exhaustive assessment to enhance disease comprehension, beyond lesion size and localization in predicting CP risks (Baak et al., 2023; Pabst et al., 2024).

## 2. Literature review on MRI imaging on Perinatal and Neonatal AIS

The literature on MRI imaging in presumed perinatal (APPIS) and neonatal arterial ischemic stroke (NAIS) has grown significantly in recent years, offering various approaches to address inter-subject variability and help predict outcomes from imaging. Outcome prediction is particularly critical, as neonatologists and pediatric neurologists need reliable information to help patients and their families anticipate adverse outcomes. This section reviews published work on MRI imaging in perinatal arterial ischemic stroke (PAIS) and NAIS, highlighting the main findings, challenges, and future perspectives.

### 2.1. Structural/Anatomic MRI

#### 2.1.1. Characterization of acute or later lesion territory and extent

Lesion localization appears to be often reproducible across patients, illustrated by the strong prevalence of the left MCA territory in NAIS, but can also be highly variable depending on the clot's position in the artery. Clearly defining the lesional territory and the stroke boundaries, whether in acute or late context (as in APPIS or diagnosed perinatal stroke where images are no longer available), is crucial for understanding and predicting early stroke outcomes.

Lesion mapping has been performed on diverse APPIS and NAIS cohorts, illustrating specific lesion distributions (Dinomais et al., 2015; Northam et al., 2018; Saunders et al., 2019; Stephan-Otto et al., 2017). However, only a few have demonstrated a predictive effect of the lesional territory on motor or cognitive outcomes (Dinomais et al., 2015). These

approaches are often deployed with diffusion imaging, which will be discussed further (see Diffusion MRI, Chapter 1, section 2.3).

Recent work has designed atlases based on arterial territories, allowing more systematic lesion classification and enabling non-specialists to perform finer lesion characterization and better exploratory studies (Liu et al., 2023; Núñez et al., 2020). These advances could greatly benefit from specifically tailored registration/segmentation processes capable of reliably segmenting regions near lesions.

### 2.1.2. Brain growth after NAIS or APPIS

Morphometric analyses, which focus on brain growth as an early indicator of brain plasticity through volume changes, have been conducted on subjects after perinatal stroke (Dunbar & Kirton, 2019). A recent study demonstrated generalized lower cortical grey matter volume, thickness, and some gyrification differences in the contralesional hemisphere compared to an age-corrected control group (Shinde et al., 2023). Other studies have highlighted lower white matter volumes along fibers connected to the lesion (Moses, 2000; Stiles et al., 2003), bilateral thalamus volume alterations (Craig, Carlson, et al., 2019), bilateral basal ganglia atrophy (Hassett et al., 2022), and crossed cerebellar atrophy (Craig, Olsen, et al., 2019). Bilateral thalamus and basal ganglia atrophy correlated with epilepsy risks (Vaheer et al., 2023), while ipsilesional atrophy correlated with poorer hand functions (N. Ilves et al., 2022) and bilateral hippocampal atrophy correlated with memory impairment (Gold & Trauner, 2014).

To our knowledge, only a few studies have delved into the brain morphometry of NAIS specifically. One study showed volume alteration in the cortico-spinal tract in centrum semiovale white matter, proposing it as a marker of cerebral palsy (Dinomais et al., 2015). Another study correlated poorer contralateral hand function with smaller volumes in the ipsilesional mediodorsal thalamus, ipsilesional corticospinal tract (superior corona radiata), posterior limb of the internal capsule, cerebral peduncle, and the ipsilesional body of the corpus callosum (Dinomais et al., 2016). The last explored thickness, volume, and gyrification alterations in both hemispheres (Al Harrach et al., 2019), identifying localized modifications in cortical areas distant from the primary lesion within the ipsilesional hemisphere, as well as in the contralesional hemisphere, emphasizing subtle differences in patterns between right and left-lesioned patients.

Most of the previously cited studies rely on small cohorts with wide age ranges and varying lesion territories and origins. Brain morphometry studies are challenging, as brain volumes depend on myriad factors (sex, age, brain asymmetry, total brain volume, environment), with lesion variability and brain plasticity adding complexity. Available cohorts are too small to explore all these factors in detail, often forcing researchers to accept sensitivity loss or imperfect correction for some unexplored factors. For example, sex is often either used as a covariate or excluded after checking for sex differences with univariate tests.

### 2.1.3. Brain segmentation and registration : A critical methodological challenge for studies of brains with lesions

Although brain segmentation and parcellation are rapidly advancing and expanding research areas, brains with lesions, especially those with severe damage, remain a

significant challenge (Cabezas et al., 2011; Craig et al., 2021). The situation gets even more complex in the case of early brain lesions, where subsequent spatially heterogeneous brain growth leads to anatomical distortions nearly impossible to account for (lesion scarring, cavities filled with Cerebrospinal Fluid (CSF), gliosis...). This issue affects several pathologies (e.g., stroke, brain tumors) and is just beginning to be addressed by gold-standard open-access softwares (Huo et al., 2016; Ledig et al., 2015; Manjón et al., 2022). For example, VolBrain launched a revised version of their segmentation tool, Vol2Brain, capable of handling small white matter lesions, but it proved incapable of accurately labeling brains with large lesions. Nevertheless, efforts are heading in the right direction, focusing mainly on white/grey matter segmentation or lesion delineation as a first step to combine with current approaches (Abbasi et al., 2023).

The limitations of current brain segmentation research are a primary reason why there are more studies on the contralesional hemisphere than on the ipsilesional hemisphere after perinatal strokes. Most ipsilesional hemisphere studies focus on very specific regions, usually driven by clinical hypotheses, to limit the necessary manual work on segmentation corrections.

## 2.2. Functional MRI

Functional MRI (fMRI) leverages blood-oxygen-level-dependent (BOLD) contrast to track deoxyhemoglobin fluctuations, which indirectly reflect neuronal activity. Neural activity increases oxygen demand in specific brain regions, triggering changes in cerebral blood flow (CBF) and altering the concentrations of oxyhemoglobin and deoxyhemoglobin. By recording BOLD response fluctuations over time, either during tasks or at rest, researchers can localize brain functions and explore the intrinsic functional connectivity between different regions.

Task-based fMRI is particularly effective in identifying brain areas involved in specific tasks. Participants generally (depending on experimental paradigm) alternate between performing a task and resting, and BOLD signal fluctuations during these periods generate statistical maps highlighting active areas. These activation maps, with millimetric spatial resolution, have successfully demonstrated patient-specific reorganization of functional areas following strokes in adults (Calautti & Baron, 2003; Lake et al., 2016; Rehme et al., 2012) or brain injuries in children (Gaberova et al., 2018).

Most fMRI studies focus on sensorimotor and language functions due to their reliable imaging procedures and significant impact on child development and integration. These functions present limited risk of failure during MRI tasks, even when cognitive difficulties are present, making them efficient targets for study.

### 2.2.1. Sensorimotor plasticity

#### 2.2.1.1. Activation patterns for sensorimotor function

Studies often employ unimanual hand tasks, such as finger tapping and hand squeezing. The typical activation pattern for such tasks involves the whole sensorimotor network including contralateral primary sensorimotor, premotor, supplementary motor, and posterior parietal cortices, as well as contralateral thalamus, basal ganglia, and ipsilateral cerebellum (Craig et al., 2021). Recent reviews on APPIS identify three activation scenarios

during paretic limb use depending on the timing of the lesion and the involvement of the motor network (Craig et al., 2021; Kirton et al., 2021):

- Ipsilesional Activation: Local functional reorganization of perilesional tissue in the lesioned hemisphere for paretic hand functions
- Contralesional Activation: Development or shift of motor function to the non-lesioned hemisphere, resulting in ipsilateral limb control. This scenario is more typical of prenatal stroke (Staudt et al., 2004), which APPIS categorization do not exclude
- Bilateral Activation: Recruitment of the motor cortex and supplementary areas in both hemispheres during movement of the paretic limb

Bilateral activation patterns might indicate mirror movement representation. Some studies compared activation peaks or activated region extents, consistently finding larger areas in subjects with perinatal stroke, reflecting increased effort to complete tasks. However, small study group sizes necessitate cautious interpretation of these metrics, as they may not directly reflect biological reality (Cao et al., 1994; Van de Winckel et al., 2013; Vandermeeren et al., 2003). Only one study has specifically explored hand function lateralization in NAIS, showing a consistent ipsilesional pattern (Al Harrach et al., 2020).

#### 2.2.1.2. Anatomical-clinical correlations of motor function after NAIS

Current literature suggests that maintaining contralateral hand control is more effective in maximizing clinical motor function (Craig et al., 2021). Some cases show a dissociation between sensory and motor functions, where only motor representation shifts to ipsilateral control, which is suspected to be maladaptive. Generally, complete contralesional ipsilateral shift correlates with poorer performance, although this effect is confounded by larger lesions.

Studies targeting activation areas and peaks indicate that higher activation in the ipsilesional central sulcus is highly correlated with motor function (in a study of 9 patients) (Van de Winckel et al., 2013). Ipsilateral (same hemisphere than the activated hand) parietal lobule and premotor cortex activations have also been linked to better performance on dexterity measures in the paretic hand (in a study of 6 subjects aged 9-17 years with high lesion variability) (Vandermeeren et al., 2003). These results must be interpreted cautiously, as older studies rely on less precise stroke classifications and diverse lesion origins within small patient cohorts.

A study of the AVCnn cohort at 7 years of age, comprising 33 subjects, specifically targeted NAIS and found a correlation between BOLD signal percentage variation in the lesioned hemisphere and dexterity levels. These findings suggest that for NAIS patients with no extensive permanent motor impairment, BOLD signal-based data analysis can be a valuable tool for evaluating functional brain networks (Al Harrach et al., 2020).

#### 2.2.2. Language function

##### 2.2.2.1. Activation patterns for language function

Functional MRI (fMRI) sequences for imaging language-related activation vary widely and include tasks such as verb generation, object naming, word chains, forward vs. reverse speech, sentence generation, and story listening. Language activation typically exhibits

left-hemisphere dominance (99% of right-handed and 75% of left-handed individuals) (Newport et al., 2017), but it involves coordinated functions across several regions. Language is a broad notion, encompassing a myriad of associated cognitive subfunctions. When focusing on sentence processing tasks, several meta-analysis reported recurrent patterns (Vigneau et al., 2006; Walenski et al., 2019). Most recent meta analysis results for sentence comprehension and production, using activation likelihood estimation (ALE), are presented in Figure 2 and Figure 3.

Sentence comprehension related functional activation encompass :

- Left Inferior frontal gyrus (pars triangularis) (Broca's area): Primarily involved in language production tasks
- Left precentral gyrus
- Left Supplementary Motor area (SMA), located on the medial side of the superior frontal gyrus
- Left middle temporal gyrus, including the temporooccipital junction
- Left posterior superior temporal gyrus (Wernicke's area): Involved in language perception tasks
- Left angular gyrus (Geschwind's area)
- Left fusiform cortex
- Right middle temporal gyrus, including the temporooccipital junction
- Right temporal pole
- Right posterior superior temporal gyrus

Sentence production tasks related functional activation encompass :

- Bilateral activation of superior division of the lateral occipital cortex
- Left superior frontal gyrus, extending to SMA
- Left Middle frontal gyrus
- Right superior frontal gyrus, extending to SMA
- Left middle temporal gyrus, temporooccipital junction

Several activations overlap between both tasks. Recent data driven atlas, based on multiple task induces activation in typical right handers encompass most of these regions, but add precuneus and most basal ganglia and hippocampus (Labache et al., 2019)

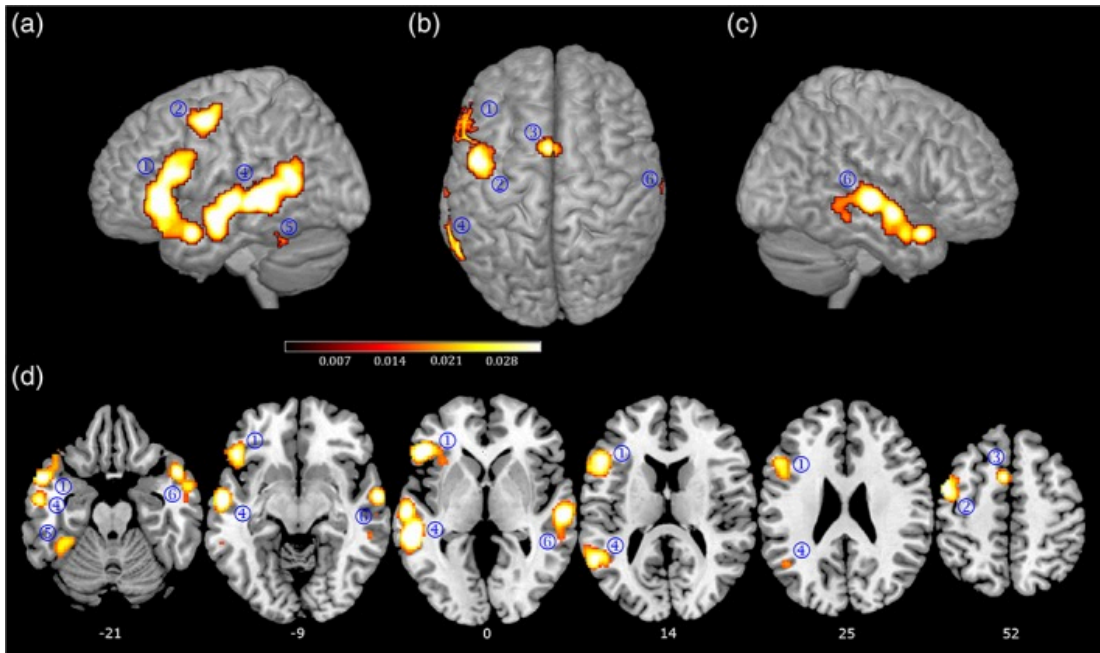


Figure 2: Significant clusters associated with sentence comprehension (both auditory and visual) derived from ALE analysis: Left lateral (a), from above (b), right lateral (c), axials by z-coordinates in MNI space (d). The scale bar reflects the ALE values (Walenski et al., 2019)

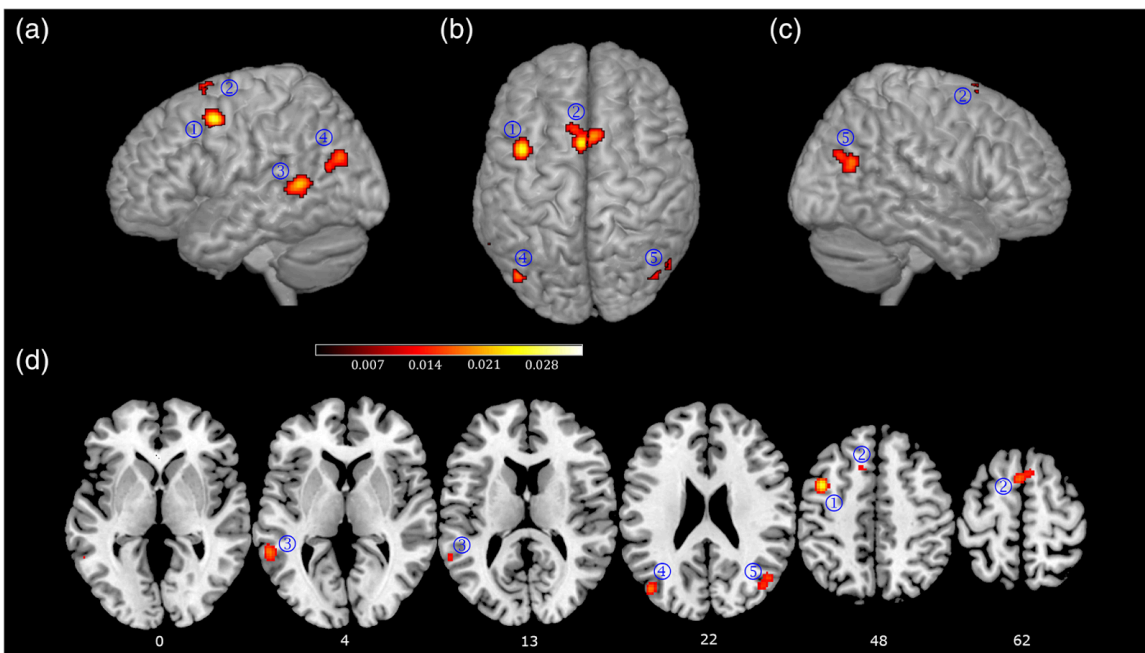


Figure 3: Significant clusters associated with sentence production derived from ALE analysis: Left lateral (a), from above (b), right lateral (c), axials by z-coordinates in MNI space (d). The scale bar reflects the ALE values (Walenski et al., 2019)

From a structural connectivity viewpoint, the language-related network is notoriously divided into separate anatomical streams (Friederici & Gierhan, 2013; Hickok & Poeppel, 2004, 2007) that arise from the posterior superior temporal gyrus (Figure 4) :

- The dorsal stream projects towards the inferior parietal and posterior frontal lobe (inferior frontal gyrus and premotor cortex) through the arcuate fasciculus

- The ventral stream links the superior and middle temporal gyri, the inferior parietal lobe, and the occipital lobe with the inferior frontal gyrus through the inferior fronto-occipital fasciculus
- The most anterior parts of the inferior frontal gyrus and the frontal operculum are connected to the anterior temporal lobe through the uncinate fasciculus

This stratification is often linked to specific language related function, and is a useful cue to understand language network, impairments, and compensation mechanisms (López-Barroso & de Diego-Balaguer, 2017)

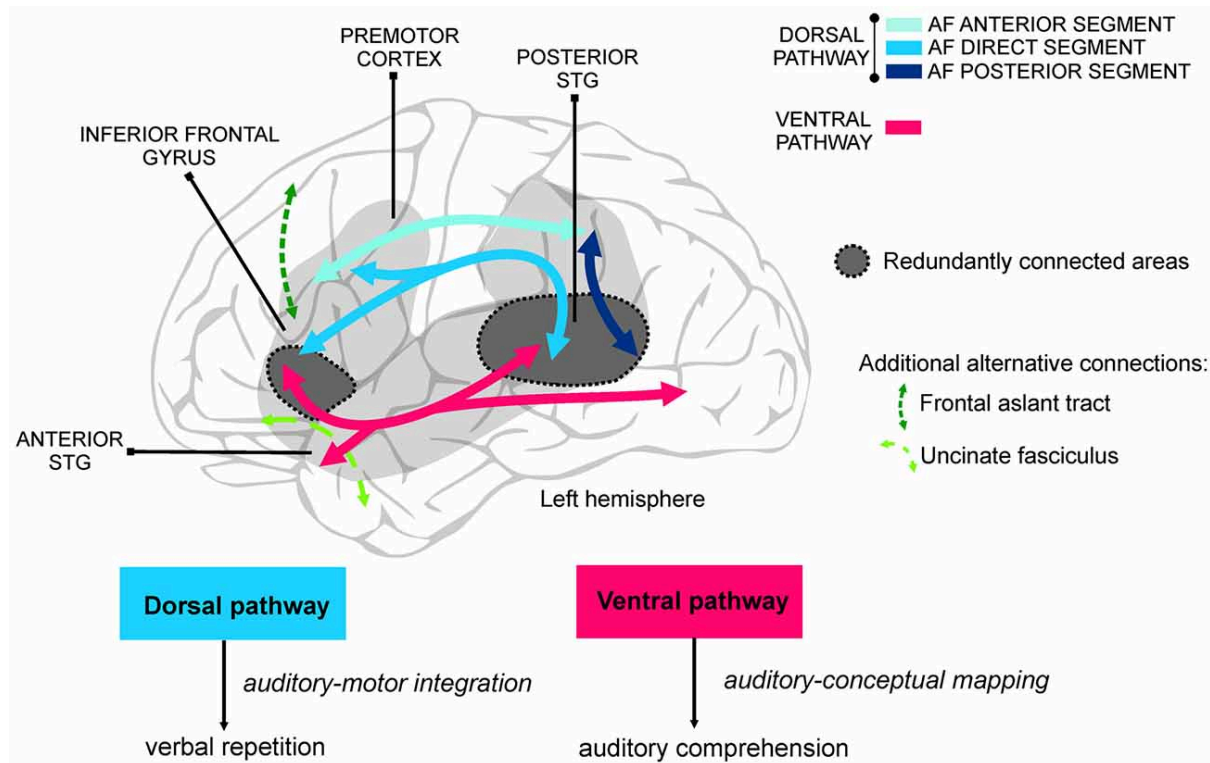


Figure 4: Schematic illustration of the main anatomical connections of the perisylvian areas in the left hemisphere, comprising the ventral and the dorsal pathways. The perisylvian cortex, covering frontal, parietal and temporal cortices, is shaded in gray (López-Barroso & de Diego-Balaguer, 2017).

Previous studies have shown that after a perinatal stroke, the lesioned language areas often reorganize within the right hemisphere, particularly in homotopic regions (François et al., 2019; Martin et al., 2023; Newport et al., 2022; Schnauffer et al., 2023; Tillema et al., 2008) (Everts et al., 2010; Fair et al., 2010). However, recent research has highlighted slight divergences in the specific regions affected (Martin et al., 2022).

It is for language specialization to remain in the left hemisphere after a perinatal stroke; this typically occurs only when the lesion is small and/or remote from the perisylvian cortex.

#### 2.1.1.1. Clinical outcomes relationship with activation pattern

The most recent review (François et al., 2021) suggests that language performance after perinatal stroke varies depending on language lateralization. This pattern is

multifactorial, influenced by lesion type (e.g., NAIS, PAIS, PVI), size, and localization. Two patterns of brain “reorganization” after early left lesion are associated with good language outcomes:

1. Interhemispheric reorganization: Temporal and frontal language areas shift to the right hemisphere, possibly accompanied by cerebellar reorganization to the left
2. Intrahemispheric reorganization with functionally active perilesional brain regions

Notably, studies with comprehensive assessments of language functions remain scarce. Previous reviews (Craig et al., 2021) suggest that bilateral or contralesional organization yields language performance comparable to typical left lateralization (P. Ilves et al., 2014) (Ballantyne et al., 2008; Staudt et al., 2002), with some evidence even favoring bilateral organization (Raja Beharelle et al., 2010).

In the context of NAIS, studies have highlighted region-dependent outcomes for language performance and lateralization (Northam et al., 2018). These studies underscore the protective effect of language relocation and identify early lesions in the dorsal language stream as related with persistent speech repetition problems, similar to conduction aphasia in adults.

Finally, one study has identified an intriguing effect where right language lateralization impacts other clinical domains, such as visuospatial scores (Lidzba et al., 2006). This phenomenon, referred to as the “crowding effect,” suggests that developing brain functions might compete for limited neural resources in a constrained brain. However, this effect has not been extensively investigated in cases of early focal lesions.

## 2.2. IRM diffusion

### 2.2.1. Role and Significance

dMRI is a crucial tool for exploring brain structure changes, particularly white matter alterations, making it instrumental in understanding long-term plasticity and impairment mechanisms in perinatal stroke. The quickest and easier metric to access is Apparent Diffusion Coefficient (ADC), computed by comparing signal intensities from diffusion-weighted MRI scans at different b-values to quantify water diffusion in tissue. It is preferred for quick detection of diffusion abnormalities. Diffusion Tensor Imaging (DTI) is the most widely used dMRI technique, which models water diffusion in the brain with a tensor, providing metrics such as Fractional Anisotropy (FA) and mean diffusivity (MD). DTI is essential for studying the microstructural correlates of motor and language outcomes in children with perinatal stroke. Improved dMRI acquisition sequences and image processing methods have facilitated tractography, which reconstructs white matter fibers to study specific tracts or perform whole-brain/whole-hemisphere analyses.

### 2.2.2. Clinical Correlations with ADC and DTI Metrics

Few studies compared dMRI metrics, with clinical performances in newborns. One has shown a relationship between mean FA asymmetry in the optic radiation and bad visuospatial performance (visual field defects at 3 months for PAIS with Posterior Cerebral Artery lesion (Koenraads et al., 2016) . Another study correlates ADC signal hyperintensities at the level of the posterior limb of the internal capsule and the cerebral peduncles in

newborn infants with arterial ischaemic stroke is followed by Wallerian degeneration and subsequent development of CP (Vries et al., 2005)

Research on older patients (children to young adults after a perinatal stroke) has investigated the cortico-spinal tract FA and diffusivity in relation to motor impairments. One study (Hodge et al., 2017) showed poor motor outcomes were associated with lower fractional anisotropy in all segments and radial diffusivity correlated with both Assisting Hand Assessment and Melbourne Assessment in a twenty-eight children APPIS cohort (6-48 years of age).

Two studies stratified by arterial versus venous perinatal stroke, showing that diffusion properties of the lesioned CST were altered after perinatal stroke, lower FA and greater MD correlated with greater movement time in visually guided reaching task for arterial stroke. The Dorsal Column-Medial Lemniscus tract, have been examined for sensory functions like proprioception and kinesthesia (Kuczynski et al., 2017), showing a correlation with impaired diffusion properties, lower FA, higher Mean Diffusivity (MD), Radial Diffusivity (RD), and Axial Diffusivity (AD), with impairments in upper limb proprioception for both stroke type.

Research also includes reconstructing dorsal and ventral streams (Northam et al., 2018), showing a correlation between left dorsal path injury and selective speech repetition impairment for nonwords and sentences for children who kept their language representation in the left hemisphere, whereas right hemisphere dominance was correlated with minimal or absent repetition deficits.

One study relied on dorsal and stream diffusion-estimated volumes and showed that patients with left perinatal stroke showed larger lateralization indices of both structural and functional connectivity of the dorsal language pathway towards the right hemisphere that, in turn, were associated with better language outcomes (François et al., 2019).

### 2.2.3. Advanced dMRI Techniques: Fixel-Based Analysis and NODDI

Fixel-based analysis addresses DTI's limitations by distinguishing individual fiber populations within a voxel, enhancing the accuracy of modeling complex fiber architecture. Key metrics include Fiber Density (FD), Fiber Cross-section (FC), and a combined measure (FDC). Fixel-based analysis has shown promise in adult stroke (Cheng et al., 2021) and was tested on the AVCnn cohort, revealing limited but distant white matter alterations (Pretzel et al., 2022), confirming inter-hemispheric alterations. Best practices for fixel-based analysis include the computation of a cohort fixel template, which can be challenging with a lesioned brain.

Neurite Orientation Dispersion and Density Imaging (NODDI) goes beyond DTI, modeling brain microstructure at the level of neurites (dendrites and axons) (Zhang et al., 2012). NODDI provides metrics like the Orientation Dispersion Index (ODI) and Neurite Density Index (NDI), as estimates of neurite density and orientation dispersion. Recent studies on CST using NODDI suggest better sensitivity and predictive power for clinical outcomes (Nemanich et al., 2019) in a perinatal stroke cohort with cerebral palsy. NODDI's capacity to explore gray matter microstructure with the NDI metric remains a significant yet underexplored strength.

#### 2.2.4. Connectomics and Graph Theory in Perinatal Stroke

Connectomics, the study of brain connectivity, uses microstructural data from dMRI to map brain networks. Graph theory (Fornito et al., 2015), applied to these networks, uses nodes to represent brain regions and edges to represent connections, analyzing the topological properties with metrics like degree, centrality, and clustering coefficient.

Edge values in structural connectomics can be computed using various methods, such as averaging a metric along a tract (a bundle of streamlines between two regions), the number of streamlines between regions, the volume of estimated streamlines, and weighting the streamlines based on whole-brain connectivity. This approach has been used with Fixel Based Analysis (FBA) metrics to investigate structural connectivity in the AVCnn cohort to predict motor outcomes (Al Harrach et al., 2021). Significant symmetric disconnections in the lesional and contralesional hemispheres of patients were found mainly within and between S1 and M1 and thalamus, in both right and left lesion patients. Significant correlations (both positive and negative) were detected between the structural connectivity metric of diverse motor areas and manuality assessed by the Box and Block Test (BBT) scores in patients. Finally, the study illustrated a potential prediction of CP with contralesional preSMA connectivity with Corpus callosum or Thalamus, depending on lesion side.

Graph theory has shown potential in predicting outcomes for cerebral palsy (Ballester-Plané et al., 2017; Englander et al., 2013) and rehabilitation (Englander et al., 2015) in stroke studies, including results in perinatal stroke cohorts, particularly in the contralesional hemisphere (Craig et al., 2020, 2022), where metrics such as global efficiency, assortativity, hierarchical coefficient of regression, local efficiency, hierarchical and average neighborhood complexity in the contralesional hemisphere, as well as clustering coefficients of M1, S1, and SMA were correlated with clinical motor function.

However, these results must be treated with caution due to the wide age range in cohorts and the diversity of perinatal stroke types. The main weakness of graph theory lies in its inherent interpretability issues, as the estimated metrics do not correspond to direct anatomical features, and sometimes do not correlate consistently with clinical predictors.

#### 2.2.5. Future Directions and Challenges

Future tractography approaches may explore broader components of sensorimotor pathways or complex cognitive pathways, elucidating the functional contributions of ipsilateral, contralateral, and interhemispheric pathways in developmental plasticity. The complementarity of the presented methods provides powerful tools for exploring the intricate brain network and its implications for health and disease, particularly in perinatal and neonatal arterial ischemic stroke. The main limitations of these approaches are the difficult registration/normalization processes, impairing brain parcellation and the potential for these methods to study the ipsilesional hemisphere (Kirton et al., 2007). The main weakness of the current literature is the diversity of stroke types and the low number of subjects per cohort.

## 2.3. Resting state fMRI as a future window into the development and plasticity of brain circuits after an early stroke ?

### 2.3.1. Principles of Resting-State fMRI (RS-fMRI)

Low-frequency BOLD (blood-oxygen-level-dependent) fluctuations can be evaluated in the absence of specific tasks using Resting-State fMRI (RS-fMRI). During RS-fMRI, participants typically fixate on a cross and refrain from thinking to specific targets (mind wandering), while BOLD sensitive images are continuously acquired. The improbability of significant temporal co-variation of BOLD signals across multiple brain areas occurring purely by chance suggests that these areas are functionally connected. Thus, higher temporal correlations of the BOLD response are interpreted as indicative of greater functional connectivity.

A range of analysis methods is available for RS-fMRI. The most common approaches assume that brain networks remain stationary over the experimental time. Seed-based analyses utilize predefined Regions Of Interest (ROIs) based on anatomical or functional atlases to establish seeds for temporal cross-correlation measurements. Another frequently used method is Independent Component Analysis (ICA), a data-driven approach that segments significantly co-varying voxels into resting-state networks from multivariate BOLD signals, without relying on predefined ROIs or atlases. The potential of RS-fMRI depends on ongoing methodological advancements, particularly in achieving consistent spatial normalization.

### 2.3.2. Importance for Perinatal Stroke

RS-fMRI is particularly valuable for imaging patients with perinatal stroke for several reasons. Its task-free nature makes it accessible to individuals with cognitive or motor impairments allowing for a more inclusive assessment of brain dysfunction. Functional connectivity as observed through low-frequency BOLD fluctuations across different brain regions is crucial for understanding how brain areas interact and coordinate, especially in patients with altered brain organization due to early brain injury. It provides insights into the brain's intrinsic baseline activity and organization over time, thus revealing long-term adaptations and reorganizations, and the neural bases of interventions effectiveness. It is thus highly valuable for longitudinal studies, which are currently very scarce in perinatal stroke literature. As a non-invasive and repeatable technique, RS-fMRI is ideal for ongoing monitoring and research. Additionally, it can help identify compensatory neural networks that may have developed to support functions impacted by the stroke, providing insights into neuroplasticity and potential targets for rehabilitation.

Very few studies investigated PAIS with resting state : One study (François et al., 2019) illustrated an increased lateralization functional connectivity of the dorsal language pathway towards the right hemisphere in a group of 4 year old, left PAIS children. This correlated with structural connectivity and better outcomes. A recent study (Carlson et al., 2019) investigated a wide age-range APPIS (arterial and venous origin) functional connectivity by seeding bilateral inferior frontal and superior temporal gyri, and showed that lower functional connectivity correlates with language impairments. In another study on the same cohort (Saunders et al., 2019), a similar approach (primary motor area seeding) was used to show differences between APPIS and controls for both strength and laterality of

motor network connections. None of these observations could be related to motor outcome scores for either stroke group

Finally, an older study on the AVCnn cohort at 7 years of age (Dinomais et al., 2012) used the interleaved resting-state data from blocked fMRI designs to investigate the somatosensory network of patients, focusing on crossed-over connectivity between S1 (primary), S2 (secondary) somatosensory cortex with cerebellum, and showed relationship between sensory deficit and functional connectivity loss in ipsilesional S2, although those results disappeared after gray matter volume correction.

### 3. PhD Aim, challenge and hypothesis

#### 3.1. Overview of the AVCnnADO Project

The neuroimaging studies of my PhD work are part of the AVCnnADO project, which explores a unique longitudinal cohort, AVCnn, comprising 100 newborns with neonatal arterial ischemic stroke (NAIS). This cohort was established between 2003 and 2006 by Dr. Stéphane Chabrier at Saint-Étienne University Hospital from different hospitals throughout France. The children have been prospectively followed and assessed at ages 2 to 3 years, 7 years, and 16 years, through successive research programs conducted by the University Hospitals of Saint-Étienne, Angers, Necker (Paris), and NeuroSpin (CEA-Paris-Saclay). For more details, refer to the relevant section.

The 7-8 and 16-18 years time windows are critical periods in the life of a child/adolescent. The 7-8 years step is that of early primary school, when most elementary learnings are ongoing (writing, reading, calculation, grammar, ...), along with the emergence of higher-level functions required by academic demands (inhibition, attention, metacognition, ...). On the biological level, this period is characterized by an excess of synapses (synaptic redundancy) that supports the intense learning possibilities. This synaptic redundancy is indirectly reflected on brain imaging through gray matter growth.

Adolescence is the second pivotal period with major behavioral changes toward increased autonomy, strong increase in academic and pre-professional requirements, and important structural and functional brain changes sustaining elaborated oral and written language, executive and attention functions, visuo-spatial abilities, etc.... On the biological level, adolescence is characterized by intense selective synaptic pruning with decreasing plasticity but increasing specialization of selected circuits, along with increasing long range intra-hemispheric connectivity and a relative decrease of interhemispheric connectivity. Grey matter decreases due to synaptic pruning, whereas white matter volume increases mostly due to the myelination processes accompanying functional specialization.

The unique setting of this longitudinal study enables to sketch the developmental trajectory of each child at the individual level, accounting for various clinical (lesion characteristics, presence of Cerebral palsy, epilepsy ...) and environmental (Socioeconomic status rehabilitation programs ...) factors, and to assess possible changes related to puberty (pre-puberty at age 7-8, and post-puberty at age 16-18)

The AVCnnADO project specifically aims to investigate several aspects:

1. **Assessment of Clinical Motor and Cognitive Outcomes:** This objective focuses on evaluating the clinical motor and cognitive outcomes of adolescents, examining the evolution of cognitive impairments and abilities, including motor skills, oral and written language, visual, spatial, and executive functions between ages 7 and 16. The goal is to identify determinants of inter-subject variability in developmental trajectories and their impact on life outcomes (e.g., schooling and vocational training) and quality of life. It is hypothesized that children with more pronounced motor and language impairments at age 7 may experience a relative decrease in higher-level cognitive abilities over time, suggesting that intellectual efficiency may not remain stable despite a fixed lesion. Additionally, quality of life indices might be more influenced by factors such as fatigue and slowness rather than specific impairments.  
This clinical/behavior research part is being handled mostly by colleagues with appropriate backgrounds within the AVCnnADO project (language outcomes after NAIS : PhD project of L Drutel, Motor outcome : Pr M Dinomais, Angers University Hospital, Clinical and neuropsychological outcome at adolescence after NAIS : S Neumane, H Costa, M Chevignard, Quality of Life after NAIS: MD practice thesis of J Arnadottir, etc.).
2. **Study of Brain Plasticity:** This objective involves examining the plasticity of brain architecture using structural and functional connectivity imaging approaches in relation to behavioral and clinical variables (e.g., age, sex, and lesion characteristics). It aims to understand the impact of ongoing brain maturation on the (re)organization of motor, language, executive, and visuospatial networks, as well as the global functional architecture following an early stroke. It is proposed that more mature systems at the time of injury (e.g., motor) may demonstrate stability over time, while still-developing cognitive functions (e.g., executive, language) may show greater deviations from normal patterns in controls, correlating with behavioral variability.
3. **Characterization of the Crowding Effect:** This objective seeks to better characterize the crowding effect, which refers to the structural and functional links between language abilities and other cognitive functions. It aims to understand the neural correlates of the crowding effect, believed to be related to the competition within a constrained 'neural' space. Previous research has indicated that visuospatial abilities are often impaired in children with left brain lesions, potentially due to right hemisphere language reorganization rather than to lesion volume.

The AVCnnADO project has several notable strengths: the precise stroke subtype inclusion criteria, the uniqueness of the cohort with a 16-year prospective follow-up for a third of the subjects (32 over 100 neonates); the repeated combination of comprehensive neuropsychological evaluations and advanced MRI research at ages 7 and 16; the expertise of the research team in advanced imaging of neurodevelopmental phenotypes at NeuroSpin; and the specialization of the clinical consortium dedicated to pediatric stroke (National Reference Center for Stroke in Children).

### 3.2. Focus of My Thesis Work

My PhD work, as presented in this manuscript, primarily focuses on the imaging part of the project with 2 directions: to directly address certain research questions (e.g. Sex effects on brain growth after NAIS) and to generate imaging metrics that may assist other researchers within the project (e.g. language lateralization index for the study of language outcomes). Over the 3 years, my work has been divided into several phases:

1. **Data Acquisition:** Spread over the first two years, this phase involved my participation in patient and parent interactions, motor assessments (e.g., Box and Block test, 9-hole peg test), MRI training, assisting the radiographer with data acquisition, and ensuring imaging quality and subject compliance with the protocol.
2. **Development and Adaptation of dedicated Methodologies:** Conducted over the three years of the PhD work, this phase focused on benchmarking image processing methods and implementing strategies to overcome the specific difficulties caused by lesion effects in a longitudinal design. Ensuring exclusive study of non-injured tissue was also crucial for investigating diffuse lesion effects. This phase also included exploring longitudinal approaches.
3. **Data Analysis and Interpretation:** This phase involved designing specific statistical tests and methods to address the project's hypotheses. The overall goal was to extract imaging biomarkers at both individual and group levels, and longitudinally when possible. Methodological issues related to spatial normalization of lesioned brains, reconstruction of lesioned bundles, and longitudinal assessment addressed in the previous phase were detrimental for this phase.

In relation to Clinical, cognitive, motor, and language data, we aimed to combine the different MRI modalities to investigate the complex sequence of anatomical, microstructural and functional development and plasticity of the immature brain after early stroke:

1. **Anatomical MRI:** Brain growth, lesion volume and location, sex differences, etc.
2. **Diffusion MRI:** Overall white matter microstructure integrity and structural connectivity, using a range of methodological approaches
3. **Activation Functional MRI:** Reorganization of motor and language networks, and the spatial competition between these functions and later-developed ones (e.g., mathematical calculation).
4. **Resting-State fMRI:** Changes in the brain architecture of cognitive networks.

### 3.3. Structure of the Manuscript

We will first detail the clinical and MRI acquisition data of the cohort, as well as the constitution of the control group. We will also outline the numerous methodological considerations surrounding acquisition, initial preprocessing, and the various approaches employed.

In chapter 2, we present the results of the multifactorial morphometric analysis of the cohort, considering factors such as age, sex, patient vs. control differences, hemisphere

side, and lesion severity, and adapted for longitudinal studies. We will discuss the consistent sex differences we found and methodological aspects in more detail. The complete reference of the article is:

Postic, P. Y., Leprince, Y., Brosset, S., Drutel, L., Peyric, E., Ben Abdallah, I., Bekha, D., Neumane, S., Duchesnay, E., Dinomais, M., Chevignard, M., Hertz-Pannier, L. (2024). Brain growth until adolescence after a neonatal focal injury: sex related differences beyond lesion effect. *Frontiers in Neuroscience*, 18, 1405381.

Chapter 3 will introduce our initial results on the exploration of structural and functional connectivity of the contralesional hemisphere to better characterize language reorganization and its impact on other functions and network development. Our preliminary results appear to challenge the crowding effect hypothesis and support the notion that right hemisphere specialization in the case of a left lesion benefits patients and mirrors a typical language network.

## 4. The AVCnn Cohort

### 4.1. Cohort constitution, assessment and imaging milestones

The AVCnn cohort is a unique global sample of 100 newborns diagnosed with neonatal arterial ischemic stroke (NAIS), established between 2003 and 2006 by Dr. Stéphane Chabrier at Saint-Étienne University Hospital, in collaboration with 39 French hospitals. NAIS (AVCnn) is characterized by ischemic stroke syndrome occurring in the neonatal period, typically presenting with focal seizures within the first days of life, and confirmed by brain MRI with diffusion sequences during the acute phase. Since then, the children have been prospectively followed and assessed at ages 2 to 3 years, 7 years, and 16 years, through successive research programs involving clinical and imaging investigations conducted by University Hospitals of Saint-Étienne (for neonates), Angers, Necker (Paris) and NeuroSpin at age 7, and by NeuroSpin (CEA Paris-Saclay and Inserm U1141 NeuroDiderot) at age 16 (PI : L Hertz-Pannier, sponsor: CEA). The research protocols at ages 7 and 16 were designed specifically for longitudinal analyses of both clinical and neuroimaging data. Clinically, assessments included detailed motor evaluations (handedness, Box and Block test, 9-hole peg test, with standardized scoring for cerebral palsy), and comprehensive oral and written language testing at both ages (N-EEL battery and Alouette at age 7; CELF-5, ECLA 16+, Chronodictées, Alouette, and pragmatics at age 16). Neuropsychological assessments utilized the Wechsler Intelligence Scales (WISC-IV at age 7 and WAIS at age 16), supplemented by evaluations of visuospatial abilities (DTVP-A) and executive functions (Stroop Test, Tower of London, Trail Making Test, BRIEF questionnaires). Quality of life and fatigue questionnaires were also administered at age 16 to evaluate the impact of disabilities on daily life.

#### 4.1.1. Clinical characterization of the cohort at 7 years of age

At age 7, all children in the cohort were able to walk independently (Chabrier et al., 2016), though approximately one-third exhibited varying degrees of hemiplegia. Nearly half of the children showed no specific impairment by age 7, while others presented with comorbidities including cerebral palsy (32%), epilepsy (11%), language impairment (49%), and rarely global intellectual disability (8%). These comorbidities had significant effects on

daily life and schooling (Chabrier et al., 2016; Darteyre et al., 2014). Language impairments were subtle but significant, with notable language plasticity sustained by homotopic network reorganization in the right hemisphere in cases of left lesions. For a comprehensive characterization of the cohort, refer to (Chabrier et al., 2016).

#### 4.1.2. Clinical characterization of the cohort at 16 years of age

Here, we provide a brief summary of the cohort characteristics. The full cohort description will be detailed in a subsequent publication.

The 16y cohort consists of 33 subjects who underwent both imaging and clinical assessments (13 females and 20 males). Socioeconomic status was assessed using the Hollingshead score computed by Emeline Peyric and Laure Drutel (independently and then through consensus), who also conducted the neuropsychological and language assessments. Motor assessments, including BFMF (Bimanual Fine Motor Function), GMFCS (Gross Motor Function Classification System), MACS (Manual Ability Classification System) scores, and cerebral palsy diagnosis, were performed by Lucie Hertz-Pannier.

	General Informations				Motor Outcomes				
	Number of subject	MCA territory lesion	SES (M/SD)	Atypical schooling (N/%)	Cerebral Palsy (N/%)	BFMF >1 (N/%)	BFMF >2 (N/%)	GMFCS >1 (N/%)	MACS >1 (N/%)
<b>Male</b>	20	70%	41.4 /14.6	3 (15)	7 (35)	5 (25)	2 (10)	1 (5)	45
<b>Female</b>	13	92%	38.9/ 13.8	1 (7.7)	3 (23)	4 (30.7)	0	7.7	15.4

**Table 1: General Informations and motor outcomes of the AVCnnADO cohort at 16 years of age**  
MCA : Middle Cerebral Artery, SES : Socioeconomic Status (Hollingshead methods), BFMF :Bimanual Fine Motor Function , GMFCS : Gross Motor Function Classification System, MACS : Manual Ability Classification System

Very few patients have followed an atypical educational path (in the institutional sense, encompasses all settings except for medical-social establishments). Overall, scores on language and neuropsychological assessments tend to be lower than the mean but staying in the normal range (with a normative score of 100 and a standard deviation of 15). Executive functions show slight deviations (BRIEF scores having a normative value of 50 and a standard deviation of 10); higher scores indicate greater difficulties.

	Epilepsy	Language scores (M/SD)				Executive functions (M/SD)		
	Active at 16yo	CELF Structure	CELF Content	CELF Expressive	CELF Receptive	BRIEF GEC	BRIEF BRI	BRIEF MI
<b>Male</b>	4(20%)	85.6 /19.30	85.55 /19.5	83.35 /18.76	88.45 /20	58.6 /13.85	59.25 /18.39	57.65 /12.85
<b>Female</b>	1(7.7%)	84 /23.15	85.07 /23.33	82.7 /24.13	85.92 /22.22	61.23 /13.32	58.62 /13.87	62.23 /15.28

**Table 2: Epilepsy, Language outcomes and executive functions of the AVCnnADO cohort at 16 years of age**

CELLF: Clinical Evaluation of Language Fundamentals, Receptive Language Index: Measures understanding of spoken language. Expressive Language Index: Measures ability to express ideas verbally. Language Content Index: Assesses knowledge of words and content. Language Structure Index: Evaluates understanding and use of grammatical rules. BRIEF : Behavior Rating Inventory of Executive Function, BRI : Behavior Regulation Index, MI : Metacognition Index, GEC : Global Executive Composite index

	WAIS (Wechsler Intelligence)			
	VCI (M/SD)	PRI (M/SD)	WMI (M/SD)	PSI (M/SD)
<b>Male</b>	90.5 /20.65	89.1 /17.41	89.65 /17.77	87.25 /17.34
<b>Female</b>	93.69 /14.96	91.85 /14.50	90.85 /13.86	95.62 /16.13

**Table 3: Cognitive and Neuropsychology assessment of the AVCnnADO cohort at 16 years of age**  
 WAIS : Wechsler Adult Intelligence Scale, VCI : Verbal Comprehension Index : Measures verbal reasoning and comprehension. PRI : Perceptual Reasoning Index, Assesses non-verbal and fluid reasoning, WMI : Working Memory Index, Evaluates short-term memory and attention, PSI : Processing Speed Index, Measures the speed of mental processing

#### 4.1.3. Control Cohorts at both ages

To understand deviations from typical development, control groups were studied at both ages (N = 37 19F/18M) at age 7, and N = 32, 16F/15M, at age 16), with some subjects assessed at both ages. These control subjects underwent the same imaging protocols as the AVCnn cohort, but with simplified clinical evaluations, lacking formal language and neuropsychological assessments while still including motor assessments.

## 4.2. Imaging protocol

### 4.2.1. 7 years of age session

The imaging system used for the 7 years of age was a Siemens MAGNETOM Trio Tim system, with a 12-channel head coil. Anatomic MRI images include T1-weighted MPRAGE (Magnetisation Prepared Rapid Gradient Echo) images (TR= 2300 ms, TE= 4.18 ms, TI = 900 ms, voxel size 1 × 1 × 1 mm<sup>3</sup>, 176 slices), T2 Flair images (TR= 5000 msec, TE= 395msec, voxel size 0.9 × 0.9 × 1 mm<sup>3</sup>, 160 slices).

Functional MRI tasks were performed using an Echo Planar Imaging (EPI) sequence without partial Fourier or GRAPPA (Generalized Autocalibrating Partially Parallel Acquisitions). These included:

- Finger tapping task for both hands, according to children capabilities, with 3 mm isotropic voxels, 40 slices, TR = 2500 ms, TE = 30 ms.
- Sentence generation task, similar to the one performed at 16 years of age, with 3 mm isotropic voxels, 40 slices, TR = 5000 ms, TE = 30 ms
- Resting-state functional imaging, 3 sequences with 3 mm isotropic voxels, 40 slices, TR = 2400 ms, TE = 30 ms.

Diffusion-weighted Spin Echo (SE)-EPI images were acquired using a single shot sequence with 30 diffusion encoding directions and a diffusion-weighting of b = 1,000 s/mm<sup>2</sup>

(TR = 9500 ms, TE = 86 ms, 40 slices, voxel size =  $1.875 \times 1.875 \times 3$  mm), GRAPPA = 2, Partial Fourier = 6/8.

Patients were filmed and recording during acquisition

#### 4.2.2. 16 years of age session

The imaging system used for the 16 years of age was a Siemens MAGNETOM Prisma fit system, with a 64 channel head coil. Anatomic MRI images include T1-weighted MPRAGE images (TR = 2300 ms, TE = 3.05ms, TI = 248 ms, voxel size=  $0.9 \times 0.9 \times 0.9$  mm<sup>3</sup>, 176 slices), T2 Flair images (TR = 5000 ms, TE = 396 ms, voxel size=  $0.9 \times 0.9 \times 0.9$  mm<sup>3</sup>, 176 slices).

Functional MRI tasks were acquired using a consistent sequence for all activation paradigm (sentence generation task, SGT, 1 run; localizer, 2 run) and all 3 resting-state run : 2 mm isotropic voxels size, 69 slices, a Repetition Time (TR) of 1.81 seconds, an Echo Time (TE) of 30.4 milliseconds, with 3 simultaneous multislice acquisitions and a partial Fourier factor of 7/8.

Diffusion-weighted SE-EPI images included two acquisitions,  $b=1,000$  s/mm<sup>2</sup>, 30 diffusion encoding directions, and  $b=1,500$  s/mm<sup>2</sup>, 60 diffusion encoding directions. Each acquisition was preceded by a reverse phase encoded  $b_0$  images. Other acquisition parameters were the same for both images, 78 slices, TR = 4,12 seconds, TE = 55 milliseconds, and a voxel resolution of  $1.8 \times 1.8 \times 1.8$  mm.

## 5. Specific methodological considerations to the AVCnnADO image processing

### 5.1. Image acquisition considerations

When working with a cohort of adolescents with NAIS, specific considerations must be addressed compared to typical subject cohorts:

- Motor Impairments: Some patients had motor impairments ranging up to cerebral palsy. These impairments could lead to discomfort, spasticity, or involuntary movements during MRI scanning. This also may impair the patient's capacity to follow motor based fMRI tasks.
- Cognitive Impairments: Some patients with cognitive impairments struggled with reading tasks at a high pace, became tired more rapidly, and had difficulty executing more challenging tasks, such as calculation tasks.

To optimize subject compliance in the scanner, each participant underwent specific training before the imaging session. They viewed a video describing the stimuli they would encounter during the scan and were asked to respond orally to ensure they understood the task and could respond promptly. This training procedure was documented consistently for each subject.

During MRI acquisition, considerable attention was given to subject comfort to prevent spasticity and involuntary movements, which can affect image quality. Subjects were allowed to move their hands and feet between image acquisitions and had to confirm their comfort verbally between sequences. Operators reminded participants of the tasks to be performed in the upcoming sequence. If unable to press buttons for the motor task, the participant was asked to clench fist instead.

Imaging sequences alternated between anatomical, diffusion, activation fMRI, and resting-state fMRI. Task instructions changed between sequences (such as watching a movie, “thinking of nothing”, or performing an active task) to prevent drowsiness and minimize fatigue. The MRI operator systematically checked for movement, and if excessive movement was detected, the sequence was repeated later in the imaging protocol.

## 5.2. Specificity of imaging a lesioned brain

The presence of a lesion, which creates a "hole" in the brain, poses several challenges from an imaging perspective:

- Morphological Landmarks: The absence of brain tissue can disrupt the identification of morphological landmarks used for brain parcellation, particularly in the ipsilesional hemisphere.
- Registration Processes: The lack of brain tissue often perturbs registration processes, both within groups and relative to templates, which are essential for most image processing pipelines.
- Lesion Variability: Differences in lesion size and location create comparability issues, necessitating either comparisons only in regions common to all subjects or managing missing data.

Imaging sessions were conducted on 2 different scanners at ages 7 and 16. Multiple scanners is a significant source of systematic bias in neuroimaging studies (Fortin et al., 2018), potentially leading to significant differences in volume estimates. This bias results not only from the machine and acquisition parameters (e.g., TR, TE, Signal-to-Noise Ratio/SNR, resolution) but also from coils, and machine reconstruction softwares.

To correct this bias, specialized corrections can be used for morphometry analysis. However, such corrections are not available for all MRI modalities. Moreover, the brain lesion posed issues with regard to scanner bias correction software hypothesis, we chose not to use these tools, to avoid artificially biasing our analysis. In the study design, controls and patients were imaged on the same scanner at each age to enable direct comparisons by age. When using both age data in our analysis, we adapted our model and our comparison to account for scanner bias to the best of our capacity.

## 5.3. Data processing

All images were exported following Brain Imaging Data Structure (BIDS) format specifications (Gorgolewski et al., 2016) to ensure anonymization, consistent naming conventions, and formatting. Data quality was systematically checked, combining manual and automated methods. Selected automated quality metrics were benchmarked against

literature standards, and manual quality control was enhanced by generating automated screenshots to expedite the process.

A significant challenge in analyzing lesioned brains is the registration process, which is crucial for brain parcellation or voxel-wise analysis across patients. Extensive efforts were made before and during the PhD to reliably register patient brains, either longitudinally within subjects for specific processes like brain growth or on a template for group analyses. Whenever possible, native space analysis was preferred.

Preliminary work included creating individual lesion masks validated by trained practitioners, generating precise brain masks using HD-BET (Isensee et al., 2019), and developing reliable registration matrices within subjects (between 7 and 16 years of age T1 images) and to symmetric and asymmetric MNI spaces. Consistent white and gray matter segmentation was achieved using a tailored CAT12 (Gaser et al., 2022) implementation. These carefully processed images were critical for the overall quality of MRI modality processing and the reliability of computed metrics, supported by our extensive quality control approach (refer to Chapter 2, for an overview of methodological considerations).

# Chapter 2 : Longitudinal Analysis of Brain Morphometry After Neonatal Stroke, Sex Differences and Developmental Changes

## 1. Introduction

The study of brain morphometry has been a cornerstone of my PhD project, offering methodological challenges to get new clinical insights into brain development after early focal injuries.

### 1.1. Clinical Relevance and rationale

Clinically, morphometric analysis is instrumental in exploring brain growth in patients with neurodevelopmental disorders. Morphometric metrics, such as gray and white matter volumes, serve as valuable proxies for understanding underlying microstructural changes (Lorio et al., 2016), (Frangou et al., 2022; Lebel & Deoni, 2018). Depending on clinical and developmental factors, these morphometric changes can correlate with functional and cognitive performances, (Shaw et al., 2006; Statsenko et al., 2022) especially in typical development and aging. Anatomic-functional inferences should be carefully addressed, and account for the intertwined nature of developmental factors and structural differences in the brain (DeCasien et al., 2022; Wierenga et al., 2014) : Brain anatomy alone is not sufficient to draw microstructural or clinical conclusions. Nevertheless, these insights are of great use to guide further hypotheses and pave the way for more targeted investigations into the long-term impacts of early brain lesions.

The investigation of brain morphometry throughout life, especially during childhood, has been the subject of extensive research. Contemporary data-driven approaches, such as normative analyses on large datasets of typical children, start to provide a comprehensive understanding of typical brain development. For example, gray matter volume is known to increase during early childhood, peak between the ages of 6 and 12 (depending on the brain region), and then decrease, a process that reflects synaptic proliferation and pruning. Conversely, white matter volume typically increases with age, corresponding to the ongoing myelination of axons. These developmental processes are neither linear nor spatially uniform. Sex differences further complicate this landscape, as both brain volumes and the timing of developmental peaks vary between males and females and across brain regions. Although the literature on this topic is not entirely consistent, we considered latest normative analyses, relying on numerous datasets and coherent sites and developmental covariate modeling as a gold standard on the matter (Bethlehem et al., 2022; Frangou et al., 2022; Rutherford et al., 2022; Wierenga et al., 2014).

Morphometric analysis typically encompasses various metrics including brain volume, cortical thickness, gyrification, and pial surface area. However, in the study presented here, we primarily focused on volume and cortical thickness, as these measures were most relevant to our research objectives.

## 1.2. Study Objectives and Hypotheses

This research project aimed at uncovering prognostic determinants of long-term outcomes in NAIS, particularly concerning the effects of sex and puberty on brain development. Given the male predominance in NAIS cases (with males comprising approximately two-thirds of patients) and the established vulnerability of males to other early developmental impairments, we aimed to determine whether significant differences existed between male and female brain volumes. Additionally, we sought to explore whether puberty influenced the divergence in developmental trajectories between patients and controls. However, variability between patients despite a uniquely homogeneous cohort (prospective design, strict criteria for NAIS, no age variability...) necessitated the inclusion of lesion side, size, and typical sex differences as covariates in our analysis.

## 1.3. Results overview and comments

In the following section of this chapter, we present our published results (Postic et al., 2024) of the longitudinal morphometric analysis of the AVCnn cohort. These results are part of a two-year process in which we investigated morphometric prognostic determinants after NAIS in a number of ways, some of which will be further detailed in the additional discussion section of this chapter, following the article. This analysis was meticulously designed to account for variables such as age, sex, patient-control differences, hemisphere side, and lesion severity.

Our study reveals significant differences between males and females in the anatomical development of the brain, particularly in the contralesional hemisphere, following dysconnectivity caused by a focal neonatal brain lesion. Lesion severity predominantly affects cortical gray matter and thalamic volumes in the ipsilesional hemisphere, while sex differences are more pronounced in the contralesional hemisphere. Notably, males exhibit significant deviations in growth patterns compared to females, and these differences persist from childhood through adolescence. The consistent effect size observed at both 7 and 16 years of age suggests that these differences primarily emerged before the age of 7 and were only minimally influenced by physiological development and changes in sex steroid exposure during puberty. This indicates that sex may play a crucial role in early post-injury plasticity and early compensatory mechanisms, and that puberty has minimal impact on these developmental trajectories.

Several hypotheses could account for these sex-related differences. One possibility involves hormonal influences arising from sex-specific differences in prenatal and early postnatal exposure to gonadal hormones, mediated by the activation of the hypothalamus-pituitary-gonadal axis. This process results in a transient "minipuberty" (Becker & Hesse, 2020) in both sexes, which may impact multiple neurobiological processes, including the neuroinflammatory response to brain injury. Another hypothesis focuses on differences in brain structure maturation at birth between males and females. Biological processes such as increased vulnerability to oxidative stress, modulation of cell death pathways, regulation of microglial activation, and differential exposure to gonadal hormones throughout developmental stages have been proposed as contributing factors (Charriaut-Marlangue et al., 2017). Recent studies further highlight that microglial cells exhibit sexual dimorphism, which influences both sexual differentiation and the immune

response to brain lesions (VanRyzin et al., 2020). A more detailed summary of literature on the matter is given in the discussion part of the article.

At this time however, univariate explorations using various neuropsychological and language assessments, conducted by neuropsychologists and speech therapists as part of the AVCnnADO protocol, did not show clear sex-related differences. We propose that the contralesional volume differences may be due to a sex-dependent expression of microstructural recovery mechanisms, rather than a male developmental disadvantage. This adds nuance to the hypothesis of heightened male vulnerability during the perinatal period with limited compensatory mechanisms later in life, suggesting that the vulnerability is more associated with the NAIS prevalence ratio, and perinatal response to the ischemic stroke than with developmental outcomes.

#### 1.4. Methodological Framework

On the methodological front, both the development and the application of our image processing pipeline were critical for achieving accurate and unbiased results in this morphometric analysis. The meticulous handling of image registration and segmentation processes at the individual level ensured the precision of registration matrices, which are also essential for subsequent fMRI and dMRI investigations. Moreover, this phase provided an opportunity to address challenges inherent to longitudinal analyses, particularly in the presence of imaging bias (scanner change between the 2 sessions at 7 and 16 years of age). Our work spanned the entire process, from quality control to the extraction and analysis of morphometric metrics, ensuring robust and reliable outcomes.

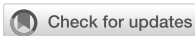
The article is completed by additional methodological discussions (Paragraph 3). We also detail a supplementary statistical analysis to address concerns on our way of accounting for brain size variability and sex related typical brain size differences underlined by one of our reviewers.

## 2. Article, Supplementary Materials

Postic, P. Y., Leprince, Y., Brosset, S., Drutel, L., Peyric, E., Ben Abdallah, I., Bekha, D., Neumane, S., Duchesnay, E., Dinomais, M., Chevignard, M., Hertz-Pannier, L. (2024).

Brain growth until adolescence after a neonatal focal injury: sex related differences beyond lesion effect.

Frontiers in Neuroscience, 18, 1405381.



## OPEN ACCESS

## EDITED BY

Daniela Tropea,  
Trinity College Dublin, Ireland

## REVIEWED BY

Jose Guerrero-Gonzalez,  
University of Wisconsin-Madison,  
United States  
Arun Bokde,  
Trinity College Dublin, Ireland

## \*CORRESPONDENCE

Pierre-Yves Postic  
✉ py.postic@gmail.com

RECEIVED 22 March 2024

ACCEPTED 26 July 2024

PUBLISHED 23 August 2024

## CITATION

Postic P-Y, Leprince Y, Brosset S, Drutel L, Peyric E, Ben Abdallah I, Bekha D, Neumane S, Duchesnay E, Dinomais M, Chevignard M and Hertz-Pannier L (2024) Brain growth until adolescence after a neonatal focal injury: sex related differences beyond lesion effect. *Front. Neurosci.* 18:1405381. doi: 10.3389/fnins.2024.1405381

## COPYRIGHT

© 2024 Postic, Leprince, Brosset, Drutel, Peyric, Ben Abdallah, Bekha, Neumane, Duchesnay, Dinomais, Chevignard and Hertz-Pannier. This is an open-access article distributed under the terms of the [Creative Commons Attribution License \(CC BY\)](https://creativecommons.org/licenses/by/4.0/). The use, distribution or reproduction in other forums is permitted, provided the original author(s) and the copyright owner(s) are credited and that the original publication in this journal is cited, in accordance with accepted academic practice. No use, distribution or reproduction is permitted which does not comply with these terms.

# Brain growth until adolescence after a neonatal focal injury: sex related differences beyond lesion effect

Pierre-Yves Postic <sup>1,2,3\*</sup>, Yann Leprince <sup>1</sup>, Soraya Brosset <sup>1,2</sup>, Laure Drutel<sup>4,5</sup>, Emeline Peyric<sup>6</sup>, Ines Ben Abdallah <sup>1,2</sup>, Dhaif Bekha<sup>1,2</sup>, Sara Neumane <sup>1,2,7</sup>, Edouard Duchesnay <sup>8</sup>, Mickael Dinomais <sup>9</sup>, Mathilde Chevignard <sup>3,10,11</sup> and Lucie Hertz-Pannier <sup>1,2</sup>

<sup>1</sup>CEA Paris-Saclay, Frederic Joliot Institute, NeuroSpin, UNIACT, Gif-sur-Yvette, France, <sup>2</sup>INSERM, Université Paris Cité, UMR 1141 NeuroDiderot, InDEV, Paris, France, <sup>3</sup>Sorbonne Université, CNRS, INSERM, Laboratoire d'Imagerie Biomédicale (LIB), Paris, France, <sup>4</sup>LP3C, Rennes 2 University, Rennes, France, <sup>5</sup>French National Reference Center for Pediatric Stroke, CHU de Saint-Etienne, Saint-Etienne, France, <sup>6</sup>Pediatric Neurology Department, HFME, Hospices Civils de Lyon, Lyon, France, <sup>7</sup>Université Paris-Saclay, UVSQ – APHP, Pediatric Physical Medicine and Rehabilitation Department, Raymond Poincaré University Hospital, Garches, France, <sup>8</sup>CEA Paris-Saclay, Frederic Joliot Institute, NeuroSpin, BAOBAB/GAIA/SIGNATURE, Gif-sur-Yvette, France, <sup>9</sup>Department of Physical Medicine and Rehabilitation, Angers University Hospital Centre, Angers, France, <sup>10</sup>Rehabilitation Department for Children with Acquired Brain Injury, Saint Maurice Hospitals, Saint Maurice, France, <sup>11</sup>Sorbonne University, GRC 24 Handicap Moteur Cognitif et Réadaptation (HaMCRE), Paris, France

**Introduction:** Early focal brain injuries lead to long-term disabilities with frequent cognitive impairments, suggesting global dysfunction beyond the lesion. While plasticity of the immature brain promotes better learning, outcome variability across individuals is multifactorial. Males are more vulnerable to early injuries and neurodevelopmental disorders than females, but long-term sex differences in brain growth after an early focal lesion have not been described yet. With this MRI longitudinal morphometry study of brain development after a Neonatal Arterial Ischemic Stroke (NAIS), we searched for differences between males and females in the trajectories of ipsi- and contralesional gray matter growth in childhood and adolescence, while accounting for lesion characteristics.

**Methods:** We relied on a longitudinal cohort (AVCnn) of patients with unilateral NAIS who underwent clinical and MRI assessments at ages 7 and 16 were compared to age-matched controls. Non-lesioned volumes of gray matter (hemispheres, lobes, regions, deep structures, cerebellum) were extracted from segmented T1 MRI images at 7 (Patients: 23 M, 16 F; Controls: 17 M, 18 F) and 16 (Patients: 18 M, 11 F; Controls: 16 M, 15 F). These volumes were analyzed using a Linear Mixed Model accounting for age, sex, and lesion characteristics.

**Results:** Whole hemisphere volumes were reduced at both ages in patients compared to controls (gray matter volume: –16% in males, –10% in females). In ipsilesional hemisphere, cortical gray matter and thalamic volume losses (average –13%) mostly depended on lesion severity, suggesting diaschisis, with minimal effect of patient sex. In the contralesional hemisphere however, we consistently found sex differences in gray matter volumes, as only male volumes were smaller than in male controls (average –7.5%), mostly in territories mirroring the contralateral lesion. Females did not significantly deviate from the typical trajectories of female controls. Similar sex differences were found in both cerebellar hemispheres.

**Discussion:** These results suggest sex-dependent growth trajectories after an early brain lesion with a contralesional growth deficit in males only. The similarity of patterns at ages 7 and 16 suggests that puberty has little

effect on these trajectories, and that most of the deviation in males occurs in early childhood, in line with the well-described perinatal vulnerability of the male brain, and with no compensation thereafter.

#### KEYWORDS

brain morphometry, brain growth trajectories, early brain injury, sex effect, multifactorial comparative analysis, male perinatal brain vulnerability

## 1 Introduction

Plasticity stands as an intrinsic property of the central nervous system, reflecting its inherent capability to dynamically respond to the environment and experiences. In the developing brain, the high level of plasticity is generally considered beneficial, but the specific advantages it confers in situations of early brain lesions remain unclear. Patients with early onset focal lesion tend to better recover impaired function at a cost of a broader impairment, suggesting dysconnectivity beyond the lesioned territory, with expected deviations in global and regional brain growth. The influence of clinical factors such as lesion characteristics and epilepsy have been explored (Sullivan et al., 2023), but other factors such as sex, environmental conditions, and intervention/rehabilitation further contribute to the complexity of understanding neural plasticity (Anderson et al., 2014). In particular, the exquisite vulnerability of male brains in the perinatal and early childhood period has been long suspected, considering the sex ratio of a number of early-onset neurodevelopmental disorders such as autism spectrum disorders (ASD) (Halladay et al., 2015), attention-deficit hyperactivity disorder (ADHD) (Ramtekkar et al., 2010), obsessive compulsive disorder (OCD) (Mathes et al., 2019). Several studies also reported a male bias in prevalence of cerebral palsy with a male/female ratio of 1.4/1 (Stanley et al., 2000; Smithers-Sheedy et al., 2014). However, long term sex-related differences in clinical outcome remain debated (Romeo et al., 2011, 2023)

Neonatal arterial ischemic stroke (NAIS) (Fluss et al., 2019; Giraud et al., 2023) is a valuable model for examining brain plasticity after an early brain lesion. Although most NAIS are considered to be idiopathic, several studies describe potential risk factors (Li et al., 2017). Notably, males are disproportionately affected by NAIS (2/3 of the NAIS population) (Dunbar and Kirton, 2018; Dunbar et al., 2020), suggesting a sex-related risk factor. Though children with NAIS form a highly homogeneous population with regard to lesion onset and localization [Middle Cerebral Artery (MCA) territory in 85% of cases, in the left hemisphere in 2/3 of cases] (Kirton and deVeber, 2013), they

exhibit a broad spectrum of long term outcome (Chabrier et al., 2011; Dunbar and Kirton, 2018).

Morphometric analyses, focusing on brain growth as a first approximation of early brain plasticity through volumes changes, have been conducted on subjects after perinatal stroke (Dunbar and Kirton, 2019). A recent study demonstrated generalized lower cortical gray matter volume, thickness, and a few gyrification differences in the contralesional hemisphere compared to an age-corrected control group (Shinde et al., 2023). Other studies have highlighted lower white matter volumes along fibers connected to the lesion (Moses, 2000; Stiles et al., 2003), bilateral thalamus volume alterations (Craig et al., 2019a), bilateral basal ganglia atrophy (Hassett et al., 2022), crossed cerebellar atrophy (Craig et al., 2019b). Bilateral thalamus and basal ganglia atrophy correlated with epilepsy risks (Vaher et al., 2023), as well ipsilesional atrophy correlated with poorer hand functions (Ilves et al., 2022) and bilateral hippocampal atrophy correlated with memory impairment (Gold and Trauner, 2014). To our knowledge, only a few studies delved into the brain morphometry of NAIS specifically. One showed volume alteration in cortico-spinal tract in centrum semiovale white matter, and proposed it as a marker of cerebral palsy (Dinomais et al., 2015). Another correlated poorer contralateral hand function with smaller volumes in ipsilesional mediodorsal thalamus, ipsilesional corticospinal tract (superior corona radiata), posterior limb of the internal capsule, the cerebral peduncle and the ipsilesional body of corpus callosum (Dinomais et al., 2016). The last explored thickness, volume, and gyrification alterations in both hemisphere (Al Harrach et al., 2019). It identified localized modifications in cortical areas distant from the primary lesion within the ipsilesional hemisphere, as well as in the contralesional hemisphere, emphasizing subtle differences in patterns between right and left-lesioned patients. In these studies, sex-related differences were not specifically investigated, as in most analyses, sex was introduced as a co-variable in the models, that also accounted for a fairly large variability in ages and clinical factors (age at lesion occurrence, side and extent of the lesion, epilepsy, cerebral palsy, etc...). Most of the previously cited studies rely on cohort with small cohorts with wide age range and different lesion territories and origins.

The goal of the present study was to investigate the contribution influence of sex among the main demographic and clinical co-variables on the longitudinal term global and regional brain growth after a unilateral NAIS, taking advantage of the exceptional resources of our prospective longitudinal French AVCnn cohort (Dinomais et al., 2015; Chabrier et al., 2016), and using i. Very strict inclusion criteria based on the combination of clinical and imaging data (only unilateral NAIS). ii. A long term follow up with a complete clinical and MRI research protocol at 2 key childhood

Abbreviations: ASD, autism spectrum disorder; WM, white matter; GM, gray matter; NAIS, neonatal arterial ischemic stroke; 7yo, acquisition session at 7 years of age; 16 yo Acquisition session at 16 years of age; M, male; F, female; MCA, middle cerebral artery; ACA, anterior cerebral artery; PCA, posterior cerebral artery; SES, socio-economic status; CP, cerebral palsy; GMFCS, gross motor function classification system; BFMF, bimanual fine motor function; DK40, Desikan-Killiany atlas; ROI, Region-of-Interest, LMM, Linear Mixed Model; FDR, false discovery rate.

ages: around 7 year old (7 yo, beginning of elementary school) and 16 year old (16 yo, before professional orientation); iii. A study design enabling a systematic and consistent longitudinal assessment (i.e., comparability between ages of clinical and behavioral tests, monocentric 3T MR evaluation with imaging parameters matched at both ages and an image analysis pipeline dedicated to longitudinal comparisons). By measuring hemispheric [cortical gray matter (GM) and white matter (WM)] volumes, as well as regional cortical and sub-cortical GM volumes, we aimed to assess: (1) the brain growth trajectories of the patients between 7 and 16 years of age, in both sexes, compared to the control groups; (2) the impact of the studied variables on growth patterns; and (3) the differences in patients volumes according to sex and age (pre-pubertal period and puberty effect). We expected global and focal growth deficits in patients, mostly in ipsilesional areas, but also within the contralesional hemisphere, more pronounced in males compared to females, and possibly evolving between 7 and 16 years of age due to puberty.

## 2 Material and methods

### 2.1 Participants

#### 2.1.1 Patients

Patients were part of the AVCnn cohort (Accident Vasculaire Cérébral du nouveau-né) (PHRC régional n80308052, and PHRC interrégional n81008026—eudract number 2010-A00329-30) (Chabrier et al., 2016). Initially, the cohort comprised 100 term neonates with a NAIS, confirmed by imaging in the acute phase. These infants were consecutively enrolled between November 2003 and October 2006 from 39 neonatology and neuropediatric units throughout mainland France.

At the age of 7–8 years (2010–2013), a research protocol involving neuropsychological and MRI investigations was proposed to the 80 children still in active file (7yo session). The clinical description of the 7-year-old cohort ( $n = 73$ ) has been published in Chabrier et al. (2016). In summary, males represented two-thirds of the patients, lesions were located in the left hemisphere in two-thirds of cases, and 85% involved the MCA territory. Of these, 52 [35 males (M), 17 females (F)] adhered to the imaging protocol.

Subsequently, at the age of 16–18 years, all AVCnn patients still in active file ( $n = 50$ ) were contacted again to participate in the AVCnnADO follow-up research project (16 yo session) (ethical approval ID-RCB 2020-100106-33). They were offered a comprehensive two-day session with clinical, language, and neuropsychological assessments, as well as MR imaging over 2 days. All responders ( $n = 32$ ) but one had participated in the 7 yo session. One patient not belonging to the original cohort (thus not having done the 7 yo session), was recruited, as this patient fulfilled all strict criteria (in terms of age and NAIS characterization according to her clinical reports and imaging in the neonatal period). Eventually, 33 patients (13 females, 20 males) participated in both the clinical assessments and the imaging protocol, after obtaining parent consents and adolescent assents.

To ensure patients homogeneity, precise lesion characterization (territory and extent) was obtained for each patient through consensus within an expert panel of pediatric neuroradiologists,

neurologists, and rehabilitation physicians. Lesion territories were defined as uni or bilateral, in Anterior Cerebral Artery (ACA), Middle Cerebral Artery (MCA), and Posterior Cerebral Artery (PCA), based on scar tissue sequelae (including tissue loss on T1w images and gliosis on FLAIR). The MCA territory was further subdivided into: i. frontal (inferior or middle frontal gyrus, frontal operculum of the insula, precentral gyrus); ii. temporal (middle and posterior parts of the superior temporal gyrus); iii. parietal (postcentral gyrus, supramarginal gyrus, intraparietal sulcus, superior parietal lobule, angular gyrus, and parietal operculum of the insula); iv. basal ganglia; and v. the entire MCA territory. A combination of several territories within the MCA territory was frequent. This *post-hoc* review led to the exclusion of 7 cases at 7 yo and 3 at 16 yo that did not fully match unilateral arterial ischemic stroke definition, mostly corresponding to bilateral junctional ischemia due to hypoxic-ischemic encephalopathy. The very few patients with PCA stroke ( $N = 2$  at 7 yo, 1 at 16 yo) were excluded from this study. NAIS in MCA and ACA territories accounted, respectively, for 93 and 7% of 7 yo cases, and 90 and 10% of 16 yo cases.

To address the variability in lesion size and severity, ranging from focal cortical ribbon interruption to strokes involving the entire MCA territory including basal ganglia, a regressor of lesion severity was deemed essential for statistical analyses. However, using lesion volumes at ages 7 or 16 was unsuitable for this purpose. Indeed, the residual cavities at 7 or 16 years poorly reflected the size of the initial stroke documented from the neonatal period due to tissue destruction, retraction, and brain growth since birth. For example, some patients missing one or more entire gyrus showed no or very limited apparent cavity, with very limited gliosis which did not reflect the extent of the initial lesion either. Obtaining lesion volume at birth was not feasible for all subjects due to inadequate neonatal MRI data collected in primary hospitals and/or the lack of digital data. We thus introduced a lesion severity score, which combined cortical and sub-cortical GM structures, based on visual assessment of involved (missing) brain tissue. This score, assessed by an expert neuroradiologist (LHP), was constructed by adding two subscores: 1. lesion affecting sub-cortical GM structures (0 = no; 1 = yes); and 2. extent of lesioned cortical territories (0 = none; 1 = one gyrus; 2 = multiple gyri; 3 = whole arterial territory), inspired by the usual clinical classification of the affected territories in ischemic strokes (superficial, deep, mixed). Building this score and including it as a correcting variable in the analysis (see Section 2.7) allows to correct for both inter- and intra-group lesion severity variability.

Active epilepsy (requiring chronic medication) at 16 y was rare ( $n = 5$ , 1 F and 4 M), and not severe (no or a few seizures per year under medication). We found no differences of socio-economic status (SES) between males and females, neither at 7 yo (F: 36.9, SD = 10.9; M: 38.4, SD = 14.1) nor at 16 yo (F: 38.3, SD = 14.2; M: 41.8, SD = 15.3, Kolmogorov-Smirnov on SES computed with Hollingshead method). No SES difference was found between patients who came back at 16 yo (longitudinal) and patients who did not (7 yo only: 35.1, SD = 14.7; longitudinal: 37.4, SD = 13.0). No differences in IQ were found between patients who came back at 16 yo (longitudinal) and patients who did not. Unilateral Cerebral Palsy (uCP) was found in 39.5% of patients, in line with previous series, with no clear changes between 7 and 16 years (37.9%), and no significant differences between males and females (Chi-Square).

All uCP children could walk, mostly with mild restrictions. Hand dysfunction was more pronounced than foot, with nearly non-functional assisting hand in two patients. The clinical presentation of the analyzed population is summarized in [Table 1](#).

### 2.1.2 Healthy controls

During the 7 yo session, a total of 37 age-matched controls (19 F, 18 M) were enlisted. These controls underwent a succinct standard clinical screening encompassing personal and family history, schooling, and a brief clinical examination. Then, they underwent an MRI study identical to that administered to the patients.

In the 16 yo session, 31 age-matched controls (16 F, 15 M) were included for comparative analysis. Similar to the earlier session, these controls underwent succinct standard clinical screening, including personal and family history, schooling, and a brief clinical examination. Furthermore, participants were underwent the Raven matrices subtest of the Weschler Adult Intelligence Scale (WAIS-IV) to screen for any conspicuous deviations from typical cognitive development. Lastly, they underwent the complete MRI study, similarly to the protocol applied to the patients.

Eventually, among all groups, 27 patients (11 F, 16 M) and 17 controls (8 F, 9 M) underwent assessments at both ages, providing unique long term longitudinal data.

In this study, the “sex” variable refers to the sex assignment made at birth by professionals and parents, and subsequently self-reported by the children then adolescents. No disparities between sex assignment and self-reported sex were identified along the study.

## 2.2 MRI acquisition

For this morphometric study, 3D T1-weighted images were acquired at both ages as part of a multimodal 3T MRI acquisition including diffusion MRI, motor and language functional MRI and resting state fMRI, in addition to FLAIR images to detect gliosis and scarring, in Neurospin, CEA-Saclay, France.

Considering the long delay between the sessions, the 3T MR scanner underwent a complete upgrade between the first and second session from a Siemens MAGNETOM Trio Tim system, with a 12-channel head coil to a Siemens MAGNETOM Prisma fit system, with a 64 channel head coil. To optimize image comparability between the two sessions, we selected MPRAGE sequence parameters to provide a similar contrast as follows: Session 7 yo, TR = 2,300 ms, TE = 4.18 ms, TI = 900 ms, voxel size  $1 \times 1 \times 1 \text{ mm}^3$ , 176 slices. Session 16 yo, TR = 2,300 ms, TE = 3.05 ms, TI = 900 ms, voxel size =  $0.9 \times 0.9 \times 0.9 \text{ mm}^3$ , 176 slices.

T2 FLAIR images were acquired for lesion delineation with the following parameters: At Session 7 yo, TR = 5,000 ms, TE = 395 ms, voxel size  $0.9 \times 0.9 \times 1 \text{ mm}^3$ , 160 slices. At Session 16 yo, TR = 5,000 ms, TE = 396 ms, voxel size =  $0.9 \times 0.9 \times 0.9 \text{ mm}^3$ , 176 slices.

## 2.3 Image processing

The methodology presented below has been designed to enable accurate image processing in the context of a developmental

study and in the presence of brain lesions, and to ensure good performance across the whole cohort.

T1-weighted images were processed as shown in [Figure 2](#). Raw DICOM images were imported, anonymized, according to the BIDS specification ([Gorgolewski et al., 2016](#)). Brain masks and extracted brain images (“skull stripping”) were generated using HD-BET ([Isensee et al., 2019](#)). A detailed Quality check was made along the process, first visually to ensure correct registration, GM/WM segmentation and ROI delineation. Raw T1 images with quality issues (mostly due to motion artifacts) were evaluated by combining Image Quality Metrics obtained with MRIQC ([Esteban et al., 2017](#)), and the Euler Number ([Rosen et al., 2018](#)) and CAT12 Image Quality Rating (IQR) ([Gaser et al., 2024](#)). By thresholding the IQR vs. Euler Number distribution, compared to visual assessments, seven images of insufficient quality at 7 yo were excluded. Post-quality check dataset comprised 37 patients at 7 yo (22 M, 15 F; 94.6% MCA, 6.4% ACA) and 29 images at 16 yo (17 M, 12 F; 90% MCA, 10% ACA).

## 2.4 Lesion mapping

Lesion masks were manually drawn at 7 yo, by two expert neuroradiologists using ITK-SNAP on both T1-weighted images (tissue destruction and porencephaly) and T2-FLAIR images (gliosis). Each final mask resulted from the fusion of both T1w and T2-FLAIR masks, followed by a morphological closing process. Discrepancies between experts were solved through consensus.

At 16 yo, lesion masks were computed from the 7 yo masks through intra-subject registration (ANTs) ([Avants et al., 2008](#)) of the T1w images between the ages of 7 and 16. This intra-subject registration used HD-BET brain masks at both 7 and 16 years as complementary inputs (registration masks). In the few instances where 16-year-old subjects lacked usable anatomical images at 7 yo, the masks were drawn using the same manual method.

Lesion mapping (overlap of lesion masks across all patients ([Figure 1](#)), was registered in MNI ICBM152 2009c symmetric space, with the same pipeline as in the subsequent sections on T1w images segmentation ([Figure 2](#)). The proportion of lesion masks overlap within each sex group signifies a comparable lesion distribution in females and males despite a disproportion in patient number (17 F, 27 M). Lesions aligned with the typical MCA/ACA territories, extending into the superior temporal gyrus, parietal lobe, central regions, and the inferior and middle frontal gyrus. A limited number of subjects had ACA territory lesions, specifically in the superior frontal gyrus.

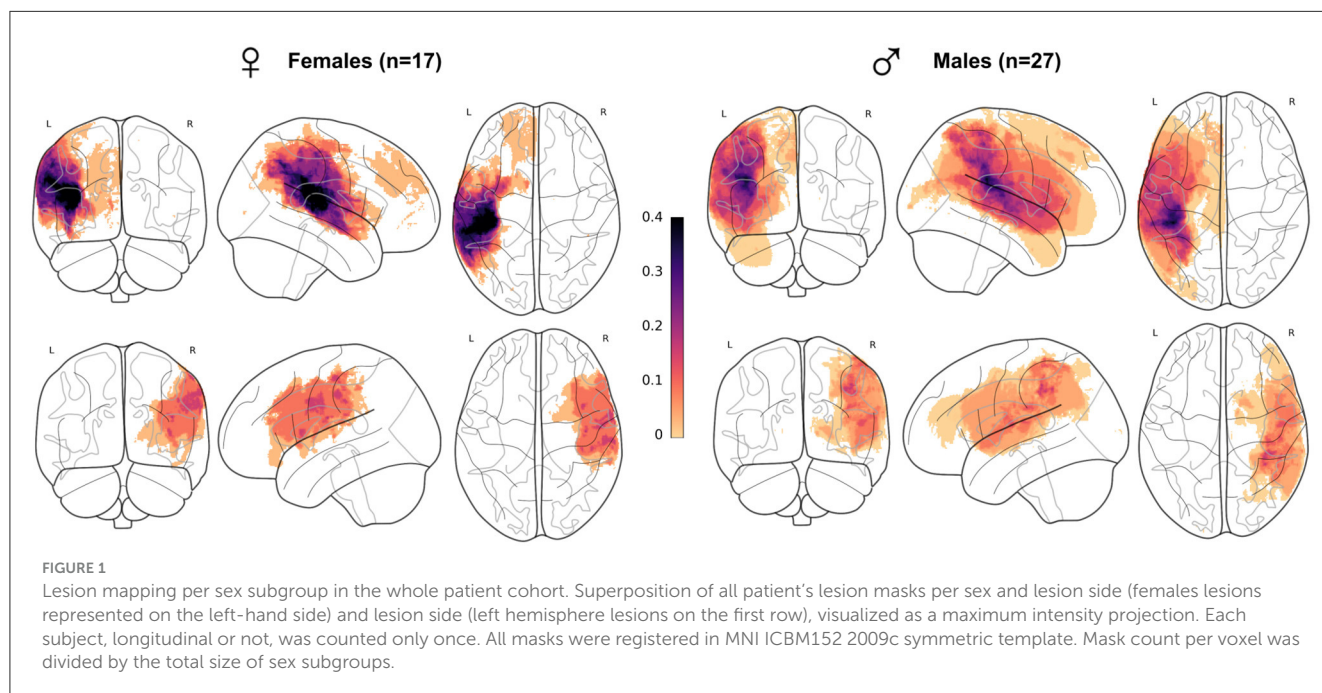
## 2.5 Image segmentation and ROIs volume extraction

We designed a dedicated complex segmentation pipeline of T1-weighted images to accurately delineate ipsi and contralateral ROIs at different scales and locations, even in the proximity of lesions. Utilizing the CAT12 segmentation function (CAT12 standalone 1839 version) in expert mode, we first successfully segmented T1-weighted images into tissue probability maps. In order to secure segmentation results and establish a robust pipeline

TABLE 1 Clinical presentation of the cohort before imaging quality check.

	Session 7 yo	Session 16 yo	Seizure	CP	GMFCS	BFMF	SES
Male	27	17	11.11%	42.86%	1.25	0.86	38.55
					SD = 0.58	SD = 1.01	SD = 13.86
Female	16	12	14.29%	35.29%	1.24	0.52	36.94
					SD = 0.66	SD = 0.72	SD = 10.54

Seizure: active (treated) or past seizure episodes; CP, cerebral palsy; GMFCS, gross motor function classification system, 84% of the subjects had a score of 1; BFMF, bimanual fine motor function, SES, socio-economic score, computed using Hollingshead method.



capable of handling lesions, the input T1 image underwent masking with both the brain mask and the lesion mask. Stroke Lesion Correction (SLC) was activated, and the skull-stripping option was deactivated. We employed HD-BET for skull stripping of T1 images (as illustrated in Figure 2) since CAT12 skull-stripping often failed in the presence of lesions. All other parameters were set to their default values. The longitudinal CAT12 pipeline was not employed, as it relies on rigid registration between imaging session, which is unable to yield a suitable average image in the presence of brain growth.

Subsequently, Desikan DK40 and Hammers' atlases (Hammers et al., 2003; Desikan et al., 2006) were registered in each native space. While the CAT12 standard setting effectively ensured a good contralesional hemisphere segmentation and atlas registration, we identified specific mislabelings and errors in the ipsilesional hemisphere due to the lesion-related anatomical distortion.

### 2.5.1 Global volumes, both hemispheres

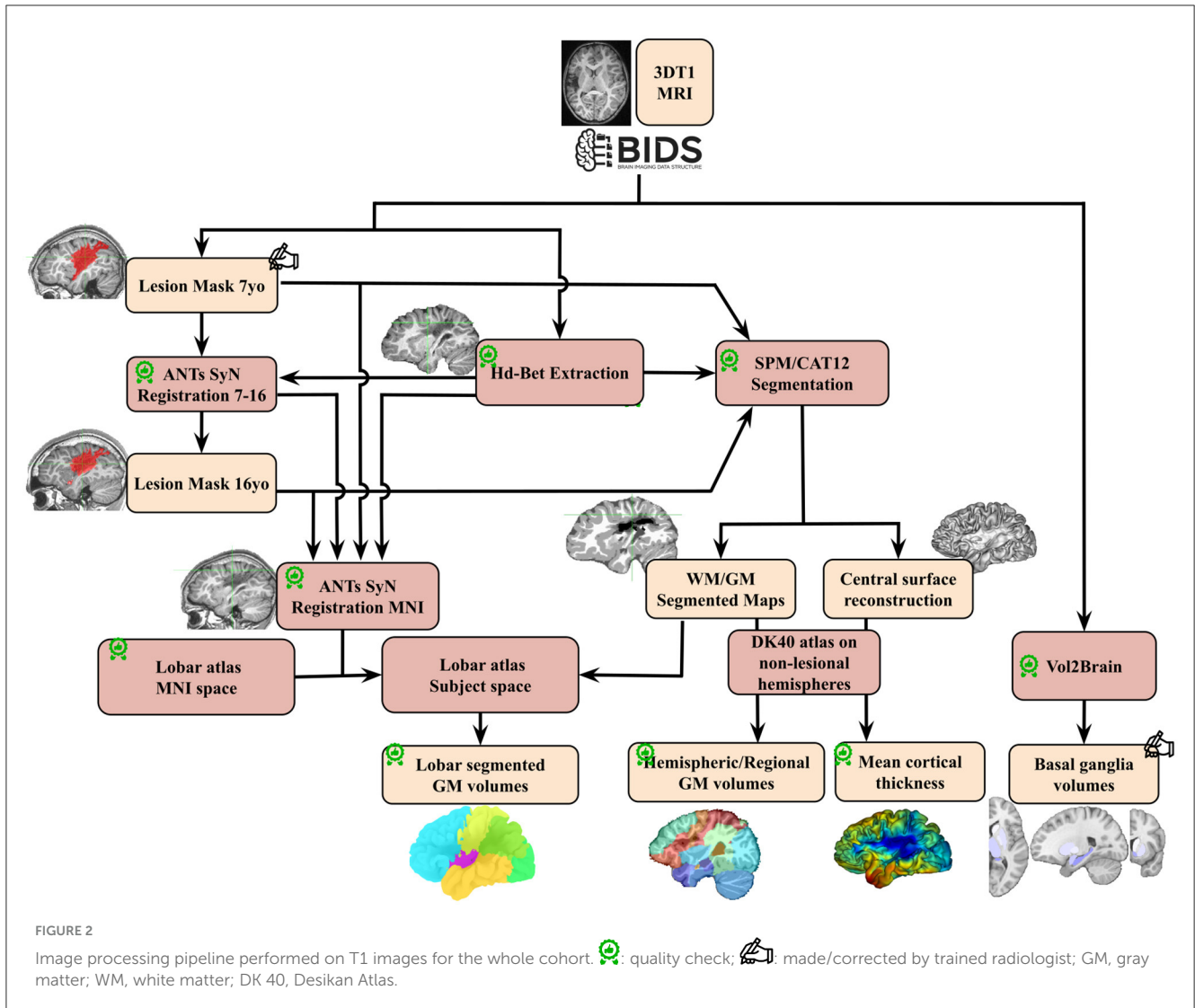
First, GM and WM volumes were computed using the white and GM partial volume maps of CAT12. We relied on the Hammers atlas registered in the native subject space to compute three hemispheric volumes: total hemisphere volumes, hemispheric WM, hemispheric cortical GM (subtracting cingulate, cerebellum and

sub-cortical structures ROIs initially present in the Hammers atlas from the hemisphere masks). Note that this parcellations did include the lesional volumes.

### 2.5.2 Lobar volumes, both hemispheres, and cerebellum

Upon conducting individual manual quality checks on the DK40 parcellation of the ipsilesional hemisphere, various mislabelings were identified. These inaccuracies were primarily attributed to the segmentation process making strong anatomical assumptions, introducing labeling biases that even extended to regions distant from the lesion territory. Consequently, we deemed the existing process unsuitable for conducting fine regional analyses in the ipsilesional hemisphere. We thus developed a mono-atlas lobar segmentation method, specifically designed to be resilient in the presence of lesions. To allow analyses on both ipsi- and contralesional hemispheres, a symmetric atlas was necessary.

We utilized the CerebrA atlas, regrouping regions to construct a lobar and cerebellum atlas in native space. This lobar atlas is divided into the frontal, central, parietal, temporal, and occipital lobes. Within this lobar atlas, the pre-, post-, and para-central gyrus were concatenated to form a "central region/lobe," distinct from the frontal or parietal lobes. The individual deformation fields



of each T1 image into MNI ICBM152 2009c symmetric space were generated using ANTs symmetric diffeomorphic registration (Avants et al., 2008), with brain masks and lesion masks serving as registration masks. These deformation fields were subsequently applied to register a Voronoi projection of the CerebrA atlas into individual space. A Voronoi projection assigns to each non-labeled voxel in the volume the same label as the closest labeled voxel.

Following individualized quality checks, this method accurately segmented lobes even in the presence of large lesions (see Supplementary material 1), with the exception of the cingulate cortex, which was excluded due to frequent misalignment of the callosal region. Individual GM probability maps were then employed to compute GM volumes in each lobe and in the cerebellum.

### 2.5.3 Contralateral cortical GM volumes and cortical thickness

To refine with a state-of-the-art parcellation method the findings obtained in the contralateral hemispheres and to ensure comparability between thickness and volume per region of interest (ROI), we conducted a volumetric analysis of the contralateral

hemisphere based on the DK40 atlas. Each GM partial volume map was parcellated according to the closest DK40 label on the individual cortical surface. Subsequently, cortical volume (as presented) and mean thickness (see Supplementary material 2, 3) per DK40 ROI were extracted and subjected to analysis.

### 2.5.4 Subcortical GM structures

Subcortical GM structures were segmented utilizing Vol2Brain (Manjón et al., 2022). During the upload of T1 images, we provided age and sex as complementary inputs to enhance segmentation performance. While the overall segmentation quality was deemed satisfactory, manual correction was carried out in ~55% of cases, primarily to rectify instances of mis-segmentation in the left hippocampus. Volumes of sub-cortical GM structures were subsequently extracted from both hemispheres.

## 2.6 ROIs exclusion criteria

Given our objective to examine the growth of preserved tissue following an early lesion, it was crucial to select on non-lesional

regions to prevent interference in statistical analyses. Consequently, lesioned territories, as described in the Patients section, were excluded by default. Additionally, areas were deemed lesioned if the intersection of the lesion mask with a specific ROI exceeded 2% of the parenchymal volume of that particular ROI. These exclusion criteria were not applied to the global ipsilesional hemispheric volumes (total volume, cortical GM, and WM) to estimate the overall impact of the lesion on the ipsilateral hemisphere.

For further analyses within the ipsilesional hemisphere, the number of subjects thus varied across ROIs due to lesion variability in both location and extent: the insula and parietal lobe were excluded from all analyses as they were lesioned in most patients (>75%). The remaining regions were analyzed in specific patient subsets: frontal lobe (12 F/15 M, and 9 F/11 M at 7 and 16 yo, respectively), central region (6 F/13 M, and 3 F/10 M at 7 and 16 yo, respectively), temporal lobe (11 F/16 M, and 6 F/10 M at 7 and 16 yo, respectively), occipital lobe (15 F/21 M, and 12 F/16 M at 7 and 16 yo, respectively), and subcortical GM structures (10 F/18 M, and 10 F/13 M at 7 and 16 yo, respectively).

In the contralesional hemisphere and the cerebellum (both hemispheres) of patients, no ROI had to be excluded, resulting in the following numbers: 15 F/22 M, and 11 F/17 M at 7 and 16 yo, respectively.

Finally, in the control group (without lesion), the total number of analyzed ROIs was 18 F/16 M and 15 F/16 M at 7 and 16 yo, respectively.

## 2.7 Statistical analysis

### 2.7.1 Model construction (LMM)

To specifically study the effect of an early lesion and its impact on developmental trajectories, we employed a Linear Mixed Model (LMM) predicting each regional volume. Despite the non-linear evolution of brain region volumes with age, the linearity assumption remains suitable for our study due to our age-constrained dataset, which comprises only two time points. The choice of an LMM enables the incorporation of a “random effect” that specifies subject identifiers, accommodating longitudinal data while also including data from subjects with only one time point.

Modeled effects are the age (volumes and thickness depending on age), sex (males and females do not have the same brain volumes), status (patients vs. controls) and all their interactions to model both typical and lesion-related sex-differences in volumes and developmental trajectories (puberty, etc.). Age was covariant with scanner change, hence the model was not adapted to investigate age effect, but corrected for additive variability due to scanner change (Fortin et al., 2018).

We also modeled a “hemisphere” effect that encodes which hemisphere side (right or left) was in input, because brain regions are known to be asymmetric and/or develop asymmetrically (Williams et al., 2021a,b, 2022). The last modeled effect was the lesion severity score, to correct for intra-group lesion size inhomogeneity with possible slight imbalance between patient subgroups. We chose not to correct for intracranial or equivalent volume as these metrics are covariant with patient status: brain growth is impaired due to missing tissue and gliosis, total brain

volume encompasses lesion volume, contralesional hemisphere volume is affected as well, and the lesioned brain exerts different biomechanical forces on the skull growth hence influencing total intracranial volume.

We standardized each ROI metric by subtracting the mean of the population and dividing by its standard deviation. Continuous variables (age, lesion severity score) were also standardized. To avoid covariance with the status effect, the lesion severity score was centered on the patient population, set to 0 for controls, and then standardized for the entire dataset. For categorical variables, the native encoding (dummy coding: [0; 1]) was retained for the status effect, where controls served as the reference group, while the hemisphere and sex effects were coded using “effect coding” ([−1;1] instead of [0,1]).

The LMM formulation for each ROI was as follows:

$$\text{Metric}_{ROI} = \text{Age} * \text{Sex} * \text{Status} + \text{Hemisphere}_{side} + \text{Lesion Severity} + (1 | \text{Participant}_{id}_{side})(1)$$

Where fixed effects are: Age as a discrete variable with two levels: 7 or 16 (before standardization); Sex as a categorical variable with two levels: male (−1) or female (+1); Status as a categorical variable with two levels: patient (+1) or control (0); Hemisphere\_side (of the studied volume) as a categorical variable with two levels: left (−1) or right (+1); Lesion Severity as a discrete variable with 5 levels [0:4]. (before standardization, see above); “\*” Signifies that both main effects and interactions were modeled; “+” Signifies that only main effects were modeled (these effects being considered independent).

1 | Participant\_id\_side is a random effect, adjusted on intercept value, estimated for each hemisphere of each subject (for example “sub-hcXXX\_left”, which correspond to the left hemisphere of control number XXX). Random effects must be independent, homoscedastic and normally distributed. This enabled to have a semi-longitudinal statistical design, while also accounting for individual left-right hemisphere variability.

The model was fitted using the LmerTest (Bates et al., 2015; Kuznetsova et al., 2017) package in R with Residual Maximum Likelihood (REML). Statistical *t*-tests (Satterthwaite’s method for degrees of freedom) were performed on the model factors for each effect and interaction, assessing whether they were significantly different from 0. For the model fit output, we chose not to correct for multiple comparisons, but we present each effect value with three different *p*-value thresholds (\* < 0.05; \*\* < 0.01; \*\*\* < 0.001).

Betas (effect factors) are expressed as standard deviations of the fitted ROI metric dataset, as each model was fitted on standardized data.

### 2.7.2 Post-hoc tests

To disentangle the multiple interaction effect terms and specifically examine the differences between males and females in patients with reference to their matched controls, *post-hoc* tests were specified using the R module Lmertest (Kuznetsova et al., 2017) and emmeans (Searle et al., 1980). This function compares marginal means (the mean volume estimated by the model for a specific group) between specified subgroups, taking into account

associated estimated standard deviations and degrees of freedom (Kenward-Roger method). The resulting *t*-tests assess whether the difference between two subgroups is significantly different from 0. The specified contrasts were designed as follows:

- **[Patients – Controls] for each sex at each age.** This design aimed to minimize the impact of sex and age-related volume variations on compared brain ROI sizes. By comparing each patient population with its corresponding control group, we could estimate the specific effects related to patient status within each sex at each age.
- **[(Patients – Controls)<sub>male</sub> – (Patients – Controls)<sub>female</sub>] at each age.** This contrast tests specifically the interaction effect between sex and status on the marginal means, hence on volume values fitted for age and sex in our cohort. This enabled a targeted investigation of potential sex differences specific to patients with early brain lesions while accounting for the typical sex differences at the group level in our cohort.

In the *post-hoc* tests, the Hemisphere\_side and Lesion\_severity effects were not explicitly defined in the contrasts. As the LMM model serves as input for the *post-hoc* test function, these effects are regressed and averaged across various subgroups before the comparison of marginal means takes place. Since the models were fit on different volume, using different image processing, they were corrected separately for multiple comparisons. False discovery rate (FDR) correction was applied to correct for three tests on whole-hemisphere metrics, six tests on contralesional hemisphere lobar approach, four tests on ipsilesional hemisphere, seven tests for basal ganglia, and 34 for DK40 atlas results. These numbers correspond to the number of ROIs per approach.

For plotting purposes on the same scale, each marginal means difference was expressed as a relative effect size (proportion of the mean control volume), by dividing the raw volume difference by the mean value of control volume across age and sex for the specific plotted ROI.

## 3 Results

### 3.1 Impact of main clinical effects on regional volumes: multifactorial analysis

Figure 3 displays the values of each factor and of their interactions in the Linear Mixed Models (LMMs) fitted on each volume of interest. As models were fitted on a normalized dataset, each factor was expressed as a proportion of its standard deviation. Associated statistical tests assessed whether the factor value significantly differed from 0. *P*-values in Figure 3 are uncorrected. Parietal lobe and insula in the ipsilesional hemisphere were excluded as they were lesioned in most patients. For further description of raw total and hemisphere volume values in each age and sex group, please refer to [Supplementary material 4](#).

#### 3.1.1 Main effect of age

The model fit results showed consistent changes between 7 and 16 years of age for cortical GM (negative) and WM trajectories

(positive), as commonly described in the literature (Bethlehem et al., 2022; Rutherford et al., 2022), and in most basal ganglia volumes (Wierenga et al., 2014). However, our study design aimed at comparing groups within age category rather than between ages.

#### 3.1.2 Main effect of sex

The results also showed consistent data with typical sex differences, recently confirmed by normative analysis (Wierenga et al., 2014; Bethlehem et al., 2022; Rutherford et al., 2022). Sex factors were significantly negative in nearly all ROIs, confirming smaller mean volumes in females than in males across all groups, a well-documented difference in the literature.

#### 3.1.3 Interaction between age and sex

The Age\*Sex interaction was weak but significant, in both ipsi and contralesional hemispheres, in the hemispheric WM volume (with a marginal effect on the whole hemisphere volume), and in some subcortical structures (putamen, pallidum, amygdala, and hippocampus). This may relate to the subtle asynchrony in GM volume developmental trajectories between males and females (Giedd et al., 2015; Bethlehem et al., 2022). No such effect was seen in the cerebellum.

#### 3.1.4 Asymmetry (hemisphere side) covariate

Model fits showed very limited effects of hemispheric side in ipsi and contralesional hemispheres, with a small negative effect on some lobar regions (temporal ipsilesional, and frontal contralesional), indicating slightly bigger left than right volumes, and positive tendencies in pallidum and accumbens, indicating bigger right than left volumes. These regional differences were however subtle.

#### 3.1.5 Differences between patients and controls (status) and effect of lesion severity

Interestingly, the effect of status (patient vs. control) and of lesion severity were different between hemispheres. In the ipsilesional hemisphere, as expected, the whole hemisphere, WM, and cortical GM volumes (that include the lesion mask) showed a strong negative effect size, i.e., smaller volumes in patients than in controls, with the effect of lesion severity adding to smaller volumes of intact brain. Indeed, in cortical regions distant from the lesion too (frontal, temporal and occipital lobes), patients had smaller volumes than controls, regardless of age, sex, or hemisphere, with an effect of lesion severity, suggesting an ipsilateral growth restriction remotely from the lesion and depending on severity. In subcortical regions, the putamen and thalamus volumes showed a similar behavior confirming previous data showing altered cortico-subcortical connectivity, that was correlated with lesion severity in the thalamus. By contrast, in the contralesional hemisphere, there were limited volume differences between patients and controls, with only hemispheric WM and putamen volumes being significantly smaller in patients. Only the contralesional reduction of the putamen volume was related to lesion severity. Pallidum exhibited a similar tendency, although the status effect was not

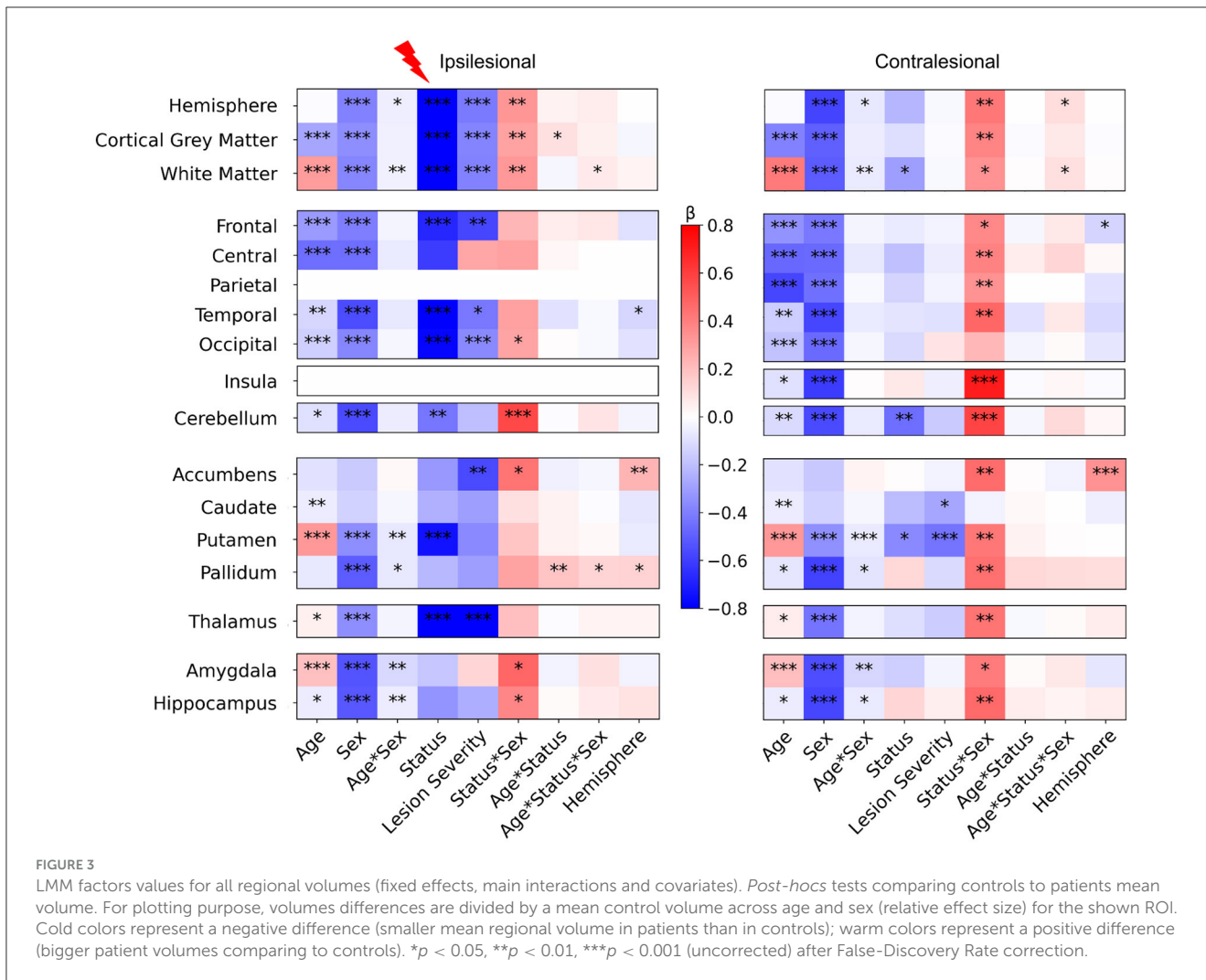


**FIGURE 3**  
 LMM factors values for all regional volumes (fixed effects, main interactions and covariates). *Post-hocs* tests comparing controls to patients mean volume. For plotting purpose, volumes differences are divided by a mean control volume across age and sex (relative effect size) for the shown ROI. Cold colors represent a negative difference (smaller mean regional volume in patients than in controls); warm colors represent a positive difference (bigger patient volumes comparing to controls). \* $p < 0.05$ , \*\* $p < 0.01$ , \*\*\* $p < 0.001$  (uncorrected) after False-Discovery Rate correction.

significant, which might indicate that only patients with the biggest lesions showed volume loss.

Eventually, cerebellar GM volumes of both hemispheres were significantly lower in patients, with no obvious impact of lesion severity.

There was a very weak interaction between status and age in the ipsilesional hemispheric GM volume, but not in ipsilesional regions distant from the lesion, except the pallidum. This may indicate minimal volume trajectory difference between 7 and 16 years between patients and controls (see *post-hoc* tests below).

### 3.1.6 Interaction between status and sex

This interaction questions whether the volume differences between patients and controls depend on the subject's sex, regardless of known typical differences due to age and sex (main effects). Interestingly we found significant interactions in both hemispheres, however much more pronounced in the contralesional hemisphere.

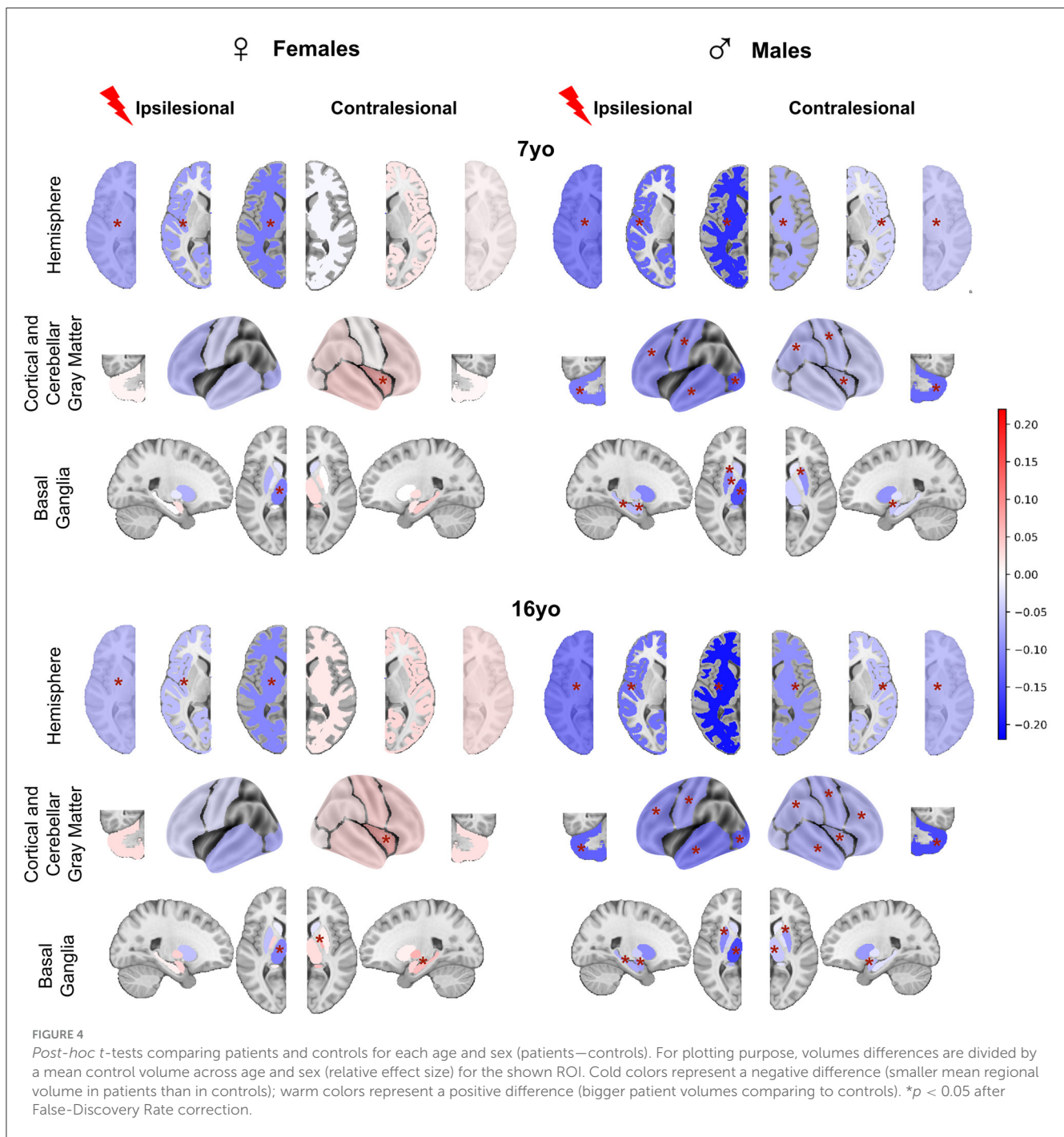
In the ipsilesional hemisphere, the Status \* Sex interaction was significantly positive for hemisphere-wise volumes, and in the occipital lobe only at the lobar scale. Among subcortical GM

volumes, it was also significantly positive in accumbens, amygdala, and hippocampus volumes. In the contralesional hemisphere however, the Status \* Sex interaction effect was significantly positive in all volumes except the occipital lobe and caudate nucleus.

The Status \* Sex interaction was significantly positive in both cerebellar hemispheres. Adding age in the interaction (Age \* Sex \* Status) showed a very weak positive effect in ipsilesional WM and pallidum, and in contralesional whole hemisphere and WM volumes.

### 3.2 Comparison between patients and controls according to sex (*post-hoc* tests)

To further explore the Status\*Sex interaction described above, we compared mean brain regional volume differences between patients and controls in all sex and age groups (Figure 4). All raw differences in volumes were divided by a mean control volume across ages and sexes of the corresponding ROI to allow better figure readability (color and effect size normalization). Therefore, all differences are expressed as proportions of a reference control volume. A negative difference (blue color) means that the mean



regional volume was smaller in patients than in controls. If positive (pink/red color), patient volumes were bigger than control ones.

### 3.2.1 In females

At 7 yo, we found very limited differences between female patients and controls. While ipsilesional hemispheric WM and cortical GM volumes were significantly lower in patients than in controls (−5.7 to 11.7% of control mean volume), there were no significant volume differences of intact lobes and of cerebellar GM volume between female patients and controls. This suggests

that the reduction of hemispheric volumes reflected the lesion extent only. Among ipsilesional subcortical GM structures, only the thalamus volume was smaller than in the controls (−11.2% of the mean control thalamus volume). This thalamus volume reduction reflects the well-known dysconnectivity of the cortico-subcortico-thalamic loop (Xia et al., 2021). Interestingly, female patients contralesional hemisphere volumes were not significantly different from controls. On the regional analysis, patient contralesional insula volumes were even significantly larger than in controls (+5.6%). No difference was found elsewhere, including in the cerebellum. At 16 yo, the pattern was similar to that of 7 yo. The

only minimal change consisted of bigger contralesional pallidum and hippocampus in female patients than in controls (+6.5 and 5.8%). These observations suggest a notable resilience of brain growth after an early brain lesion in females, and even maybe some compensation mechanism, whose cellular mechanisms cannot be informed by mere volumetric descriptions (synaptic densities, myelination? ...).

### 3.2.2 In males

By contrast, we found significant volume reductions in male patients as compared to male controls, in both hemispheres, and at both ages. At 7 yo, ipsilesional hemisphere, WM, and cortical GM volumes were significantly smaller than controls (−12.1 to −20.3%). All ipsilesional lobes and subcortical GM structures distant from the lesion showed significant volume reductions in patients compared to controls (lobes = −9.3 to −19.6%, hippocampus = −6.1%, amygdala = −5.3%, putamen = −10%, pallidum = −5.1%, and thalamus = −14%). This demonstrates a volume reduction of all ipsilesional remote structures in addition to the direct lesion effect.

In the contralesional hemisphere, whole hemisphere, WM, and cortical GM volumes were also significantly lower in male patients than in controls (−3.9 to −9.6%). Lobar analysis showed significantly lower volumes in contralesional parietal lobe, central region and insula (−5.6%), as well as in amygdala (−5%) and putamen (−9.2%). Cerebellum was smaller on both sides (−10%). At 16 yo, the pattern was essentially identical to that of 7 years in the ipsilesional hemisphere. In the contralesional hemisphere, minimal changes were seen as volume reduction also reached significance in the frontal and temporal lobes (−5.8 and 7.4%), in the thalamus (−4.9%), and the hippocampus (−2.6%).

## 3.3 Comparison between male and female patients accounting for typical sex differences

To assess whether these sex differences according to the clinical status were really significant, while accounting for the known differences in typical subjects, we used the interaction product contrast ( $[(patient - control) male - (patient - control) female]$ ) (Figure 5). In nearly all ROIs, volumes were smaller in males than in females, reaching significance in almost all contralesional regions, and also in a number of ipsilesional ones, with an identical pattern at 7 and 16 years of age. Ipsilesional hemispheric volumes were significantly smaller in male than in female patients at both ages (on the average −2.5 and −3.5% at 7 and 16 yo, respectively). This difference is independent from lesion severity, as the model already corrected for it. In ipsilesional lobes distant from the lesion, male and female cortical GM volumes were not significantly different, although the trend in all regions was toward smaller volumes in males. Ipsilesional pallidum, hippocampus and amygdala were also significantly smaller in male than female patients at 16 yo (−3.9, −4.1, −5.9%, respectively).

In the contralesional hemisphere, the male-female differences were even more pronounced, especially at 16 yo. Hemispheric

volumes were significantly smaller in males at 16 yo only (−5.8%). The lobe-wise pattern was the same at both ages: parietal (−4.1%), temporal (−4.1 to −5.4%) and insula (−6.2 to −6.7%), or at 16 yo only (frontal lobe and central region, −5.6 and −4.8%, respectively). Contralesional accumbens (−7.7, −6.3%), pallidum (−2.7, −4.5%), putamen (−4.7, −4.9%), thalamus (−3.5, −3.8%) and hippocampus (−3.6, −4.2%) were all significantly smaller in male than in female patients at both ages, and amygdala volume difference was significant only at 16 yo, −4.7%. Cerebellum was significantly smaller in male than in female patients at both ages and on both sides (ipsilesional: −5.8 and −7.9%, and contralesional: −5.8 and −8.3% at 7 and 16 years of age, respectively).

## 3.4 Regional study of the contralesional hemisphere in the Desikan-Killiany (DK40) atlas

Beyond this relatively coarse analysis of ipsi and contralesional hemispheric and lobar volumes, we aimed at a finer contralesional ROIs parcellation in order to test whether regions homotopic to the lesion would show a particular vulnerability in terms of cortical GM growth. This hypothesis stems from the well-known diaschisis that affects regions connected to a lesioned territory, especially through callosal interhemispheric homotopic fibers (Pretzel et al., 2022). To investigate this, we designed a finer contralesional parcellation, in DK40 atlas, and applied the same model and analysis grid (Figure 6).

### 3.4.1 Impact of the clinical variables

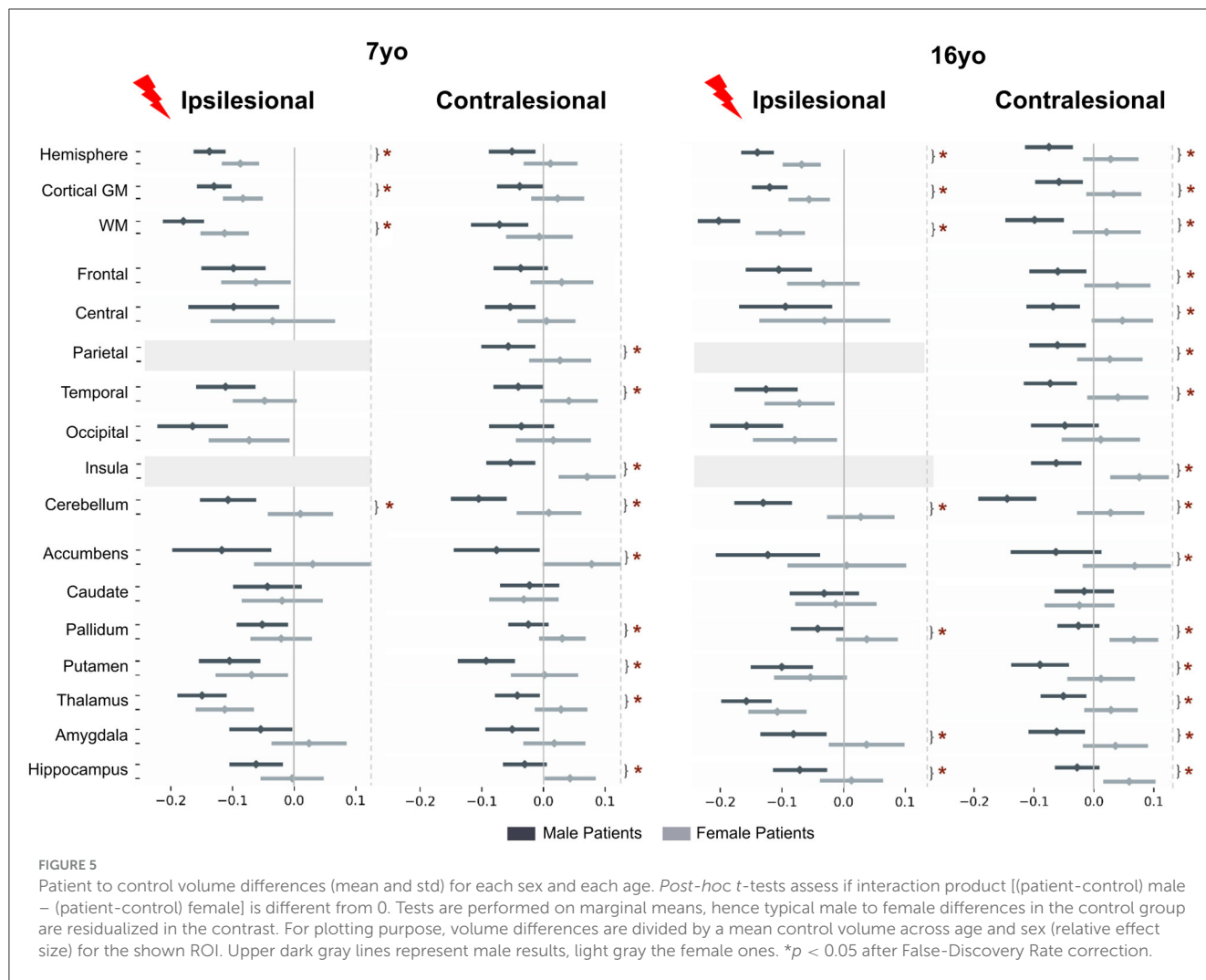
Figure 6A displays the coefficients obtained from the models. Consistently with the lobar results, the Age and Sex effects were negative in most regions, indicating lower volumes at 16 than at 7 yo and lower volumes in females than males. Age\*Sex effect was rarely significant (uncorrected) with a small effect size. Status and lesion severity had little to no effect. We confirmed the positive Status\*Sex interaction effect in several regions, suggesting a divergence from the norm in male vs. female patients, like in the previous analysis.

Age\*Status interaction effect showed a similar behavior than in previous analysis, but reached significant (uncorrected) in a few regions (lateral orbitofrontal gyrus, middle and inferior temporal gyrus). This may indicate a slightly more pronounced volume decrease between 7 and 16 yo in patients than in controls. As for previous results, no Age\*Sex\*Status interaction was significant.

However, unlike lobar scale results, the Hemisphere effect was significant in many ROIs. Most effects were in line with recent studies on brain asymmetries studied with similar brain parcellation (Williams et al., 2022).

### 3.4.2 Comparison between patients and controls per sex group

In Figure 6B, sex and age-paired comparisons between patients and controls revealed distinct patterns: In females, there was no difference in any regional volume between patients and controls



at both ages. In males, the supramarginal gyrus and insula were significantly smaller in patients than in controls (–11.6 and –5.9%, respectively) at 7 yo. At 16 yo, volumes were smaller in superior temporal gyrus (–9.1%), supramarginal gyrus (–10%), postcentral (–9.5%) and precentral gyrus (–7.6%), rostral middle frontal gyrus (–10%), lateral orbitofrontal (–9.5%), and insula (–6%). Thus, this finer parcellation confirmed the trends observed previously, with very little deviation from the typical trajectories in females, and decreased volumes in male patients, mostly in perisylvian regions, mirroring the lesion distribution in the opposite hemisphere.

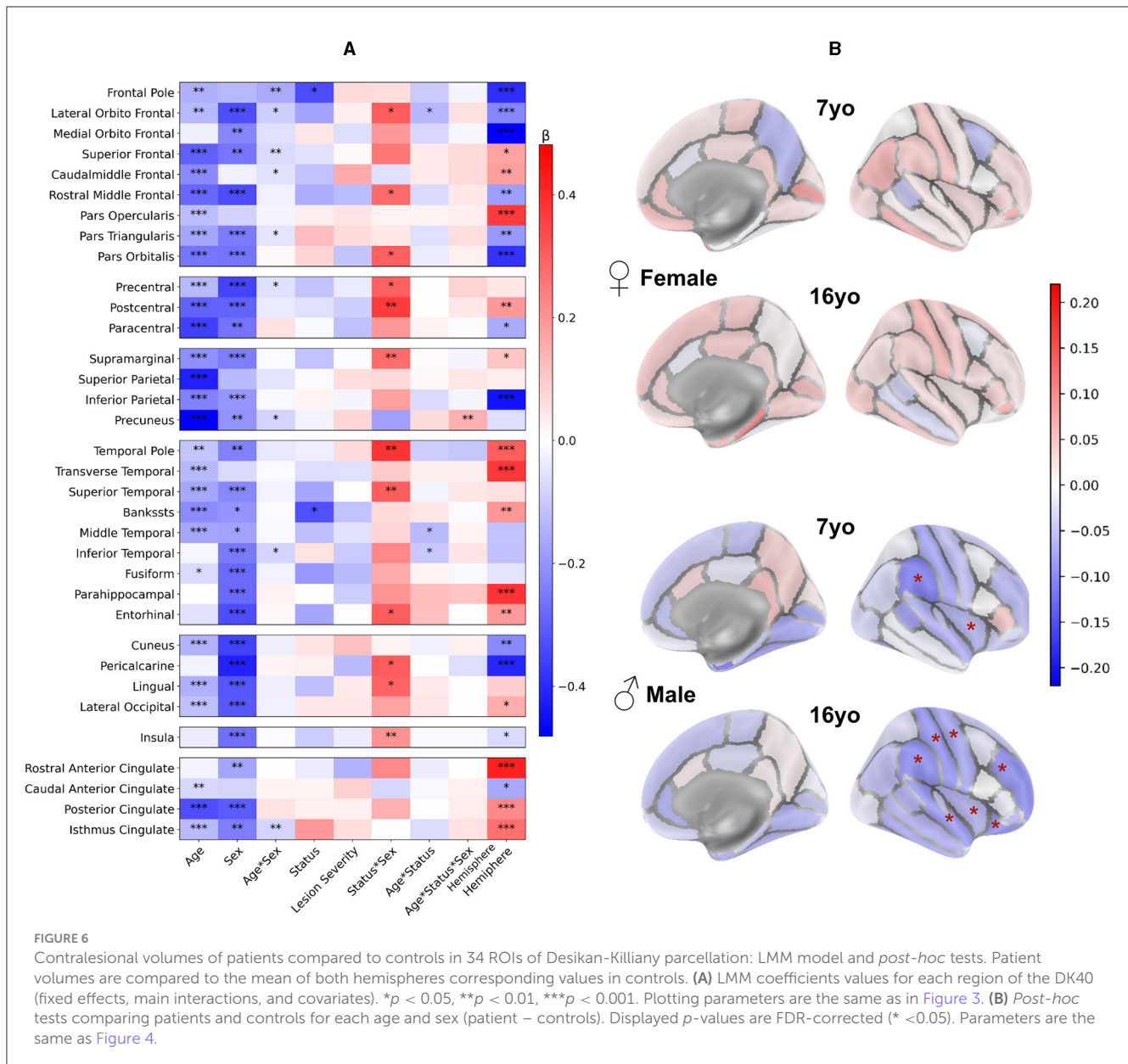
When looking at male to female volume differences specific to the patient status effect (see [Supplementary material 5](#)) we found similar tendencies in DK40 atlas as with the lobar atlas in almost all regions, consistently at 7 and 16 yo. However, no differences survived the FDR correction. This was probably due to several reasons: (i) As ROIs were smaller, the data variability was bigger compared to the observed effect size; (ii) Volume differences between patients and controls were smaller than on the lobe wise analysis, with lower effect size, and as such, less significant results; (iii) The multiple tests correction was more stringent given the number of tests with regard to the limited number of patients.

We confirmed these sex differences by exploring two alternative models: a sex by sex analysis, and a residualised approach, where we fitted a Age \* Sex Generalized Model before fitting an adapted Linear Mixed Model (see [Supplementary material 6–11](#)).

The same analysis was performed on mean cortical thickness (see [Supplementary material 1, 2](#)) in DK40. Model factors exhibited more dispersed tendencies, leading to inconclusive results in *post-hoc* tests. This inconclusiveness primarily stemmed from smaller effect sizes, typically below 3%.

## 4 Discussion

This study is the first step of a larger protocol aiming at studying the long-term plasticity of the brain during childhood and adolescence after an early focal brain injury, through a combination of multimodal clinical and MRI markers. In this paper, we present the first longitudinal multifactorial MRI morphometry analysis of the long-term sequels after a neonatal stroke, accounting for developmental and clinical factors (age, sex, lesion side and extent). Relying on a carefully curated cohort of subjects with unilateral



NAIS studied longitudinally within specific age ranges (7–8 and 16–18 years of age), we underlined the impact of the different factors on the ipsi- and contra-lesional cortical, subcortical and cerebellar GM distant from the lesion growth trajectories, with reference to age-matched controls.

We designed a robust image processing and segmentation pipelines capable of handling the lesion-related anatomical modifications. Volumes were extracted at different scales (from hemispheric to regional parcels). Age-matched controls were recruited for normative purposes, with more than half of those also studied longitudinally. Utilizing a Linear Mixed Model with numerous regressors, we obtained reproducible and congruent results across different morphometry pipelines and granularity levels.

We found an overall reduction of most volumes distant from the lesion in patients compared to controls, with different

patterns in ipsi- and contra-lesional hemispheres depending on sex (after controlling for all other variables, including lesion severity). As expected, volumes distant from the lesion were more reduced in the ipsi-lesional hemisphere than in contra-lesional one, and depended on lesion extent, reflecting intrahemispheric disconnectivity. The ipsilesional volume reductions were slightly more pronounced in males than in females. In the contralesional hemisphere, sex differences were much more pronounced, with males exhibiting smaller regional cortical (and some subcortical) GM volumes, while females showed little deviations from the typical trajectories. When utilizing finer parcellations, the volume reductions were mostly seen in homotopic regions to the lesion within the contralesional hemisphere, suggesting specific interhemispheric homotopic disconnectivity after a unilateral NAIS. The hippocampus/amygdala volumes followed a similar pattern with reduction in males, and stability/increase in females.

Bilateral cerebellar gray matter was reduced in males only. Interestingly, the impact of puberty was weak, as volume differences between patients and controls exhibited similar magnitudes at age 7 and 16, suggesting that most, if not all, deviations had occurred in early childhood (before 7 yo).

Among previous morphometric studies on perinatal stroke, very few investigated specifically sex differences in volume trajectories. Most of them controlled for sex ratio differences in each group composition before conducting analysis without including sex as covariate (Gold and Trauner, 2014; Dinomais et al., 2015; Craig et al., 2019a,b; Hassett et al., 2022; Ilves et al., 2022; Shinde et al., 2023; Vaher et al., 2023). One study explicitly stated controlling analysis for sex before not including it as covariable (Al Harrach et al., 2019), and two compared each patient to an age and sex paired control group (Moses, 2000; Stiles et al., 2009). To our knowledge, our study is the first one tackling specifically sex differences in brain volumetry after a neonatal stroke.

#### 4.1 GM volumes reduction in ipsilesional hemisphere

In the ipsilesional hemisphere, GM volumes distant from the lesion were consistently smaller in patients compared to controls, in both sexes and ages, independently of the stroke side and severity. Additionally, these volumes exhibited a dependence on lesion extent in cortical lobar regions (except the central region) and in the thalamus. *Post-hoc* tests revealed significant differences in lobar parcels for males. The total hemisphere volumes (WM and cortical GM volumes) do include the lesioned area (that is accounted for in the lesion severity regressor). Thus, differences between patients and controls at the hemispheric level can be explained by the difference of volumes distant from the lesion as seen in each lobe, adding to the lesion effect. Moreover, subcortical GM volumes were also altered, with thalamic volumes significantly smaller in both sexes, in line with (Craig et al., 2019a; Vaher et al., 2023).

This pattern likely relates to distributed intrahemispheric disconnectivity, leading to changes in brain areas functionally connected but structurally remote from the primary lesion (i.e., diaschisis), and resulting in the reduction in GM volumes distant from the lesion in all associative territories with long range connectivity. The exception of the central region might come from the peculiar connectivity of this primary projection cortex that essentially connects with subcortical and cerebellar regions. In premature babies, WM lesions such as periventricular leucomalacia (PVL) have been shown to lead to reduced GM volumes at term (Inder et al., 1999). Previous diffusion studies of NAIS have also consistently identified diaschisis in GM and WM, such as in the thalamus or the corpus callosum (Srivastava et al., 2019), and beyond corpus callosum (Pretzel et al., 2022). As expected, we also found a global reduction in hemispheric WM (beyond the lesion volume), but more detailed study of WM bundles will help to correlate the altered structural connectivity pattern following NAIS with GM volumes. Thalamus volume was significantly smaller in both sexes, in line with (Craig et al., 2019a; Vaher et al., 2023), its central position making it susceptible

to diaschisis, as described by previous analyses (Carrera and Bogousslavsky, 2006) linking regional thalamic injuries to many cortical lesion syndromes.

While diaschisis has been extensively studied in adult stroke using older imaging modalities, the contemporary definition of “connectomal” diaschisis (Carrera and Tononi, 2014), made possible by advanced imaging modalities, presents a promising avenue for understanding the clinical impairment and recovery after NAIS (Shi et al., 2019; Umarova and Thomalla, 2020; Siddiqi et al., 2022).

#### 4.2 Differentiated pattern of GM volumes in the contralesional hemisphere

In the contralesional hemisphere, only male patients exhibited significantly smaller GM volumes than controls. This pattern was reproduced by the DK40 parcellation, albeit more focused on homotopic regions mirroring the lesion. By contrast, female patients did not deviate from the controls values and had an even slightly larger insula than controls, that could illustrate sex differences in compensatory mechanisms.

Sub-cortical analysis revealed smaller putamen and amygdala at both ages, along with a smaller thalamus at 16 years in male patients. Female patients, on the other hand, exhibited larger hippocampus and pallidum than controls at 16 yo. Patient sex-related differences were significant only at 16 years, in hippocampus, amygdala and putamen. Lower volumes were found in pallidum and hippocampus in perinatal AIS (Ilves et al., 2022), and hippocampus, amygdala and putamen lower volumes correlated with poorer hand function. To our knowledge, the sex-difference we found in subcortical GM has never been described before.

These congruent and robust results at different scales and with different atlases indicate long-term contralesional differences in GM growth between male and female patients after NAIS. Specific *post-hoc* tests yielded significant results at both ages, encompassing whole hemisphere volumes, all lobes but the occipital, and almost all subcortical volumes but the caudate. However, significance was not reached when using the DK40 parcellation after correcting for multiple comparisons.

Divergences between these two scales can be attributed to various methodological factors. Inter-individual variability is more prominent in smaller regions, where subtle segmentation errors also contribute to a larger variability. Smaller regions also tend to exhibit greater asymmetry, particularly during development. Regional asymmetries are a key feature of mature brain, and start during prenatal development (Chi et al., 1977; Toga and Thompson, 2003; Maingault et al., 2016; Williams et al., 2022). Brain maturation unfolds asynchronously, with finer associative functions maturing later than primary ones, and with a precise spatiotemporal sequence. In our model, this asynchrony was accounted for by the hemisphere regressor, but this correction may be improved, as recent large scale studies pointed sex differences in these asymmetries (Williams et al., 2022). Finally, significantly more tests were conducted on the DK40, making multiple tests correction more stringent, given our limited sample size (although

the largest sample to date of NAIS patients studied longitudinally over 17 years).

### 4.3 Cerebellum morphometry

Consistently with prior results, we observed smaller cerebellar hemispheric GM volumes in male patients compared to controls (but not in females) at both ages and in both hemispheres. In this study, we did not intend to study specifically cerebellar asymmetries nor subcerebellar parcels, and no differences were identified between ipsi- and contra-lesional hemispheric cerebellar GM volumes in any group. Cross cerebellar diaschisis has been observed repeatedly (Dinomais et al., 2012; Craig et al., 2019b). The role of the ipsilesional cerebellar hemisphere volume alterations on cognitive outcome after perinatal stroke has been recently suggested (Craig et al., 2019b).

### 4.4 Sex related differences

Overall, our study shows a significant difference between males and females in the brain developmental anatomical evolution, especially within the contralesional hemisphere, following the dysconnectivity induced by a focal neonatal brain lesion. Numerous factors may contribute to these sex differences on brain architecture and organization (DeCasien et al., 2022), including chromosomal differences and sex bias in autosomal gene expression (Shi et al., 2016). Our results are in line with the vast literature validating the neurobiological differences between males and females with respect to the response to brain injuries and in particular the early vulnerability of the male brain (Smith et al., 2014; Charriaut-Marlangue et al., 2018; Kelly et al., 2023). While the mechanisms underlining this early sex difference remain unclear, several biological processes have been suggested: vulnerability to oxidative stress, modulation of cell death, regulation of microglial activation and gonadal hormones exposure across developmental stages (Charriaut-Marlangue et al., 2018).

As our results indicate a same order effect size at 7 and 16 years, we infer that most observed differences occurred before 7 years of age and were minimally impacted by the physiological development and by the shift in sex steroid exposure during puberty. This suggests that sex might influence early post-injury plasticity and other compensation mechanisms. Several non-exclusive hypotheses can be proposed. One is hormonal, given the differences in prenatal and early post-natal exposure to gonadal hormones, due to a sex-difference on the hypothalamus-pituitary gonadal axis activation. This induces in both sexes a transient “minipuberty” (Becker and Hesse, 2020), that could impact several neurobiological mechanisms including the neuroinflammatory response to the lesion. Another hypothesis involves differences in brain structure maturation at birth between males and females. Recent studies have shown that microglia cells are sexually dimorphic and play a role in sexual differentiation, but they also intervene in the immune response to brain lesions (VanRyzin et al., 2020).

Sex related differences have been described in preclinical inflammation models showing an upregulated immune response and increased microglial activation in males following neonatal hypoxia (Kelly et al., 2023). Also, the materno-fetal innate immune signaling shows a more prominent inflammation in males than in females, with sex specific decreased myelination, decreased WM thickness, microglial depletion in the corpus callosum, and neuronal apoptosis (Giraud et al., 2017; Allard et al., 2019). In a placental study in twins, male placentas were shown to have more inflammation than girls (Jahanfar and Lim, 2018). Sex-specific placental and fetal pro-inflammatory responses are in keeping with the higher susceptibility of males for preterm birth, early brain injuries, and neurodevelopmental disorders such as CP, and ASD. Eventually, sex differentiated segregation of genetic polymorphisms might contribute to this pattern (Dewing et al., 2003; McCarthy et al., 2017; Raznahan et al., 2018). Independently of the underlying mechanisms, our observations concur to an early deviation from typical trajectory in males, while females seem to be more resilient, and to present less morphological changes in later childhood and adolescence.

### 4.5 Functional correlates

The relationship between atypical brain size/growth and the variability of neurocognitive outcomes remains unclear. In most cases, cognitive deficits suggest cortical and/or subcortical neuronal dysfunction, that often translates in reduced volumes/growth, especially in case of characterized perinatal brain lesions (i.e., hypoxic-ischemic encephalopathies). On the other hand, reduced volumes do not always translate into clinically relevant correlates, as shown by the large inter-subject variability of brain volume in the typical population (Bethlehem et al., 2022; DeCasien et al., 2022; Rutherford et al., 2022).

Beyond the sex ratio in the occurrence of NAIS (two males for one female) (Chabrier et al., 2016), data on sex related functional/clinical consequences correlated to the morphological brain changes after early brain lesions remain scarce. For example, as some volumes are larger in female patients than controls (e.g., insula, hippocampus), it may be tempting to conclude that females compensate anatomically for their lesions, whereas males do not. However, this hypothesis might be somewhat simplistic, as previous work has highlighted volume variations outside the norm that do not correlate with clinical variables (Craig et al., 2019b). In general, the anatomo-functional correlations between morphometry and clinical scores remain deceiving in a number of situations (Gur and Gur, 2017; Peper et al., 2020). In previous literature, no clear sex differences have emerged so far on behavioral analysis, suggesting that the contribution of sex remains moderate in comparison to major clinical variables such as lesion extent and co-morbidities. More thoughtful designs may address this issue in depth.

### 4.6 Methodological considerations

This study is a pioneering endeavor, distinguished by its reliance on a partly longitudinal cohort of both patients and

controls. This unique design facilitates the utilization of a Linear Mixed Model, incorporating a linear model of age, given our two strictly defined age ranges. This enhances the statistical power of the analyses, enabling a multifactorial investigation that accounts for various developmental factors, for the first time in this pathology. Notably, to our knowledge, this is the first comprehensive exploration of the ipsilesional hemisphere and of sex effects in this context.

Our segmentation methodology proved robust to the presence of lesions, and we expect that improved volumetric parcellation will contribute to more reliable results in subsequent diffusion and functional imaging analyses. Rigorous quality checks were applied to the images to ensure the absence of artifacts that could corrupt the analyses. Lesions were characterized based on clinical and imaging criteria, ensuring a highly reproducible phenotype and restricting its clinical and structural variability. To further address lesion variability in the model, we designed a specific lesion severity score. We developed a methodology to strictly select regions distant from the lesion and secure analyses on the cortical regions of the ipsilesional hemisphere. We accounted for brain local asymmetry directly in the model as well as in the imaging pipeline by using symmetric templates. The use of complementary image processing and segmentation methodologies resulted in consistent tendencies increasing confidence in the findings.

Some limitations should however be acknowledged in the current study. While we did our best to avoid selection biases and checked the different subgroups clinical characteristics, we cannot fully assert a perfect generalizability of our results to the NAIS population.

In addition to the fact that NAIS is a rare disease, the AVCnn cohort is a unique cohort that, from a clinical perspective, present a large number of subjects studied longitudinally over nearly 20 years. From an imaging and statistical perspective however, this sample remains relatively small, especially for the female subgroup. Although the statistical models used estimate standard errors and degrees of freedom based on subgroup sizes, the limited population of 16 yo females with a right lesion may not be generalizable. We however remain confident in our results on the female subgroup, given the excellent coherence of the results at age 16 with those at age 7 with more subjects.

Also, because of the limited sample size, we could not include more variables in the LMM analysis. To alleviate this possible confound, we checked beforehand that there were no differences between females and males characteristics, in particular for variables that may induce a bias, including the presence of epilepsy (Vaher et al., 2023), cerebral palsy (Dinomais et al., 2015), and the family socio-economic status

In this long-term longitudinal study, we could not avoid a scanner bias due to MRI scanner change between 7 and 16 years of age (covariance with age). This problem was solved by regressing the scanner bias in conjunction with the age effect in the model.

Despite our best efforts to design our registration pipeline, and a thorough quality check we cannot exclude some residual misregistration in the ipsilesional hemisphere, due to non-linear brain growth around the lesion scar. However, this effect is unlikely to affect the results in remote regions and it has been mitigated in the close vicinity of the lesion by our stringent exclusion criteria

of lesioned ROIs. Lastly, given the complexity of hemispheric asymmetries specially in the presence of a lesion, lesion side effect might be imperfectly accounted for by the hemisphere side regressor.

## 5 Conclusion

This first longitudinal study on long-term global and regional brain growth after NAIS highlights sex differences in contralesional brain volumes. Notably, while females did not deviate from controls, males exhibited smaller volumes of gray matter in both cortical and subcortical compartments, and in the cerebellum. These sex related differences were apparent in early childhood, and puberty did not change the pattern.

Thus, beyond the known increased frequency of early setbacks in males, this study demonstrates intrinsic sex-related differences in brain growth *after* the initial event, at the expense of males that show an early restricted growth compared to male controls. The biological mechanisms of male brain response to injury results in a multifactorial cascade that takes place in early childhood, with a continuing deviation from the typical pattern that is not much influenced by puberty. Further work on detailed assessment of white matter growth and connectivity will provide a more comprehensive understanding of the neurobiological underpinnings of sex-related differences in the aftermath of NAIS.

How this translates into clinical sex-related differences will also need to be further detailed.

Eventually, this study underscores the critical importance of accounting for typical sex-related volume differences in the developing brain where the temporality and amplitude of brain maturation follow a non-linear trajectory, varying by sex and brain region.

## Data availability statement

The raw data supporting the conclusions of this article will be made available by the authors, without undue reservation.

## Ethics statement

The studies involving humans were approved by Data at 7 years of age: PHRC régional n80308052, and PHRC interrégional n81008026—eudract number 2010-A00329-30 and Data at 16 years of age: ethical approval ID-RCB 2020-100106-33 (CPP Devine). The studies were conducted in accordance with the local legislation and institutional requirements. Written informed consent for participation in this study was provided by the participants' legal guardians/next of kin.

## Author contributions

P-YP: Conceptualization, Data curation, Formal analysis, Investigation, Methodology, Software, Validation, Visualization, Writing – original draft, Writing – review & editing. YL: Conceptualization, Data curation, Formal analysis, Methodology,

Software, Supervision, Visualization, Writing – review & editing. SB: Data curation, Investigation, Methodology, Software, Writing – review & editing. LD: Conceptualization, Data curation, Investigation, Methodology, Writing – review & editing. EP: Conceptualization, Data curation, Investigation, Methodology, Writing – review & editing. IB: Conceptualization, Investigation, Methodology, Validation, Writing – review & editing. DB: Methodology, Software, Writing – review & editing. SN: Data curation, Validation, Writing – review & editing. ED: Methodology, Software, Writing – review & editing. MD: Conceptualization, Data curation, Funding acquisition, Investigation, Methodology, Writing – review & editing. MC: Writing – review & editing, Conceptualization, Methodology, Supervision, Visualization. LH-P: Formal analysis, Funding acquisition, Investigation, Methodology, Project administration, Supervision, Validation, Visualization, Writing – review & editing, Conceptualization, Data curation.

## Funding

The author(s) declare financial support was received for the research, authorship, and/or publication of this article. Data collection has been funded by the Fondation de Recherche sur l'AVC. Data analysis was partially funded by the French National Reference Center for Pediatric Stroke.

## Acknowledgments

We warmly thank Dr. Stephane Chabrier for constituting the AVCnn cohort, Dr. Cyrille Renaud and Gaëlle Mediouni for

patient recruitment and organization of data collection sessions, the clinical team of UNIACT lab at NeuroSpin for continuing support in data acquisition, Dr. Maxime de Malherbe for manual extraction of lesion masks at age 7 yo, Noémie Palay for her help in dealing with clinical and neuropsychological data, the Drs. Jessica Dubois, David Germanaud, and Catherine Chiron for the rich and valuable scientific exchanges throughout the study. We are grateful to The Fondation de Recherche sur l'AVC and the French National Reference Center for Pediatric Stroke for funding the study.

## Conflict of interest

The authors declare that the research was conducted in the absence of any commercial or financial relationships that could be construed as a potential conflict of interest.

## Publisher's note

All claims expressed in this article are solely those of the authors and do not necessarily represent those of their affiliated organizations, or those of the publisher, the editors and the reviewers. Any product that may be evaluated in this article, or claim that may be made by its manufacturer, is not guaranteed or endorsed by the publisher.

## Supplementary material

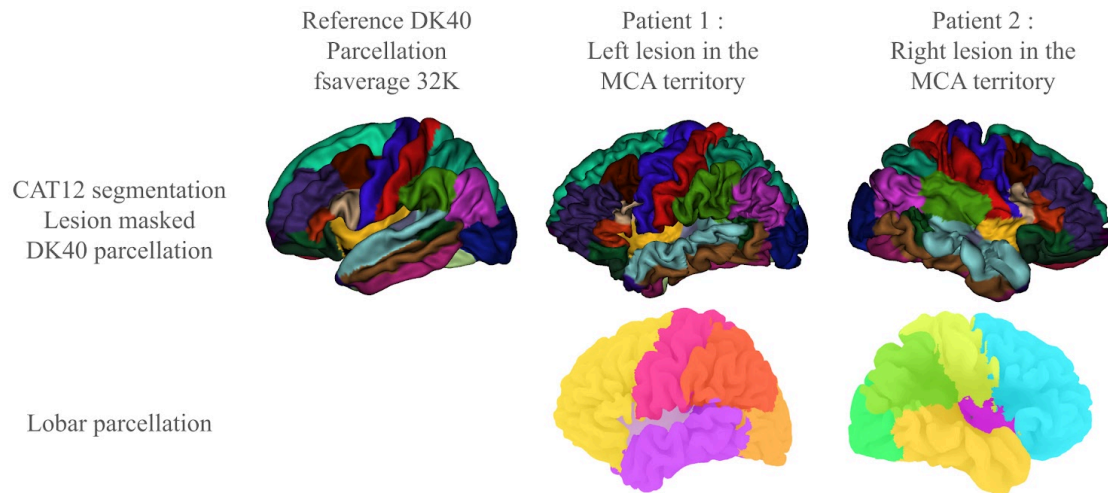
The Supplementary Material for this article can be found online at: <https://www.frontiersin.org/articles/10.3389/fnins.2024.1405381/full#supplementary-material>

## References

- Al Harrach, M., Rousseau, F., Groeschel, S., Wang, X., Hertz-pannier, L., Chabrier, S., et al. (2019). Alterations in cortical morphology after neonatal stroke: compensation in the contralesional hemisphere? *Dev. Neurobiol.* 79, 303–316. doi: 10.1002/dneu.22679
- Allard, M.-J., Giraud, A., Segura, M., and Sebire, G. (2019). Sex-specific maternofetal innate immune responses triggered by group B Streptococci. *Sci. Rep.* 9:8587. doi: 10.1038/s41598-019-45029-x
- Anderson, V. A., Spencer-Smith, M. M., Coleman, L., Anderson, P. J., Greenham, M., Jacobs, R., et al. (2014). Predicting neurocognitive and behavioural outcome after early brain insult. *Develop. Med. Child. Neuro.* 56, 329–336. doi: 10.1111/dmcn.12387
- Avants, B., Tustison, N., and Song, G. (2008). Advanced normalization tools (ANTS). *Insight J.* 1–35. doi: 10.54294/uvnhn
- Bates, D., Mächler, M., Bolker, B., and Walker, S. (2015). Fitting Linear Mixed-Effects Models Using lme4. *J. Stat. Soft.* 67. doi: 10.18637/jss.v067.i01
- Becker, M., and Hesse, V. (2020). Minipuberty: why does it happen? *Horm. Res. Paediatr.* 93, 76–84. doi: 10.1159/000508329
- Bethlehem, R. A. I., Seidlitz, J., White, S. R., Vogel, J. W., Anderson, K. M., Adamson, C., et al. (2022). Brain charts for the human lifespan. *Nature* 604, 525–533. doi: 10.1038/s41586-022-04554-y
- Carrera, E., and Bogousslavsky, J. (2006). The thalamus and behavior: effects of anatomically distinct strokes. *Neurology* 66, 1817–1823. doi: 10.1212/01.wnl.0000219679.95223.4c
- Carrera, E., and Tononi, G. (2014). Diaschisis: past, present, future. *Brain* 137, 2408–2422. doi: 10.1093/brain/awu101
- Chabrier, S., Husson, B., Dinomais, M., Landrieu, P., and Nguyen The Tich, S. (2011). New insights (and new interrogations) in perinatal arterial ischemic stroke. *Thromb. Res.* 127, 13–22. doi: 10.1016/j.thromres.2010.10.003
- Chabrier, S., Peyric, E., Drutel, L., Deron, J., Kossorotoff, M., Dinomais, M., et al. (2016). Multimodal outcome at 7 years of age after neonatal arterial ischemic stroke. *J. Pediatr.* 172, 156–161.e3. doi: 10.1016/j.jpeds.2016.01.069
- Charriaut-Marlangue, C., Besson, V. C., and Baud, O. (2018). Sexually dimorphic outcomes after neonatal stroke and hypoxia-ischemia. *Int. J. Mol. Sci.* 19:61. doi: 10.3390/ijms19010061
- Chi, J. G., Dooling, E. C., and Gilles, F. H. (1977). Left-right asymmetries of the temporal speech areas of the human fetus. *Arch. Neurol.* 34, 346–348. doi: 10.1001/archneur.1977.00500180040008
- Craig, B. T., Carlson, H. L., and Kirton, A. (2019a). Thalamic diaschisis following perinatal stroke is associated with clinical disability. *NeuroImage Clin.* 21:101660. doi: 10.1016/j.nicl.2019.101660
- Craig, B. T., Olsen, C., Mah, S., Carlson, H. L., Wei, X.-C., and Kirton, A. (2019b). Crossed cerebellar atrophy in perinatal stroke. *Stroke* 50, 175–177. doi: 10.1161/STROKEAHA.118.022423
- DeCasien, A. R., Guma, E., Liu, S., and Raznahan, A. (2022). Sex differences in the human brain: a roadmap for more careful analysis and interpretation of a biological reality. *Biol. Sex Differ.* 13:43. doi: 10.1186/s13293-022-00448-w
- Desikan, R. S., Ségonne, F., Fischl, B., Quinn, B. T., Dickerson, B. C., Blacker, D., et al. (2006). An automated labeling system for subdividing the human cerebral cortex on MRI scans into gyral based regions of interest. *Neuroimage* 31, 968–980. doi: 10.1016/j.neuroimage.2006.01.021

- Dewing, P., Shi, T., Horvath, S., and Vilain, E. (2003). Sexually dimorphic gene expression in mouse brain precedes gonadal differentiation. *Mol. Brain Res.* 118, 82–90. doi: 10.1016/S0169-328X(03)00339-5
- Dinomais, M., Groeschel, S., Staudt, M., Krägeloh-Mann, I., and Wilke, M. (2012). Relationship between functional connectivity and sensory impairment: Red flag or red herring? *Hum. Brain Mapp.* 33, 628–638. doi: 10.1002/hbm.21227
- Dinomais, M., Hertz-Pannier, L., Groeschel, S., Chabrier, S., Delion, M., Husson, B., et al. (2015). Long term motor function after neonatal stroke: Lesion localization above all. *Hum. Brain Mapp.* 36, 4793–4807. doi: 10.1002/hbm.22950
- Dinomais, M., Hertz-Pannier, L., Groeschel, S., Delion, M., Husson, B., Kossorotoff, M., et al. (2016). Does contralesional hand function after neonatal stroke only depend on lesion characteristics? *Stroke* 47, 1647–1650. doi: 10.1161/STROKEAHA.116.013545
- Dunbar, M., and Kirton, A. (2018). Perinatal stroke: mechanisms, management, and outcomes of early cerebrovascular brain injury. *Lancet Child Adolesc. Health* 2, 666–676. doi: 10.1016/S2352-4642(18)30173-1
- Dunbar, M., and Kirton, A. (2019). Perinatal stroke. *Semin. Pediatr. Neurol.* 32:100767. doi: 10.1016/j.spn.2019.08.003
- Dunbar, M., Mineyko, A., Hill, M., Hodge, J., Floer, A., and Kirton, A. (2020). Population based birth prevalence of disease-specific perinatal stroke. *Pediatrics* 146:e2020013201. doi: 10.1542/peds.2020-013201
- Esteban, O., Birman, D., Schaer, M., Koyejo, O. O., Poldrack, R. A., and Gorgolewski, K. J. (2017). MRIQC: advancing the automatic prediction of image quality in MRI from unseen sites. *PLoS ONE* 12:e0184661. doi: 10.1371/journal.pone.0184661
- Fluss, J., Dinomais, M., and Chabrier, S. (2019). Perinatal stroke syndromes: similarities and diversities in aetiology, outcome and management. *Eur. J. Paediatr. Neurol.* 23, 368–383. doi: 10.1016/j.ejpn.2019.02.013
- Fortin, J.-P., Cullen, N., Sheline, Y. I., Taylor, W. D., Aselcioglu, I., Cook, P. A., et al. (2018). Harmonization of cortical thickness measurements across scanners and sites. *Neuroimage* 167, 104–120. doi: 10.1016/j.neuroimage.2017.11.024
- Gaser, C., Dahnke, R., Thompson, P. M., Kurth, F., Luders, E., and The Alzheimer's Disease Neuroimaging Initiative. (2024). CAT: a computational anatomy toolbox for the analysis of structural MRI data. *Gigascience* 13:giae049. doi: 10.1093/gigascience/giae049
- Giedd, J. N., Raznahan, A., Alexander-Bloch, A., Schmitt, E., Gogtay, N., and Rapoport, J. L. (2015). Child psychiatry branch of the national institute of mental health longitudinal structural magnetic resonance imaging study of human brain development. *Neuropsychopharmacol* 40, 43–49. doi: 10.1038/npp.2014.236
- Giraud, A., Guiraut, C., Chevin, M., Chabrier, S., and Sèbire, G. (2017). Role of perinatal inflammation in neonatal arterial ischemic stroke. *Front. Neurol.* 8:612. doi: 10.3389/fneur.2017.00612
- Giraud, A., Stephens, C. M., Fluss, J., Kossorotoff, M., Walsh, B. H., and Chabrier, S. (2023). Long-term developmental condition following neonatal arterial ischemic stroke: a systematic review. *Arch. Pédiatr.* 30, 600–606. doi: 10.1016/j.arcped.2023.07.007
- Gold, J. J., and Trauner, D. A. (2014). Hippocampal volume and memory performance in children with perinatal stroke. *Pediatr. Neurol.* 50, 18–25. doi: 10.1016/j.pediatrneurol.2013.08.029
- Gorgolewski, K. J., Auer, T., Calhoun, V. D., Craddock, R. C., Das, S., Duff, E. P., et al. (2016). The brain imaging data structure, a format for organizing and describing outputs of neuroimaging experiments. *Sci. Data* 3:160044. doi: 10.1038/sdata.2016.44
- Gur, R. C., and Gur, R. E. (2017). Complementarity of sex differences in brain and behavior: from laterality to multimodal neuroimaging. *J. Neurosci. Res.* 95, 189–199. doi: 10.1002/jnr.23830
- Halladay, A. K., Bishop, S., Constantino, J. N., Daniels, A. M., Koenig, K., Palmer, K., et al. (2015). Sex and gender differences in autism spectrum disorder: summarizing evidence gaps and identifying emerging areas of priority. *Mol. Autism* 6:36. doi: 10.1186/s13229-015-0019-y
- Hammers, A., Allom, R., Koeppe, M. J., Free, S. L., Myers, R., Lemieux, L., et al. (2003). Three-dimensional maximum probability atlas of the human brain, with particular reference to the temporal lobe. *Hum. Brain Mapp.* 19, 224–247. doi: 10.1002/hbm.10123
- Hassett, J., Carlson, H., Babwani, A., and Kirton, A. (2022). Bihemispheric developmental alterations in basal ganglia volumes following unilateral perinatal stroke. *NeuroImage Clin.* 35:103143. doi: 10.1016/j.nicl.2022.103143
- Ivles, N., Lõo, S., Ivles, N., Laugesaar, R., Loorits, D., Kool, P., et al. (2022). Ipsilesional volume loss of basal ganglia and thalamus is associated with poor hand function after ischemic perinatal stroke. *BMC Neurol.* 22:23. doi: 10.1186/s12883-022-02550-3
- Inder, T. E., Huppi, P. S., Warfield, S., Kikinis, R., Zientara, G. P., Barnes, P. D., et al. (1999). Periventricular white matter injury in the premature infant is followed by reduced cerebral cortical gray matter volume at term. *Ann Neurol.* 46, 755–760. doi: 10.1002/1531-8249(199911)46:5<755::AID-ANA11>3.0.CO;2-0
- Isensee, F., Schell, M., Pflueger, I., Brugnara, G., Bonekamp, D., Neuberger, U., et al. (2019). Automated brain extraction of multisequence MRI using artificial neural networks. *Hum. Brain Mapp.* 40, 4952–4964. doi: 10.1002/hbm.24750
- Jahanfar, S., and Lim, K. (2018). Is there a relationship between fetal sex and placental pathological characteristics in twin gestations? *BMC Pregn. Childb.* 18:285. doi: 10.1186/s12884-018-1896-9
- Kelly, L. A., Branagan, A., Semova, G., and Molloy, E. J. (2023). Sex differences in neonatal brain injury and inflammation. *Front. Immunol.* 14:1243364. doi: 10.3389/fimmu.2023.1243364
- Kirton, A., and deVeber, G. (2013). Life after perinatal stroke. *Stroke* 44, 3265–3271. doi: 10.1161/STROKEAHA.113.000739
- Kuznetsova, A., Brockhoff, P. B., and Christensen, R. H. B. (2017). lmerTest package: tests in linear mixed effects models. *J. Stat. Softw.* 82, 1–26. doi: 10.18637/jss.v082.i13
- Li, C., Miao, J. K., Xu, Y., Hua, Y. Y., Ma, Q., Zhou, L. L., et al. (2017). Prenatal, perinatal and neonatal risk factors for perinatal arterial ischaemic stroke: a systematic review and meta-analysis. *Eur. J. Neurol.* 24, 1006–1015. doi: 10.1111/ene.13337
- Maingault, S., Tzourio-Mazoyer, N., Mazoyer, B., and Crivello, F. (2016). Regional correlations between cortical thickness and surface area asymmetries: a surface-based morphometry study of 250 adults. *Neuropsychologia* 93, 350–364. doi: 10.1016/j.neuropsychologia.2016.03.025
- Manjón, J. V., Romero, J. E., Vivo-Hernando, R., Rubio, G., Aparici, F., De La Iglesia-Vaya, M., et al. (2022). vol2Brain: a new online pipeline for whole brain MRI analysis. *Front. Neuroinform.* 16:862805. doi: 10.3389/fninf.2022.862805
- Mathes, B. M., Morabito, D. M., and Schmidt, N. B. (2019). Epidemiological and clinical gender differences in OCD. *Curr. Psychiatry Rep.* 21:36. doi: 10.1007/s11920-019-1015-2
- McCarthy, M. M., Nugent, B. M., and Lenz, K. M. (2017). Neuroimmunology and neuroepigenetics in the establishment of sex differences in the brain. *Nat. Rev. Neurosci.* 18, 471–484. doi: 10.1038/nrn.2017.61
- Moses, P. (2000). Regional size reduction in the human corpus callosum following perinatal and perinatal brain injury. *Cereb. Cortex* 10, 1200–1210. doi: 10.1093/cercor/10.12.1200
- Peper, J. S., Burke, S. M., and Wierenga, L. M. (2020). “Chapter 3 - sex differences and brain development during puberty and adolescence,” in *Handbook of Clinical Neurology*, eds. R. Lanzenberger, G. S. Kranz, and I. Savić (Elsevier), 25–54.
- Pretzel, P., Dholander, T., Chabrier, S., Al-Harrach, M., Hertz-Pannier, L., Dinomais, M., et al. (2022). Structural brain connectivity in children after neonatal stroke: a whole-brain fixel-based analysis. *NeuroImage Clin.* 34:103035. doi: 10.1016/j.nicl.2022.103035
- Ramtekkar, U. P., Reiersen, A. M., Todorov, A. A., and Todd, R. D. (2010). Sex and Age Differences in attention-deficit/hyperactivity disorder symptoms and diagnoses: implications for DSM-V and ICD-11. *J. Am. Acad. Child Adolesc. Psychiatry* 49, 217–228.e3. doi: 10.1097/00004583-201003000-00005
- Raznahan, A., Parikshak, N. N., Chandran, V., Blumenthal, J. D., Clasen, L. S., Alexander-Bloch, A. F., et al. (2018). Sex-chromosome dosage effects on gene expression in humans. *Proc. Natl. Acad. Sci. U. S. A.* 115, 7398–7403. doi: 10.1073/pnas.1802889115
- Romeo, D. M., Venezia, I., Pede, E., and Brogna, C. (2023). Cerebral palsy and sex differences in children: a narrative review of the literature. *J. Neurosci. Res.* 101, 783–795. doi: 10.1002/jnr.25020
- Romeo, D. M. M., Cioni, M., Battaglia, L. R., Palermo, F., and Mazzone, D. (2011). Spectrum of gross motor and cognitive functions in children with cerebral palsy: Gender differences. *Eur. J. Paediatr. Neurol.* 15, 53–58. doi: 10.1016/j.ejpn.2010.05.007
- Rosen, A. F. G., Roalf, D. R., Ruparel, K., Blake, J., Seelaus, K., Villa, L. P., et al. (2018). Quantitative assessment of structural image quality. *Neuroimage* 169, 407–418. doi: 10.1016/j.neuroimage.2017.12.059
- Rutherford, S., Kia, S. M., Wolfers, T., Frazza, C., Zabihi, M., Dinga, R., et al. (2022). The normative modeling framework for computational psychiatry. *Nat. Protoc.* 17, 1711–1734. doi: 10.1038/s41596-022-00696-5
- Searle, S. R., Speed, F. M., and Milliken, G. A. (1980). Population marginal means in the linear model: an alternative to least squares means. *Am. Stat.* 34, 216–221. doi: 10.1080/00031305.1980.10483031
- Shi, K., Tian, D.-C., Li, Z.-G., Ducruet, A. F., Lawton, M. T., and Shi, F.-D. (2019). Global brain inflammation in stroke. *Lancet Neurol.* 18, 1058–1066. doi: 10.1016/S1474-4422(19)30078-X
- Shi, L., Zhang, Z., and Su, B. (2016). Sex biased gene expression profiling of human brains at major developmental stages. *Sci. Rep.* 6:21181. doi: 10.1038/srep21181
- Shinde, K., Craig, B. T., Hassett, J., Dlamini, N., Brooks, B. L., Kirton, A., et al. (2023). Alterations in cortical morphometry of the contralesional hemisphere in children, adolescents, and young adults with perinatal stroke. *Sci. Rep.* 13:11391. doi: 10.1038/s41598-023-38185-8

- Siddiqi, S. H., Kording, K. P., Parvizi, J., and Fox, M. D. (2022). Causal mapping of human brain function. *Nat. Rev. Neurosci.* 23, 361–375. doi: 10.1038/s41583-022-00583-8
- Smith, A. L., Alexander, M., Rosenkrantz, T. S., Sadek, M. L., and Fitch, R. H. (2014). Sex differences in behavioral outcome following neonatal hypoxia ischemia: insights from a clinical meta-analysis and a rodent model of induced hypoxic ischemic brain injury. *Exp. Neurol.* 254, 54–67. doi: 10.1016/j.expneurol.2014.01.003
- Smithers-Sheedy, H., Badawi, N., Blair, E., Cans, C., Himmelmann, K., Krägeloh-Mann, I., et al. (2014). What constitutes cerebral palsy in the twenty-first century? *Dev. Med. Child Neurol.* 56, 323–328. doi: 10.1111/dmcn.12262
- Srivastava, R., Rajapakse, T., Carlson, H. L., Keess, J., Wei, X.-C., and Kirton, A. (2019). Diffusion imaging of cerebral diaschisis in neonatal arterial ischemic stroke. *Pediatr. Neurol.* 100, 49–54. doi: 10.1016/j.pediatrneurol.2019.04.012
- Stanley, F. J., Blair, E., Alberman, E., and Alberman, E. D. (2000). *Cerebral Palsies: Epidemiology and Causal Pathways*. Cambridge: Cambridge University Press.
- Stiles, J., Moses, P., Roe, K., Akshoomoff, N. A., Trauner, D., Hesselink, J., et al. (2003). Alternative brain organization after prenatal cerebral injury: Convergent fMRI and cognitive data. *J. Int. Neuropsychol. Soc.* 9, 604–622. doi: 10.1017/S135561770394001X
- Stiles, J., Nass, R., Levine, S., Moses, P., and Reilly, J. (2009). “Perinatal stroke: effects and outcomes,” in *Pediatric Neuropsychology: Research, Theory, and Practice, 2nd Edn*, eds. K. O. Yeates, M. D. Ris, H. G. Taylor, and B. Pennington (New York, NY: The Guilford Press).
- Sullivan, A. W., Johnson, M. K., Boes, A. D., and Tranel, D. (2023). Implications of age at lesion onset for neuropsychological outcomes: a systematic review focusing on focal brain lesions. *Cortex* 163, 92–122. doi: 10.1016/j.cortex.2023.03.002
- Toga, A. W., and Thompson, P. M. (2003). Mapping brain asymmetry. *Nat. Rev. Neurosci.* 4, 37–48. doi: 10.1038/nrn1009
- Umarova, R., and Thomalla, G. (2020). Indirect connectome-based prediction of post-stroke deficits: prospects and limitations. *Brain* 143, 1966–1970. doi: 10.1093/brain/awaa186
- Vaher, U., Ilves, N., Ilves, N., Laugesaar, R., Männamaa, M., Loorits, D., et al. (2023). The thalamus and basal ganglia are smaller in children with epilepsy after perinatal stroke. *Front. Neurol.* 14:1252472. doi: 10.3389/fneur.2023.1252472
- VanRyzin, J. W., Marquardt, A. E., Pickett, L. A., and McCarthy, M. M. (2020). Microglia and sexual differentiation of the developing brain: a focus on extrinsic factors. *Glia* 68, 1100–1113. doi: 10.1002/glia.23740
- Wierenga, L., Langen, M., Ambrosino, S., Van Dijk, S., Oranje, B., and Durston, S. (2014). Typical development of basal ganglia, hippocampus, amygdala and cerebellum from age 7 to 24. *Neuroimage* 96, 67–72. doi: 10.1016/j.neuroimage.2014.03.072
- Williams, C. M., Peyre, H., Toro, R., and Ramus, F. (2021a). Neuroanatomical norms in the UK Biobank: the impact of allometric scaling, sex, and age. *Hum. Brain Mapp.* 42, 4623–4642. doi: 10.1002/hbm.25572
- Williams, C. M., Peyre, H., Toro, R., and Ramus, F. (2021b). Sex differences in the brain are not reduced to differences in body size. *Neurosci. Biobehav. Rev.* 130, 509–511. doi: 10.1016/j.neubiorev.2021.09.015
- Williams, C. M., Peyre, H., Toro, R., and Ramus, F. (2022). Comparing brain asymmetries independently of brain size. *Neuroimage* 254:119118. doi: 10.1016/j.neuroimage.2022.119118
- Xia, C., Zhou, J., Lu, C., Wang, Y., Tang, T., Cai, Y., et al. (2021). Characterizing diaschisis-related thalamic perfusion and diffusion after middle cerebral artery infarction. *Stroke* 52, 2319–2327. doi: 10.1161/STROKEAHA.120.032464

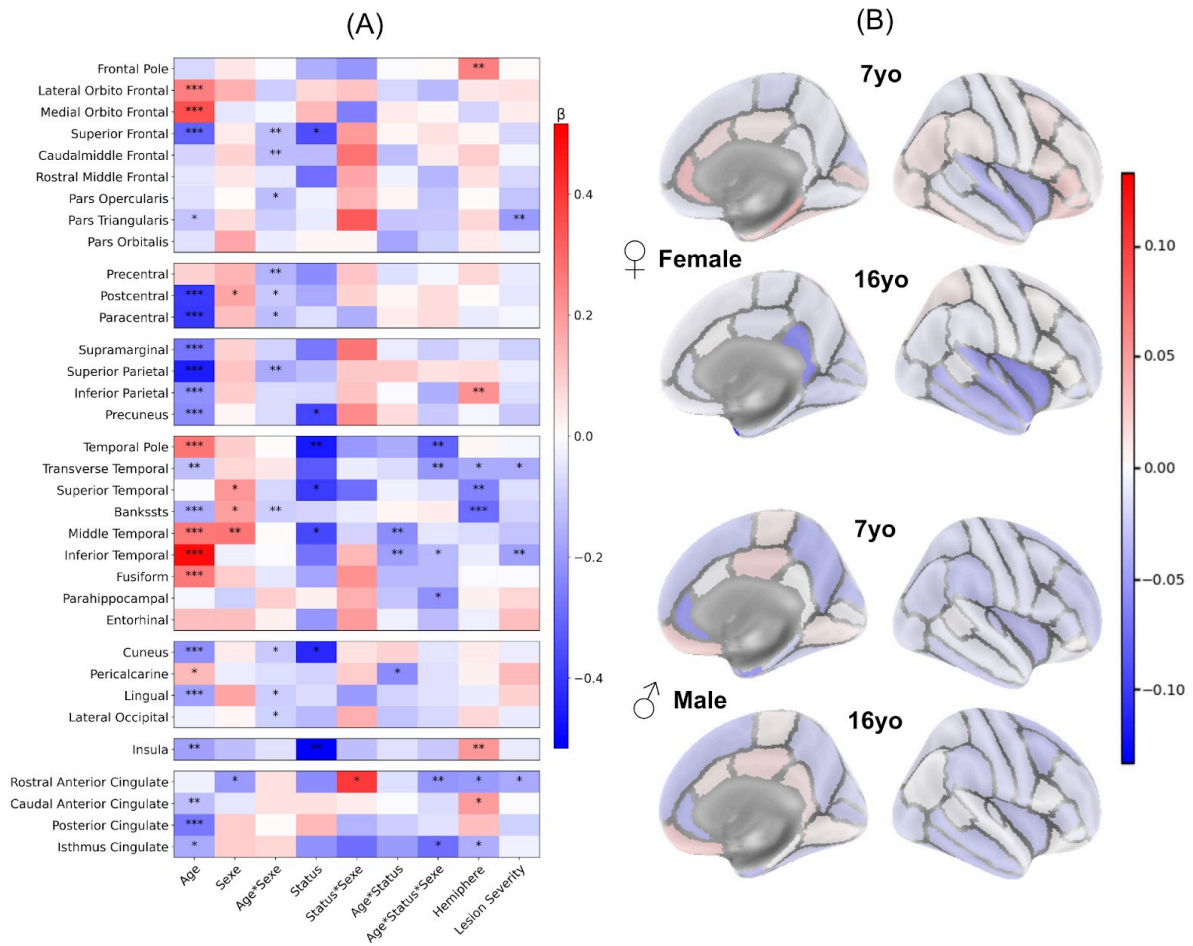


**Supplementary 1 : Parcellation on two lesioned hemisphere.**

Patient 1 misses a superior temporal gyrus. CAT12 parcellation wrongfully affected the superior temporal gyrus label (cyan) to the middle temporal gyrus. This error spreads to the inferior temporal gyrus, identified as the middle temporal gyrus.

Patient 2 misses a superior temporal gyrus, a part of the parietal lobe, precentral gyrus and inferior frontal gyrus. CAT12 parcellation wrongfully affected a part of the occipital lobe as inferior temporal gyrus. In the same manner the precentral gyrus spreads on the rest of the central region, inferior frontal gyrus regions are now labeled on the middle temporal gyrus.

In those two cases, the lobar parcellation, although coarser, is more robust to anatomical deformation due to the lesion, and correctly identifies the lobar boundaries.



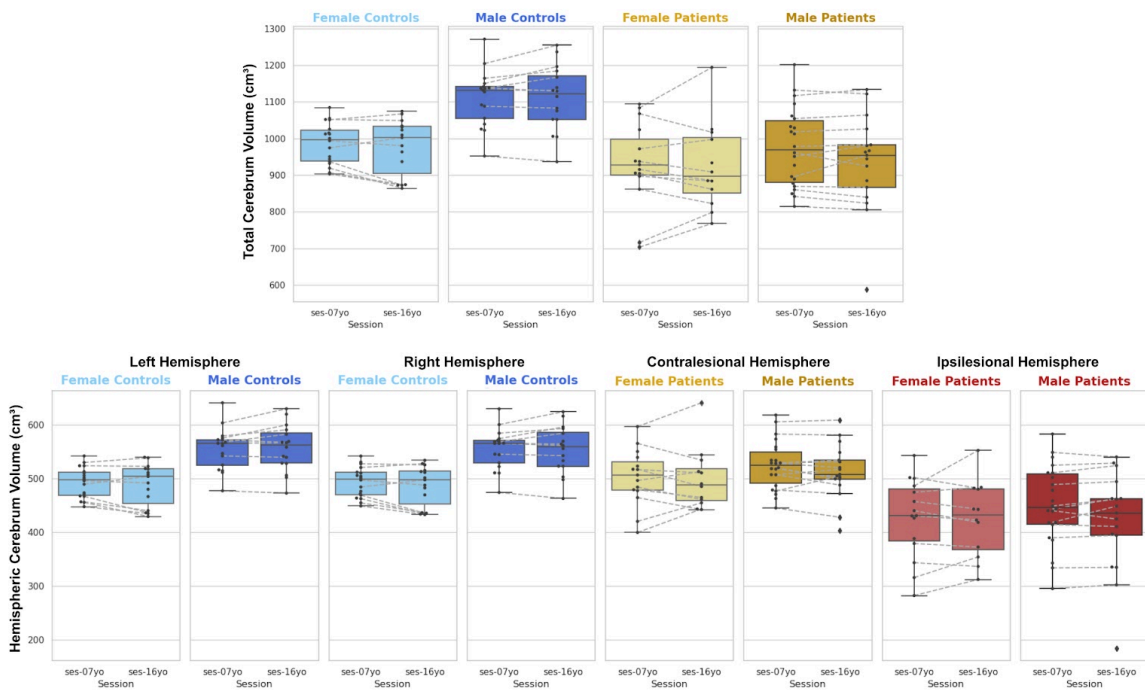
**Supplementary 2 : Contralesional mean thickness of patients compared to controls in 34 ROIs of Desikan-Killiany parcellation : LMM model and post hoc tests**

- (A) LMM coefficients values for each region of the DK40 (fixed effects, main interactions, and covariates). Plotting parameters are the same as in Figure 3
- (B) Post hoc tests comparing patients and control for each age and sex (patient - controls). Displayed p-values are FDR-corrected. Parameters are the same as in figure 4



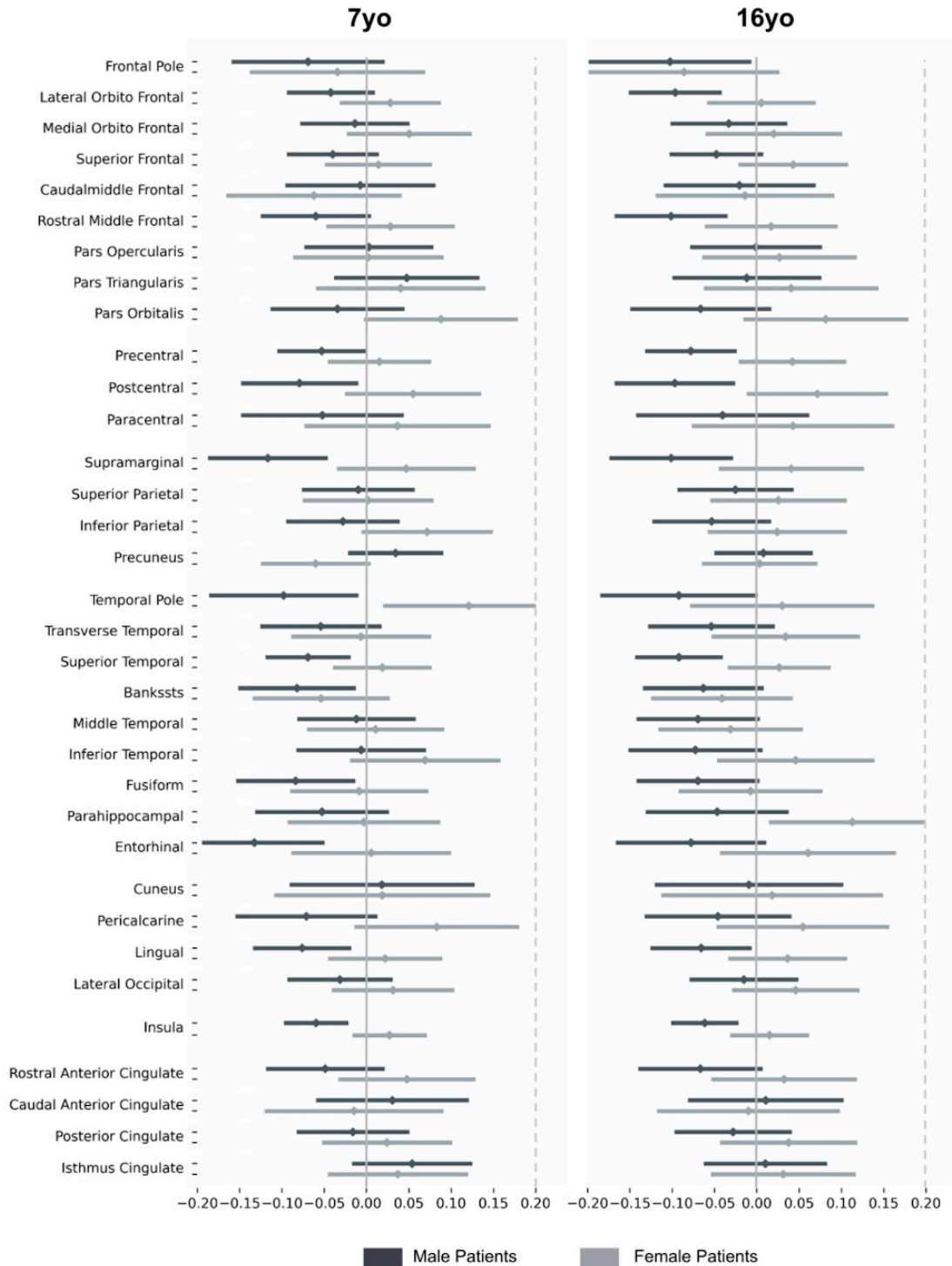
**Supplementary 3 : Contralesional patient to control mean thickness difference (mean and std) for each sex, in 34 ROIs of Desikan-Killiany parcellation. Post hoc t-tests assess if interaction product [(patient-control)male - (patient-control)female] is different from 0.**

Tests are performed on marginal means, hence account for typical male to female differences in the control group. For plotting purpose, volume differences are divided by a mean control thickness across age and sex (relative effect size) for the shown ROI. Upper dark grey lines represent male results, light grey the female ones. \* :  $p < 0.05$  after False-Discovery Rate correction



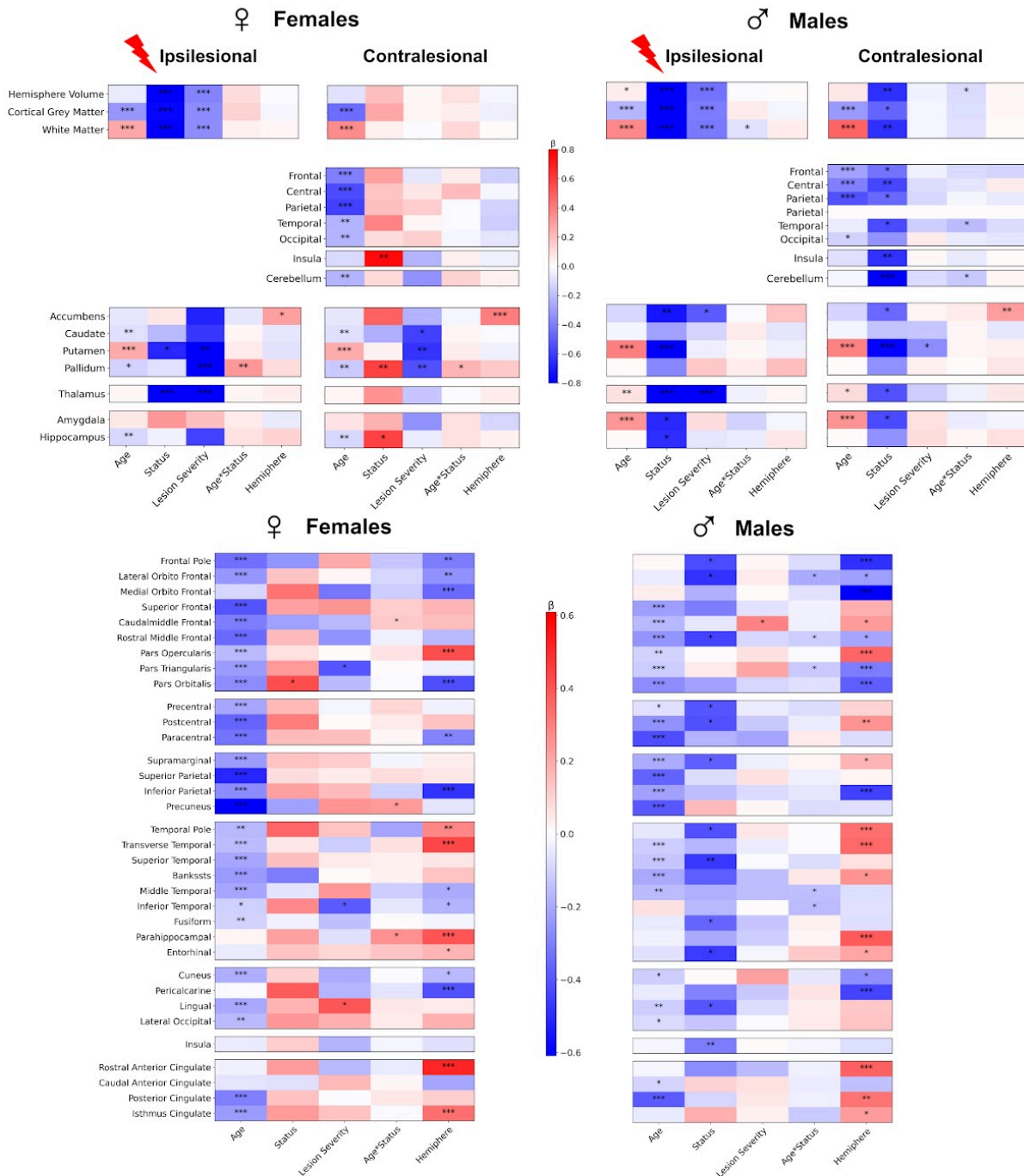
**Supplementary 4 : Raw total brain and hemispheric volume (cerebrum) of the cohort in cm<sup>3</sup> for both acquisition sessions**

The box shows the quartiles of the dataset while the whiskers extend to show the rest of the distribution, except for points that are determined to be “outliers” using a method that is a function of the inter-quartile range. Dotted lines represent longitudinal subjects



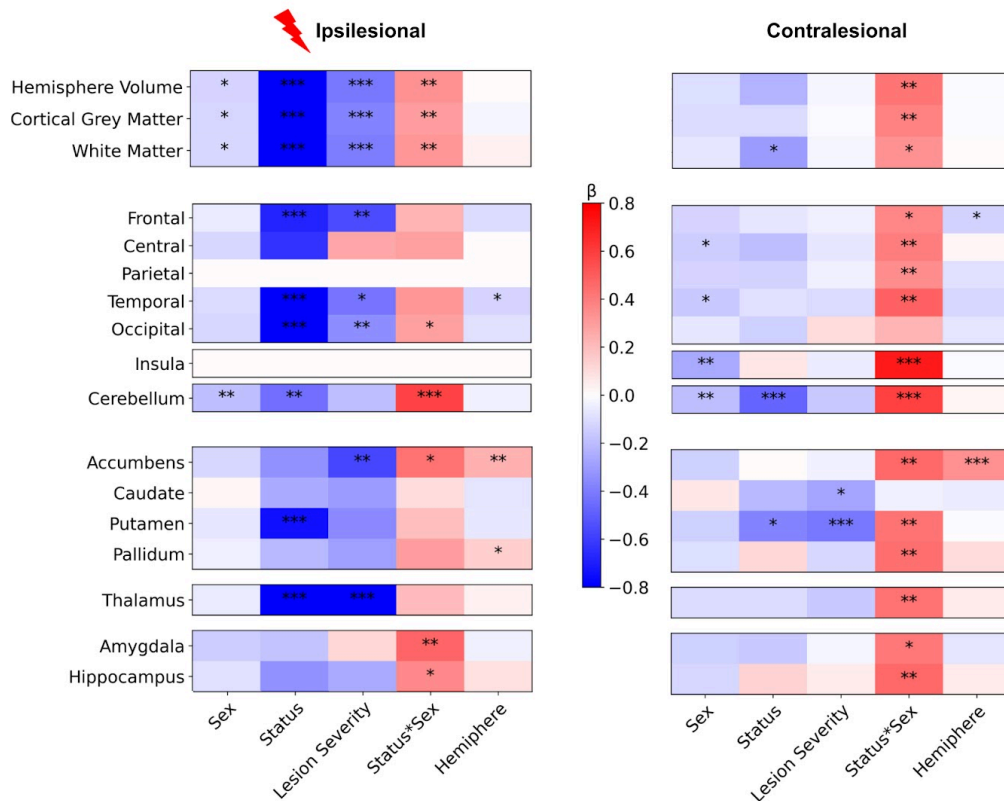
**Supplementary 5 : Contralesional patient to control volume difference (mean and std) for each sex, in 34 ROIs of Desikan-Killiany parcellation. Post hoc t-tests assess if interaction product  $[(\text{patient-control})_{\text{male}} - (\text{patient-control})_{\text{female}}]$  is different from 0.**

Test are performed on marginal means, hence it account for typical male to female differences in the control group. For plotting purpose, volume differences are divided by a mean control thickness across age and sex (relative effect size) for the shown ROI. Upper dark grey lines represent male results, light grey the female ones. \* :  $p < 0.05$  after False-Discovery Rate correction



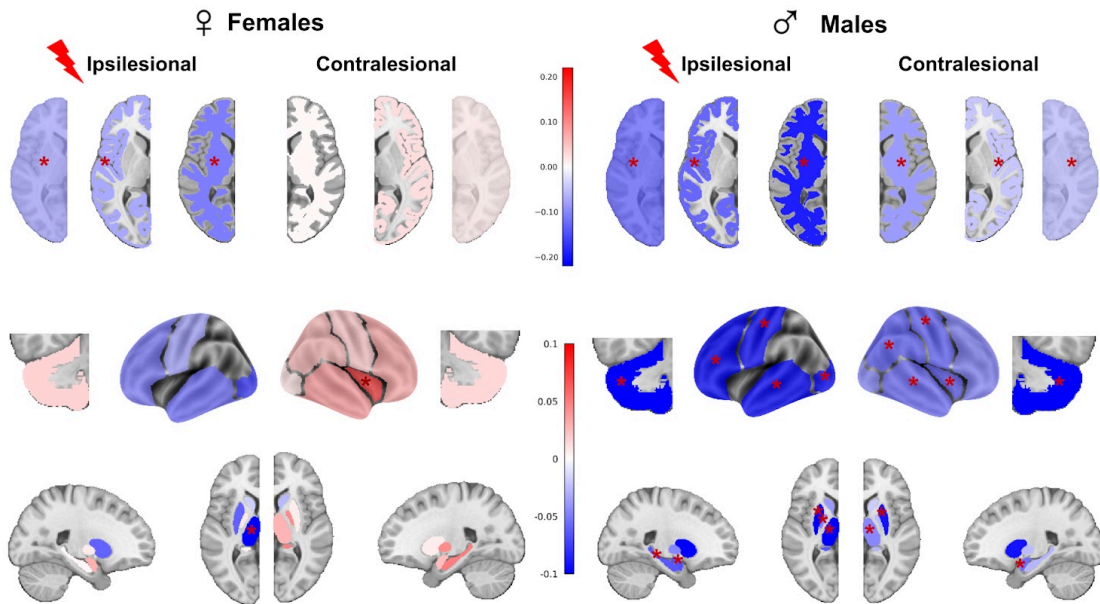
**Supplementary 6 : Factors values for all regional volumes (fixed effects, main interactions and covariates), for LMM fitted individually on male and female group**

Coefficients are expressed as a proportion of the region volume standard deviation (std). The reference population is the 7 years old control group. Hemisphere variables is coded using “effect coding”, being positive in females and in the right hemisphere. Lesion severity is modelled by a centered 5 level continuous covariate. (see Material and Method, Statistical Analysis). Ipsilesional whole hemisphere metrics comprise lesion volume. \* :  $p < 0.05$ , \*\* :  $p < 0.01$ , \*\*\* :  $p < 0.001$  (uncorrected)



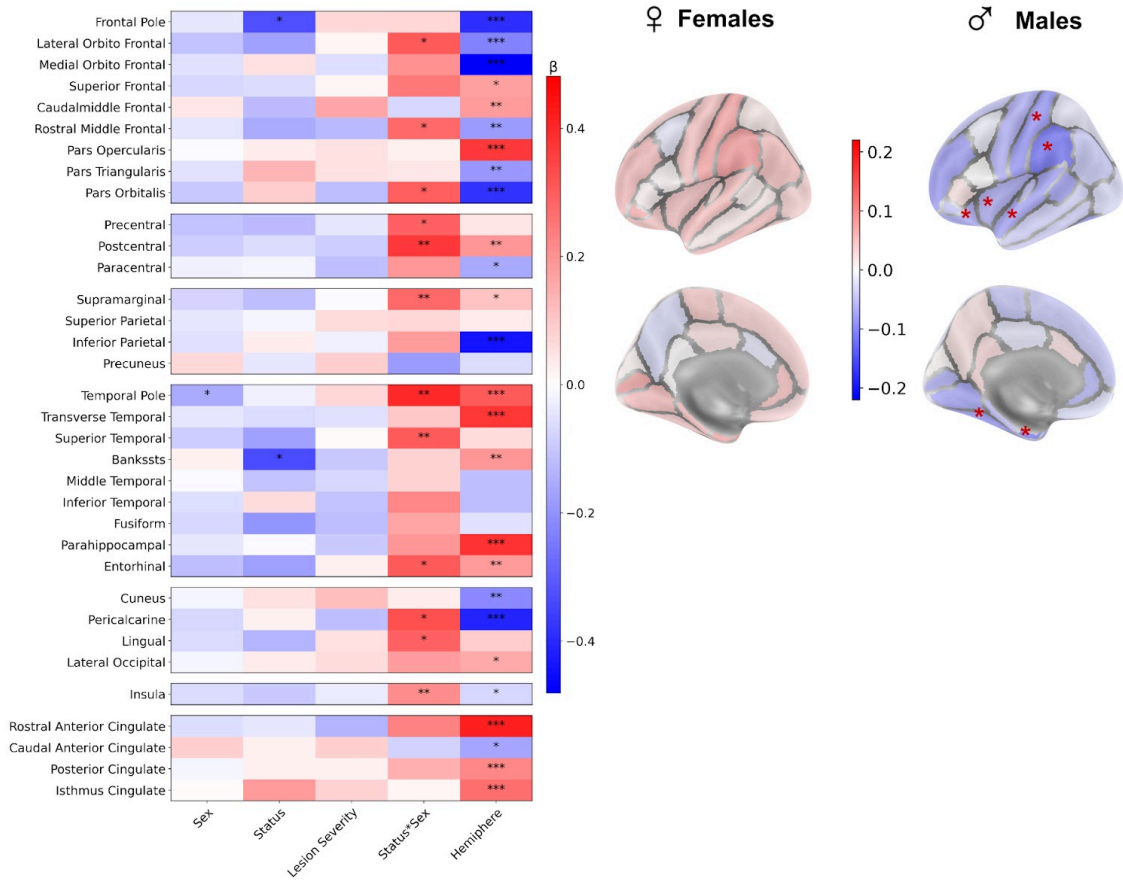
**Supplementary 7 : Factors values for all regional volumes (fixed effects, main interactions and covariates), for LMM fitted on residualized data for Sex and Age**

Coefficients are expressed as a proportion of the region dataset standard deviation (std). Sex and Hemisphere variables are coded using “effect coding”, being positive in females and in the right hemisphere. Lesion severity is modelled by a centered 5 level continuous covariate. (see Material and Method, Statistical Analysis). Ipsilesional whole hemisphere metrics comprise lesion volume. \* : p<0.05, \*\* : p<0.01, \*\*\* : p<0.001 (uncorrected)



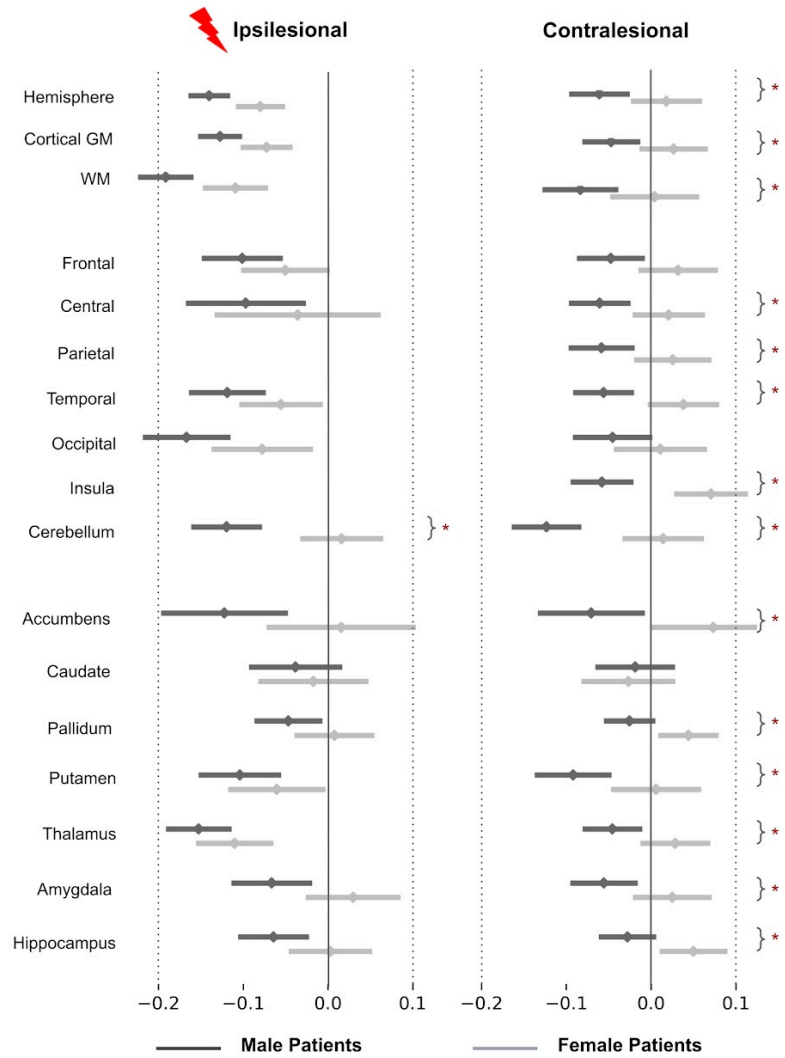
**Supplementary 8 : Post hoc t-tests comparing patients and control volume for each sex (patient - controls) for LMM residualized for Age and Sex effect beforehand.**

Post-hocs tests comparing controls to patients volume marginal means. For plotting purpose, volumes differences are divided by a mean control volume across age and sex (relative effect size) for the shown ROI. Cold colours represent a negative difference (smaller mean regional volume in patients than in controls); warm colours represent a positive difference (bigger patient volumes comparing to controls). \* :  $p < 0.05$  after False-Discovery Rate correction



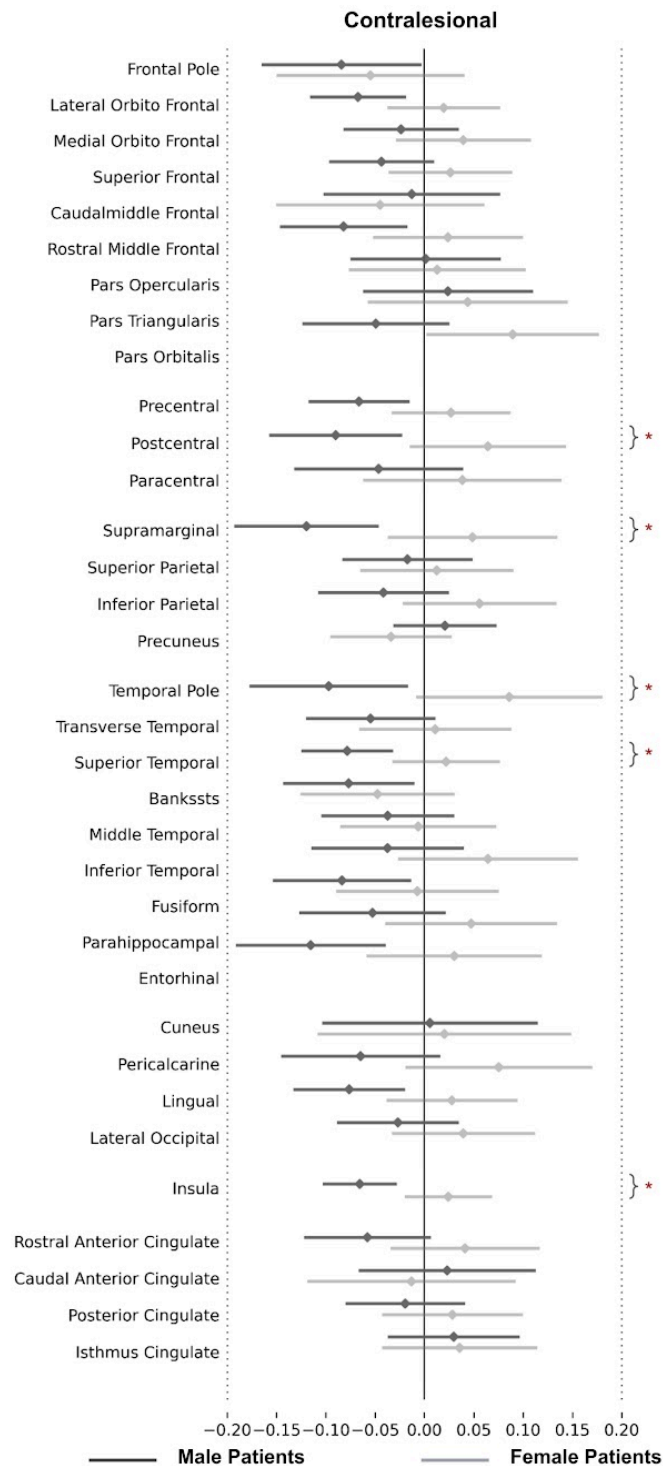
**Supplementary 9 : Contralateral volumes of patients compared to controls in 34 ROIs of Desikan-Killiany parcellation : LMM fitted on residualized data for Sex and Age and post hoc tests**  
 Patient volumes are compared to the mean of both hemispheres corresponding values in controls.

- LMM coefficients values for each region of the DK40 (fixed effects, main interactions, and covariates). \* :  $p < .05$ , \*\* :  $p < .01$ , \*\*\* :  $p < .001$ . Plotting parameters are the same as in Figure 3
- Post hoc tests comparing patients and controls for each age and sex (patient - controls). Displayed p-values are FDR-corrected (\*  $< 0.05$ ). Parameters are the same as in figure 4



**Supplementary 10 : Patient to control volume difference (mean and std) for each sex. Post hoc t-tests assess if interaction product  $[(\text{patient-control})_{\text{male}} - (\text{patient-control})_{\text{female}}]$  is different from 0.**

Tests are performed on marginal means, hence account for typical male to female differences in the control group. For plotting purpose, volume differences are divided by a mean control thickness across age and sex (relative effect size) for the shown ROI. Upper dark grey lines represent male results, light grey the female ones. \* :  $p < 0.05$  after False-Discovery Rate correction



**Supplementary 11 : Contralesional patient versus control volume difference (mean and std) for each sex in 34 ROIs of Desikan-Killiany parcellation. Post hoc t-tests assess if interaction product [(patient-control)male - (patient-control)female] is different from 0. Test is performed on marginal means, hence it account for typical male to female differences in the control group.**

Tests are performed on marginal means, hence account for typical male to female differences in the control group. For plotting purpose, volume differences are divided by a mean control thickness across age and sex (relative effect size) for the shown ROI. Upper dark grey lines represent male results, light grey the female ones. \* :  $p < 0.05$  after False-Discovery Rate correction.

### 3. Complementary discussion

In this section, we delve deeper into supplementary considerations related to the article. We detailed alternative statistical approaches confirming that the sex differences observed are specific to the patient population. We also discuss how we appropriately correct for typical sex differences given our study design and constraints. This is part of supplementary materials in the Journal, in response to a reviewer concern.

#### 3.1. Whole brain volume correction bias in morphometric analyses

Whole-brain or intracranial volumes are often used as regressors in morphometric analyses that are looking for spatially specific effects. However, in the case of our cohort, whole-brain volume measures are impacted by lesion cavity and extent, and total intracranial volume results from both lesion extent and reduced growth due to the lack of biomechanical pressure during brain growth in the lesioned area. Our first results show that non-lesioned hemispheres are also impaired (see Article, Figure 4), as visible in raw data (see Supplementary material 4). By including one of these volumes in our analysis, we would have added a variable that is covariant with the status effect. By choosing to compare each region independently without including total brain volume, we lost some sensitivity but avoided biasing the analysis. Our model therefore does not aim at directly testing the regional specificity of the volumetric effects compared to brain volume evolution. However, the figures and plotting format enable to directly compare the relative amplitude of a regional volume variation in proportion to its contralesional hemisphere volume variation.

#### 3.2. Confirming That Sex Differences Are Specific To Patients

The [(patient – control) male – (patient – control) female] contrast on the fitted model and its suitability for assessing sex differences in patients while controlling for typical sex differences in brain volume can be questioned. In this study, we ensured to adequately manage sex-related brain size differences by performing this contrast on the model marginal means, hence the mean volume estimated by the model, which encompasses sex effect estimation. However, we also performed two complementary analyses :

Fitting separate models for male and female populations. We fitted a Linear Mixed Model (Age \* Status + Hemi\_side + Lesion Severity + (1|participant\_id)) on each sex subgroup independently for the contralesional hemisphere. Our analysis confirmed several brain areas where the volume was significantly lower in male patients but not in female patients (see Supplementary Material 6). This approach confirms our results shown in figure 3 and 4 of the paper but does not allow for direct comparison of sex-related brain volume differences.

Residualizing the data beforehand for age and sex effects, then evaluating the pathology effect on data that has been corrected for these effects. We first fitted a classic Generalized Linear Model (GLM) (Age \* Sex) on the data. We ensured for each volume that the mean and variance of the residuals were equivalent between sexes on the whole cohort. We then fitted a Linear Mixed Model (Sex \* Status + Hemi\_Side + Lesion severity + (1|Participant\_id)) on the residuals. This approach ensured that all volumes were corrected for age and sex differences on the whole cohort before testing for status effects. The

sex\*status interaction in this residual model was of the same amplitude and significance as in the original model (see Supplementary Material 7 and 9). We also performed the same post hoc tests as in the article and obtained similar results (see Supplementary Material 8, 10 and 11). Although this approach is less subtle and more susceptible to overfitting, it strongly confirms our findings while explicitly addressing non-specific volume differences. We still observed a significant residual sex effect in some brain regions. This arises because, even after accounting for age and sex differences at the level of the whole cohort, male patients tend to have lower brain volumes compared to male controls, while female controls tend to have lower brain volumes compared to female patients. As our model uses the control group as the reference group, the effects we observe are relative to the controls. This tendency is therefore consistent with our previous observations and the results of post hoc tests (see Supplementary Material 8, 10 and 11).

These complementary analyses confirm there is a sex difference in the post-NAIS growth, whereby male patients exhibit lower contralesional volumes than male controls, while females do not show such a reduction, but contralesional volumes similar to female controls.

### 3.3. Methodological considerations

#### 3.3.1. Quality Control in Scanner-Biased Longitudinal Data

When analyzing a longitudinal dataset, it is crucial to use a quality metric enabling to reliably assess image quality and understand potential imaging biases or correlations between subject status and artifacts, despite the use of different scanners at 7 and 16 years of age. Based on a benchmark study in the literature [source], we chose the Euler number, automatically computed during CAT12 segmentation, as our Quality Check (QC) metric. Figure 5 illustrates the Euler number computed for all T1-weighted images from both sessions (7 and 16) and compares it with another quality metric, the Image Quality Ratio (IQR), also automatically computed by CAT12. We analyzed the distribution of these metrics across sessions and subject status. The Euler number demonstrated greater independence from session effects (i.e., scanner and resolution differences). Based on these visualizations, we identified outliers, primarily patients at 7 years of age, and excluded low-quality or motion-affected images from our analysis. Images at the far end of the distribution are considered to be at-risk images and were investigated with regard to visual inspections and segmentation quality and excluded individually.

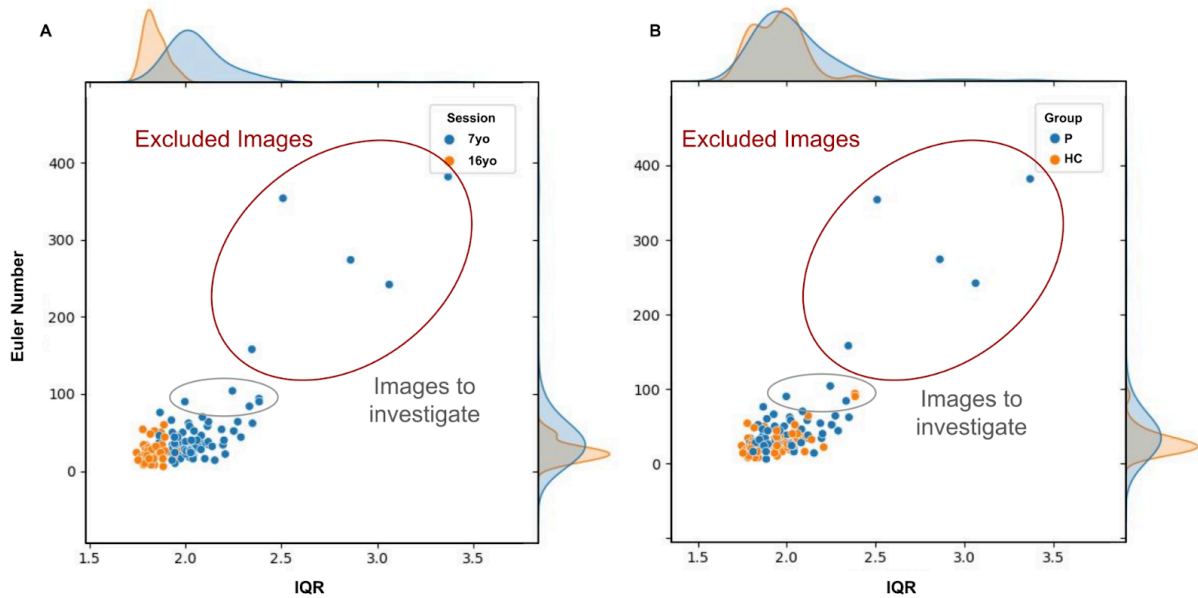


**Figure 5: Euler Number and IQR distribution the AVCnn cohort**

- **A : Metric distribution depending on acquisition session.**
- **B : Metric distribution depending on subject status (patient/controls)**

### 3.3.2. Deformation-based Morphometry

Deformation-based morphometry analysis leverages highly precise intra-subject registrations to extract local deformations and assess brain growth, even in lesioned hemispheres, using the registration process between ages 7 and 16. This approach was the first we used to explore morphometric variations, as it quite straightforwardly used our registration optimization efforts and allowed us to make early visual observations on morphometric changes depending on subject status (patient/control) and sex. The presented parts were parts of the results shown during the OHBM 2022 poster session in Glasgow.

We expected to observe variations in gray matter, due to sex differences in developmental trajectories (Bethlehem et al., 2022), as well as local variations in gray and white matter for patients, mostly mirroring lesion trajectory and connectivity.

We employed ANTs registration with a cross-correlation similarity metric at each registration step and a registration mask that included brain extraction and lesion masking. Figure 6 presents the Jacobian determinant values for each voxel, averaged for controls, right-lesion, and left-lesion patients, registered in the MNI symmetric template. The Jacobian values exhibited typical patterns of gray matter reduction (blue) and white matter increase (red) between ages 7 and 16. We masked these determinants using gray and white matter masks and conducted comparisons between controls and hemispheres, and between contralesional and ipsilesional hemispheres (Figure 7).

As expected, white matter volume increased between 7 and 16 years (positive Jacobian determinant) and male systematically had a bigger white matter increase than females. This trajectory divergence is known and shown by latest normative modeling of typical brain growth (Bethlehem et al., 2022; Rutherford et al., 2022). Although the white matter Jacobians were lower in the ipsilesional hemisphere, the difference between patient

and control hemispheres was not significant, notably due to the small number of subjects included in the analysis.

Unexpectedly, gray matter Jacobians were positive for most subjects, mainly due to positive Jacobian determinants of white matter overlapping with cortical gray matter in sulci. Although a sex-dependent pattern, echoing typical developmental patterns, was also visible, we chose to abandon this approach due to the lack of spatial specificity of this method.

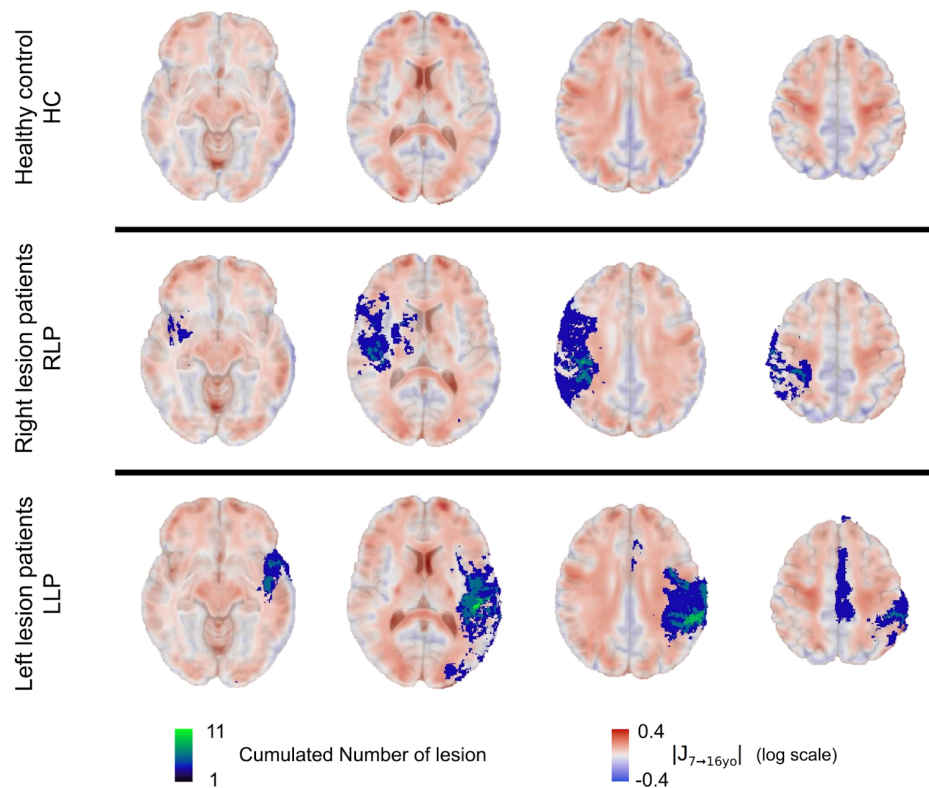


Figure 6: Mean Jacobian Determinant of the deformation field between 7 and 16 years old (logarithmic scale)

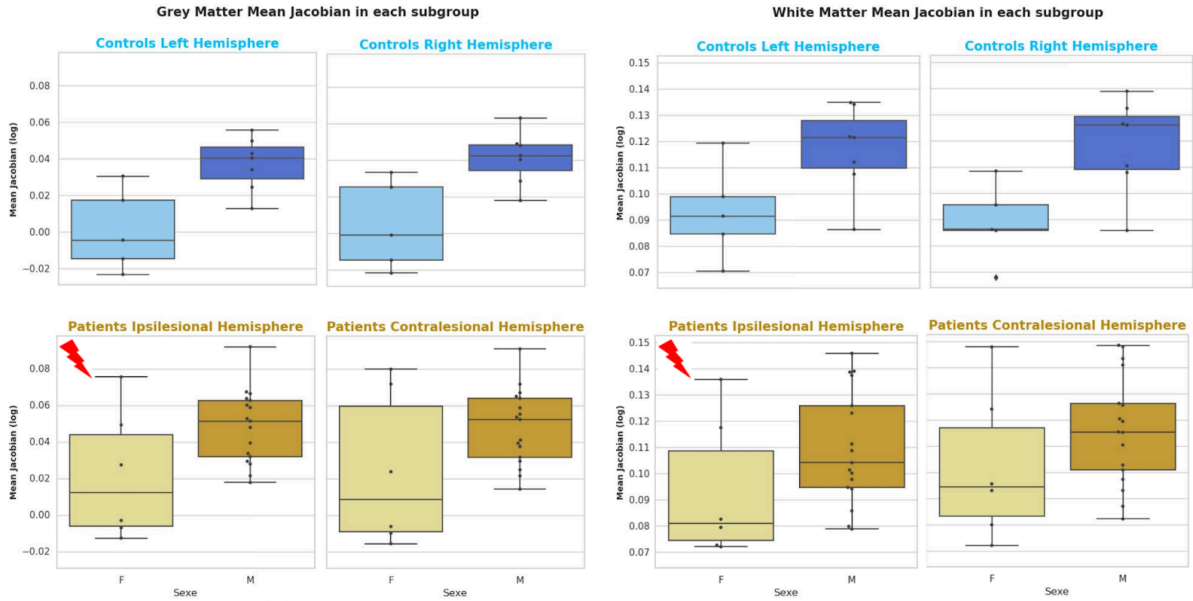


Figure 7: Mean Jacobian Determinant of the deformation field between 7 and 16 years old (logarithmic scale), for each tissue type and hemisphere

### 3.3.3. Using Surface Parcellation for Volumetric Analysis

When approaching morphometry variations as a proxy of brain tissue microstructural changes, volume and surface metrics variations might have different sensibility to microstructural variations. To allow comparison between different metrics, we needed to investigate these metrics at the same spatial granularity. Among the parcellation methods available in CAT12, there is no direct equivalent for comparing volume and surface parcellations, limiting our direct comparison capacities. To solve this issue, we had to convert an atlas from one space to another, either from volume to surface or surface to volume. As surface parcellation relies on surface inflating and sulci registration, instead of conventional deformation-based registration for volume parcellation, it is often more precise and less susceptible to local deformations and local errors. This makes surface to volume projection more reliable for high granularity parcellation such as DK40 parcellation, although not suitable for ipsilesional parcellation. We reviewed the literature on studies that analyze volumes using the Desikan-Killiany (DK40) parcellation (Yaakub et al., 2020), (Jao et al., 2021), (Potvin et al., 2017). Most studies align native surface mesh and project the surface atlas into volume space, using different tools.

We initially computed the volume in Desikan-Killiany atlas by multiplying vertex-wise thickness by the surface. Note that vertex surface computation is not implemented per se in CAT12. It is accessible only using expert mode and batch hidden options, and does not work properly with ROI Based Morphometry functions.

As a complementary investigation, we compared our approach with a surface projection we had performed using the central surface in the fsaverage32K mesh in native space to native grey matter probability maps. Figure 8 presents the comparison between both approaches for each subject and region in the DK40 parcellation. The volumes computed by both methods were highly correlated and yielded similar results, indicating that

both approaches are suitable for surface and volume morphometry analysis. In the published article, we utilized projected volumes as regional volumes.

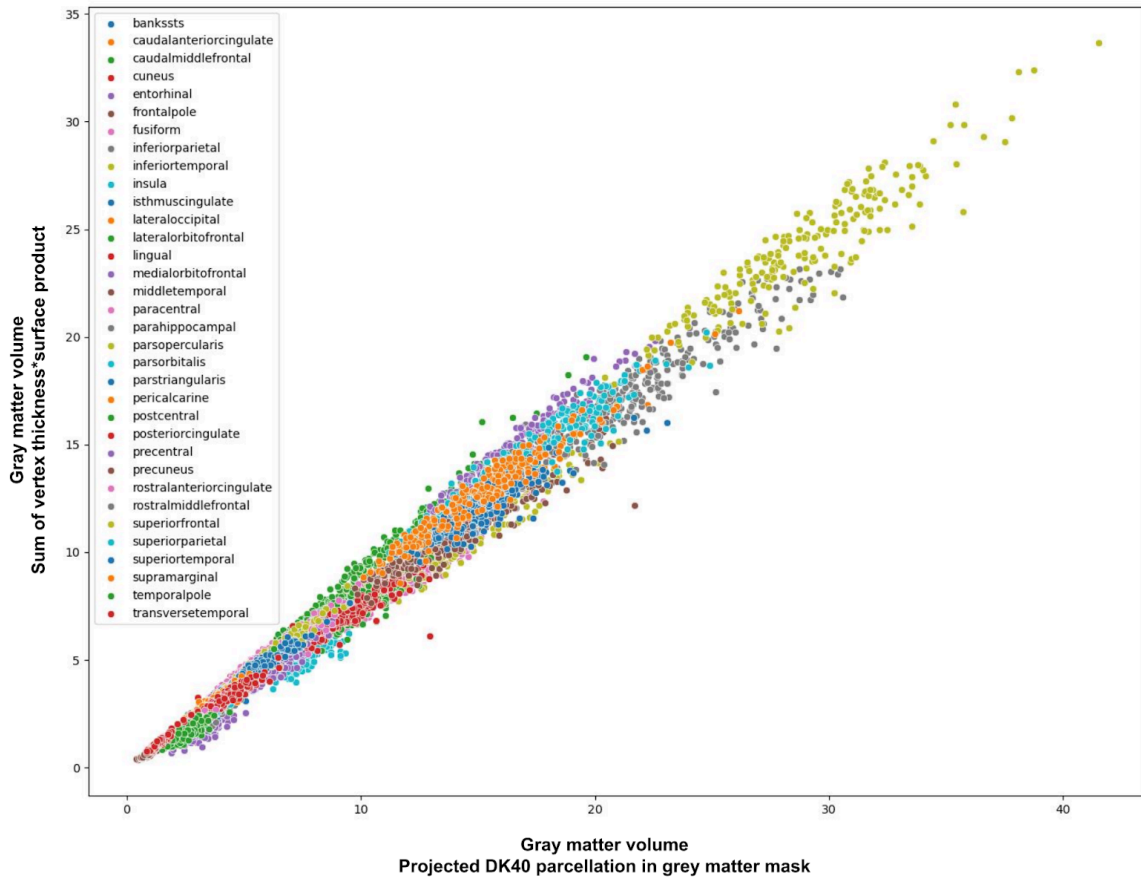


Figure 8: Grey matter volume for each subject and each DK40 regions, Computed with two different methods:

DK 40 projection into native space gray matter mask (x-axis)

Vertex-wise sum of thickness \* surface product (y-axis)

### 3.3.4. Exploration of cortical thickness with Threshold-Free Cluster Enhancement (TFCE)

The observed effect sizes in cortical thickness variations between groups were not large enough relative to intrinsic data dispersion. This could relate to multiple reasons :

- Desikan-Killiany Atlas Limitations: The parcellation provided by the Desikan-Killiany atlas may be too coarse to capture subtle and localized thickness variations, averaging dynamic changes in some areas with other regions that vary in the opposite direction or do not vary at all within the considered age range.
- Multiple Comparisons Correction: The numerous regions investigated necessitate corrections for multiple comparisons, which reduces sensitivity. We were constrained to use correction methods that are not ideally suited to the specificities of our data.

To enhance our analysis of cortical thickness of the contralesional hemisphere, we explored an alternative approach to address the limitations of our ROI-based analysis, detailed in the article. We thus employed the TFCE toolbox within CAT12 to further investigate cortical thickness variations in our cohort. We designed a 4x2 ANOVA model

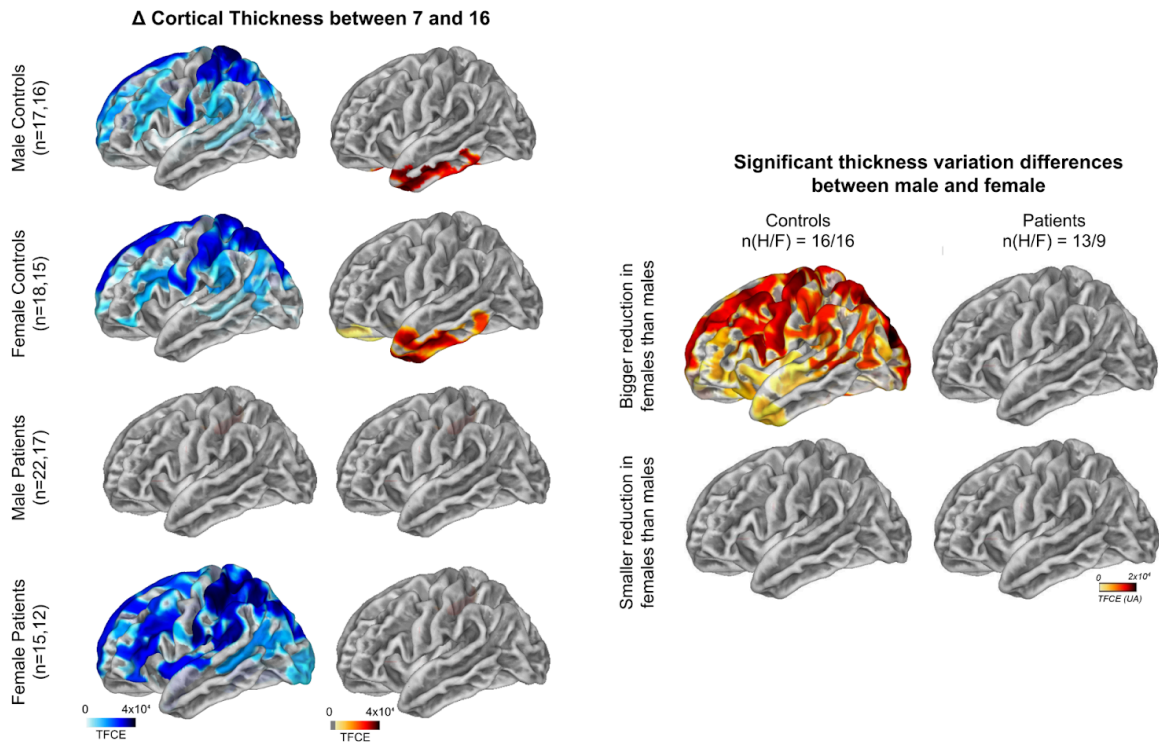
where Session, Sex, Status, and Hemisphere Side were encoded with two levels for each variable. All surfaces were computed in the fsaverage 32K template, ensuring vertex-to-vertex correspondence between right and left hemisphere meshes (symmetric atlas).

Figure 9 displays the TFCE results of cortical thickness, expressed in TFCE metric thresholded for  $p > 0.05$  and FDR corrected.

The left panel (A) shows the cortical thickness variations between ages 7 and 16 in typical boys and girls, in left and right hemispheres in controls, and in the contralesional hemisphere only in patients. Red color displays regions where gray matter cortical thickness increases between 7 and 16, whereas blue color shows regions where cortical thickness decreases in this age range. Controls showed consistent results between males and females, with a reduction in cortical thickness almost everywhere except in the occipital gyrus and an increase in the inferior temporal gyrus and temporal pole, this is consistent with normative modeling literature on cortical thickness (Bethlehem et al., 2022; Frangou et al., 2022). In the contralesional hemisphere of patients, female patients exhibited a pattern close to controls, though with some cortical thickness reduction in the occipital lobe and no increase in the temporal lobe. Male patients, however, showed no significant changes between 7 and 16 years of age, confirming our results on a morphometric deviation between male and female trajectory in the contralesional hemisphere.

The right panel (B) directly compares the amplitude of age-related cortical thickness variations between males and females for both controls and patients longitudinally. The results showed a bigger reduction in female than male controls in all regions that exhibited cortical thinning between 7 and 16. By contrast, no significant differences were found between male and female patients, probably due to a lack of statistical power regarding the variability of our data.

Given that the hemisphere side had a substantial and composite effect size in both volume and thickness assessments in our article, we performed similar tests while separating the right and left hemispheres. No test reached significance when separating hemispheres, neither in the presented results nor in further comparisons of patients versus controls differences. While these results indirectly support morphometric differences between male and female patients, our statistical power was insufficient for deeper analysis. This is likely due to the inability of our design in performing longitudinal statistical analysis or in regressing qualitative nuisance variables.



**Figure 9:**

**A. Cortical thickness (CT) changes between 7 and 16 years of age in males and females of both groups (controls and patients) assessed with TFCE (CAT12). Decreases of CT in blue, increases in red.**  
**B. Cortical thickness difference amplitude comparison between male and female for both group**

## 4. Final Conclusion

This chapter illustrates the complexity and the diversity of approaches we tested to adequately study brain morphometry, accounting for both developmental factors and specific NAIS factors. This complexity necessitated tailored image processing and statistical methods to properly control for confounding variables and accurately address NAIS outcomes.

Despite the careful selection and design of these methods, many approaches lacked statistical power, primarily because of the small and multifactorial effect size of the investigated phenomena. A larger sample size would be required to explore these effects comprehensively. However, these avenues of investigation and improvement request meticulous quality control beforehand, as the pathology involved makes image processing highly susceptible to errors and distortions at every stage.

Some morphometry metrics, such as the gyrification index and surface area, were not investigated in this study primarily due to the absence of specific hypotheses regarding these measures. Additionally, time constraints were a factor, as this image preprocessing and morphometry analysis took over almost 2 years, while the project intended to also explore functional aspects of brain plasticity using multiple imaging modalities.

# Chapter 3 : Exploration of functional and structural brain connectivity and their relationship with clinical and language outcomes after a neonatal stroke

## 1. Introduction

In most adults, language processing is strongly lateralized to the left hemisphere, a phenomenon that occurs in both right and left handers (99% of right-handed and 75% of left-handed individuals) (Knecht, Deppe, et al., 2000; Knecht, Dräger, et al., 2000; Szaflarski et al., 2002, 2006) and regardless of whether the language is spoken or signed (MacSweeney et al., 2008; Newman et al., 2015; Petitto et al., 2000). Consequently, a stroke affecting the left frontotemporal cortex in adults typically results in lifelong language impairment (Martin et al., 2023). However, in the case of neonatal stroke, despite the frequent involvement of this region, language is often only mildly impaired, and the extent of impairment is significantly less severe than that observed in adults (Trauner et al., 2013).

Recent advances in neuroimaging, particularly functional MRI (fMRI), have provided greater insight into the recovery mechanisms underlying this phenomenon. These advances have illustrated a shift in language processing lateralization, with homotopic regions in the right hemisphere being recruited to compensate for the damaged left hemisphere language networks (François et al., 2021; Martin et al., 2023).

The benefit of this atypical lateralization is still a matter of debate. On one hand, language recovery and development are critical milestones for cognitive growth and social adaptation. Thus, the minimal long-term language impairment following a neonatal arterial ischemic stroke (NAIS) may serve as the foundation for nearly typical cognitive and social development, despite the loss of brain matter and connectivity. On the other hand, the early development of language function in the right hemisphere may lead to spatial competition within the impaired brain, potentially affecting the development of other functions. This phenomenon, known as the "crowding effect" (Lidzba et al., 2006), may partially account for the more diffuse and generalized impairments observed following early-onset stroke (Sullivan et al., 2023).

The implication of atypical language lateralization remains superficially investigated, especially its intertwinement with other functional and microstructural development. In the following chapter, we present the first steps of our ongoing exploration of brain functional and structural connectivity alteration depending on language lateralization after NAIS in the AVCnn cohort at 16 years of age.

### 1.1. Main Hypothesis and experimental plan

We first investigated the language lateralization in the AVCnn cohort, and used it as a new cohort stratification. We investigated the sentence processing activation pattern for patients depending on their language lateralization and verified the homotopy of atypical lateralization regarding typical one. We finally studied the relationship between language lateralization and clinical outcomes.

In a second part we investigated the “crowding effect” hypothesis, hence the impact of language lateralization on other functional spatial and functional development, with an emphasis on mental calculation.

## 1.2. Known functional patterns for sentence processing and calculation tasks

Language network regions typically involved in sentence processing tasks are described in chapter 1, section 2.2.2.1. They encompass both middle and superior temporal gyrus, as well as left inferior frontal gyrus, precentral gyrus, SMA and preSMA, and left angular gyrus.

Although less extensively studied than language network, calculation tasks usually involves, inferior parietal lobule (Cantlon et al., 2006; Davis et al., 2009; Dehaene & Cohen, 2007), with a right dominance for number tasks and a left dominance for calculation task (Arsalidou et al., 2017), left claustrum, the cingulate gyrus extending medially from superior frontal and medial frontal gyrus.

Overall, overlapping regions between calculation and language are task-dependant, and conjunction analysis exhibited mostly small areas in superior frontal cortex and intraparietal sulcus (Amalric & Dehaene, 2016) or posterior cingulate, precuneus, and inferior parietal lobe (Arora et al., 2020), although inconsistently shown in the current state of the literature. Sentence processing network is activated in the same way for math and non-math sentences (Amalric & Dehaene, 2019).

## 2. Material and Methods

### 2.1. Participants

This study focused on the 16-year-old cohort. For a more detailed description, please refer to Chapter 1 section 4. Preliminary exclusions based on lesion territory were applied similarly to those in the morphology study, resulting in a population of 31 patients (15 females, 16 males) and 31 controls (16 females, 15 males).

### 2.2. Image acquisition

#### 2.2.1. Imaging procedure

The detailed imaging protocol can be found in Chapter IV, Subsection 5 of the Introduction. The scans were performed using a Siemens MAGNETOM Prisma fit system equipped with a 64-channel head coil.

Functional MRI tasks were acquired using a consistent sequence: 2 mm isotropic voxels size, 69 slices, a repetition time (TR) of 1.81 seconds, an echo time (TE) of 30.4 milliseconds, with 3 simultaneous multislice acquisitions and a partial Fourier factor of 7/8.

Diffusion-weighted SE-EPI images included two acquisitions,  $b=1,000$  s/mm<sup>2</sup>, 30 diffusion encoding directions, and  $b=1,500$  s/mm<sup>2</sup>, 60 diffusion encoding directions. Each acquisition was preceded by a reverse phase encoded  $b_0$  images. Other acquisition parameters were the same for both images, 78 slices, TR = 4,12 seconds, TE = 55 milliseconds, and a voxel resolution of  $1.8 \times 1.8 \times 1.8$  mm

#### 2.2.2. Functional MRI paradigms

Sentence Generation Task (SGT) :



Localizer :

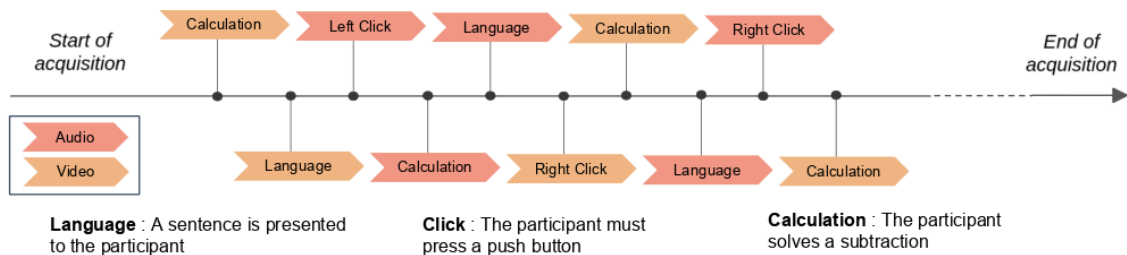


Figure 10: Experimental paradigm deployed for the AVCnnADO activation fMRI

The subjects were presented with two tasks (Figure 10):

Sentence Generation Task (SGT): This task was presented once in a block design format. Subjects were successively presented orally five concrete words (one every 5 seconds), with which they were required to construct a simple sentence. Alternatively, the word "rest" was presented five times while the subject maintained a resting state. This coarse language paradigm has been demonstrated to be highly robust in assessing language processing in cognitively impaired subjects. The primary reason for its effectiveness is that severely impaired children were allowed to create sentences using simple phrases such as "I like/I don't like" if they encountered difficulties. Average acquisition time is ~4.5 min.

The contrast investigated for the Sentence Generation Task compared the brain response evoked by sentence generation (language) to the response evoked by a passive auditory stimulus (rest).

"Localizer" Task: This task was a slower version (one stimulation every 5 seconds) of a previously published experimental paradigm (Pinel et al., 2007), in order to make it more accessible to children, especially those with cognitive impairments. Subjects were presented with a sequence of tasks involving passive language processing (short sentences composed of a subject, verb and object), subtraction (positive results, with numbers < 20), and 3-time push-button pressing, all instructions being presented in both visual and auditory modalities. The sequence length and delay were designed to identify specific functional areas activated by each task. Average acquisition time is ~4.65 min.

The following contrasts were examined :

- Right vs. Left Hand motor Activation: This contrast allowed for a rapid assessment of upper limb functional organization.
- Audio vs. Video: This contrast compared the brain's response when the subject received auditory stimuli versus visual stimuli, regardless of the specific content of the stimuli.
- Language vs. Calculation: This contrast compared the brain's response during language input processing versus when the subject was asked to solve a subtraction problem.

All tasks were required to be performed silently hence we could not control whether they were correctly performed.

## 2.3. Image preprocessing

### 2.3.1. Image preprocessing and Quality control

Functional Image quality metrics were extracted using MRIQC (Esteban et al., 2017), and images were preprocessed with fMRIPrep (version 22.1.1) (Esteban et al., 2019). The preprocessed images, stimuli, and movement matrices were then used to perform first-level analyses (Statistical parametric maps computation indicating the level of activation for each voxel in the brain for each individual) with Nilearn (Python version 3.10, Nilearn version 0.10.4).

Outliers in the MRIQC group report were pre-identified based on a set of quality metrics, following MRIQC guidelines. These metrics included the Entropy Focused Criterion (EFC), Framewise Displacement (measured in percentage and time points), temporal Signal-to-Noise Ratio (tSNR), and Ghost to Signal Ratio (GSR). We investigated task-movement correlations and whether movement affected the overall performance of the first-level analysis.

Based on these criteria, one control subject and one patient were excluded from the individual and group analysis based on the SGT. Final group composition was 30 controls (14F/16M), 14 typical (5F/9M), 16 atypical (8F/8G) language lateralized patients (Refer to section 2.4.1. for language lateralization criteria).

One patient was excluded from group analysis based on the Localizer tasks, and one additional patient was excluded a priori, as this patient reported being unable to read the instructions quickly enough during the pre-MRI training. Final group composition was 31 controls (15F/16M), 14 typical (5F/9M), 15 atypical (7F/8G) language lateralized patients (Refer to section 2.4.1. for language lateralization criteria).

Diffusion MRI (dMRI) data were preprocessed using the MRtrix software suite (Tournier et al., 2019). The preprocessing steps included denoising, motion and distortion correction via FSL's TOPUP and EDDY tools, slice-to-volume registration, and bias correction (Andersson et al., 2016, 2017; Andersson & Sotiropoulos, 2016; S. M. Smith et al., 2004). Given the alternating acquisition of fMRI and dMRI, and the care taken to ensure subject comfort, subject head might have slightly moved between  $b=1000$  and  $b=1500$  images. Minor adjustments were made to the TOPUP and EDDY inputs to account for this issue. Specifically, as  $b_0$  images were systematically acquired before a diffusion-weighted MRI image, corresponding Anterior-Posterior (AP) and Posterior-Anterior (PA) encoded  $b_0$  images were specified for each corresponding imaging shell. During preprocessing, the brain mask computed during the morphometric analysis was registered in individual diffusion space. Automated quality control was conducted using EDDY QC and EDDY Squad tools (Bastiani et al., 2019), generating individual reports for each subject as well as a group report.

Subjects with deviations from the distribution, primarily due to movement during acquisition, were reviewed individually. No subjects were excluded from the analysis, although artifacts in  $b_0$  images were corrected individually by excluding the motion-affected volumes. For the comparison of metrics between fMRI and dMRI images, the subject pool remained consistent with that used in the SGT-related tasks.

## 2.4. fMRI Images analysis

### 2.4.1. First level analysis

The first-level analysis deals with the data from an individual subject, focusing on identifying brain regions that are activated in response to specific tasks or stimuli, by using a statistical model. From this analysis we obtained individual Z-maps and model fit information.

The images preprocessed by fMRIprep were first detrend, smoothed with a gaussian filter (full width at half maximum = 5 mm). An individual design matrix was compiled from individual event files (containing stimulation exact timings) and confound (movement and

rotation in all axes and their derivatives, white matter and CSF signal) compiled with fMRIprep. Z-scores maps and model fit were computed with a GLM, Glover Hemodynamic Response Function model, a cosine drift model of the first order, a cut frequency of 1/128 and a AR1 (autoregressive) temporal variance model.

#### 2.4.2. Language lateralization index in each subject

To study language lateralization patterns in the cohort and use it as a stratification criterion to evaluate the functional consequences of atypical language lateralization, we computed a language lateralization index (LI) for all patients and controls from first level Z-maps. This LI is based on individual subject SGT contrast using the SPM12 LI toolbox (Wilke & Lidzba, 2007, 2007). This index represents the proportion of activated voxels in the left hemisphere compared to the right hemisphere.

$$\frac{\sum \text{activated voxels left hemisphere} - \sum \text{activated voxels right hemisphere}}{\sum \text{activated voxels}}$$

The LI computation was enhanced with bootstrap methods to ensure its robustness against varying statistical thresholds, artifacts, and imaging biases. As shown in Figure 11, the LI tends to approach 1 for left-hemisphere lateralization and -1 for right-hemisphere dominance.

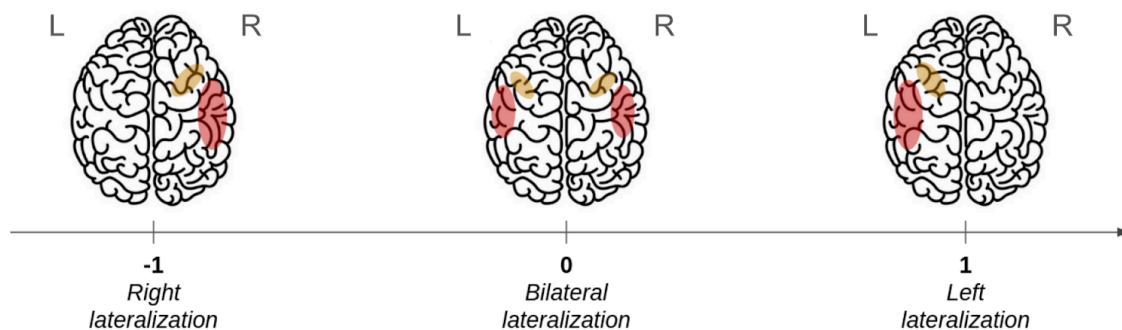


Figure 11: LI values depending on the hemispheric specialization of language activation

Due to the high morphological variability within our cohort, we could not rely on the toolbox's default affine registration and lobe atlas to compute lateralization indexes on a lobe-specific scale. To address this, we created a custom mask for LI computation, by merging LI toolbox regions. We excluded the occipital lobe to compute a hemispheric LI, and used a separate cerebellum mask for the cerebellar LI.

This approach enabled us to stratify the cohort into groups based on their language hemispheric specialization: left-lateralized (LI > 0.2), right-lateralized (LI < -0.2), and bilateral (-0.2 ≤ LI ≤ 0.2) language specialization, or into two main groups : typical (LI > 0.2) and atypical (LI < 0.2) language lateralisation. The latter categorization was used in this ongoing study.

#### 2.4.3. Correlation between LI and clinical score

Selected clinical scores were plotted against the LI. When a specific group appeared to exhibit a correlation based on the clinical score in question, a Pearson correlation test was conducted on all scores using scipy (1.8.0) and scikit-learn (1.5.1) packages.

#### 2.4.4. Group analysis of functional contrast (second-level analysis)

Second level analysis is a group-level statistical map that highlights areas of the brain where there are consistent effects across subjects, such as regions that show significant activation during a task in multiple subjects. In order to investigate spatial activation patterns depending on language lateralization, we performed a second level analysis on control, typical and atypical language lateralization patients groups.

To ensure spatial comparability between subjects and comparison of homotopic regions, all individual Z-maps from patients were registered into MNI ICBM152 2009c symmetric space using the deformation fields derived from the morphometric study. fMRIPrep preprocessing ensured fMRI to structural MRI space rigid registration, allowing us to directly apply our own deformation fields toward MNI space.

We conducted group second-level analyses based on the individual Z-maps using Nilearn. In these analyses, all subjects were encoded as intercepts in the design matrix of a parametric GLM. Second-level analysis included gaussian smoothing with a 8mm full width at half maximum.

To correct for multiple comparisons while accounting for spatial information and clustering, we utilized the non-parametric second-level inference functionalities available in Nilearn. We employed the Threshold-Free Cluster Enhancement (TFCE) method with 500 permutations. The TFCE-computed p-value map was then used to threshold the second-level analysis Z-maps at  $p < 0.05$ , corrected for false discovery rate.

#### 2.4.5. Creation of a Language Activation Atlas based on Group SGT contrast maps

In order to specifically investigate spatial, functional and microstructural homotopy of language networks in the patient cohort, we created a symmetric atlas derived from group activation maps. This atlas was designed to facilitate the extraction of BOLD signal and GLM coefficients from regions of interest (ROIs) identical in all subjects. Overall, this atlas was also used to perform fMRI driven tractography on language activated areas and investigate microstructural properties of white matter bundles connected to language activated regions.

ROI size and delineation were determined based on Z-maps, with Family-Wise Error (FWE) corrections applied at  $p < 0.01$  and  $p < 0.001$ . The control group served as the reference for generating most of the ROIs, with thresholds chosen to ensure the correct segregation of regions. After symmetrizing the atlas, we verified potential divergences between the template and the patient activation maps. No major divergences were observed, as atypical language specialization predominantly activated homotopic regions of the typical language network. Resulting Atlas is presented in Figure 12.

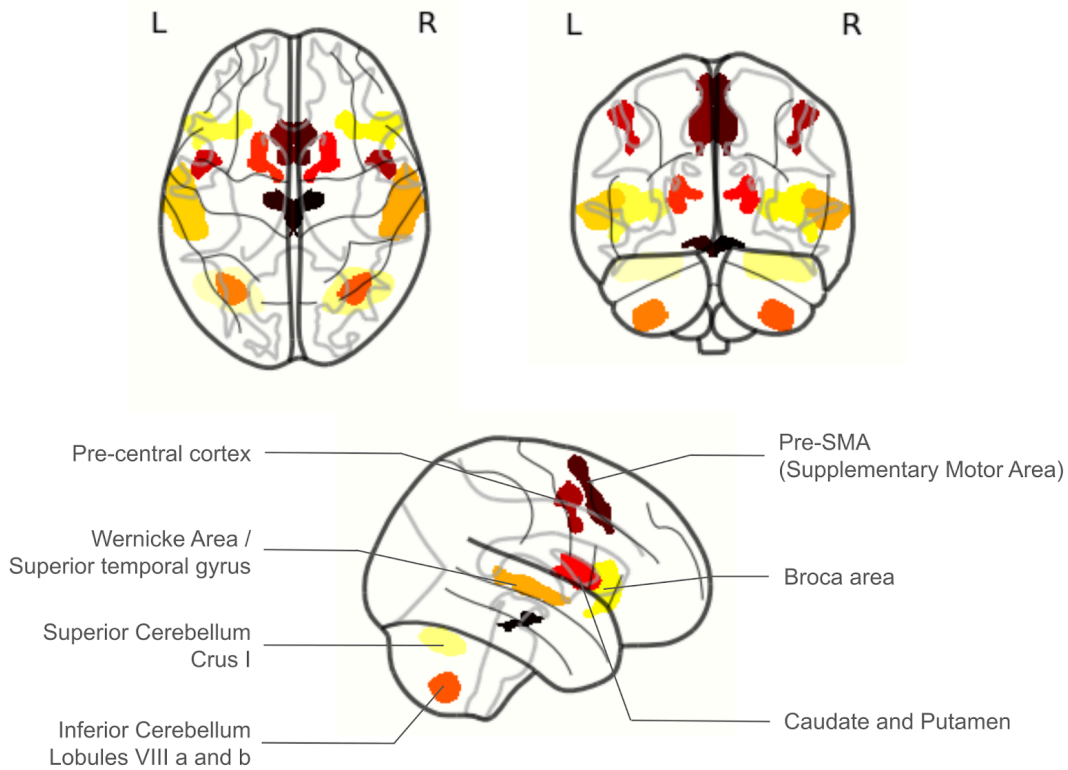


**Figure 12: Language functional atlas extracted from the cohort data**

Figure 12 presents the language ROI atlas constructed from the 3 groups SGT activation maps within the cohort. With such a global task, these regions include nearly all the typical areas known to be involved in language processing, such as Broca's area (inferior frontal gyrus), Wernicke's area (superior temporal gyrus), the pre-SMA (mesial region anterior to precentral gyrus), the precentral cortex, subcortical structures linked to speech production, and the cerebellum.

However, some dorsal stream areas, including the temporo-parietal junction, were not activated enough by our contrast and could not be delineated. The Sentence Generation Task, though simple and suitable for young individuals with cognitive challenges, is purely auditory and contrasted with a passive auditory stimulus. As a result, visual or reading-related areas were weakly activated or not activated at all, and primary auditory functions were canceled out by the resting contrast (repeated presentation of the word "rest," without sentence generation).

#### 2.4.6. Group comparisons between typical and atypical language representation

In the second part of our study, after having characterized language activation in our cohort, we investigated whether there were differences or similarities between patient groups. Our main focus was the tasks included in the localizer, including primary functions (auditory, visual, hand motor), as well as relatively late developing complex associative functions (mental calculation). This was a first approach to investigate the "crowding effect" hypothesis, suggesting spatial competition between atypical language network and other

later developing functions. We investigated whether other tasks exhibited different activation patterns depending on language lateralization.

To this end, we designed two complementary second-level analyses :

- One analysis where we grouped all patients together, and performed a simple group second level analysis. This aimed at assessing common activation regions irrespective of language lateralization in patients. One advantage is that the overall number of patients was similar to the number of controls, allowing us to compare all patients second level analysis with control
- One analysis where we looked for differences between the two patient groups, with a +1 (Atypical), -1 (Typical) encoding contrast. This method allowed us to perform group comparisons as interaction products.

#### 2.4.7. Extraction of cluster and peaks localization

To precisely isolate activation clusters and peaks, we relied on native Nilearn peak detection functionalities (`get_cluster_table`), on which we added peak detection conditions, with a minimal cluster size of 100 voxels, a minimal z-score of 3 and a minimal distance of 35mm between peaks within a same activated region.

Peaks localization were overlaid on Harvard-Oxford Cortical and Subcortical atlas (Desikan et al., 2006; Frazier et al., 2005; Goldstein et al., 2007; N et al., 2006) and SUI Cerebellar atlas (Diedrichsen et al., 2009, 2011) to have an overview of task related activation localization.

As a supplementary analysis, although the corresponding tables are only presented in Appendix 2 to 9, we developed a 3D watershed algorithm to subdivide activation clusters from peaks position, and computed cluster overlay on these atlases, as both a cluster percentage and atlas ROI percentage (not in the manuscript). These analyses will be investigated in further research.

#### 2.4.8. BOLD temporal signal extraction in clusters identified with group comparisons

As group comparison Z-maps can be challenging to interpret, we conducted supplementary analyses, including extraction of the BOLD signal variation over time and first-level Generalized Linear Model (GLM) coefficient, reflecting the strength of activation for each individual stimulus.

The BOLD signal extraction involved registering the fMRIPrep-preprocessed fMRI images into MNI space, standardizing, centering, and regressing the confounds from the whole-brain BOLD signal. The BOLD signal within an anatomical ROI was then extracted and averaged over time.

The individual event files were used to predict the temporal window of the BOLD response for each stimulus, and the temporal responses were averaged over iterations of a specific stimulus. The beta coefficients from the first-level analysis GLM were extracted similarly from the beta maps generated for each subject.

## 2.5. Diffusion MRI images analysis

### 2.5.1. Fractional anisotropy (FA)

From the curated diffusion images, Fractional Anisotropy (FA) was computed for each subject. A benchmark comparison between FA maps derived from the  $b=1000$  and  $b=1500$  shells revealed no significant differences, except at the image borders, which do not impact the regions of interest for further analysis. Consequently, all FA results presented were computed using the  $b=1000$  shell.

### 2.5.2. Probabilistic Tractography

Tissue response function calculation and Probabilistic Anatomically Constrained Tractography (ACT) was performed using 5-tissue-type (5tt) images (Tournier et al., 2010). The 5tt images are 4D brain images containing five volumes, each corresponding to a tissue mask: cortical gray matter, subcortical gray matter, white matter, CSF, and pathological tissue (lesion or blank image for control subjects) (R. E. Smith et al., 2012). These tissue masks were derived from the anatomical tissue probability maps generated with CAT12 and the lesion mask we created (refer to section 2.4.4).

To ensure tractography comparability, we averaged controls' tissue response and used this unique response to generate Fiber Orientation Distributions (FODs) in the whole group via spherical deconvolution (Tournier et al., 2007). We then performed another normalization on FOD amplitude, ensuring a fixed density of streamlines should be used to reconstruct a given FOD amplitude between subjects, and then the cross-sectional area of fibers represented by each streamline is also identical between subjects. (Dhollander, Tabbara, et al., 2021)

To increase tractography quality, preprocessed diffusion images and brain masks were upsampled to achieve an isotropic voxel size of  $1.25 \text{ mm}^3$ . A whole-brain tractography was generated with 3 million streamlines. The tractography was anatomically constrained using 5tt images and a dynamic seeding method (R. E. Smith et al., 2015). The whole-brain tractography was subsequently filtered and weighted using SIFT2 (Spherical-deconvolution Informed Filtering of Tractograms) methods, which adjust streamline densities to match the FOD lobe integrals.

### 2.5.3. Language network Tractography

To specifically investigate the white matter microstructure of the language network, we utilized the functional atlas presented in Figure 12 to extract both streamlines between the atlas ROIs and associated diffusion metrics (e.g., the number of streamlines per bundle, mean FA for each bundle). Bundles containing fewer than 70 streamlines were considered spurious. This threshold was empirically benchmarked and validated through team consensus.

To explore the equivalence of homotopic language network reorganization with a typical network, we limited our analysis to anatomically plausible bundles. Non-homotopic interhemispheric bundles, as well as bundles linking the cerebellum with hemispheric ROIs, were excluded (cerebellar tracts typically connect with basal ganglia, which in turn connect with cortical territories). The bundles investigated included :

- Streamline bundle between Broca and Caudate/Putamen
- Streamline bundle between Broca and Precentral
- Streamline bundle between Broca and PreSMA
- Streamline bundle between Broca and Wernicke
- Streamline bundle between Caudate/Putamen and Contralateral Cerebellum

These streamlines were analyzed within the language-specialized hemisphere, as determined by the Lateralization Index (LI), as well as the contralateral (non-dominant) hemisphere.

### 3. Results

#### 3.1. Language Hemispheric specialization and its correlation with clinical outcomes and microstructure

##### 3.1.1. Distribution of Hemispheric Language Specialization within the Cohort

In this first part, language lateralization within the cohort during the Sentence Generation Task (SGT) was used to create a new group stratification. Figure 13 shows the distribution of the hemispheric lateralization index (LI) compared to cerebellar LI. This visualization reveals an inversion of the typical language specialization pattern in most patients with left hemisphere lesions (in blue), where language activation was more prominent in the right hemisphere and the left cerebellum. In contrast, patients with right hemisphere lesions (in red) exhibited a typical pattern similar to controls (in green), with predominant activation in the left hemisphere and right cerebellum. Although such a shift was expected and has been described in the literature, the changes in cerebellar lateralization have been less frequently reported.

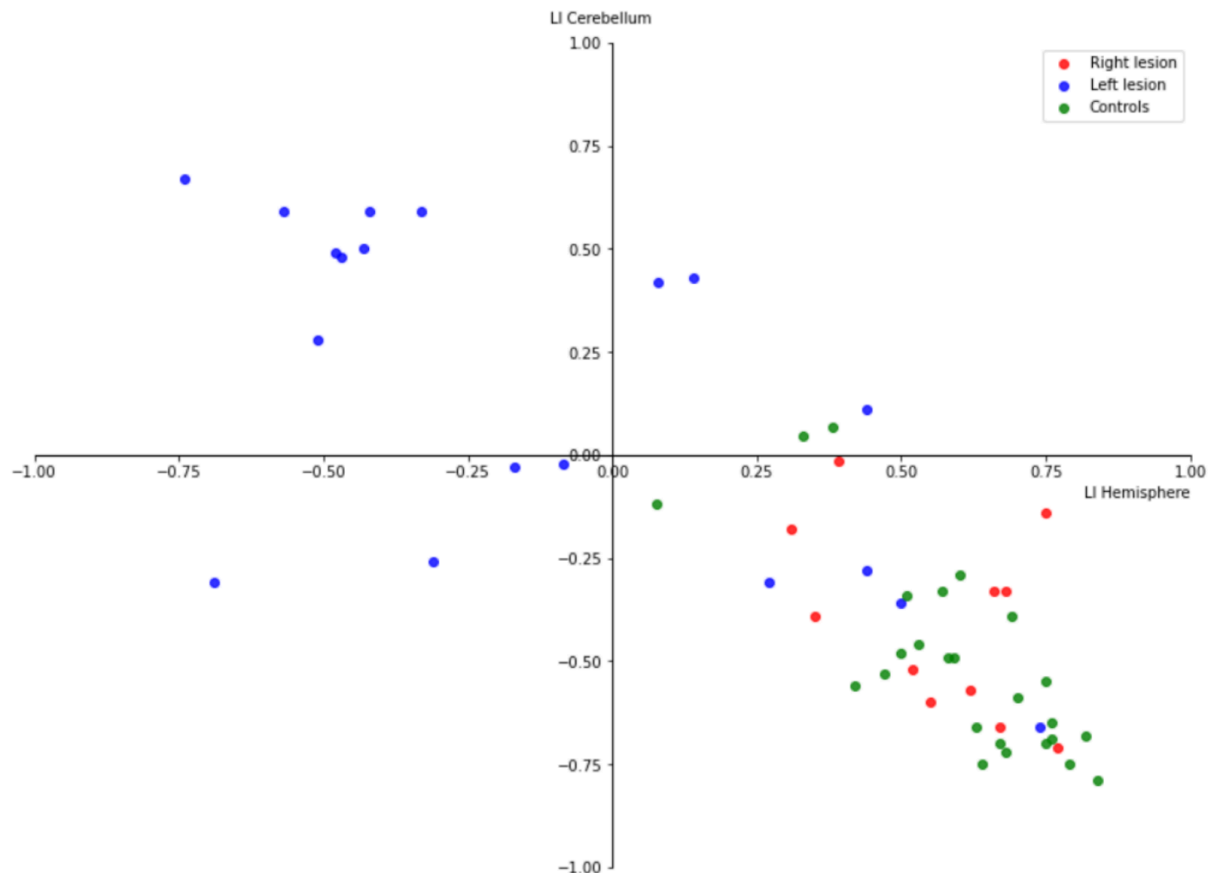


**Figure 13: Hemisphere and Cerebellum Language Lateralization according to lesion side**

Based on hemisphere LI, the patients cohort was stratified into two groups: Typical (left activation,  $LI > 0.2$ ) and atypical (bilateral and right activation,  $LI < 0.2$ ) language lateralization. The activation maps displayed in Figure 14 show the second-level model Z-maps for SGT contrast based on this new group stratification we will use from now on. These maps are FDR corrected and thresholded for  $p < 0.05$  based on TFCE statistics. Cluster peaks for patients are reported in Table 4 and 5. The group contrasts support the inversion pattern shown in Figure 13 and reported in the literature.

Controls showed rather widespread left-lateralized language activation, involving the Inferior frontal gyrus and the lateral prefrontal cortex, the pre-SMA, the basal ganglia, and the posterior part of the superior temporal gyrus (planum temporale), bilateral activation of the anterior part of the superior temporal gyrus, and right cerebellum (crus 1 and 2). Which is highly congruent with the literature

Typically lateralized patients exhibited a less widespread but highly asymmetric activation pattern. Activation peaks in Table 2 were found in the left supplementary motor area, Broca and Frontal Pole region. Significant activation involved the entire left superior temporal gyrus and the right cerebellar hemisphere, like in controls. More details can be found in the appendix where we computed cluster coverage of the different regions.

Atypically lateralized patients showed smaller activation clusters (Table 3) in the right hemisphere, with a mirror pattern when compared to both previous groups: right superior temporal gyrus (both anterior and posterior division, right inferior frontal gyrus and supplementary motor area, as well as several cerebellar clusters, mostly on the left side.

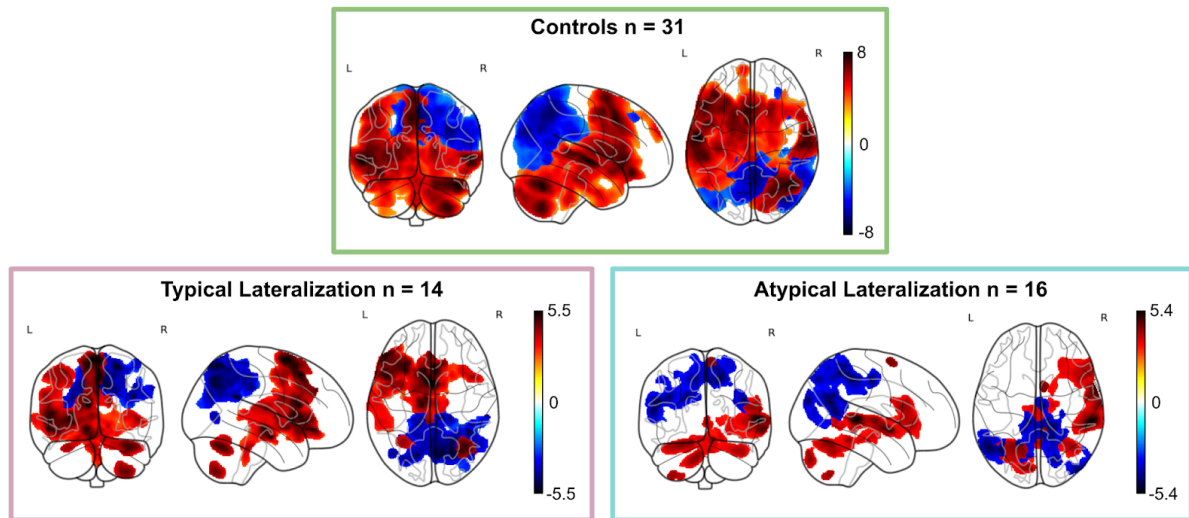


Figure 14: Activation maps depending for Controls, Left and Right Language Lateralization Patient Groups Defined based on Hemispheric LI

Peak Z Score	X (mm)	Y (mm)	Z (mm)	Harvard-Oxford	SUIT
5.83	2.0	4.0	67.0	Right Juxtapositional Lobule Cortex (Supplementary Motor Cortex)	
5.61	-50.0	36.0	-10.0	Left Frontal Pole	
5.54	-11.0	-18.0	-4.0	Left Thalamus	
5.54	-50.0	14.0	7.0	Left Inferior Frontal Gyrus, pars opercularis	
5.23	34.0	-64.0	-28.0		Right_CrusI
4.92	34.0	-69.0	-57.0		Right_VIIb
4.67	-31.0	-59.0	-29.0		Left_VI

Table 4 : Typical language specialization patients group z-map positive peaks position (Figure 14). Coordinates are expressed in symmetric MNI referential

Peak Z Score	X (mm)	Y (mm)	Z (mm)	Harvard-Oxford	SUIT
5.61	60.0	-33.0	5.0	Right Superior Temporal Gyrus, posterior division	
4.93	64.0	4.0	-7.0	Right Superior Temporal Gyrus, anterior division	
4.49	48.0	15.0	18.0	Right Inferior Frontal Gyrus, pars opercularis	
4.11	49.0	-38.0	-8.0	Right Middle Temporal Gyrus posterior division	
4.62	7.0	5.0	66.0	Right Juxtapositional Lobule Cortex (Supplementary Motor Cortex)	
4.69	-17.0	-65.0	-21.0		Left_VI

4.35	35.0	-60.0	-30.0		Right_CrusI
4.32	8.0	-44.0	-18.0		Right_I_IV
3.49	-6.0	-76.0	-25.0		Left_VI
4.59	-8.0	-86.0	-35.0		Left_CrusII
4.44	-36.0	-64.0	-57.0		Left_VIIb
4.2	0.0	-57.0	0.0		Right_I_IV

**Table 5 : Atypical language specialization patients group z-map peaks position (Figure 14). Coordinates are expressed in symmetric MNI referential**

To have a finer insight into language activation in the different groups, we investigated language activation during SGT task in the atlas we designed from our own cohort, results are presented in Figure 15. Time series visualization exhibits expected block activation signal. Controls, in green, showed higher cortical bold signals in the left than in the right hemisphere, especially visible in the Broca and Precentral area. Conversely, higher activation is exhibited in the right than in the left cerebellum.

Typically lateralized patients, plum-colored, exhibited a really similar activation pattern to controls, except for no activation peak in the right Precentral Gyrus and Basal Ganglia.

Atypically lateralized patients, in cyan, exhibited less activation in the left cortical areas, and no activation in Wernicke and Precentral cortex, and less activation in right cerebellum. Conversely, the bold signal in the right Pre-SMA, Precentral, Broca, as well as in the left Cerebellum is higher than in control and typical language patients.

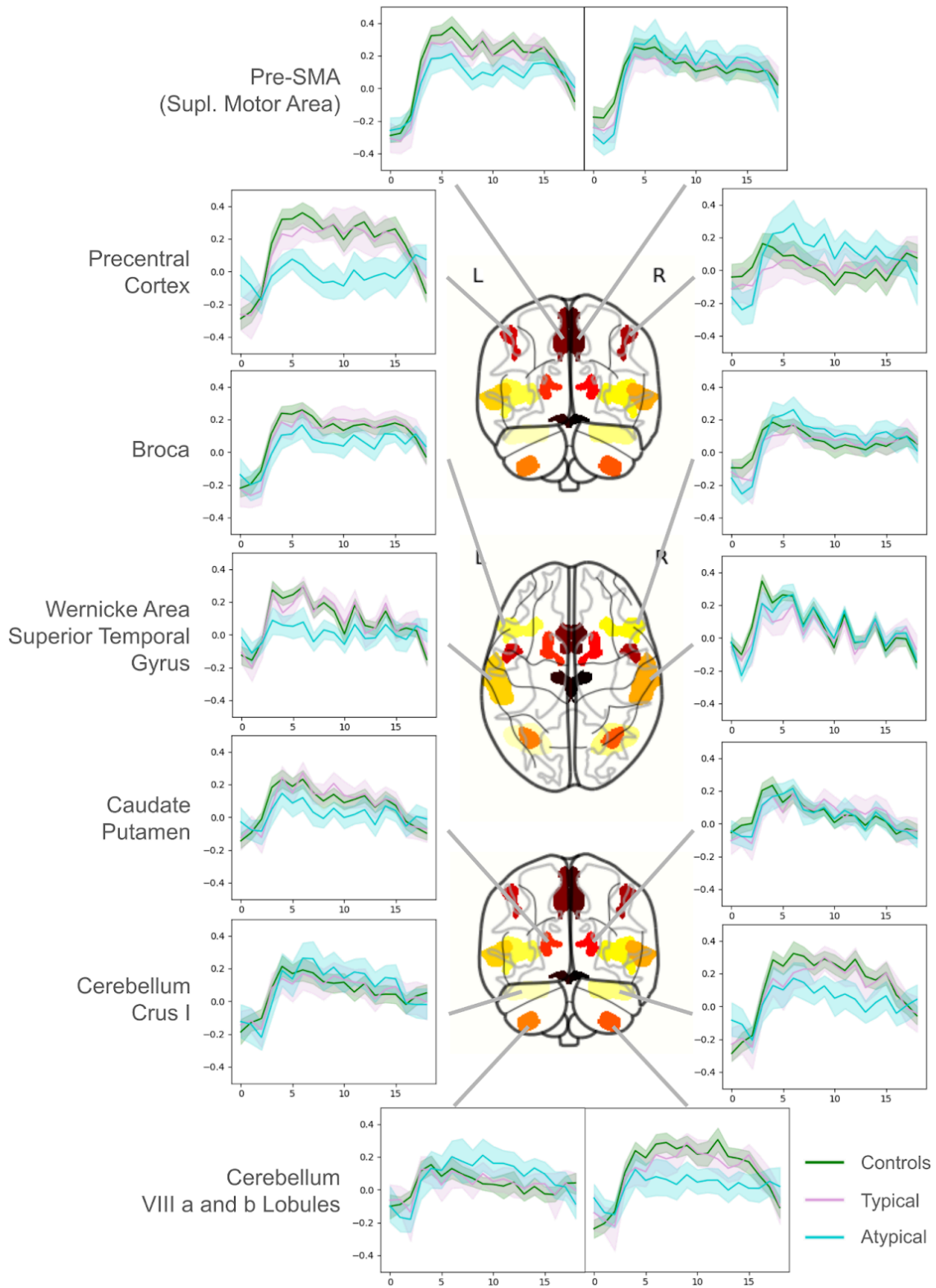
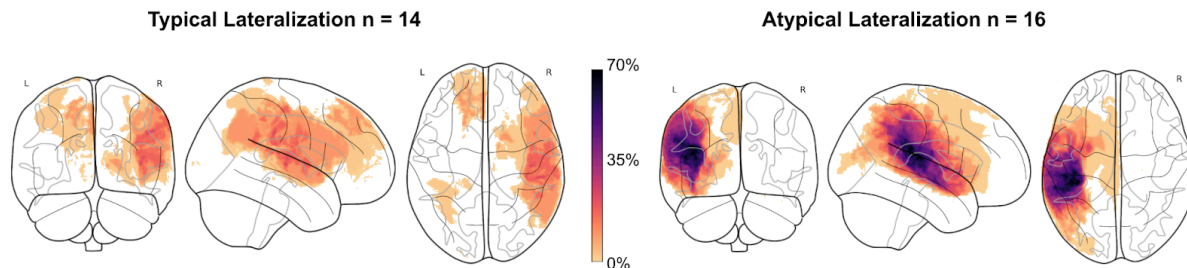


Figure 15: Detrend and standardized BOLD signal in control, typical and atypical language lateralization for SGT task

### 3.1.2. Lesion Distribution Depending on Language Lateralization

Figure 16 shows the lesion distribution depending on language hemispheric specialization. Typically lateralized patients have mostly right lesions in the MCA territory, as well as a few left lesion patients (in the territory of the anterior cerebral artery, or very small lesions in the parietal lobe). Atypically lateralized patients show only left lesions, which seem to affect in most cases the perisylvian regions.



**Figure 16: Superposition of all patient's lesion masks depending on their language LI visualized as a maximum intensity projection. All masks were registered in MNI ICBM152 2009c symmetric template. Mask count per voxel was divided by the total size of each lateralization subgroups**

### 3.1.3. Correlation of Clinical Scores with Language Lateralization

As we aimed at investigating the “crowding effect” and at checking whether patients' outcomes were worse due to spatial functional competition when the language is atypically lateralized, we compared LIs with several clinical scores. Figure 17 and 18 displays respectively the relationships between CELF and WAIS main scores and the language lateralization index in each subject.

Patients with right hemisphere lesions (and left lateralization) did not exhibit a significant relationship between their scores and LI. We explored qualitatively other potential variability causes such as lesion severity score, but did not find any pattern.

Conversely, patients with left hemisphere lesions and frequent atypical language lateralization demonstrated a significant correlation between their scores and LI; the more right-lateralized their language network was, the better was their performance, except for the PSI and WMI subtests. One male subject with a left lesion was identified as an outlier, but was not excluded from the statistical analyses; this subject had been graded as HIP (High Intellectual Potential) at neuropsychological assessments and had a very small lesion. Overall, most patients had scores below 100, indicating average suboptimal performances.

These findings challenge the “crowding effect” hypothesis, as the more right-lateralized the language network was, the better subjects performed in both language and cognitive functioning. This seems to indicate a synergy rather than a competition between language and cognitive function. Although we did not directly test this hypothesis with dedicated statistics, no significant sex-related patterns emerged from these observations.

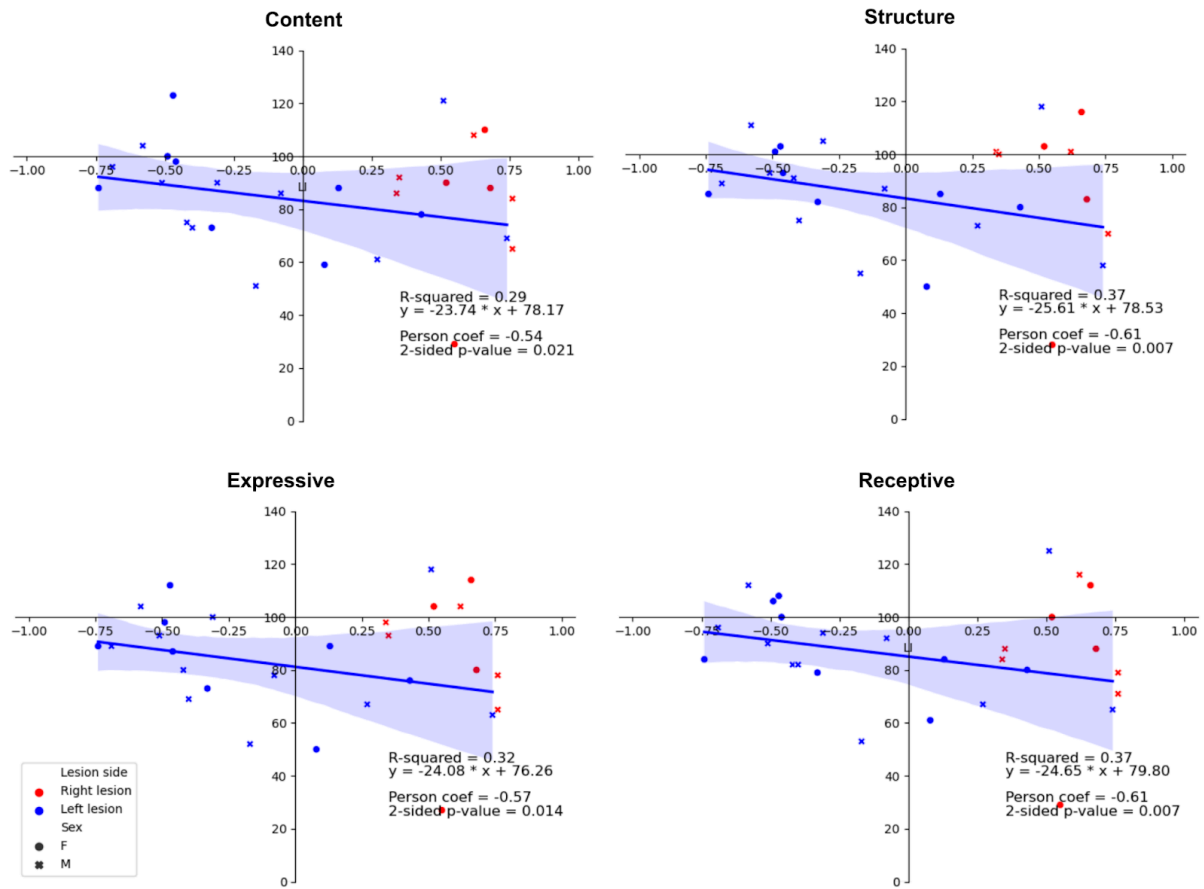


Figure 17: CELF main scores distribution in the cohort as a function of LI, Sex and Lesion Side. Correlations were computed only for left lesion patients, and performed without excluding HIP outlier

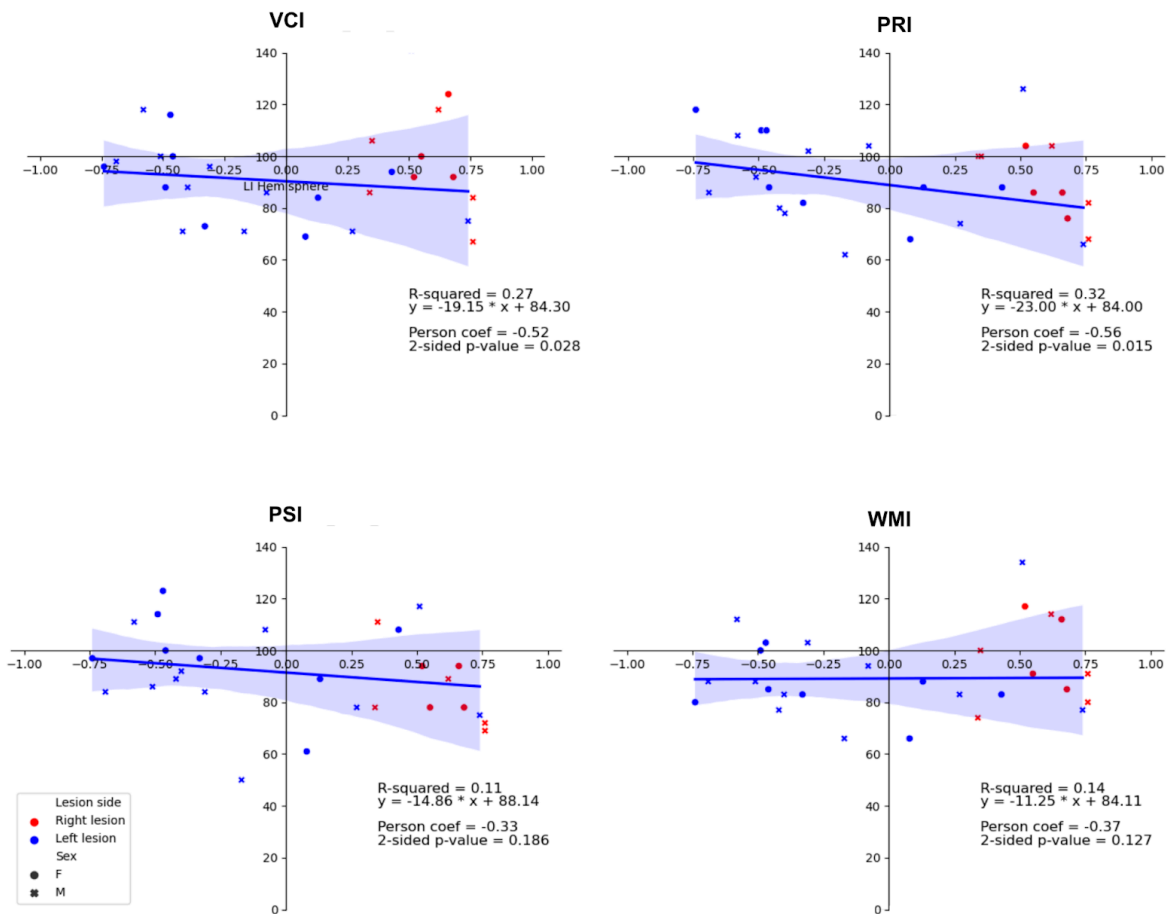


Figure 18: WAIS main scores distribution in the cohort as a function of LI, Sex and Lesion Side. Correlations were computed only for left lesion patients, and performed without excluding HIP outlier

### 3.1.4. Microstructural changes according to language lateralization

After confirming that atypical functional organization follows a pattern homotopic to the typical language network, we started to investigate whether the microstructural organization of right language networks in right-lateralized individuals is comparable to the left networks in subjects with typical left-hemisphere lateralization. This analysis is still in progress and will be completed in the coming months. To that end, we utilized diffusion MRI images and the functional atlas defined in the Materials and Methods section.

Figure 19 illustrates the white matter bundles that were studied, along with the proportion of subjects for whom we were able to successfully reconstruct the fiber bundles. Bundles comprising fewer than 70 streamlines were considered insufficiently well reconstructed and excluded from further analyses. The patients group exhibited lower reconstruction rates compared to the control group.

Based on qualitative observation of Figure 19, reconstruction in typically language lateralized patients performed at lower rates:

- Lesional hemisphere (for the majority of subjects) : Right PreSMA - Right Caudate/Putamen ; Right Broca - Right Caudate/Putamen
- Inter-Hemispheric Bundles : Left - Right PreSMA ; Left-Right Caudate/Putamen ; Right Caudate/Putamen - Left Inf. Cerebellum
- Bundles that do not correspond to well-known white matter fibre tracts bundles : Right PreSMA - Left Caudate/Putamen ; Right PreSMA - Left Broca ; Right Precentral - Left Inf. Cerebellum

In patients with atypical language lateralized patients similarly, lower reconstruction rates were found in:

- Lesional hemisphere : Left PreSMA - Left Broca ; Left PreSMA - Left Precentral ; Left PreSMA - Left Caudate/Putamen ; Left Broca - Left Wernicke ; Left Broca - Left Precentral ; Left Broca - Left Caudate/Putamen ; Left Caudate/Putamen - Left Sup. & Inf. Cerebellum
- Inter-Hemispheric Bundles : Left - Right PreSMA ; Left - Right Caudate/Putamen
- Bundles that do not correspond to well-known white matter fibre tracts bundles : Left Pre-SMA - Right Wernicke; Left Pre-SMA - Right Precentral ; Left Broca - Right Pre-SMA ; Left Caudate/Putamen - Right Broca

In many of these cases, the reconstructed bundles appeared to be composed of several bundles that were merged to form a 'pseudo-unique path between the 2 ROIS concerned. Overall, the reconstruction performances seemed worse in the lesional territory and in inter-hemispheric bundles directly connected to the lesion territory. Many "bundles" did not correspond to known anatomical bundles, yet exhibited worse reconstruction performances in patients. This indicates a need to refine the ROI parcellation, notably to ensure WM-GM interface is included in the region of interest. We statistically tested the reconstruction rate differences between these groups with a Chi<sup>2</sup> test. No test was significant after FDR correction for  $p < 0.05$ .

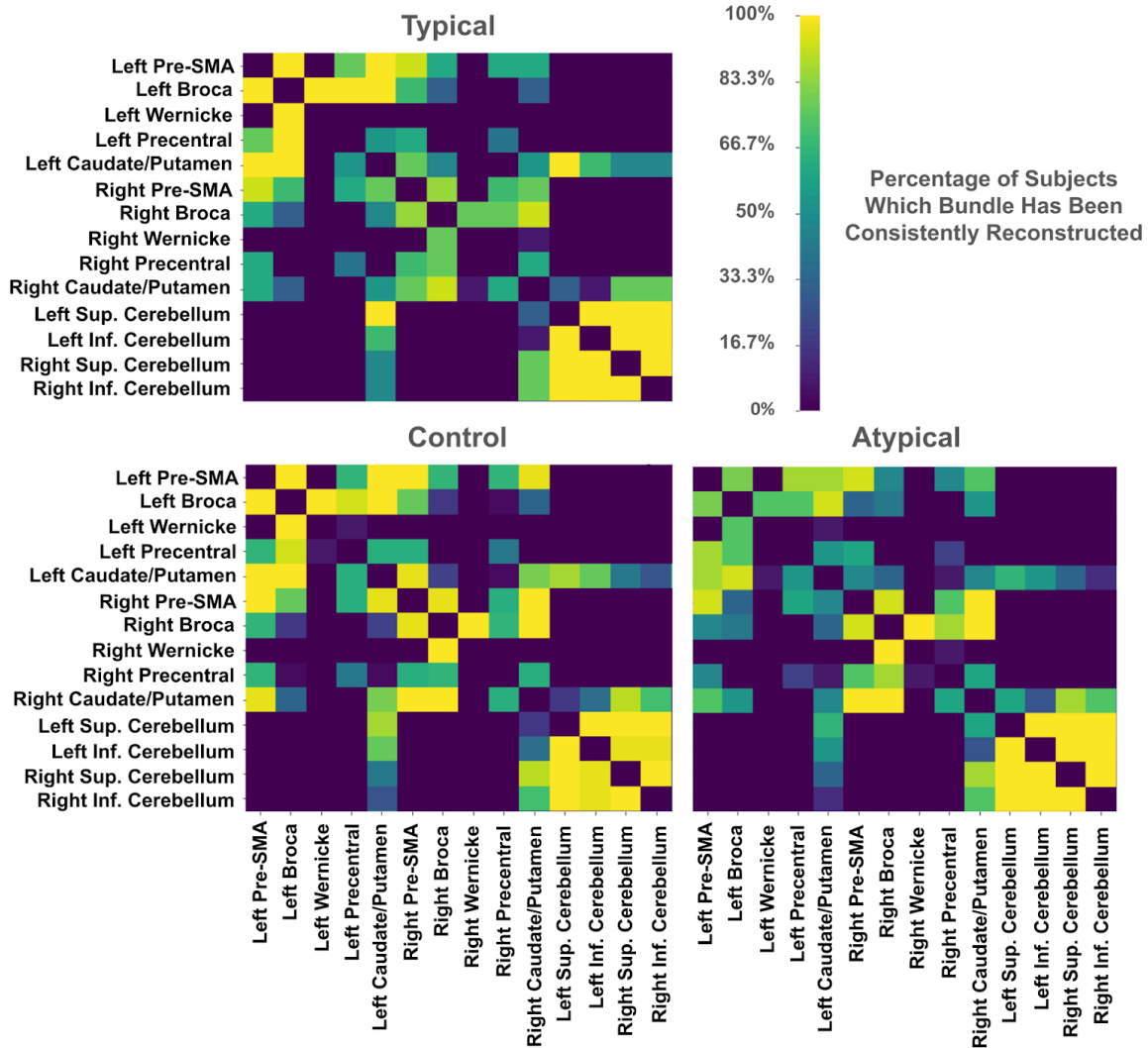


Figure 19: Proportion of subjects in the 3 groups (Controls, Patients with typical and atypical language representation) for whom we were able to correctly reconstruct white fiber bundle (more than 70 streamlines)

In a simplification effort, we focused more specifically on bundles corresponding to well-established anatomical connections, including: Broca–Caudate/Putamen, Broca–Precentral, Broca–PreSMA, Broca–Wernicke (Arcuate Fasciculus), and Caudate/Putamen–Contralateral Superior Cerebellum. We examined the mean fractional anisotropy (FA) as a function of on lateralization index (LI), to test whether there were differences according to the side of hemispheric language dominance. We also studied the correlations between mean FA in both hemispheres and main CELF/WAIS scores to test whether there was any link between the microstructure of the bundles in the dominant hemisphere and language/IQ performances. Unfortunately, no significant correlations were found between mean FA and LI nor between FA and test scores.

Figure 20 shows the FA vs LI results for the Arcuate Fasciculus. No patient-specific patterns were observed, nor were there significant correlations between LI and mean FA. Additionally, no sex-specific differences were identified. The only notable finding was that in the non-dominant hemisphere, we were unable to consistently reconstruct the arcuate

fasciculus in 27% of atypical and 23% of typical patients. This "attrition" was evident across all studied bundles, with an attrition rate ranging from 10% to 30%, likely due to the lesion territory.

Moreover, the Caudate/Putamen–Contralateral Cerebellum bundle exhibited poor reconstruction reliability even in control subjects, limiting its utility for further analysis and raising caution on the overall parcellation pertinence.

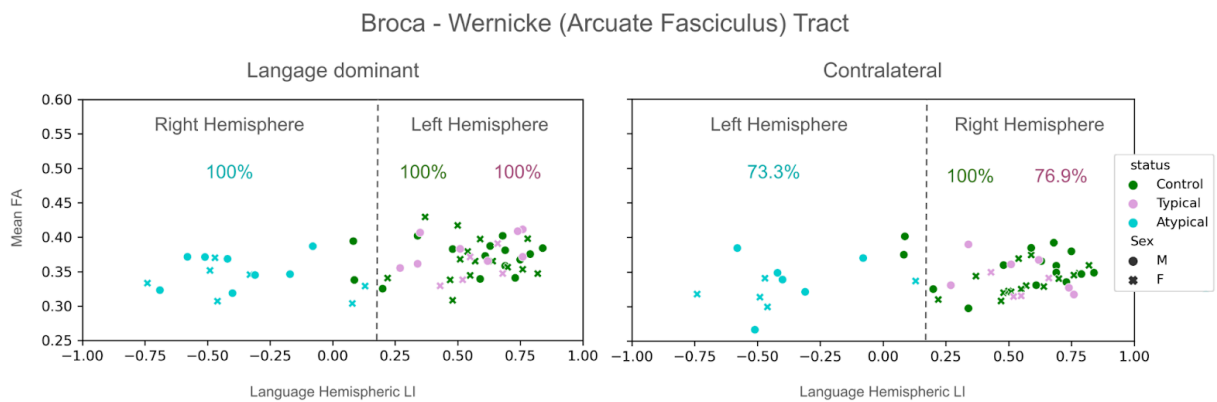


Figure 20: Mean FA in the arcuate fasciculus (streamline bundle between Broca and Wernicke area). Right plot shows FA value in the language dominant hemisphere and left plot in the non dominant hemisphere, as a LI  $\geq 0.2$  or  $< 0.2$ . Percentages are the proportion of subjects in each group with a high quality reconstruction of the bundle (more than 70 streamlines).

### 3.1.5. Discussion

In this still ongoing study, we examined the distribution of hemispheric language lateralization in the 3 groups (controls, left or right lesion) and the implications of atypical language representation following neonatal arterial ischemic stroke (NAIS), specifically investigating the functional and microstructural homotopy between the typically language-dominant left hemisphere and the atypically dominant right hemisphere.

#### *Language Reorganization in Patients with Left-Hemisphere Lesions*

Our study confirms the recruitment of homotopic regions in the right hemisphere, as well as an inversion of cerebellar activation in patients with left-hemispheric lesions. These findings corroborate prior results in the literature (Martin et al., 2023). However, not all patients with left-hemisphere lesions showed a shift of language function to the right hemisphere. Lesion mapping suggests that this reorganization is associated with peri-sylvian territory lesions, especially involving the dorsal stream, a pattern previously noted in the literature (Pahs et al., 2013).

Interestingly, our findings suggest that higher degree of language lateralization correlates with better language and cognitive outcomes, indicating that the homotopic reorganization of the language may play a protective role against language impairment. As cognitive outcomes tend to align with language outcomes and lateralization, our results challenge the initial observations that led to the "crowding effect" hypothesis (Lidzba et al., 2006). Nevertheless, these observations are insufficient to conclusively refute the crowding effect. It is plausible that two opposing mechanisms influence outcomes: on one hand, the

crowding effect may lead to diffuse and long-term impairment, while on the other hand, typical or near-typical language development may provide protective benefits, promoting better social interactions, alternative learning pathways, and more normative experiences.

### *Structural Connectivity and White Matter Integrity Depending on Hemispheric Language Dominance*

Preliminary analyses suggest that structural connectivity and white matter integrity are similar between right- and left-lateralized language networks. Mean FA values were more variable in the non-dominant hemispheres of patients, although no significant differences were observed between subgroups, and no correlations were found between FA, LI, or clinical scores.

A key trend in our result is the difference in reconstruction performance, with up to 30% of subjects failing to yield a successful reconstruction of the fiber bundles in the non-dominant hemisphere (in most cases also the lesioned hemisphere), although not significant according to preliminary statistical tests. This contrasts with the reliable reconstruction observed in the dominant hemisphere (in most cases, not lesioned). Notably, one bundle, connecting the basal ganglia to the contralateral superior cerebellum (Crus I), demonstrated poor reconstruction across all subgroups.

Although the literature on correlations between BOLD activation and FA remains heterogeneous, with results being highly task-, region-, and population-dependent (Jarret et al., 2022), it was unexpected that FA results in our cohort were so poorly sensitive to both language lateralization and cognitive scores. We hypothesize that methodological limitations, such as the relevance of parcellation and the lack of sensitivity of mean FA values, likely contributed to these outcomes. These findings remain preliminary, and we will address these issues by employing improved methodologies and alternative analytical approaches.

## 3.2. Hypothesis of functional competition within the right dominant hemisphere

In the subsequent part of this study, we aimed to further investigate the "crowding effect" hypothesis. Specifically, we intended to assess whether atypical language specialization adversely affects the spatial activation of other cognitive functions. Special attention was given to mental calculation, an associative function which partly relies on the sentence-processing network. Mental calculation shares overlapping activation of small regions with sentence processing in the intraparietal sulcus (Amalric & Dehaene, 2019). Through the study of brain activation during the "localizer" sequence, we hoped to elucidate the relationship between atypical language lateralization and the spatial organization of other cognitive functions.

### 3.2.1. Investigation of localizer tasks per subgroup depending on language lateralization

We first examined group-wise activation contrasts based on language lateralization (typical left vs atypical), focusing on three contrasts: audio versus video, left versus right hand motor activation (button pressing), and language (sentence processing) versus silent calculation (subtraction). This analysis is an initial step for understanding activation patterns

across groups for different functions depending on the subject's language lateralization. A summary of all results is presented in Figure 21, with detailed contrast-specific activation clusters described below. All contrast peaks described are defined in the Harvard-Oxford atlas and cerebellar regions were defined in SUIT atlas.

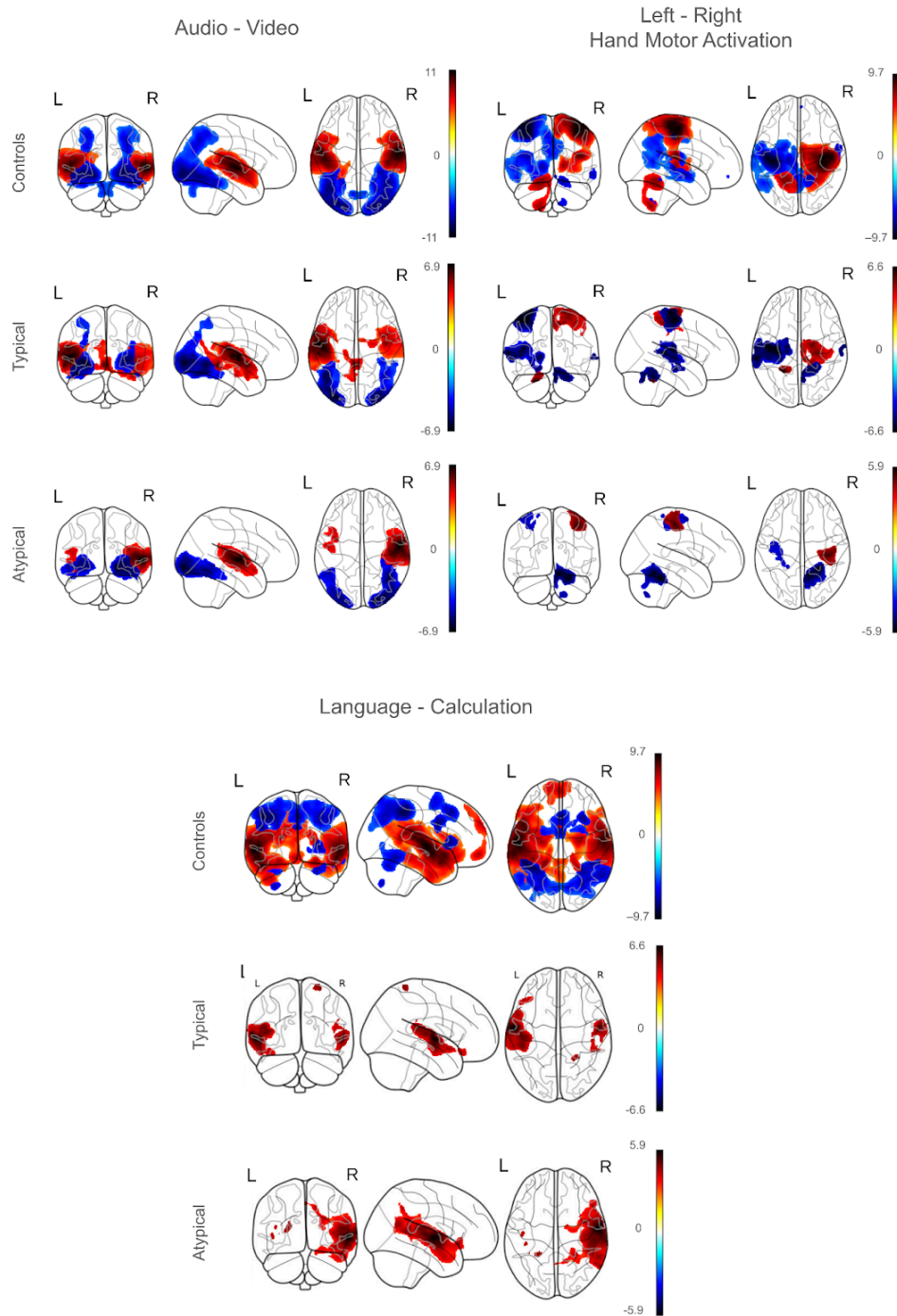


Figure 21: Second level analysis for the localizer task (TFCE thresholded for  $p < 0.05$ ). Contrasts are shown for Controls ( $n=30$ ) and Patients with Typical ( $n=14$ ) and Atypical ( $n=15$ ) language lateralization. Red areas indicate a significantly bigger BOLD activation for the first condition (e.g., audio, right hand, language) and blue for the second (e.g., video, left hand, calculation).

#### 3.2.1.1. Audio – video contrast

In the control group, the activation maps for the audio-video contrast revealed an expected bilateral and grossly symmetric activation of both temporal cortices in the audio tasks, and in the occipitoparietal primary and secondary visual cortices for the video condition. Four activation peaks were found for audio stimuli, located in the right planum temporale, right temporal pole, the anterior division of the left superior temporal gyrus, and the left thalamus. For video stimuli, seven peaks were detected, predominantly in the occipital cortex, except for one peak in the temporo-occipital part of the inferior right temporal gyrus and another in the left cerebellum (Cerebellum Left VI).

In patients with typical language dominance, activation maps showed a pattern more asymmetric than controls with a left predominance of all activations, likely due to the lesion impact in the right hemisphere. Analysis revealed for audio stimuli, including the left central opercular cortex, posterior division of the left supramarginal gyrus, left precuneus cortex, left accumbens, right planum temporale, right central opercular cortex, and right cerebellum (Cerebellum Right I-IV). For video stimuli, peaks were mainly in the occipital cortex and the posterior divisions of the temporal fusiform cortex bilaterally.

In patients with atypical language lateralization, the activation pattern was reversed with right predominance of activation, areas were smaller and did not reach significance in the right parietal lobe, while it was the case on the left side in patients left dominance. Two peaks were observed for audio stimuli, located in the right planum temporale and the left insular cortex. For video stimuli, peaks were identified in the right occipital pole, and the left lateral occipital cortex, inferior division.

Overall, activation localizations were similar across subgroups, with bilateral activations for both audio and video stimuli. However, peak intensities were stronger in the contralesional hemisphere for patients.

#### 3.2.1.2. Left – Right contrast

In the control group, activation during left-hand motor tasks was observed as expected in the right precentral gyrus, right parietal opercular cortex, right superior parietal lobule, and left cerebellum (Left V, VIIIb). For right-hand motor tasks, activations were found in the left precentral gyrus, left caudate, right superior temporal gyrus (anterior division), and right cerebellum (Right V, VIIIb).

In typical patients, left-hand activation peaks included the primary somatosensory cortex and the left cerebellum (Left VI). For right-hand tasks, activation was observed in the left precentral gyrus, left superior temporal gyrus (posterior division), left caudate, left planum temporale, right superior temporal gyrus (posterior division), the corticospinal tract, and right cerebellum (Right VI).

In atypical patients, left-hand activation exhibited a single to the right postcentral gyrus (although the cluster extend to precentral gyrus), while right-hand activation showed two peaks in the left postcentral gyrus (extending to precentral as well) and activation in the right cerebellum (Right V, VIIb, VIIIa).

As with the audio-video contrast, motor activation was mostly bilateral across subgroups, with some unilateral activations in the atypical language group left hand, in pre/postcentral area. The cluster sizes in patients were generally smaller than in controls, possibly due to the limited sample size. Interestingly, no contralateral cerebellar activation was found for left hand activation in atypical language lateralization patients group.

#### 3.2.1.3. Language – Calculation contrast

In the control group, language-related activations formed a bilateral though left lateralized network composed of perisylvian and temporal regions and bilateral anterior cingulum. Peaks were observed in the left superior temporal gyrus (anterior division), right superior temporal gyrus (posterior division), left planum temporale, left temporal pole, left frontal pole, and the callosal body.

Calculation-related activations showed a bilateral network involving dorsal precentral/prefrontal areas along with both superior parietal lobules (intra-parietal sulcus), and inferior-posterior temporo-occipital clusters. Peaks included the left supramarginal gyrus (anterior division), left lateral occipital cortex (superior division), left precentral gyrus, left superior frontal gyrus, and multiple areas in the right hemisphere, including the superior parietal lobule, supramarginal gyrus (posterior division), insular cortex, paracingulate gyrus, inferior temporal gyrus (temporo-occipital part), and middle frontal gyrus. The cerebellum (Left VIIb and Left Crus I) also showed activation.

In typical patients, language-related activation was primarily observed in the left superior temporal gyrus (anterior division), left frontal orbital cortex, along with a few right areas (planum temporale, superior parietal lobule, and planum polare). No cluster emerged in the group contrast for calculation tasks.

In atypical patients, language-related activation was right lateralized, in right planum temporale, middle temporal gyrus (temporo-occipital part), insular cortex, precuneus cortex, but also the left thalamus, and left Heschl's gyrus (H1 and H2). No cluster emerged in the group contrast for calculation tasks.

The activation patterns for patients differed considerably from those of the control group, with language-dominant temporal regions being activated primarily during language tasks, similar to the temporal clusters seen in the audio contrast, but no activation cluster emerging for calculation tasks. This divergence is difficult to explain and could be attributed to a higher variability in patients, the smaller sample size leading to insufficient statistical power, or external factors such as fatigue and difficulty in maintaining focus during the paradigm.

#### 3.2.2. Activation pattern differences between typical and atypical hemispheric language specialization

To illustrate potential differences between patients with atypical and typical language lateralization, we conducted direct group comparisons. In Nilearn, these comparisons are encoded as interaction effects, meaning that clusters identified in the group comparisons require further investigation to fully understand the source of the observed differences. As a complementary approach, we also created a combined “patient” group activation map. This

z-map, generated from the whole patient population, irrespective of the language lateralization, allowed us to assess the similarities between them and make a more direct comparison with the control group, given the similar number of subjects. The results are presented in Figure 22, and the analysis follows the same format used for the group activation maps.

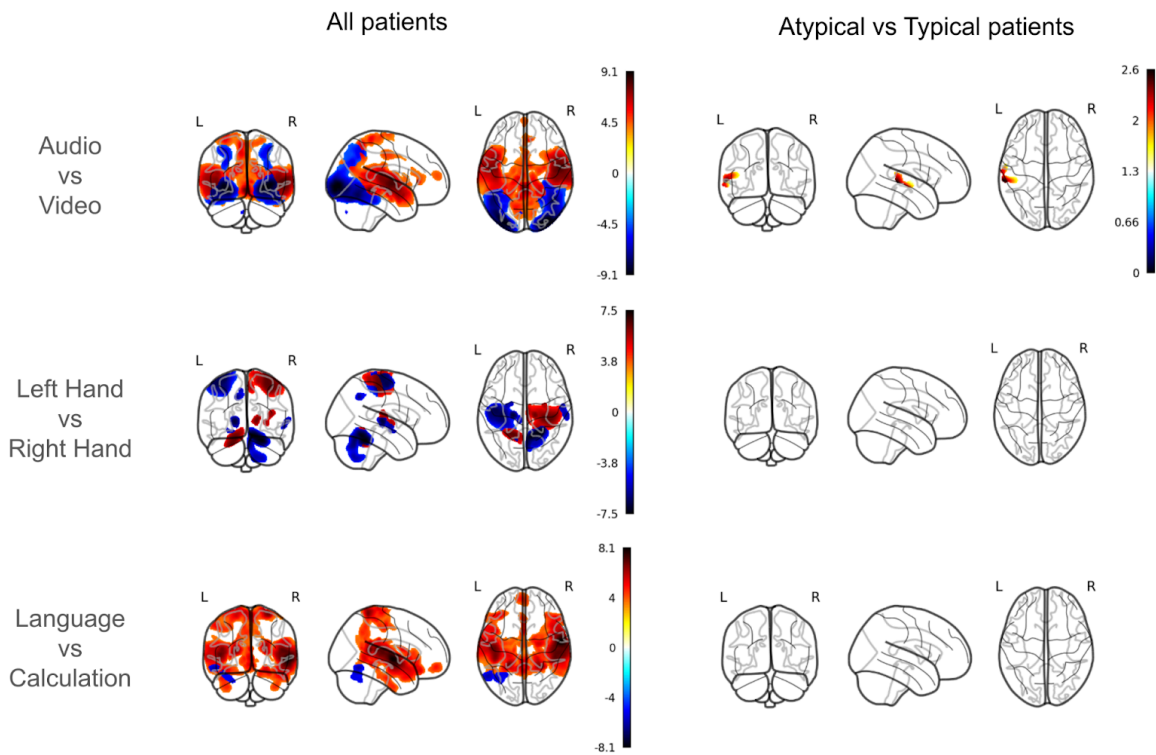


**Figure 22: Group comparison 2nd level analysis, TFCE thresholded z-maps (FDR,  $p < 0.05$ ). On the right, all patients are analyzed as the same group, regions in red are regions consistently activated for the first condition in the two groups, blue for the second. On the left, differences between typical and atypical subjects, any significant regions would need further investigation to better assess origin of the difference**

### 3.2.2.1. Audio – Video contrast

For the audio stimuli in the whole patients group, activation was very similar to that of the control group (Fig 12). Peaks were observed in the right Heschl's gyrus (including H1 and H2), right planum polare, left hippocampus, left insular cortex and left precentral gyrus. An unusual activation in the precentral cortices was noted for this contrast, which was not observed in the control group and requires further examination.

For the video stimuli, the pattern was again close to that of controls, and the most prominent activations were in the occipital regions, including the left inferior temporal gyrus (temporo-occipital part), left superior parietal lobule, and the cerebellum (Left VIIb).

The comparison between typical and atypical patient groups exhibited a small cluster in the left superior temporal gyrus, but was not captured by cluster detection in Nilearn, likely due to the small cluster size. This will be investigated further in future analyses

### 3.2.2.2. Left – Right hand motor contrast

For left-hand motor tasks in patients, activation was seen in the right postcentral gyrus, right precentral gyrus, right parietal opercular cortex, right caudate, and the left cerebellum (Left V), as expected.

For right-hand motor tasks, two peaks were identified in the left precentral gyrus, along with activation in the left caudate, the Left amygdala, and cerebellar regions (Right V, Right VIIIa).

We found no differences between the typical and atypical language groups. The activation pattern for all patients hand-motor contrast is very similar to controls group activation pattern, suggesting that differences seen in group activation maps previously seen between patients subgroups and controls was likely due to a difference in statistical power.

### 3.2.2.3. Language – Calculation contrast

Language activations for all-patient group resembled that of controls' (Fig 12), but with some rightward asymmetry of perisylvian activation and a strong activation of bilateral superior parietal lobules (upper part of the intraparietal/post central sulcus).

In the right hemisphere, activation peaks were observed in the parietal opercular cortex, superior parietal lobule, amygdala, and frontal orbital cortex. In the left hemisphere, activation involved Heschl's gyrus (including H1 and H2), parietal opercular cortex, frontal pole, posterior part of the temporal fusiform cortex and two distinct peaks in the thalamus.

For calculation tasks, the pattern of the whole patient group was very different from that of controls (Fig 12), as we found no clear activation of the intraparietal sulcus region in the superior parietal lobules, nor any prefrontal activation. Activation was primarily seen in the left inferior temporal and fusiform gyri.

Peak Z Score	X (mm)	Y (mm)	Z (mm)	Harvard-Oxford	SUIT
-6.14	-54.0	-62.0	-13.0	Left Inferior Temporal Gyrus, temporooccipital part	
-5.90	-42.0	-65.0	-20.0	Left Occipital Fusiform Gyrus	

**Table 6 : Calculation task z-map peaks position for the all patient group analysis, coordinates are expressed in symmetric MNI referential**

Figure 23 displays the BOLD signal response for language and calculation tasks for the 3 groups (controls, typical, atypical) in those two regions. The plots show that activation patterns in both regions were similar between the 2 patient groups and the control group (no activation during language and a small peak during calculation). This highly localized activation pattern in patients suggests greater dispersion in their brain activations, or lower task compliance, hence incomplete activation patterns.

Overall, these results suggest a weaker activation of the calculation networks in patients than in controls, and no specific differences between networks engaged in language and calculation processing in patients.

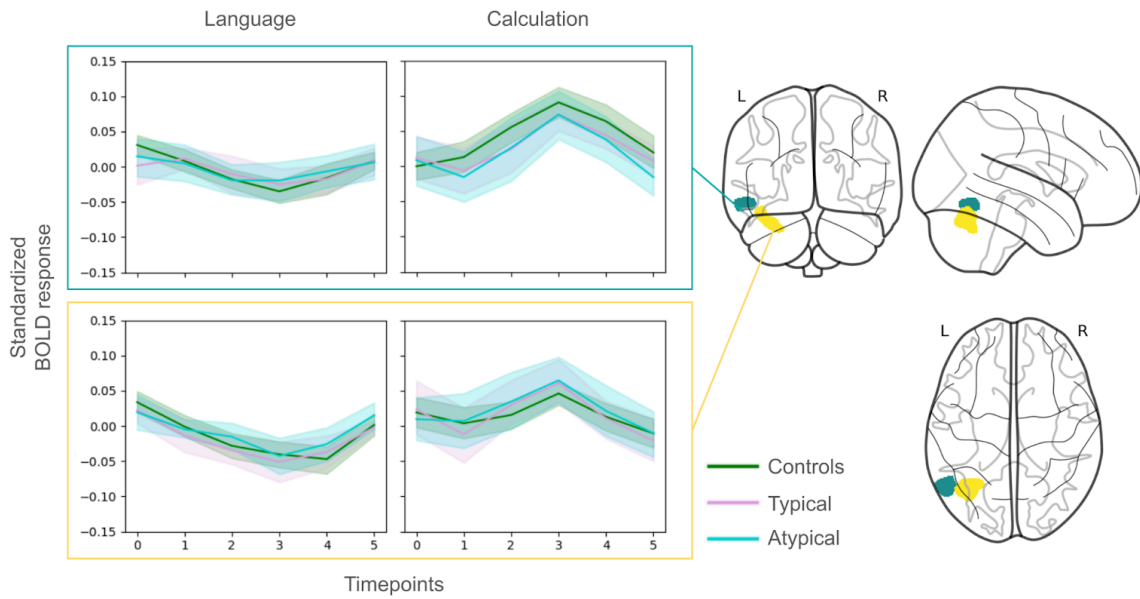


**Figure 23: Standardized BOLD time-serie for Language and Calculation activation in the left inferior temporo-occipital cluster (green) and in the fusiform gyrus (yellow)**

### 3.2.3. Investigation of activation pattern differences between dominant and non-dominant hemisphere

To better understand the differences between dominant and non-dominant hemispheres during language and calculation, we shifted along the x-plane the z-maps (registered in the MNI symmetric template) of patients with atypical language lateralization to directly compare the language-dominant hemispheres across all patients. The purpose of this approach was to explore whether there were distinct activation patterns specific to either the dominant or non-dominant hemisphere, whether left or right. Figure 24 presents the results processed and thresholded in the same manner as the previous analyses. Only the whole patient population results are shown, as the comparison between the two patient groups did not yield significant findings.

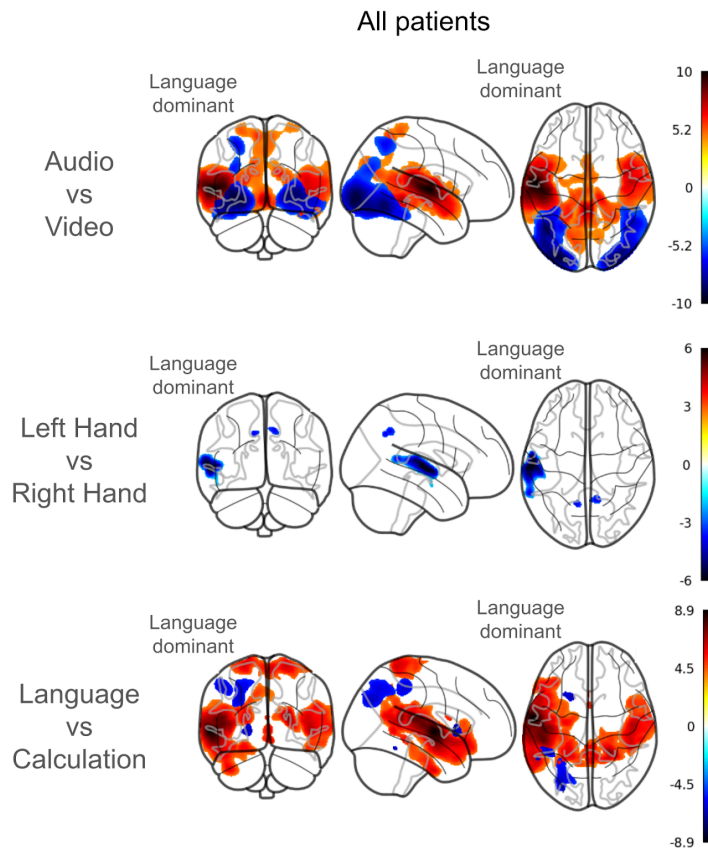


**Figure 24: Group analysis of all patients where all dominant hemispheres are shifted to the left. 2nd level analysis, TFCE thresholded z-maps (FDR,  $p < 0.05$ ). All patients are analyzed as the same group, regions in red are regions consistently activated for the first condition in the two groups, blue for the second.**

### 3.2.3.1. Audio – Video contrast

For the audio stimuli, activation was observed in both the dominant and non-dominant hemispheres, with the expected asymmetry toward the dominant hemisphere. The dominant hemisphere showed activation in Heschl's gyrus (including H1 and H2) and the hippocampus. In the non-dominant hemisphere, activation was detected in Heschl's gyrus and the thalamus.

For the video stimuli, bilateral activation was seen in the occipital pole, temporal occipital fusiform cortex, lateral occipital cortex (superior division), and in the superior parietal lobule in the dominant hemisphere only.

### 3.2.3.2. Left–Right Hand Motor Activation Contrast

No left-hand motor activation was observed.

For the right-hand motor tasks, activation in the language-dominant hemisphere was particularly notable, as it suggests right hemisphere activation in patients with atypical language lateralization (left hemisphere lesions). It might imply partly motor lateralization shifts. Activation was found in the dominant hemisphere planum temporale and in both dominant and non-dominant hemispheres of the precuneus cortex.

These surprising findings regarding motor activation warrant further investigation, particularly examining hand motor activation lateralization as a potential metric of interest.

### 3.2.3.3. Language – Calculation contrast

During the language tasks, activation was primarily observed in the dominant hemisphere, including expected regions such as the superior temporal gyrus (anterior division), the middle temporal gyrus (temporo-occipital part), and the temporal pole. Additionally, activation was detected in the hippocampus, thalamus, and the superior parietal lobule.

In the non-dominant hemisphere, activation occurred in the superior temporal gyrus, temporal pole, and the superior parietal lobule; peaks did not reflect the overall activation pattern, and cluster recovery on the atlases may be more informative.

For calculation tasks, the dominant hemisphere showed peak activation in the lateral occipital cortex (superior division), the inferior temporal gyrus (temporo-occipital part), and the supramarginal gyrus (anterior division). We found no activation for calculation in the non-dominant hemisphere. More information is tabulated in Table 5.

Peak Z Score	X (mm)	Y (mm)	Z (mm)	Harvard-Oxford	SUIT
-6.58	-20.0	16.0	1.0	Dominant Hemisphere Insula	
-6.43	-30.0	-77.0	36.0	Dominant Hemisphere Lateral Occipital Cortex, superior division	
-6.34	-55.0	-51.0	-17.0	Dominant Hemisphere Inferior Temporal Gyrus, temporooccipital part	
-6.24	-48.0	-40.0	48.0	Dominant Hemisphere Supramarginal Gyrus, anterior division	

**Table 7 : Calculation task z-map peaks position for the all patient group analysis in language dominant hemisphere, coordinates are expressed in symmetric MNI referential**

Figure 25, displays the BOLD signal response for language and calculation tasks in the four regions of the dominant hemisphere highlighted by the group contrasts across all patients. In all regions except the small insular cluster, BOLD response amplitude is of the same amplitude as left activation in controls for both patient populations.

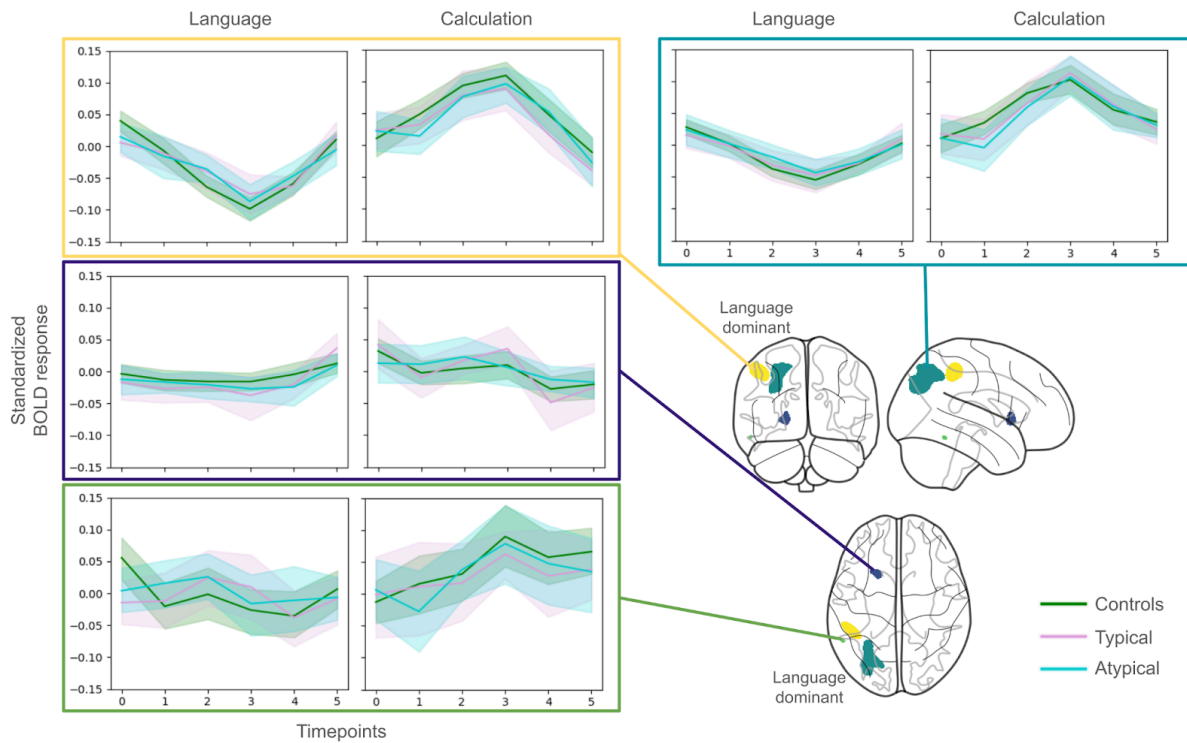


**Figure 25: Standardized BOLD time-series for Language and Calculation activation. Investigated regions are the regions activated for calculation contrast when all patients are analyzed as the same group. fMRI images were shifted to superpose all language dominant hemispheres on the left side.**

Combined together, these results suggest a calculation task lateralization in the language dominant hemisphere, whether left or right, with a consistent activation cluster in the Supramarginal (intraparietal sulcus) and lateral occipital cortex, highlighting a specialized role for this hemisphere in handling computational and linguistic tasks.

### 3.2.4. Discussion

In this second part, we present our ongoing exploration of the spatial organization of primary (hand motor activation, auditory and visual) and associative functions (mental calculation) in patients with either typical or atypical language lateralization, compared to controls.

#### *Primary function activation pattern depending on language specialization*

We showed that the activation patterns of primary functions (motor, visual, audio) in patients were largely similar to those of controls. Group contrasts, combining data from all patients, suggest that most differences between subgroups were likely due to differences in statistical power, as there were 30 controls, 15 patients with atypical language lateralization, and 14 with typical language lateralization. A few areas, notably those observed when comparing patients' dominant hemispheres, suggested a potential atypical motor activation for the right-hand motor function in the right hemisphere of atypically lateralized patients. This observation warrants further analysis.

#### *Associative (calculation) function activation pattern depending on language specialization*

Regarding calculation, we were unable to detect significant activation in either the typical or atypical language lateralization groups alone, nor significant differences between

the two groups. However, when analyzing all patients together, we identified common activation clusters in the left fusiform gyrus, as well as small activation clusters in the supramarginal, superior occipital, and inferior temporal gyri within the language-dominant hemisphere.

These findings suggest a higher lateralization of the mental calculation network, particularly around the supramarginal gyrus, in alignment with language hemispheric specialization. However, not all calculation activations followed language hemispheric dominance, as we observed small activation in the left fusiform gyrus common to both patient groups.

Overall, our results suggest a partial spatial covariance between the language and calculation activation networks following an early focal lesion like a NAIS. This spatial covariance may be explained by the dependence on language networks of calculation processing (Amalric & Dehaene, 2019). These activation areas were notably fewer and smaller in patients than in controls, indicating increased variability, likely due to cognitive impairments affecting task compliance. However, it is also possible that spatial variability in activation contributed to these findings.

#### *Conclusions on the "crowding effect"*

Our results, particularly the dominant hemisphere activation for both language and calculation, do not support the hypothesis of a "crowding effect" in the sense originally hypothesized as spatial cortical competition. However, our first investigations were not ideally suited to fully address this hypothesis. Further explorations, such as lateralization indices (LI) computed for calculation or motor tasks, or investigations of overlapping activations using other fMRI analysis tools (e.g., SPM, (Friston, 2011)), would be beneficial. In addition, the exploration of the clinical correlates are still pending.

## 4. Conclusion

In this ongoing study, we have confirmed the homotopic reorganization of the right hemisphere for atypical language lateralization following a left neonatal arterial ischemic stroke. This atypical pattern typically occurs in cases of left hemisphere lesions, particularly within the peri-sylvian areas (MCA territory), involving the dorsal pathways. Additionally, We found that stronger right-hemisphere lateralization was associated with better language scores in patients with left lesions.

We examined the "crowding effect" hypothesis and uncovered several findings that challenge this theory :

- In patients with left-hemisphere lesions, the cognitive scores were higher when patients exhibited stronger right-hemisphere language lateralization, suggesting a beneficial or protective effect of pronounced atypical hemispheric specialization for language.
- We found evidence that BOLD activation associated with calculation in the parietal lobe lateralizes in the language-dominant hemisphere. This could indicate a language-dependent integration mechanism, as aspects of mental calculation involve sentence processing tasks.

However, this evidence is not sufficient to fully challenge the crowding effect hypothesis. Lateralization indices correlate with both CELF and WAIS scores [Appendix 1], suggesting a potential protective effect of typical language development, which may contribute to a more normative life experience and overall typical development. This could, in turn, compensate for the "crowding effect". The activation patterns for calculation are relatively weak compared to those in controls, even when considering all patients, potentially indicating greater spatial variability or reduced task compliance due to cognitive difficulties.

To further investigate these results and considerations, additional approaches could be considered, such as investigating overlapping activations between language and calculation networks and employing resting-state fMRI, to investigate mental calculation clusters without relying on subject compliance. To this end, we could use the cluster highlighted with group fMRI or use a specific atlas.

# Perspectives and Considerations on the Presented Studies

NAIS presents a particularly compelling model for studying brain plasticity after an early lesion in children :

- Its relatively high incidence compared to other forms of pediatric stroke, combined with the high prevalence of left MCA involvement, make it the perinatal stroke with the greatest potential for building a cohort with sufficient homogeneity. This offers a promising opportunity to isolate specific mechanisms of brain development and plasticity after a focal neonatal lesion.
- The precise timing of the stroke induces lesser plasticity of primary functions (e.g., auditory, visual, motor) and higher plasticity of associative functions, allowing to study a broad spectrum of brain plasticity mechanisms and response to injury.

While it has become clear that subjects with NAIS tend to have suboptimal clinical performance on average, identifying neuroimaging markers that finely predict cognitive or developmental outcomes remains challenging. In this context, the AVCnn cohort, with its extensive and longitudinal clinical follow-up and neuroimaging data, represents a valuable resource for exploring such markers. To our knowledge, it is currently one of the most uniform cohorts in terms of pathology definition and is among the largest. Another substantial cohort (deVeber et al., 2000) exists but it is less well-defined and includes a wider age range.

## 1. Remarks on Morphometry studies

### 1.1. Strengths

A key strength of our study lies in the emphasis we placed on thorough manual quality checks at every step of the process. Although time-consuming, this rigorous attention to methodological details underscores the challenges rarely acknowledged in the literature. This diligence, particularly with respect to the lesioned hemisphere, strengthens the validity of our conclusions, countering the trend of some studies to quickly overlook such concerns.

In addition, thanks to the age-restricted design of our cohort, we were able to cancel the common age-related variability of the developmental cohorts. This allowed us to employ simpler models for tracking developmental changes and expand the number of variables analyzed using a mixed-model approach.

We consistently observed similar effects across different models and volumetric methodologies after controlling for various developmental variables. These findings strengthen our confidence that the results are not due to model overfitting, but reflect a genuine morphological patient-specific sex-difference in our cohort.

## 1.2. Weaknesses

### 1.2.1. Scanner bias

The heterogeneity of scanner equipment poses a challenge in most large multicenter neuroimaging studies. In our case, the scanner change from TRIO to Prisma Fit 3T Magnetom (Siemens) was strictly covariant with the age variable (7 and 16 years). Scanner changes mostly introduce both additive and multiplicative biases (Fortin et al., 2018) and nonlinear biases potentially. The mixed-model was useful to that extent, as additive bias is accounted for by the age regressor, which makes our design unsuitable at precisely estimating age-related volume variations alone, but still suitable for regressing age and scanner additive variability to isolate status effect.

We considered using scanner bias correction algorithms such as ComBat (Fortin et al., 2018), and consulted with researchers who have optimized these tools. However, we ultimately decided against applying it, as this tool assumes mean and variance equivalence between site/scanner, which was not our case due to lesion variability. It would have risked introducing supplementary bias in our data.

### 1.2.2. Effect of whole brain volume

One unresolved issue, acknowledged by reviewers, is the difficulty in accounting for total brain volume, a major source of variability in morphometry studies. In typical groups, correcting for brain volume is standard, but in our case, it is not independent of lesion presence. Although we adopted a comparative approach showing volume differences across regions to evaluate global trends, this method reduced the sensitivity of the results.

We eventually considered a potentially unbiased way to study region-specific trajectories by residualizing contralesional hemisphere volume and introducing this residual as a covariate in regional models. This aimed to create a brain volume variable independent of developmental and lesion effects. However, the implications of this approach and its interaction with LMM random variables need further exploration.

### 1.2.3. Generalization of this study

A major limitation of our study is the generalizability of the results. Although it is one of the largest NAIS cohorts to date, it remains small by contemporary MRI standards, and it remains uncertain to what extent our cohort is representative of the entire NAIS population, although we took special attention to avoid any recruitment bias (based on the data at age 7 years, we confirmed that the group of adolescents studied at age 16 had the same characteristics as the adolescents that were not). Furthermore, our control group was recruited largely from a suburban area of Paris (the Saclay area), where there is a concentration of universities and research institutions, potentially introducing a sociological bias.

## 1.3. Perspectives

### 1.3.1. Normative Analysis: Addressing Generalizability and Scanner Bias

One promising avenue to overcome these limitations is the normative analysis approach. Recent papers have proposed leveraging large databases to correct for factors such as age, sex, hemispheric asymmetry, and site bias (Bethlehem et al., 2022; Rutherford et al., 2022; Williams et al., 2021). Neurospin has a large number of data acquired on the same imager with a wide age range and could, subject to regulatory requirements, take advantage of these data to enable all teams working on rare diseases (including our own) to have effective means of correcting scanner bias and get access to a comparison more representative of the global population. This implementation would benefit our morphometric studies, as well as all other small cohort projects.

Hypothetical applications might include integrating new datasets to refine model predictions, generating population distributions by quartile, training models to account for site, scanner, or processing biases, and returning bias correction coefficients or models. It could also support allometric studies and offer different approaches to modeling. Recent normative approaches, allometric models or deep learning based tools already perform on one or several of these applications.

The overarching vision would be to develop a versatile tool capable of delivering results across multiple levels and stages of analysis, adaptable to various experimental designs. While highly speculative and requiring a long-term, ambitious effort, such a tool could foster better collaborative practices and reduce data redundancy.

### 1.3.2. Normalization and parcellation methods for lesional brain in children

As previously discussed in the article and its supplementary materials, brain normalization, particularly ipsilesional parcellation, presents significant challenges in perinatal stroke research. These challenges explain why much of the research has focused on the contralesional hemisphere rather than the ipsilesional hemisphere. Studies examining the ipsilesional side typically concentrate on very specific regions, often guided by clinical hypotheses. This is done to limit the extensive manual work required for correcting segmentation errors. However, this approach undermines the comprehensiveness and consistency of morphometric findings and poses challenges for other imaging modalities that rely on parcellation or normalization to the MNI space.

A promising approach to address these limitations is the concept of "Virtual Brain Grafting" (VBG) (Radwan et al., 2021). VBG is a fully automated, open-source workflow designed to facilitate reliable parcellation of MRI datasets in the presence of focal brain pathologies, such as large lesions. By simulating brain tissue in the lesioned areas, VBG generates a lesion-free T1-weighted image, allowing for more accurate normalization and parcellation, thus overcoming some of the challenges associated with brain normalization in stroke research.

Another potential solution involves using anatomical landmarks for registration, such as sulci. This approach could reduce the risk of significant mislabeling errors. Currently available software for sulci-based analyses, such as the DISCO method implemented in BrainVISA (Auzias et al., 2011; Lebenberg et al., 2018), holds promise but still requires considerable manual correction, limiting its scalability and efficiency.

These approaches have limitations, as the process of post-lesional brain growth alters anatomy in ways that are not yet fully understood. As a result, the concept of spatial correspondence remains poorly defined, even in cases where realignment is performed manually.

### 1.3.3. Exploring differences between cortical thickness and volume results

As we did observe weaker effects for cortical thickness than for volumes, it suggests several hypotheses on cortical surface evolution and gyrification to explain this divergence. These issues would require many supplementary investigations, particularly on brain surface and gyrification. As brain gyrification fine study is an emerging research area, there are few studies that delved into gyrification after a perinatal stroke (Al Harrach et al., 2019), finding very focal alterations.

The exploration of gyrification encompasses various methodologies. A commonly used approach involves calculating a regional gyrification index, as implemented in tools such as CAT12 or FreeSurfer. For a more in-depth investigation, sulcus-based morphometry tools, such as those available in BrainVISA can be considered. These tools allow for the detailed analysis of individual sulcal characteristics and offer alternative parcellation methods that may be less affected by lesion-induced deformations. However further evaluation is required to determine the strategic value of adopting such methods in case of an early injured brain.

## 2. Perspectives for Functional and Structural Connectivity studies

### 2.1. Further investigation of homotopic language lateralization consequences

Further exploration is needed, particularly of the significance of activation clusters in group maps and their overlap in group comparisons. Variability of individual activation maps is a growing focus in the literature, and future studies should explore this area. However, there are currently no clear methodological guidelines nor statistical frameworks for individual studies, despite their obvious major interest for clinical applications. In our sample, lesion variability in location and size required a dedicated effort for the extraction of relevant morphometric, functional and microstructural markers applicable to the entire population.

## 2.2. Avenues for investigating microstructural connectivity with Diffusion MRI

As we only preliminary explored the area of structural connectivity and white matter microstructure, there is still a great potential for methodological exploration and improvement in numerous ways.

Among the literature which combined fMRI and dMRI, our study lies in the “integration approaches” category (Jarret et al., 2022), as we used fMRI-based atlas to restrain tractography. As no clear guidelines exist on the matter, and as few studies compared their results to reference populations, it is difficult to evaluate the potential of such approaches.

### 2.2.1. White matter tracts parcellation

The first avenue for improvement lies in the white matter tracts parcellation methods. Our functional regions of interest (ROIs) were relatively small, which may have posed a problem. One potential improvement would be to adopt more widely used cortical atlases, as our study confirmed the hemispheric homotopy of language networks. This would provide a valuable white matter bundle reconstruction to compare with our actual reconstructions.

Additionally, white matter bundle atlases, such as TRACTSEG (Wasserthal et al., 2018), a convolutional neural network trained on 105 healthy subjects from the Human Connectome Project (HCP), to segment 72 anatomically well-defined white matter tracts, could be employed. This approach would assume structural connectivity remains relatively stable in patients in the contralesional hemisphere compared to controls but would imperfectly work in the lesioned hemisphere.

We did not implement one safeguard that may improve the relevance of parcellation: ensuring that ROIs encompass gray-white matter interface, thus ensuring compatibility with Anatomically-Constrained Tractography (ACT) deployed for our analysis. This approach could also reduce inter-individual variability.

### 2.2.2. White Matter Integrity metrics

Our preliminary analysis is still incomplete, as we did not yet perform the data processing pipeline for other conventional DTI metrics (MD, AD, RD, ...). Although mean tract metrics like FA are widely used, it is also common knowledge that this approach is far from perfect, and very prone to false negative/Type II error (Gomez et al., 2015). One way to mitigate this weakness would be to use track profiling approaches, which measure metric changes along a tract. However, there is no clear consensus on the best approach, as this method introduces difficulties in the interpretation of inter-subject variability. Moreover, FA is sensitive to the presence of crossing fibers (in areas with crossing fibers, FA values can be artificially lowered), which can lead to misinterpretation of the underlying tissue microstructure.

NODDI model provides more specific measures of brain microstructure compared to traditional diffusion tensor imaging, including in gray matter (Chung et al., 2016). This

approach would allow us to further investigate the sex-related gray matter volume differences highlighted in our paper. At the same time, it would provide diffusion metrics more sensitive to white matter microstructure than those from DTI, without engaging in the complex image processing required for Fixel-Based Analysis

Structural connectomics enables the quantitative analysis of brain network properties through graph theoretical approaches, providing valuable insights into the structural basis of brain function and plasticity. However, its main limitation lies in the unclear relationship between structural connectivity measures (e.g., streamline count, fractional anisotropy) and actual axonal connectivity. Moreover, the accuracy of results can be highly dependent on the parcellation and reconstruction methods employed. (Straathof et al., 2019).

Fixel-based analysis is particularly well-suited for regions with complex fiber configurations, as it enables the characterization of individual fiber populations within a voxel, thereby addressing the issue of crossing fibers that confounds traditional DTI measures. This approach can potentially detect more subtle changes in white matter microstructure compared to voxel-based methods, offering metrics more directly related to the underlying white matter anatomy, such as fiber density and fiber cross-section. However, as a relatively new technique, FBA requires further validation against histological measures and across various clinical populations. Additionally, group analyses rely on the construction of a cohort-specific fixel template, which can be challenging in cases of atypical brain anatomy and will require extensive validation (Dhollander, Clemente, et al., 2021).

### 3. Using multimodal and clinical data to extract risk factors and outcome predictors

The initial overarching goal of this study was to extract bioimaging markers, at different scale and abstraction levels (voxel, local/ROI, network, ...), by performing a multimodal imaging and clinical data investigation of protective or risk markers. While some progress has been made in this direction, not all imaging modalities have been explored, some analyses require further refinement, and several clinical markers are still undergoing descriptive analysis.

Once these challenges are addressed, the question remains of how to combine and analyze the numerous markers within a relatively small cohort of subjects.

Multivariate approaches are a promising initial avenue for such explorations, as they are well-suited for situations requiring the reduction or grouping of explanatory variables, and for isolating those with strong variance-explaining capabilities. Principal Component Analysis (PCA) is a simple example that could serve as a proof of concept. More advanced techniques such as Multiple Factor Analysis (MFA), Factor Analysis for Mixed Data (FAMD), or Mixed PCA, which handle both continuous and categorical variables, could also be considered. Other, more complex models or those based on different assumptions could be explored as well, but they would require formalization of constraints after a thorough review of the relevant literature. It is important to acknowledge the limitations of our dataset, which is relatively small, only partially longitudinal, and affected by missing data, due in part to

variability in the application of exclusion criteria based on image quality across imaging modalities.

The use of deep learning approaches may appear attractive given the current focus on this field, particularly in neuroimaging. However, in our case, most deep learning methods are impractical due to the "curse of dimensionality," which necessitates a large number of subjects to train a model capable of avoiding overfitting and achieving generalizability when dealing with data containing numerous features, such as images. While dimensionality reduction techniques, such as creating connectomes, may help manage the complexity of imaging data, they are unlikely to suffice for training robust deep learning models.

One potentially feasible approach could involve the use of foundation models, large-scale machine learning models pre-trained on extensive, diverse datasets, which can be adapted or fine-tuned for specific tasks, such as predicting risk factors or outcomes from multimodal imaging and clinical data. However, this lies outside our current expertise, and there are multiple potential sources of complexity that would need to be addressed.

## 4. Outcomes of Brain Plasticity after an Early lesion

### 4.1. Language homotopy functional outcomes and microstructure

Despite known brain anatomical and functional asymmetries at birth (Dehaene-Lambertz et al., 2002), our results confirmed that homotopic language lateralization in the contralesional hemisphere is common after an early left lesion. This organization was observed with group activation maps and individual LIs. In addition, our preliminary microstructural exploration showed no microstructural differences between a typical left lateralized language network and an atypically right lateralized language network.

In our cohort, the data suggest that this homotopic reorganization is beneficial for language performance in patients with a left lesion. Our current data and methods do not allow us to delve deeper into this interpretation. To refine our results, we would need to compute LIs on more granular atlases tailored to the language network, obtaining more specific indices and investigate the contribution of individual regions. A key challenge would be ensuring the accuracy of the registration steps in the SPM LI toolbox, or, if necessary, bypassing automatic registrations to manage the process manually.

### 4.2. "Crowding Effect"

The "crowding effect" hypothesis posits that atypical language specialization could create spatial competition, particularly with associative functions that develop later, such as mental arithmetic (e.g., subtraction). Our current (and incomplete) findings challenge this hypothesis:

- Calculation tasks appear to become more lateralized in the language-dominant hemisphere, while primary functions maintain a typical organization.
- Greater atypical lateralization of language in patients with left-hemisphere lesions correlates significantly with better clinical performance, even in non-language functions.

Based on these observations, it is difficult to fully support the crowding effect hypothesis in our study at this stage. Although our results do not allow us to investigate this hypothesis directly, they suggest that any potential "crowding effect" might be compensated for by effective language development, a significant developmental advantage.

## Final conclusion

Beyond well-known risk factors like epilepsy and Cerebral Palsy, little is known about the long-term outcomes after neonatal stroke (NAIS). Neuroimaging is a growing field of research that benefits from a highly advanced open-source methodological research environment and significantly capitalizes on the advancements in artificial intelligence. Neuroimaging holds great promise for exploring the brain development and plasticity after early setbacks, through the numerous metrics available in these rich datasets. However, doing so requires many improvements and developments in managing long term longitudinal data, dealing with missing data, and characterizing inter-individual variability, especially in patients with distorted anatomy.

Further exploration of the crowding effect hypothesis will involve precisely examining the overlap of functional activations during language and mental computation. Resting-state fMRI is very promising for investigating the crowding effect hypothesis. Its major advantage is that it does not require complex tasks, allowing us to explore the brain's functional organization in patients while minimizing compliance bias due to cognitive difficulties. However, this requires robust statistical handling of missing data if we want to use both 7yo and 16yo acquisitions, enabling group comparisons that are reliable and interpretable.

The approaches developed in this thesis will be expanded during my postdoctoral research, with a particular focus on functional connectivity using resting-state fMRI. This work is the first step to create a database of markers for multimodal exploration, helping to further identify risk factors linked to NAIS and providing a deeper understanding of early brain plasticity to guide clinicians in establishing a prognosis and implementing early personalized care and rehabilitation programs in future neonates with NAIS.

## Bibliography

- Abbasi, H., Orouskhani, M., Asgari, S., & Zadeh, S. S. (2023). Automatic brain ischemic stroke segmentation with deep learning : A review. *Neuroscience Informatics*, 3(4), 100145. <https://doi.org/10.1016/j.neuri.2023.100145>
- Al Harrach, M., Pretzel, P., Groeschel, S., Rousseau, F., Dhollander, T., Hertz-Pannier, L., Lefevre, J., Chabrier, S., Dinomais, M., & the AVCnn study group. (2021). A connectome-based approach to assess motor outcome after neonatal arterial ischemic stroke. *Annals of Clinical and Translational Neurology*, 8(5), 1024-1037. <https://doi.org/10.1002/acn3.51292>
- Al Harrach, M., Rousseau, F., Groeschel, S., Chabrier, S., Hertz-Pannier, L., Lefevre, J., Dinomais, M., & The AVCnn Study Team. (2020). Is the Blood Oxygenation Level-Dependent fMRI Response to Motor Tasks Altered in Children After Neonatal Stroke? *Frontiers in Human Neuroscience*, 14. <https://doi.org/10.3389/fnhum.2020.00154>
- Al Harrach, M., Rousseau, F., Groeschel, S., Wang, X., Hertz-pannier, L., Chabrier, S., Bohi, A., Lefevre, J., Dinomais, M., & on behalf of the AVCnn group. (2019). Alterations in Cortical Morphology after Neonatal Stroke : Compensation in the Contralesional Hemisphere? *Developmental Neurobiology*, 79(4), 303-316. <https://doi.org/10.1002/dneu.22679>
- Amalric, M., & Dehaene, S. (2016). Origins of the brain networks for advanced mathematics in expert mathematicians. *Proceedings of the National Academy of Sciences*, 113(18), 4909-4917. <https://doi.org/10.1073/pnas.1603205113>
- Amalric, M., & Dehaene, S. (2019). A distinct cortical network for mathematical knowledge in the human brain. *NeuroImage*, 189, 19-31. <https://doi.org/10.1016/j.neuroimage.2019.01.001>
- Andersson, J. L. R., Graham, M. S., Drobnyak, I., Zhang, H., Filippini, N., & Bastiani, M. (2017). Towards a comprehensive framework for movement and distortion correction

- of diffusion MR images : Within volume movement. *NeuroImage*, *152*, 450-466.  
<https://doi.org/10.1016/j.neuroimage.2017.02.085>
- Andersson, J. L. R., Graham, M. S., Zsoldos, E., & Sotiropoulos, S. N. (2016). Incorporating outlier detection and replacement into a non-parametric framework for movement and distortion correction of diffusion MR images. *NeuroImage*, *141*, 556-572.  
<https://doi.org/10.1016/j.neuroimage.2016.06.058>
- Andersson, J. L. R., & Sotiropoulos, S. N. (2016). An integrated approach to correction for off-resonance effects and subject movement in diffusion MR imaging. *NeuroImage*, *125*, 1063-1078. <https://doi.org/10.1016/j.neuroimage.2015.10.019>
- Arora, A., Pletzer, B., Aichhorn, M., & Perner, J. (2020). What's in a Hub?-Representing Identity in Language and Mathematics. *Neuroscience*, *432*.  
<https://doi.org/10.1016/j.neuroscience.2020.02.032>
- Arsalidou, M., Pawliw-Levac, M., Sadeghi, M., & Pascual-Leone, J. (2017). Brain areas associated with numbers and calculations in children : Meta-analyses of fMRI studies. *Developmental Cognitive Neuroscience*, *30*, 239-250.  
<https://doi.org/10.1016/j.dcn.2017.08.002>
- Auzias, G., Colliot, O., Glaunes, J. A., Perrot, M., Mangin, J.-F., Trouve, A., & Baillet, S. (2011). Diffeomorphic Brain Registration Under Exhaustive Sulcal Constraints. *IEEE Transactions on Medical Imaging*, *30*(6), 1214-1227. *IEEE Transactions on Medical Imaging*. <https://doi.org/10.1109/TMI.2011.2108665>
- Baak, L. M., van der Aa, N. E., Verhagen, A. A. E., Dudink, J., Groenendaal, F., Nijboer, C. H. A., Benders, M. J. N. L., & Wagenaar, N. (2023). Early predictors of neurodevelopment after perinatal arterial ischemic stroke : A systematic review and meta-analysis. *Pediatric Research*, *94*(1), 20-33.  
<https://doi.org/10.1038/s41390-022-02433-w>
- Ballantyne, A. O., Spilkin, A. M., Hesselink, J., & Trauner, D. A. (2008). Plasticity in the developing brain : Intellectual, language and academic functions in children with ischaemic perinatal stroke. *Brain*, *131*(11), 2975-2985.

<https://doi.org/10.1093/brain/awn176>

- Ballester-Plané, J., Schmidt, R., Laporta-Hoyos, O., Junqué, C., Vázquez, É., Delgado, I., Zubiaurre-Elorza, L., Macaya, A., Póo, P., Toro, E., de Reus, M. A., van den Heuvel, M. P., & Pueyo, R. (2017). Whole-brain structural connectivity in dyskinetic cerebral palsy and its association with motor and cognitive function. *Human Brain Mapping*, 38(9), 4594-4612. <https://doi.org/10.1002/hbm.23686>
- Bastiani, M., Cottaar, M., Fitzgibbon, S. P., Suri, S., Alfaro-Almagro, F., Sotiropoulos, S. N., Jbabdi, S., & Andersson, J. L. R. (2019). Automated quality control for within and between studies diffusion MRI data using a non-parametric framework for movement and distortion correction. *NeuroImage*, 184, 801-812. <https://doi.org/10.1016/j.neuroimage.2018.09.073>
- Becker, M., & Hesse, V. (2020). Minipuberty : Why Does it Happen? *Hormone Research in Paediatrics*, 93(2), 76-84. <https://doi.org/10.1159/000508329>
- Bethlehem, R. A. I., Seidlitz, J., White, S. R., Vogel, J. W., Anderson, K. M., Adamson, C., Adler, S., Alexopoulos, G. S., Anagnostou, E., Areces-Gonzalez, A., Astle, D. E., Auyeung, B., Ayub, M., Bae, J., Ball, G., Baron-Cohen, S., Beare, R., Bedford, S. A., Benegal, V., ... Alexander-Bloch, A. F. (2022). Brain charts for the human lifespan. *Nature*, 604(7906), 525-533. <https://doi.org/10.1038/s41586-022-04554-y>
- Boardman, J. P., Ganesan, V., Rutherford, M. A., Saunders, D. E., Mercuri, E., & Cowan, F. (2005). Magnetic resonance image correlates of hemiparesis after neonatal and childhood middle cerebral artery stroke. *Pediatrics*, 115(2), 321-326. <https://doi.org/10.1542/peds.2004-0427>
- Cabezas, M., Oliver, A., Lladó, X., Freixenet, J., & Bach Cuadra, M. (2011). A review of atlas-based segmentation for magnetic resonance brain images. *Computer Methods and Programs in Biomedicine*, 104(3), e158-e177. <https://doi.org/10.1016/j.cmpb.2011.07.015>
- Calautti, C., & Baron, J.-C. (2003). Functional Neuroimaging Studies of Motor Recovery After Stroke in Adults. *Stroke*, 34(6), 1553-1566.

<https://doi.org/10.1161/01.STR.0000071761.36075.A6>

- Cantlon, J. F., Brannon, E. M., Carter, E. J., & Pelphrey, K. A. (2006). Functional Imaging of Numerical Processing in Adults and 4-y-Old Children. *PLOS Biology*, *4*(5), e125. <https://doi.org/10.1371/journal.pbio.0040125>
- Cao, Y., Vikingstad, E. M., Huttenlocher, P. R., Towle, V. L., & Levin, D. N. (1994). Functional magnetic resonance studies of the reorganization of the human hand sensorimotor area after unilateral brain injury in the perinatal period. *Proceedings of the National Academy of Sciences*, *91*(20), 9612-9616. <https://doi.org/10.1073/pnas.91.20.9612>
- Carlson, H. L., Sugden, C., Brooks, B. L., & Kirton, A. (2019). Functional connectivity of language networks after perinatal stroke. *NeuroImage: Clinical*, *23*, 101861. <https://doi.org/10.1016/j.nicl.2019.101861>
- Chabrier, S., Peyric, E., Drutel, L., Deron, J., Kossorotoff, M., Dinomais, M., Lazaro, L., Lefranc, J., Thébault, G., Dray, G., Fluss, J., Renaud, C., Nguyen The Tich, S., Darteyre, S., Dégano, C., Delion, M., Groeschel, S., Hertz-Pannier, L., Husson, B., ... Vuillerot, C. (2016). Multimodal Outcome at 7 Years of Age after Neonatal Arterial Ischemic Stroke. *The Journal of Pediatrics*, *172*, 156-161.e3. <https://doi.org/10.1016/j.jpeds.2016.01.069>
- Charriaut-Marlangue, C., Besson, V., & Baud, O. (2017). Sexually Dimorphic Outcomes after Neonatal Stroke and Hypoxia-Ischemia. *International Journal of Molecular Sciences*, *19*(1), 61. <https://doi.org/10.3390/ijms19010061>
- Cheng, B., Petersen, M., Schulz, R., Boenstrup, M., Krawinkel, L., Gerloff, C., & Thomalla, G. (2021). White matter degeneration revealed by fiber-specific analysis relates to recovery of hand function after stroke. *Human Brain Mapping*, *42*(16), 5423-5432. <https://doi.org/10.1002/hbm.25632>
- Chung, A. W., Seunarine, K. K., & Clark, C. A. (2016). NODDI reproducibility and variability with magnetic field strength : A comparison between 1.5 T and 3 T. *Human Brain Mapping*, *37*(12), 4550-4565. <https://doi.org/10.1002/hbm.23328>
- Craig, B. T., Carlson, H. L., & Kirton, A. (2019). Thalamic diaschisis following perinatal stroke

- is associated with clinical disability. *NeuroImage: Clinical*, 21, 101660.  
<https://doi.org/10.1016/j.nicl.2019.101660>
- Craig, B. T., Hilderley, A., Kinney-Lang, E., Long, X., Carlson, H. L., & Kirton, A. (2020). Developmental neuroplasticity of the white matter connectome in children with perinatal stroke. *Neurology*, 95(18). <https://doi.org/10.1212/WNL.0000000000010669>
- Craig, B. T., Hilderley, A., Kirton, A., & Carlson, H. L. (2021). Imaging Developmental and Interventional Plasticity Following Perinatal Stroke. *Canadian Journal of Neurological Sciences / Journal Canadien Des Sciences Neurologiques*, 48(2), 157-171.  
<https://doi.org/10.1017/cjn.2020.166>
- Craig, B. T., Kinney-Lang, E., Hilderley, A. J., Carlson, H. L., & Kirton, A. (2022). Structural connectivity of the sensorimotor network within the non-lesioned hemisphere of children with perinatal stroke. *Scientific Reports*, 12(1), 3866.  
<https://doi.org/10.1038/s41598-022-07863-4>
- Craig, B. T., Olsen, C., Mah, S., Carlson, H. L., Wei, X.-C., & Kirton, A. (2019). Crossed Cerebellar Atrophy in Perinatal Stroke. *Stroke*, 50(1), 175-177.  
<https://doi.org/10.1161/STROKEAHA.118.022423>
- Darmency-Stamboul, V., Cordier, A. G., & Chabrier, S. (2017). Accident vasculaire cérébral ischémique artériel chez le nouveau-né à terme ou proche du terme : Prévalence et facteurs de risque. *Archives de Pédiatrie*, 24(9, Supplement), 9S3-9S11.  
[https://doi.org/10.1016/S0929-693X\(17\)30325-1](https://doi.org/10.1016/S0929-693X(17)30325-1)
- Darteyre, S., Renaud, C., Vuillerot, C., Presles, E., Kossorotoff, M., Dinomais, M., Lazaro, L., Gautheron, V., & Chabrier, S. (2014). Quality of life and functional outcome in early school-aged children after neonatal stroke : A prospective cohort study. *European Journal of Paediatric Neurology*, 18(3), 347-353.  
<https://doi.org/10.1016/j.ejpn.2014.01.006>
- Davis, N., Cannistraci, C. J., Rogers, B. P., Gatenby, J. C., Fuchs, L. S., Anderson, A. W., & Gore, J. C. (2009). The neural correlates of calculation ability in children : An fMRI study. *Magnetic Resonance Imaging*, 27(9), 1187-1197.

<https://doi.org/10.1016/j.mri.2009.05.010>

Debillon, T., De Launay, C., & Ego, A. (2017). Recommandations pour la prise en charge de l'infarctus cérébral artériel à révélation néonatale chez le nouveau-né à terme ou proche du terme. *Archives de Pédiatrie*, 24(9), 9S1-9S2.

[https://doi.org/10.1016/S0929-693X\(17\)30324-X](https://doi.org/10.1016/S0929-693X(17)30324-X)

DeCasien, A. R., Guma, E., Liu, S., & Raznahan, A. (2022). Sex differences in the human brain : A roadmap for more careful analysis and interpretation of a biological reality. *Biology of Sex Differences*, 13(1), 43. <https://doi.org/10.1186/s13293-022-00448-w>

Dehaene, S., & Cohen, L. (2007). Cultural Recycling of Cortical Maps. *Neuron*, 56(2), 384-398. <https://doi.org/10.1016/j.neuron.2007.10.004>

Dehaene-Lambertz, G., Dehaene, S., & Hertz-Pannier, L. (2002). Functional Neuroimaging of Speech Perception in Infants. *Science*, 298(5600), 2013-2015.

<https://doi.org/10.1126/science.1077066>

Desikan, R. S., Ségonne, F., Fischl, B., Quinn, B. T., Dickerson, B. C., Blacker, D., Buckner, R. L., Dale, A. M., Maguire, R. P., Hyman, B. T., Albert, M. S., & Killiany, R. J. (2006). An automated labeling system for subdividing the human cerebral cortex on MRI scans into gyral based regions of interest. *NeuroImage*, 31(3), 968-980.

<https://doi.org/10.1016/j.neuroimage.2006.01.021>

deVeber, G. A., MacGregor, D., Curtis, R., & Mayank, S. (2000). Neurologic Outcome in Survivors of Childhood Arterial Ischemic Stroke and Sinovenous Thrombosis. *Journal of Child Neurology*, 15(5), 316-324. <https://doi.org/10.1177/088307380001500508>

Dhollander, T., Clemente, A., Singh, M., Boonstra, F., Civier, O., Duque, J. D., Egorova, N., Enticott, P., Fuelscher, I., Gajamange, S., Genc, S., Gottlieb, E., Hyde, C., Imms, P., Kelly, C., Kirkovski, M., Kolbe, S., Liang, X., Malhotra, A., ... Caeyenberghs, K. (2021). Fixel-based Analysis of Diffusion MRI : Methods, Applications, Challenges and Opportunities. *NeuroImage*, 241, 118417.

<https://doi.org/10.1016/j.neuroimage.2021.118417>

Dhollander, T., Tabbara, R., Rosnarho-Tornstrand, J., Tournier, J.-D., Raffelt, D., & Connelly,

- A. (2021, mai 15). *Multi-tissue log-domain intensity and inhomogeneity normalisation for quantitative apparent fibre density*.
- Diedrichsen, J., Balsters, J. H., Flavell, J., Cussans, E., & Ramnani, N. (2009). A probabilistic MR atlas of the human cerebellum. *NeuroImage*, *46*(1), 39-46.  
<https://doi.org/10.1016/j.neuroimage.2009.01.045>
- Diedrichsen, J., Maderwald, S., Küper, M., Thürling, M., Rabe, K., Gizewski, E. R., Ladd, M. E., & Timmann, D. (2011). Imaging the deep cerebellar nuclei : A probabilistic atlas and normalization procedure. *NeuroImage*, *54*(3), 1786-1794.  
<https://doi.org/10.1016/j.neuroimage.2010.10.035>
- Dinomais, M., Groeschel, S., Staudt, M., Krägeloh-Mann, I., & Wilke, M. (2012). Relationship between functional connectivity and sensory impairment : Red flag or red herring? *Human Brain Mapping*, *33*(3), 628-638. <https://doi.org/10.1002/hbm.21227>
- Dinomais, M., Hertz-Pannier, L., Groeschel, S., Chabrier, S., Delion, M., Husson, B., Kossorotoff, M., Renaud, C., Nguyen The Tich, S., & for the AVCnn Study Group. (2015). Long term motor function after neonatal stroke : Lesion localization above all. *Human Brain Mapping*, *36*(12), 4793-4807. <https://doi.org/10.1002/hbm.22950>
- Dinomais, M., Hertz-Pannier, L., Groeschel, S., Delion, M., Husson, B., Kossorotoff, M., Renaud, C., Chabrier, S., & The Tich, S. N. (2016). Does Contralesional Hand Function After Neonatal Stroke Only Depend on Lesion Characteristics? *Stroke*, *47*(6), 1647-1650. <https://doi.org/10.1161/STROKEAHA.116.013545>
- Dudink, J., Mercuri, E., Al-Nakib, L., Govaert, P., Counsell, S., Rutherford, M., & Cowan, F. M. (2009). Evolution of Unilateral Perinatal Arterial Ischemic Stroke on Conventional and Diffusion-Weighted MR Imaging. *AJNR. American journal of neuroradiology*, *30*, 998-1004. <https://doi.org/10.3174/ajnr.A1480>
- Dunbar, M., & Kirton, A. (2018). Perinatal stroke : Mechanisms, management, and outcomes of early cerebrovascular brain injury. *The Lancet Child & Adolescent Health*, *2*(9), 666-676. [https://doi.org/10.1016/S2352-4642\(18\)30173-1](https://doi.org/10.1016/S2352-4642(18)30173-1)
- Dunbar, M., & Kirton, A. (2019). Perinatal Stroke. *Seminars in Pediatric Neurology*, *32*,

100767. <https://doi.org/10.1016/j.spen.2019.08.003>

Dunbar, M., Mineyko, A., Hill, M., Hodge, J., Floer, A., & Kirton, A. (2020). Population Based Birth Prevalence of Disease-Specific Perinatal Stroke. *Pediatrics*, *146*(5), e2020013201. <https://doi.org/10.1542/peds.2020-013201>

Ecury-Goossen, G. M., van der Haer, M., Smit, L. S., Feijen-Roon, M., Lequin, M., de Jonge, R. C. J., Govaert, P., & Dudink, J. (2016). Neurodevelopmental outcome after neonatal perforator stroke. *Developmental Medicine & Child Neurology*, *58*(1), 49-56. <https://doi.org/10.1111/dmcn.12857>

Englander, Z. A., Pizoli, C. E., Batrachenko, A., Sun, J., Worley, G., Mikati, M. A., Kurtzberg, J., & Song, A. W. (2013). Diffuse reduction of white matter connectivity in cerebral palsy with specific vulnerability of long range fiber tracts. *NeuroImage: Clinical*, *2*, 440-447. <https://doi.org/10.1016/j.nicl.2013.03.006>

Englander, Z. A., Sun, J., Laura Case, Mikati, M. A., Kurtzberg, J., & Song, A. W. (2015). Brain structural connectivity increases concurrent with functional improvement : Evidence from diffusion tensor MRI in children with cerebral palsy during therapy. *NeuroImage: Clinical*, *7*, 315-324. <https://doi.org/10.1016/j.nicl.2015.01.002>

Esteban, O., Birman, D., Schaer, M., Koyejo, O. O., Poldrack, R. A., & Gorgolewski, K. J. (2017). MRIQC : Advancing the automatic prediction of image quality in MRI from unseen sites. *PLOS ONE*, *12*(9), e0184661. <https://doi.org/10.1371/journal.pone.0184661>

Esteban, O., Markiewicz, C. J., Blair, R. W., Moodie, C. A., Isik, A. I., Erramuzpe, A., Kent, J. D., Goncalves, M., DuPre, E., Snyder, M., Oya, H., Ghosh, S. S., Wright, J., Durnez, J., Poldrack, R. A., & Gorgolewski, K. J. (2019). fMRIPrep : A robust preprocessing pipeline for functional MRI. *Nature Methods*, *16*(1), 111-116. <https://doi.org/10.1038/s41592-018-0235-4>

Everts, R., Lidzba, K., Wilke, M., Kiefer, C., Wingeier, K., Schroth, G., Perrig, W., & Steinlin, M. (2010). Lateralization of cognitive functions after stroke in childhood. *Brain Injury*, *24*(6), 859-870. <https://doi.org/10.3109/02699051003724978>

- Fair, D. A., Choi, A. H., Dosenbach, Y. B. L., Coalson, R. S., Miezin, F. M., Petersen, S. E., & Schlaggar, B. L. (2010). The functional organization of trial-related activity in lexical processing after early left hemispheric brain lesions : An event-related fMRI study. *Brain and Language*, *114*(2), 135-146. <https://doi.org/10.1016/j.bandl.2009.09.001>
- Fluss, J., Dinomais, M., & Chabrier, S. (2019). Perinatal stroke syndromes : Similarities and diversities in aetiology, outcome and management. *European Journal of Paediatric Neurology*, *23*(3), 368-383. <https://doi.org/10.1016/j.ejpn.2019.02.013>
- Fornito, A., Zalesky, A., & Breakspear, M. (2015). The connectomics of brain disorders. *Nature Reviews Neuroscience*, *16*(3), 159-172. <https://doi.org/10.1038/nrn3901>
- Fortin, J.-P., Cullen, N., Sheline, Y. I., Taylor, W. D., Aselcioglu, I., Cook, P. A., Adams, P., Cooper, C., Fava, M., McGrath, P. J., McInnis, M., Phillips, M. L., Trivedi, M. H., Weissman, M. M., & Shinohara, R. T. (2018). Harmonization of cortical thickness measurements across scanners and sites. *NeuroImage*, *167*, 104-120. <https://doi.org/10.1016/j.neuroimage.2017.11.024>
- François, C., Garcia-Alix, A., Bosch, L., & Rodriguez-Fornells, A. (2021). Signatures of brain plasticity supporting language recovery after perinatal arterial ischemic stroke. *Brain and Language*, *212*, 104880. <https://doi.org/10.1016/j.bandl.2020.104880>
- François, C., Ripollés, P., Ferreri, L., Muchart, J., Sierpowska, J., Fons, C., Solé, J., Rebollo, M., Zatorre, R. J., Garcia-Alix, A., Bosch, L., & Rodriguez-Fornells, A. (2019). Right Structural and Functional Reorganization in Four-Year-Old Children with Perinatal Arterial Ischemic Stroke Predict Language Production. *Eneuro*, *6*(4), ENEURO.0447-18.2019. <https://doi.org/10.1523/ENEURO.0447-18.2019>
- Frangou, S., Modabbernia, A., Williams, S. C. R., Papachristou, E., Doucet, G. E., Agartz, I., Aghajani, M., Akudjedu, T. N., Albajes-Eizaguirre, A., Alnæs, D., Alpert, K. I., Andersson, M., Andreasen, N. C., Andreassen, O. A., Asherson, P., Banaschewski, T., Bargallo, N., Baumeister, S., Baur-Streubel, R., ... Dima, D. (2022). Cortical thickness across the lifespan : Data from 17,075 healthy individuals aged 3–90 years. *Human Brain Mapping*, *43*(1), 431-451. <https://doi.org/10.1002/hbm.25364>

- Frazier, J. A., Chiu, S., Breeze, J. L., Makris, N., Lange, N., Kennedy, D. N., Herbert, M. R., Bent, E. K., Koneru, V. K., Dieterich, M. E., Hodge, S. M., Rauch, S. L., Grant, P. E., Cohen, B. M., Seidman, L. J., Caviness, V. S., & Biederman, J. (2005). Structural Brain Magnetic Resonance Imaging of Limbic and Thalamic Volumes in Pediatric Bipolar Disorder. *American Journal of Psychiatry*, *162*(7), 1256-1265.  
<https://doi.org/10.1176/appi.ajp.162.7.1256>
- Friederici, A. D., & Gierhan, S. M. (2013). The language network. *Current Opinion in Neurobiology*, *23*(2), 250-254. <https://doi.org/10.1016/j.conb.2012.10.002>
- Friston, K. J. (2011). *Statistical parametric mapping : The analysis of functional brain images*. Academic Press.
- Gaberova, K., Pacheva, I., & Ivanov, I. (2018). Task-related fMRI in hemiplegic cerebral palsy—A systematic review. *Journal of Evaluation in Clinical Practice*, *24*(4), 839-850. <https://doi.org/10.1111/jep.12929>
- Gaser, C., Dahnke, R., Thompson, P. M., Kurth, F., Luders, E., & Alzheimer's Disease Neuroimaging Initiative. (2022). *CAT – A Computational Anatomy Toolbox for the Analysis of Structural MRI Data* [Preprint]. Neuroscience.  
<https://doi.org/10.1101/2022.06.11.495736>
- Giraud, A., Guiraut, C., Chevin, M., Chabrier, S., & Sébire, G. (2017). Role of Perinatal Inflammation in Neonatal Arterial Ischemic Stroke. *Frontiers in Neurology*, *8*, 612.  
<https://doi.org/10.3389/fneur.2017.00612>
- Gold, J. J., & Trauner, D. A. (2014). Hippocampal Volume and Memory Performance in Children With Perinatal Stroke. *Pediatric Neurology*, *50*(1), 18-25.  
<https://doi.org/10.1016/j.pediatrneurol.2013.08.029>
- Goldstein, J. M., Seidman, L. J., Makris, N., Ahern, T., O'Brien, L. M., Caviness, V. S., Kennedy, D. N., Faraone, S. V., & Tsuang, M. T. (2007). Hypothalamic Abnormalities in Schizophrenia : Sex Effects and Genetic Vulnerability. *Biological Psychiatry*, *61*(8), 935-945. <https://doi.org/10.1016/j.biopsych.2006.06.027>
- Gomez, J., Pestilli, F., Witthoft, N., Golarai, G., Liberman, A., Poltoratski, S., Yoon, J., &

- Grill-Spector, K. (2015). Functionally Defined White Matter Reveals Segregated Pathways in Human Ventral Temporal Cortex Associated with Category-Specific Processing. *Neuron*, 85(1), 216-227. <https://doi.org/10.1016/j.neuron.2014.12.027>
- Gorgolewski, K. J., Auer, T., Calhoun, V. D., Craddock, R. C., Das, S., Duff, E. P., Flandin, G., Ghosh, S. S., Glatard, T., Halchenko, Y. O., Handwerker, D. A., Hanke, M., Keator, D., Li, X., Michael, Z., Maumet, C., Nichols, B. N., Nichols, T. E., Pellman, J., ... Poldrack, R. A. (2016). The brain imaging data structure, a format for organizing and describing outputs of neuroimaging experiments. *Scientific Data*, 3(1), 160044. <https://doi.org/10.1038/sdata.2016.44>
- Hassett, J., Carlson, H., Babwani, A., & Kirton, A. (2022). Bihemispheric developmental alterations in basal ganglia volumes following unilateral perinatal stroke. *NeuroImage: Clinical*, 35, 103143. <https://doi.org/10.1016/j.nicl.2022.103143>
- Hickok, G., & Poeppel, D. (2004). Dorsal and ventral streams : A framework for understanding aspects of the functional anatomy of language. *Cognition*, 92(1), 67-99. <https://doi.org/10.1016/j.cognition.2003.10.011>
- Hickok, G., & Poeppel, D. (2007). The cortical organization of speech processing. *Nature Reviews Neuroscience*, 8(5), 393-402. <https://doi.org/10.1038/nrn2113>
- Hodge, J., Goodyear, B., Carlson, H., Wei, X.-C., & Kirton, A. (2017). Segmental Diffusion Properties of the Corticospinal Tract and Motor Outcome in Hemiparetic Children With Perinatal Stroke. *Journal of Child Neurology*, 32(6), 550-559. <https://doi.org/10.1177/0883073817696815>
- Huo, Y., Plassard, A. J., Carass, A., Resnick, S. M., Pham, D. L., Prince, J. L., & Landman, B. A. (2016). Consistent cortical reconstruction and multi-atlas brain segmentation. *NeuroImage*, 138, 197-210. <https://doi.org/10.1016/j.neuroimage.2016.05.030>
- Husson, B., Hertz-Pannier, L., Renaud, C., Allard, D., Presles, E., Landrieu, P., Chabrier, S., & for the AVCnn Group. (2010). Motor Outcomes After Neonatal Arterial Ischemic Stroke Related to Early MRI Data in a Prospective Study. *Pediatrics*, 126(4), e912-e918. <https://doi.org/10.1542/peds.2009-3611>

- Ilves, N., Lõo, S., Ilves, N., Laugesaar, R., Loorits, D., Kool, P., Talvik, T., & Ilves, P. (2022). Ipsilesional volume loss of basal ganglia and thalamus is associated with poor hand function after ischemic perinatal stroke. *BMC Neurology*, *22*(1), 23.  
<https://doi.org/10.1186/s12883-022-02550-3>
- Ilves, P., Tomberg, T., Kepler, J., Laugesaar, R., Kaldoja, M.-L., Kepler, K., & Kolk, A. (2014). Different Plasticity Patterns of Language Function in Children With Perinatal and Childhood Stroke. *Journal of Child Neurology*, *29*(6), 756-764.  
<https://doi.org/10.1177/0883073813489350>
- Isensee, F., Schell, M., Pflueger, I., Brugnara, G., Bonekamp, D., Neuberger, U., Wick, A., Schlemmer, H., Heiland, S., Wick, W., Bendszus, M., Maier-Hein, K. H., & Kickingereder, P. (2019). Automated brain extraction of multisequence MRI using artificial neural networks. *Human Brain Mapping*, *40*(17), 4952-4964.  
<https://doi.org/10.1002/hbm.24750>
- Jao, C.-W., Lau, C. I., Lien, L.-M., Tsai, Y.-F., Chu, K.-E., Hsiao, C.-Y., Yeh, J.-H., & Wu, Y.-T. (2021). Using Fractal Dimension Analysis with the Desikan–Killiany Atlas to Assess the Effects of Normal Aging on Subregional Cortex Alterations in Adulthood. *Brain Sciences*, *11*(1), Article 1. <https://doi.org/10.3390/brainsci11010107>
- Jarret, J., Boré, A., Bedetti, C., Descoteaux, M., & Brambati, S. M. (2022). A methodological scoping review of the integration of fMRI to guide dMRI tractography. What has been done and what can be improved : A 20-year perspective. *Journal of Neuroscience Methods*, *367*, 109435. <https://doi.org/10.1016/j.jneumeth.2021.109435>
- Kirton, A., & deVeber, G. (2009). Advances in Perinatal Ischemic Stroke. *Pediatric Neurology*, *40*(3), 205-214. <https://doi.org/10.1016/j.pediatrneurol.2008.09.018>
- Kirton, A., & deVeber, G. (2013). Life After Perinatal Stroke. *Stroke*, *44*(11), 3265-3271.  
<https://doi.org/10.1161/STROKEAHA.113.000739>
- Kirton, A., Metzler, M. J., Craig, B. T., Hilderley, A., Dunbar, M., Giuffre, A., Wrightson, J., Zewdie, E., & Carlson, H. L. (2021). Perinatal stroke : Mapping and modulating developmental plasticity. *Nature Reviews Neurology*, *17*(7), 415-432.

<https://doi.org/10.1038/s41582-021-00503-x>

Kirton, A., Shroff, M., Visvanathan, T., & deVeber, G. (2007). Quantified corticospinal tract diffusion restriction predicts neonatal stroke outcome. *Stroke*, *38*(3), 974-980.

<https://doi.org/10.1161/01.STR.0000258101.67119.72>

Knecht, S., Deppe, M., Dräger, B., Bobe, L., Lohmann, H., Ringelstein, E.-B., & Henningsen, H. (2000). Language lateralization in healthy right-handers. *Brain*, *123*(1), 74-81.

<https://doi.org/10.1093/brain/123.1.74>

Knecht, S., Dräger, B., Deppe, M., Bobe, L., Lohmann, H., Flöel, A., Ringelstein, E.-B., & Henningsen, H. (2000). Handedness and hemispheric language dominance in healthy humans. *Brain*, *123*(12), 2512-2518.

<https://doi.org/10.1093/brain/123.12.2512>

Koenraads, Y., Porro, G. L., Braun, K. P. J., Groenendaal, F., Vries, L. S. de, & Aa, N. E. van der. (2016). Prediction of visual field defects in newborn infants with perinatal arterial ischemic stroke using early MRI and DTI-based tractography of the optic radiation. *European Journal of Paediatric Neurology*, *20*(2), 309-318.

<https://doi.org/10.1016/j.ejpn.2015.11.010>

Kuczynski, A. M., Carlson, H. L., Lebel, C., Hodge, J. A., Dukelow, S. P., Semrau, J. A., & Kirton, A. (2017). Sensory tractography and robot-quantified proprioception in hemiparetic children with perinatal stroke. *Human Brain Mapping*, *38*(5), 2424-2440.

<https://doi.org/10.1002/hbm.23530>

Labache, L., Joliot, M., Saracco, J., Jobard, G., Hesling, I., Zago, L., Mellet, E., Petit, L., Crivello, F., Mazoyer, B., & Tzourio-Mazoyer, N. (2019). A SENSentence Supramodal Areas Atlas (SENSAAS) based on multiple task-induced activation mapping and graph analysis of intrinsic connectivity in 144 healthy right-handers. *Brain Structure and Function*, *224*(2), 859-882. <https://doi.org/10.1007/s00429-018-1810-2>

Lake, E. M. R., Bazzigaluppi, P., & Stefanovic, B. (2016). Functional magnetic resonance imaging in chronic ischaemic stroke. *Philosophical Transactions of the Royal Society B: Biological Sciences*, *371*(1705), 20150353. <https://doi.org/10.1098/rstb.2015.0353>

- Lebel, C., & Deoni, S. (2018). The Development of Brain White Matter Microstructure. *NeuroImage*, *182*, 207-218. <https://doi.org/10.1016/j.neuroimage.2017.12.097>
- Lebenberg, J., Labit, M., Auzias, G., Mohlberg, H., Fischer, C., Rivière, D., Duchesnay, E., Kabdebon, C., Leroy, F., Labra, N., Poupon, F., Dickscheid, T., Hertz-Pannier, L., Poupon, C., Dehaene-Lambertz, G., Hüppi, P., Amunts, K., Dubois, J., & Mangin, J.-F. (2018). A framework based on sulcal constraints to align preterm, infant and adult human brain images acquired in vivo and post mortem. *Brain Structure and Function*, *223*(9), 4153-4168. <https://doi.org/10.1007/s00429-018-1735-9>
- Ledig, C., Heckemann, R. A., Hammers, A., Lopez, J. C., Newcombe, V. F. J., Makropoulos, A., Lötjönen, J., Menon, D. K., & Rueckert, D. (2015). Robust whole-brain segmentation : Application to traumatic brain injury. *Medical Image Analysis*, *21*(1), 40-58. <https://doi.org/10.1016/j.media.2014.12.003>
- Lee, S., Mirsky, D. M., Beslow, L. A., Amlie-Lefond, C., Danehy, A. R., Lehman, L., Stence, N. V., Vossough, A., Wintermark, M., & Rivkin, M. J. (2017). Pathways for Neuroimaging of Neonatal Stroke. *Pediatric Neurology*, *69*, 37-48. <https://doi.org/10.1016/j.pediatrneurol.2016.12.008>
- Lequin, M. H., Dudink, J., Tong, K. A., & Obenaus, A. (2009). Magnetic resonance imaging in neonatal stroke. *Seminars in Fetal and Neonatal Medicine*, *14*(5), 299-310. <https://doi.org/10.1016/j.siny.2009.07.005>
- Li, C., Miao, J. K., Xu, Y., Hua, Y. Y., Ma, Q., Zhou, L. L., Liu, H. J., & Chen, Q. X. (2017). Prenatal, perinatal and neonatal risk factors for perinatal arterial ischaemic stroke : A systematic review and meta-analysis. *European Journal of Neurology*, *24*(8), 1006-1015. <https://doi.org/10.1111/ene.13337>
- Lidzba, K., Küpper, H., Kluger, G., & Staudt, M. (2017). The time window for successful right-hemispheric language reorganization in children. *European Journal of Paediatric Neurology: EJPN: Official Journal of the European Paediatric Neurology Society*, *21*(5), 715-721. <https://doi.org/10.1016/j.ejpn.2017.06.001>
- Lidzba, K., Staudt, M., Wilke, M., & Krägeloh-Mann, I. (2006). Visuospatial deficits in patients

- with early left-hemispheric lesions and functional reorganization of language :  
Consequence of lesion or reorganization? *Neuropsychologia*, *44*(7), 1088-1094.  
<https://doi.org/10.1016/j.neuropsychologia.2005.10.022>
- Liu, C.-F., Hsu, J., Xu, X., Kim, G., Sheppard, S. M., Meier, E. L., Miller, M. I., Hillis, A. E., & Faria, A. V. (2023). Digital 3D Brain MRI Arterial Territories Atlas. *Scientific Data*, *10*(1). <https://doi.org/10.1038/s41597-022-01923-0>
- López-Barroso, D., & de Diego-Balaguer, R. (2017). Language Learning Variability within the Dorsal and Ventral Streams as a Cue for Compensatory Mechanisms in Aphasia Recovery. *Frontiers in Human Neuroscience*, *11*.  
<https://doi.org/10.3389/fnhum.2017.00476>
- Lorio, S., Kherif, F., Ruef, A., Melie-Garcia, L., Frackowiak, R., Ashburner, J., Helms, G., Lutti, A., & Draganski, B. (2016). Neurobiological origin of spurious brain morphological changes : A quantitative MRI study. *Human Brain Mapping*, *37*(5), 1801-1815. <https://doi.org/10.1002/hbm.23137>
- MacSweeney, M., Capek, C. M., Campbell, R., & Woll, B. (2008). The signing brain : The neurobiology of sign language. *Trends in Cognitive Sciences*, *12*(11), 432-440.  
<https://doi.org/10.1016/j.tics.2008.07.010>
- Manjón, J. V., Romero, J. E., Vivo-Hernando, R., Rubio, G., Aparici, F., De La Iglesia-Vaya, M., & Coupé, P. (2022). vol2Brain : A New Online Pipeline for Whole Brain MRI Analysis. *Frontiers in Neuroinformatics*, *16*, 862805.  
<https://doi.org/10.3389/fninf.2022.862805>
- Martin, K. C., Seydell-Greenwald, A., Berl, M. M., Gaillard, W. D., Turkeltaub, P. E., & Newport, E. L. (2022). A Weak Shadow of Early Life Language Processing Persists in the Right Hemisphere of the Mature Brain. *Neurobiology of Language*, *3*(3), 364-385. [https://doi.org/10.1162/nol\\_a\\_00069](https://doi.org/10.1162/nol_a_00069)
- Martin, K. C., Seydell-Greenwald, A., Turkeltaub, P. E., Chambers, C. E., Giannetti, M., Dromerick, A. W., Carpenter, J. L., Berl, M. M., Gaillard, W. D., & Newport, E. L. (2023). One right can make a left : Sentence processing in the right hemisphere after

- perinatal stroke. *Cerebral Cortex*, 33(23), 11257-11268.  
<https://doi.org/10.1093/cercor/bhad362>
- Moses, P. (2000). Regional Size Reduction in the Human Corpus Callosum Following Pre- and Perinatal Brain Injury. *Cerebral Cortex*, 10(12), 1200-1210.  
<https://doi.org/10.1093/cercor/10.12.1200>
- N, M., Jm, G., D, K., Sm, H., Vs, C., Sv, F., Mt, T., & Lj, S. (2006). Decreased volume of left and total anterior insular lobule in schizophrenia. *Schizophrenia Research*, 83(2-3).  
<https://doi.org/10.1016/j.schres.2005.11.020>
- Nemanich, S. T., Mueller, B. A., & Gillick, B. T. (2019). Neurite orientation dispersion and density imaging quantifies corticospinal tract microstructural organization in children with unilateral cerebral palsy. *Human Brain Mapping*, 40(17), 4888.  
<https://doi.org/10.1002/hbm.24744>
- Newman, A. J., Supalla, T., Fernandez, N., Newport, E. L., & Bavelier, D. (2015). Neural systems supporting linguistic structure, linguistic experience, and symbolic communication in sign language and gesture. *Proceedings of the National Academy of Sciences*, 112(37), 11684-11689. <https://doi.org/10.1073/pnas.1510527112>
- Newport, E. L., Landau, B., Seydell-Greenwald, A., Turkeltaub, P. E., Chambers, C. E., Dromerick, A. W., Carpenter, J., Berl, M. M., & Gaillard, W. D. (2017). Revisiting Lenneberg's Hypotheses About Early Developmental Plasticity : Language Organization After Left-Hemisphere Perinatal Stroke. *Biolinguistics*, 11, 407-422.
- Newport, E. L., Seydell-Greenwald, A., Landau, B., Turkeltaub, P. E., Chambers, C. E., Martin, K. C., Rennert, R., Giannetti, M., Dromerick, A. W., Ichord, R. N., Carpenter, J. L., Berl, M. M., & Gaillard, W. D. (2022). Language and developmental plasticity after perinatal stroke. *Proceedings of the National Academy of Sciences*, 119(42), e2207293119. <https://doi.org/10.1073/pnas.2207293119>
- Northam, G. B., Adler, S., Eschmann, K. C. J., Chong, W. K., Cowan, F. M., & Baldeweg, T. (2018). Developmental conduction aphasia after neonatal stroke. *Annals of Neurology*, 83(4), 664-675. <https://doi.org/10.1002/ana.25218>

- Núñez, C., Arca, G., Agut, T., Stephan-Otto, C., & García-Alix, A. (2020). Precise neonatal arterial ischemic stroke classification with a three-dimensional map of the arterial territories of the neonatal brain. *Pediatric Research*, *87*(7), 1231-1236.  
<https://doi.org/10.1038/s41390-019-0724-x>
- Okabe, T., Aida, N., Niwa, T., Nozawa, K., Shibasaki, J., & Osaka, H. (2014). Early magnetic resonance detection of cortical necrosis and acute network injury associated with neonatal and infantile cerebral infarction. *Pediatric Radiology*, *44*(5), 597-604.  
<https://doi.org/10.1007/s00247-013-2846-3>
- Pabst, L., Hoyt, C. R., Felling, R. J., Smith, A. E., Harpster, K., Pardo, A. C., Bridge, J. A., Jiang, B., Gehred, A., & Lo, W. (2024). Neuroimaging and Neurological Outcomes in Perinatal Arterial Ischemic Stroke : A Systematic Review and Meta-Analysis. *Pediatric Neurology*, *157*, 19-28. <https://doi.org/10.1016/j.pediatrneurol.2024.04.029>
- Pahs, G., Rankin, P., Helen Cross, J., Croft, L., Northam, G. B., Liegeois, F., Greenway, S., Harrison, S., Vargha-Khadem, F., & Baldeweg, T. (2013). Asymmetry of planum temporale constrains interhemispheric language plasticity in children with focal epilepsy. *Brain*, *136*(10), 3163-3175. <https://doi.org/10.1093/brain/awt225>
- Petitto, L. A., Zatorre, R. J., Gauna, K., Nikelski, E. J., Dostie, D., & Evans, A. C. (2000). Speech-like cerebral activity in profoundly deaf people processing signed languages : Implications for the neural basis of human language. *Proceedings of the National Academy of Sciences*, *97*(25), 13961-13966.  
<https://doi.org/10.1073/pnas.97.25.13961>
- Pinel, P., Thirion, B., Meriaux, S., Jobert, A., Serres, J., Le Bihan, D., Poline, J.-B., & Dehaene, S. (2007). Fast reproducible identification and large-scale databasing of individual functional cognitive networks. *BMC Neuroscience*, *8*(1).  
<https://doi.org/10.1186/1471-2202-8-91>
- Postic, P.-Y., Leprince, Y., Brosset, S., Drutel, L., Peyric, E., Ben Abdallah, I., Bekha, D., Neumane, S., Duchesnay, E., Dinomais, M., Chevignard, M., & Hertz-Pannier, L. (2024). Brain growth until adolescence after a neonatal focal injury : Sex related

- differences beyond lesion effect. *Frontiers in Neuroscience*, *18*, 1405381.  
<https://doi.org/10.3389/fnins.2024.1405381>
- Potvin, O., Dieumegarde, L., & Duchesne, S. (2017). Freesurfer cortical normative data for adults using Desikan-Killiany-Tourville and ex vivo protocols. *NeuroImage*, *156*, 43-64. <https://doi.org/10.1016/j.neuroimage.2017.04.035>
- Pretzel, P., Dhollander, T., Chabrier, S., Al-Harrach, M., Hertz-Pannier, L., Dinomais, M., & Groeschel, S. (2022). Structural brain connectivity in children after neonatal stroke : A whole-brain fixel-based analysis. *NeuroImage: Clinical*, *34*, 103035.  
<https://doi.org/10.1016/j.nicl.2022.103035>
- Radwan, A. M., Emsell, L., Blommaert, J., Zhylyka, A., Kovacs, S., Theys, T., Sollmann, N., Dupont, P., & Sunaert, S. (2021). Virtual brain grafting : Enabling whole brain parcellation in the presence of large lesions. *NeuroImage*, *229*, 117731.  
<https://doi.org/10.1016/j.neuroimage.2021.117731>
- Raja Beharelle, A., Dick, A. S., Josse, G., Solodkin, A., Huttenlocher, P. R., Levine, S. C., & Small, S. L. (2010). Left hemisphere regions are critical for language in the face of early left focal brain injury. *Brain*, *133*(6), 1707-1716.  
<https://doi.org/10.1093/brain/awq104>
- Raju, T. N. K., Nelson, K. B., Ferriero, D., Lynch, J. K., & and the NICHD-NINDS Perinatal Stroke Workshop Participants. (2007). Ischemic Perinatal Stroke : Summary of a Workshop Sponsored by the National Institute of Child Health and Human Development and the National Institute of Neurological Disorders and Stroke. *Pediatrics*, *120*(3), 609-616. <https://doi.org/10.1542/peds.2007-0336>
- Rehme, A. K., Eickhoff, S. B., Rottschy, C., Fink, G. R., & Grefkes, C. (2012). Activation likelihood estimation meta-analysis of motor-related neural activity after stroke. *NeuroImage*, *59*(3), 2771-2782. <https://doi.org/10.1016/j.neuroimage.2011.10.023>
- Reilly, J. S., Wasserman, S., & Appelbaum, M. (2013). Later language development in narratives in children with perinatal stroke. *Developmental Science*, *16*(1), 67-83.  
<https://doi.org/10.1111/j.1467-7687.2012.01192.x>

- Ricci, D., Mercuri, E., Barnett, A., Rathbone, R., Cota, F., Haataja, L., Rutherford, M., Dubowitz, L., & Cowan, F. (2008). Cognitive outcome at early school age in term-born children with perinatally acquired middle cerebral artery territory infarction. *Stroke*, *39*(2), 403-410. <https://doi.org/10.1161/STROKEAHA.107.489831>
- Rutherford, S., Frazza, C., Dinga, R., Kia, S. M., Wolfers, T., Zabihi, M., Berthet, P., Worker, A., Verdi, S., Andrews, D., Han, L. K., Bayer, J. M., Dazzan, P., McGuire, P., Mocking, R. T., Schene, A., Sripada, C., Tso, I. F., Duval, E. R., ... Marquand, A. F. (2022). Charting brain growth and aging at high spatial precision. *ELife*, *11*, e72904. <https://doi.org/10.7554/eLife.72904>
- Saunders, J., Carlson, H. L., Cortese, F., Goodyear, B. G., & Kirton, A. (2019). Imaging functional motor connectivity in hemiparetic children with perinatal stroke. *Human Brain Mapping*, *40*(5), 1632-1642. <https://doi.org/10.1002/hbm.24474>
- Schnauffer, L., Gschaidmeier, A., Heimgärtner, M., Driever, P. H., Hauser, T., Wilke, M., Lidzba, K., & Staudt, M. (2023). Atypical language organization following perinatal infarctions of the left hemisphere is associated with structural changes in right-hemispheric grey matter. *Developmental Medicine & Child Neurology*, dmcn.15751. <https://doi.org/10.1111/dmcn.15751>
- Shaw, P., Greenstein, D., Lerch, J., Clasen, L., Lenroot, R., Gogtay, N., Evans, A., Rapoport, J., & Giedd, J. (2006). Intellectual ability and cortical development in children and adolescents. *Nature*, *440*(7084), 676-679. <https://doi.org/10.1038/nature04513>
- Shinde, K., Craig, B. T., Hassett, J., Dlamini, N., Brooks, B. L., Kirton, A., & Carlson, H. L. (2023). Alterations in cortical morphometry of the contralesional hemisphere in children, adolescents, and young adults with perinatal stroke. *Scientific Reports*, *13*(1), 11391. <https://doi.org/10.1038/s41598-023-38185-8>
- Smith, R. E., Tournier, J.-D., Calamante, F., & Connelly, A. (2012). Anatomically-constrained tractography : Improved diffusion MRI streamlines tractography through effective use of anatomical information. *NeuroImage*, *62*(3), 1924-1938. <https://doi.org/10.1016/j.neuroimage.2012.06.005>

- Smith, R. E., Tournier, J.-D., Calamante, F., & Connelly, A. (2015). SIFT2 : Enabling dense quantitative assessment of brain white matter connectivity using streamlines tractography. *NeuroImage*, *119*, 338-351.  
<https://doi.org/10.1016/j.neuroimage.2015.06.092>
- Smith, S. M., Jenkinson, M., Woolrich, M. W., Beckmann, C. F., Behrens, T. E. J., Johansen-Berg, H., Bannister, P. R., De Luca, M., Drobnjak, I., Flitney, D. E., Niazy, R. K., Saunders, J., Vickers, J., Zhang, Y., De Stefano, N., Brady, J. M., & Matthews, P. M. (2004). Advances in functional and structural MR image analysis and implementation as FSL. *NeuroImage*, *23*, S208-S219.  
<https://doi.org/10.1016/j.neuroimage.2004.07.051>
- Statsenko, Y., Habuza, T., Smetanina, D., Simiyu, G. L., Uzianbaeva, L., Neidl-Van Gorkom, K., Zaki, N., Charykova, I., Al Koteesh, J., Almansoori, T. M., Belghali, M., & Ljubisavljevic, M. (2022). Brain Morphometry and Cognitive Performance in Normal Brain Aging : Age- and Sex-Related Structural and Functional Changes. *Frontiers in Aging Neuroscience*, *13*. <https://doi.org/10.3389/fnagi.2021.713680>
- Staudt, M., Gerloff, C., Grodd, W., Holthausen, H., Niemann, G., & Krägeloh-Mann, I. (2004). Reorganization in congenital hemiparesis acquired at different gestational ages. *Annals of Neurology*, *56*(6), 854-863. <https://doi.org/10.1002/ana.20297>
- Staudt, M., Lidzba, K., Grodd, W., Wildgruber, D., Erb, M., & Krägeloh-Mann, I. (2002). Right-Hemispheric Organization of Language Following Early Left-Sided Brain Lesions : Functional MRI Topography. *NeuroImage*, *16*(4), 954-967.  
<https://doi.org/10.1006/nimg.2002.1108>
- Stephan-Otto, C., Núñez, C., Arca, G., Agut, T., & García-Alix, A. (2017). Three-Dimensional Map of Neonatal Arterial Ischemic Stroke Distribution From Early Multimodal Brain Imaging. *Stroke*, *48*(2), 482-485. <https://doi.org/10.1161/STROKEAHA.116.014186>
- Stiles, J., Moses, P., Roe, K., Akshoomoff, N. A., Trauner, D., Hesselink, J., Wong, E. C., Frank, L. R., & Buxton, R. B. (2003). Alternative brain organization after prenatal cerebral injury : Convergent fMRI and cognitive data. *Journal of the International*

*Neuropsychological Society*, 9(4), 604-622.

<https://doi.org/10.1017/S135561770394001X>

- Straathof, M., Sinke, M. R., Dijkhuizen, R. M., & Otte, W. M. (2019). A systematic review on the quantitative relationship between structural and functional network connectivity strength in mammalian brains. *Journal of Cerebral Blood Flow & Metabolism*, 39(2), 189-209. <https://doi.org/10.1177/0271678X18809547>
- Sullivan, A. W., Johnson, M. K., Boes, A. D., & Tranel, D. (2023). Implications of age at lesion onset for neuropsychological outcomes : A systematic review focusing on focal brain lesions. *Cortex*, 163, 92-122. <https://doi.org/10.1016/j.cortex.2023.03.002>
- Szaflarski, J. P., Binder, J. R., Possing, E. T., McKiernan, K. A., Ward, B. D., & Hammeke, T. A. (2002). Language lateralization in left-handed and ambidextrous people. *Neurology*, 59(2), 238-244. <https://doi.org/10.1212/WNL.59.2.238>
- Szaflarski, J. P., Holland, S. K., Schmithorst, V. J., & Byars, A. W. (2006). fMRI study of language lateralization in children and adults. *Human Brain Mapping*, 27(3), 202-212. <https://doi.org/10.1002/hbm.20177>
- Tillema, J.-M., Byars, A. W., Jacola, L. M., Schapiro, M. B., Schmithorst, V. J., Szaflarski, J. P., & Holland, S. K. (2008). Cortical reorganization of language functioning following perinatal left MCA stroke. *Brain and Language*, 105(2), 99-111. <https://doi.org/10.1016/j.bandl.2007.07.127>
- Tournier, J.-D., Calamante, F., & Connelly, A. (2007). Robust determination of the fibre orientation distribution in diffusion MRI : Non-negativity constrained super-resolved spherical deconvolution. *NeuroImage*, 35(4), 1459-1472. <https://doi.org/10.1016/j.neuroimage.2007.02.016>
- Tournier, J.-D., Calamante, F., & Connelly, A. (2010). Improved probabilistic streamlines tractography by 2nd order integration over fibre orientation distributions. *Proc. Intl. Soc. Mag. Reson. Med. (ISMRM)*, 18.
- Tournier, J.-D., Smith, R., Raffelt, D., Tabbara, R., Dhollander, T., Pietsch, M., Christiaens, D., Jeurissen, B., Yeh, C.-H., & Connelly, A. (2019). *MRtrix3 : A fast, flexible and*

*open software framework for medical image processing and visualisation.*

<https://doi.org/10.1101/551739>

- Trauner, D. A., Eshagh, K., Ballantyne, A. O., & Bates, E. (2013). Early language development after peri-natal stroke. *Brain and Language*, *127*(3), 399-403.  
<https://doi.org/10.1016/j.bandl.2013.04.006>
- Vaher, U., Ilves, N., Ilves, N., Laugesaar, R., Männamaa, M., Loorits, D., Kool, P., & Ilves, P. (2023). The thalamus and basal ganglia are smaller in children with epilepsy after perinatal stroke. *Frontiers in Neurology*, *14*, 1252472.  
<https://doi.org/10.3389/fneur.2023.1252472>
- Van de Winckel, A., Klingels, K., Bruyninckx, F., Wenderoth, N., Peeters, R., Sunaert, S., Van Hecke, W., De Cock, P., Eyssen, M., De Weerd, W., & Feys, H. (2013). How does brain activation differ in children with unilateral cerebral palsy compared to typically developing children, during active and passive movements, and tactile stimulation? An fMRI study. *Research in Developmental Disabilities*, *34*(1), 183-197.  
<https://doi.org/10.1016/j.ridd.2012.07.030>
- van der Aa, N., Benders, M., Groenendaal, F., & de Vries, L. (2014). Neonatal stroke : A review of the current evidence on epidemiology, pathogenesis, diagnostics and therapeutic options. *Acta Paediatrica*, *103*(4), 356-364.  
<https://doi.org/10.1111/apa.12555>
- Vandermeeren, Y., Sébire, G., Grandin, C. B., Thonnard, J.-L., Schlögel, X., & De Volder, A. G. (2003). Functional reorganization of brain in children affected with congenital hemiplegia : FMRI study. *NeuroImage*, *20*(1), 289-301.  
[https://doi.org/10.1016/S1053-8119\(03\)00262-3](https://doi.org/10.1016/S1053-8119(03)00262-3)
- VanRyzin, J. W., Marquardt, A. E., Pickett, L. A., & McCarthy, M. M. (2020). Microglia and sexual differentiation of the developing brain : A focus on extrinsic factors. *Glia*, *68*(6), 1100-1113. <https://doi.org/10.1002/glia.23740>
- Vigneau, M., Beaucousin, V., Hervé, P. Y., Duffau, H., Crivello, F., Houdé, O., Mazoyer, B., & Tzourio-Mazoyer, N. (2006). Meta-analyzing left hemisphere language areas :

- Phonology, semantics, and sentence processing. *NeuroImage*, 30(4), 1414-1432.  
<https://doi.org/10.1016/j.neuroimage.2005.11.002>
- Vries, L. S. D., Grond, J. V. der, Haastert, I. C. V., & Groenendaal, F. (2005). Prediction of Outcome in New-Born Infants with Arterial Ischaemic Stroke Using Diffusion-Weighted Magnetic Resonance Imaging. *Neuropediatrics*, 36(1), 12-20.  
<https://doi.org/10.1055/s-2005-837544>
- Wagenaar, N., Martinez-Biarge, M., Van Der Aa, N. E., Van Haastert, I. C., Groenendaal, F., Benders, M. J. N. L., Cowan, F. M., & De Vries, L. S. (2018). Neurodevelopment After Perinatal Arterial Ischemic Stroke. *Pediatrics*, 142(3), e20174164.  
<https://doi.org/10.1542/peds.2017-4164>
- Walenski, M., Europa, E., Caplan, D., & Thompson, C. K. (2019). Neural networks for sentence comprehension and production : An ALE-based meta-analysis of neuroimaging studies. *Human Brain Mapping*, 40(8), 2275-2304.  
<https://doi.org/10.1002/hbm.24523>
- Wasserthal, J., Neher, P., & Maier-Hein, K. H. (2018). TractSeg—Fast and accurate white matter tract segmentation. *NeuroImage*, 183, 239-253.  
<https://doi.org/10.1016/j.neuroimage.2018.07.070>
- Westmacott, R., Askalan, R., Macgregor, D., Anderson, P., & Deveber, G. (2010). Cognitive outcome following unilateral arterial ischaemic stroke in childhood : Effects of age at stroke and lesion location. *Developmental Medicine & Child Neurology*, 52(4), 386-393. <https://doi.org/10.1111/j.1469-8749.2009.03403.x>
- Wierenga, L., Langen, M., Ambrosino, S., Van Dijk, S., Oranje, B., & Durston, S. (2014). Typical development of basal ganglia, hippocampus, amygdala and cerebellum from age 7 to 24. *NeuroImage*, 96, 67-72.  
<https://doi.org/10.1016/j.neuroimage.2014.03.072>
- Wilke, M., & Lidzba, K. (2007). LI-tool : A new toolbox to assess lateralization in functional MR-data. *Journal of Neuroscience Methods*, 163(1), 128-136.  
<https://doi.org/10.1016/j.jneumeth.2007.01.026>

Williams, C. M., Peyre, H., Toro, R., & Ramus, F. (2021). Neuroanatomical norms in the UK Biobank: The impact of allometric scaling, sex, and age. *Human Brain Mapping*, 42(14), 4623-4642. <https://doi.org/10.1002/hbm.25572>

Yaakub, S. N., Heckemann, R. A., Keller, S. S., McGinnity, C. J., Weber, B., & Hammers, A. (2020). On brain atlas choice and automatic segmentation methods: A comparison of MAPER & FreeSurfer using three atlas databases. *Scientific Reports*, 10(1), 2837. <https://doi.org/10.1038/s41598-020-57951-6>

Zhang, H., Schneider, T., Wheeler-Kingshott, C. A., & Alexander, D. C. (2012). NODDI: Practical *in vivo* neurite orientation dispersion and density imaging of the human brain. *NeuroImage*, 61(4), 1000-1016. <https://doi.org/10.1016/j.neuroimage.2012.03.072>

## List of figures

[Figure 1](#) : Synthesis of perinatal stroke types, mechanisms, clinical findings and outcomes (Fluss et al., 2019) **Page 17**

[Figure 2](#) : Significant clusters associated with sentence comprehension (both auditory and visual) derived from ALE analysis: Left lateral (a), from above (b), right lateral (c), axials by z-coordinates in MNI space (d). The scale bar reflects the ALE values (Walenski et al., 2019) **Page 25**

[Figure 3](#) : Significant clusters associated with sentence production derived from ALE analysis: Left lateral (a), from above (b), right lateral (c), axials by z-coordinates in MNI space (d). The scale bar reflects the ALE values (Walenski et al., 2019) **Page 25**

[Figure 4](#) : Schematic illustration of the main anatomical connections of the perisylvian areas in the left hemisphere, comprising the ventral and the dorsal pathways. The perisylvian cortex, covering frontal, parietal and temporal cortices, is shaded in gray (López-Barroso & de Diego-Balaguer, 2017). **Page 26**

[Figure 5](#) : Euler Number and IQR distribution the AVCnn cohort A : Metric distribution depending on acquisition session. B : Metric distribution depending on subject status (patient/controls) **Page 74**

[Figure 6](#) : Mean Jacobian Determinant of the deformation field between 7 and 16 years old (logarithmic scale) **Page 75**

[Figure 7](#) : Mean Jacobian Determinant of the deformation field between 7 and 16 years old (logarithmic scale), for each tissue type and hemisphere **Page 76**

[Figure 8](#): Grey matter volume for each subject and each DK40 regions, Computed with two different methods: DK 40 projection into native space gray matter mask (x-axis) & Vertex-wise sum of thickness \* surface product (y-axis) **Page 77**

[Figure 9](#): A. Cortical thickness (CT) changes between 7 and 16 years of age in males and females of both groups (controls and patients) assessed with TFCE (CAT12). Decreases of CT in blue, increases in red. B. Cortical thickness difference amplitude comparison between male and female for both group **Page 79**

[Figure 10](#): Experimental paradigm deployed for the AVCnnADO activation fMRI **Page 82**

[Figure 11](#): LI values depending on the hemispheric specialization of language activation **Page 85**

[Figure 12](#): Language functional atlas extracted from the cohort data **Page 87**

[Figure 13](#): Hemisphere and Cerebellum Language Lateralization according to lesion side **Page 91**

[Figure 14](#): Activation maps depending for Controls, Left and Right Language Lateralization Patient Groups Defined based on Hemispheric LI **Page 92**

[Figure 15](#): Detrend and standardized BOLD signal in control, typical and atypical language lateralization for SGT task **Page 94**

[Figure 16](#): Superposition of all patient's lesion masks depending on their language LI visualized as a maximum intensity projection. All masks were registered in MNI ICBM152 2009c symmetric template. Mask count per voxel was divided by the total size of each lateralization subgroups **Page 95**

[Figure 17](#): CELF main scores distribution in the cohort as a function of LI, Sex and Lesion Side. Correlations were computed only for left lesion patients, and performed without excluding HIP outlier **Page 96**

[Figure 18](#): WAIS main scores distribution in the cohort as a function of LI, Sex and Lesion Side. Correlations were computed only for left lesion patients, and performed without excluding HIP outlier **Page 97**

[Figure 19](#): Proportion of subjects in the 3 groups (Controls, Patients with typical and atypical language representation) for whom we were able to correctly reconstruct white fiber bundle (more than 70 streamlines). **Page 99**

[Figure 20](#): Mean FA in the arcuate fasciculus (streamline bundle between Broca and Wernicke area). Right plot shows FA value in the language dominant hemisphere and left on the non dominant hemisphere, defined depending on LI value according to a LI = 0.2

threshold. Percentages are proportion of subjects in each group for whom we were able to correctly reconstruct white fiber bundle (more than 70 streamlines) **Page 100**

[Figure 21:](#) Second level analysis for the localizer task (TFCE thresholded for  $p < 0.05$ ). Contrasts are shown for Controls ( $n=30$ ) and Patients with Typical ( $n=14$ ) and Atypical ( $n=15$ ) language lateralization. Red areas indicate a significantly bigger BOLD activation for the first condition (e.g., audio, right hand, language) and blue for the second (e.g., video, left hand, calculation). **Page 102**

[Figure 22:](#) Group comparison 2nd level analysis, TFCE thresholded z-maps (FDR,  $p < 0.05$ ). On the right, all patients are analyzed as the same group, regions in red are regions consistently activated for the first condition in the two groups, blue for the second. On the left, differences between typical and atypical subjects, any significant regions would need further investigation to better assess origin of the difference **Page 105**

[Figure 23:](#) Standardized BOLD time-series for Language and Calculation activation in the left inferior temporo-occipital cluster (green) and in the fusiform gyrus (yellow). **Page 107**

[Figure 24:](#) Group comparison 2nd level analysis, TFCE thresholded z-maps (FDR,  $p < 0.05$ ). All patients are analyzed as the same group, regions in red are regions consistently activated for the first condition in the two groups, blue for the second. **Page 108**

[Figure 25:](#) Standardized BOLD time-serie for Language and Calculation activation. Investigated regions are the regions activated for calculation contrast when all patients are analyzed as the same group. fMRI images were shifted to superpose all language dominant hemispheres on the left side. **Page 110**

## List of Tables

[Table 1:](#) General Informations and motor outcomes of the AVCnnADO cohort at 16 years of age. MCA : Middle Cerebral Artery, SES : Socioeconomic Status (Hollingshead methods), BFMF :Bimanual Fine Motor Function , GMFCS : Gross Motor Function Classification System, MACS : Manual Ability Classification System. **Page 35**

[Table 2:](#) Epilepsy, Language outcomes and executive functions of the AVCnnADO cohort at 16 years of age. CELF: Clinical Evaluation of Language Fundamentals, Receptive Language Index: Measures understanding of spoken language. Expressive Language Index: Measures ability to express ideas verbally. Language Content Index: Assesses knowledge of words and content. Language Structure Index: Evaluates understanding and use of grammatical rules. BRIEF : Behavior Rating Inventory of Executive Function, BRI : Behavior Regulation Index, MI : Metacognition Index, GEC : Global Executive Composite index. **Page 35**

[Table 3:](#) Cognitive and Neuropsychology assessment of the AVCnnADO cohort at 16 years of age. WAIS : Wechsler Adult Intelligence Scale, VCI : Verbal Comprehension Index : Measures verbal reasoning and comprehension. PRI : Perceptual Reasoning Index, Assesses non-verbal and fluid reasoning, WMI : Working Memory Index, Evaluates short-term memory and attention, PSI : Processing Speed Index, Measures the speed of mental processing. **Page 36**

[Table 4:](#) Typical language specialization patients group z-map positive peaks position (Figure 14).Coordinates are expressed in symmetric MNI referential **Page 92**

[Table 5:](#) Atypical language specialization patients group z-map peaks position (Figure 14).Coordinates are expressed in symmetric MNI referential **Page 93**

[Table 6:](#) Calculation task z-map peaks position for the all patient group analysis, coordinates are expressed in symmetric MNI referential **Page 106**

[Table 7:](#) Calculation task z-map peaks position for the all patient group analysis in language dominant hemisphere, coordinates are expressed in symmetric MNI referential. **Page 109**

# Appendix

**Appendix 1** : Exploratory plot of CELF and WAIS main scores, Total IQ (QIT), Handedness (EHI, Edinburgh Handedness Inventory), Socioeconomic Status (SES)

**Appendix 2** : Typical language lateralized patients, Language activation z-maps from SGT task : activation clusters peak z-score, position in MNI space, and cluster overlap on Harvard-Oxford Atlas (Cortical and subcortical) and SUIF Atlas, as a percentage of cluster volume. ROIs were included if overlap represented more than 3% of the cluster volume.

**Appendix 3** : Atypical language lateralized patients, Language activation z-maps from SGT task : activation clusters peak z-score, position in MNI space, and cluster overlap on Harvard-Oxford Atlas (Cortical and subcortical) and SUIF Atlas, as a percentage of cluster volume. ROIs were included if overlap represented more than 3% of the cluster volume.

**Appendix 4** : Controls, Language activation z-maps from SGT task : activation clusters peak z-score, position in MNI space, and cluster overlap on Harvard-Oxford Atlas (Cortical and subcortical) and SUIF Atlas, as a percentage of cluster volume. ROIs were included if overlap represented more than 3% of the cluster volume.

**Appendix 5** : All patients, Language (positive z-score) and Calculation (negative z-score) activation z-maps from Localizer task : activation clusters peak z-score, position in MNI space, and cluster overlap on Harvard-Oxford Atlas (Cortical and subcortical) and SUIF Atlas, as a percentage of cluster volume. ROIs were included if overlap represented more than 3% of the cluster volume.

**Appendix 6** : All patients, Atypical language patients were shifted : “Left” correspond to language dominant hemisphere, “Right” to non-dominant hemisphere  
Language (positive z-score) and Calculation (negative z-score) activation z-maps from Localizer task : activation clusters peak z-score, position in MNI space, and cluster overlap on Harvard-Oxford Atlas (Cortical and subcortical) and SUIF Atlas, as a percentage of cluster volume. ROIs were included if overlap represented more than 3% of the cluster volume.

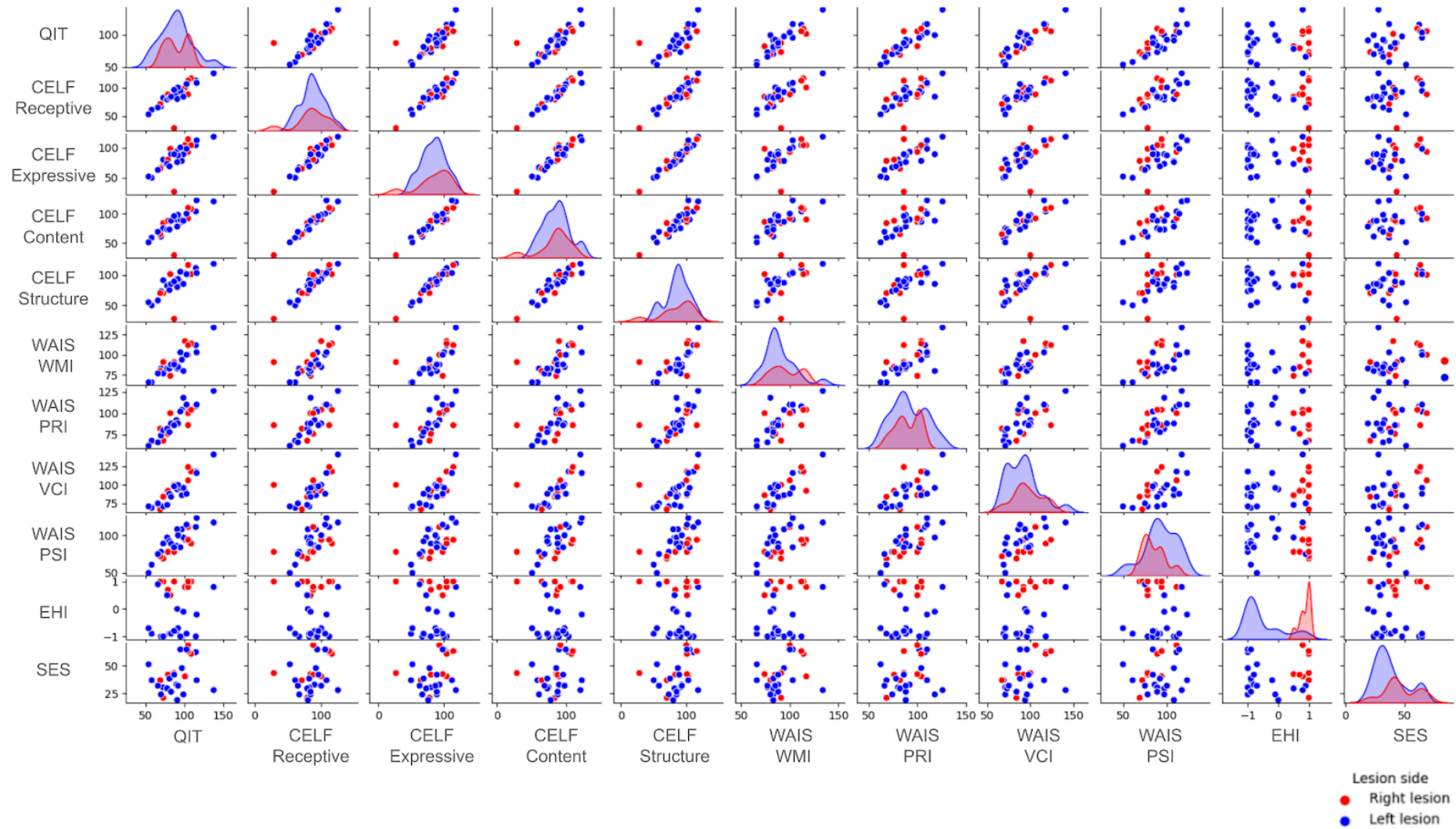
**Appendix 7** : All patients, Right hand (positive z-score) and Hand (negative z-score) motor activation z-maps from Localizer task : activation clusters peak z-score, position in MNI space, and cluster overlap on Harvard-Oxford Atlas (Cortical and subcortical) and SUIF Atlas, as a percentage of cluster volume. ROIs were included if overlap represented more than 3% of the cluster volume.

**Appendix 8** : All patients, Atypical language patients were shifted : “Left” correspond to language dominant hemisphere, “Right” to non-dominant hemisphere  
Right hand (positive z-score) and Hand (negative z-score) motor activation z-maps from Localizer task : activation clusters peak z-score, position in MNI space, and cluster overlap on Harvard-Oxford Atlas (Cortical and subcortical) and SUIF Atlas, as a percentage of

cluster volume. ROIs were included if overlap represented more than 3% of the cluster volume

**Appendix 9** : All patients, Audio (positive z-score) and Video (negative z-score) activation z-maps from Localizer task : activation clusters peak z-score, position in MNI space, and cluster overlap on Harvard-Oxford Atlas (Cortical and subcortical) and SUIT Atlas, as a percentage of cluster volume. ROIs were included if overlap represented more than 3% of the cluster volume

**Appendix 1** : Exploratory plot of CELF and WAIS main scores, Total IQ (QIT), Handedness (EHI, Edinburgh Handedness Inventory), Socio-Economic Status (SES)



**Appendix 2** : Typical language lateralized patients, Language activation z-maps from SGT task : activation clusters peak z-score, position in MNI space, and cluster overlap on Harvard-Oxford Atlas (Cortical and subcortical) and SUI Atlas, as a percentage of cluster volume. ROIs were included if overlap represented more than 3% of the cluster volume.

z-score	X (mm)	Y (mm)	Z (mm)	Harvard-Oxford cortical and subcortical atlas	SUIT
5.83	2.0	4.0	67.0	Left Frontal Pole: 25.92, Right Frontal Pole: 21.37, Left Insular Cortex: 4.26, Right Insular Cortex: 7.51, Left Superior Frontal Gyrus: 5.09, Right Superior Frontal Gyrus: 3.42, Right Inferior Frontal Gyrus, pars opercularis: 9.48, Left Precentral Gyrus: 14.98, Left Paracingulate Gyrus: 6.29, Right Paracingulate Gyrus: 3.95, Left Cingulate Gyrus, anterior division: 4.68	
5.61	-50.0	36.0	-10.0	Right Frontal Pole: 100.00	
5.54	-11.0	-18.0	-8.0	Left Frontal Pole: 7.86, Right Insular Cortex: 6.50, Right Middle Frontal Gyrus: 37.68, Left Inferior Frontal Gyrus, pars triangularis: 4.90	
5.54	-50.0	14.0	7.0	Left Frontal Pole: 23.93, Right Frontal Pole: 73.04, Left Frontal Orbital Cortex: 8.67, Left Frontal Opercular Cortex: 4.66	
5.23	34.0	-64.0	-28.0		Right_V: 8.08, Right_VI: 42.40, Right_CrusI: 41.71
4.92	34.0	-69.0	-57.0		Right_CrusII: 4.74, Right_VIIb: 74.41, Right_VIIIa: 20.06
4.67	-31.0	-59.0	-29.0		Left_VI: 89.23, Left_CrusI: 10.77

**Appendix 3** : Atypical language lateralized patients, Language activation z-maps from SGT task : activation clusters peak z-score, position in MNI space, and cluster overlap on Harvard-Oxford Atlas (Cortical and subcortical) and SUI Atlas, as a percentage of cluster volume. ROIs were included if overlap represented more than 3% of the cluster volume.

z-score	X (mm)	Y (mm)	Z (mm)	Harvard-Oxford cortical and subcortical atlas	SUIT
5.61	60.0	-33.0	5.0	Right Inferior Frontal Gyrus, pars opercularis: 28.11, Left Precentral Gyrus: 71.02, Right Middle Temporal Gyrus, posterior division: 5.63, Right Middle Temporal Gyrus, temporooccipital part: 7.12, Right Supramarginal Gyrus, posterior division: 4.04, Right Planum Temporale: 3.65	No region
4.93	64.0	4.0	-7.0	Left Precentral Gyrus: 100.00	No region
4.49	48.0	15.0	18.0	Right Inferior Frontal Gyrus, pars opercularis: 22.17, Left Precentral Gyrus: 73.90, Right Frontal Orbital Cortex: 9.45, Right Frontal Opercular Cortex: 10.44	No region
4.11	49.0	-38.0	-8.0	Right Inferior Frontal Gyrus, pars opercularis: 100.00	No region
4.69	-17.0	-65.0	-21.0	Right Frontal Pole: 9.14, Left Occipital Fusiform Gyrus: 4.50	Left_VI
4.35	35.0	-60.0	-30.0		Right_CrusI
4.32	8.0	-44.0	-18.0	Right Middle Frontal Gyrus: 19.83, Left Superior Temporal Gyrus, posterior division: 4.61	Right_I_IV
3.49	-6.0	-76.0	-25.0		Left_VI
4.62	7.0	5.0	66.0	Right Inferior Frontal Gyrus, pars opercularis: 8.38, Left Precentral Gyrus: 91.62, Right Juxtapositional Lobule Cortex (formerly Supplementary Motor Cortex): 49.88	No region
4.59	-8.0	-86.0	-35.0		Left_CrusII
4.44	-36.0	-64.0	-57.0		Left_VIIb
4.2	0.0	-57.0	0.0	Left Precentral Gyrus: 34.98, Right Lingual Gyrus: 20.05	Right_I_IV

**Appendix 4** : Controls, Language activation z-maps from SGT task : activation clusters peak z-score, position in MNI space, and cluster overlap on Harvard-Oxford Atlas (Cortical and subcortical) and SUI Atlas, as a percentage of cluster volume. ROIs were included if overlap represented more than 3% of the cluster volume.

z-score	X (mm)	Y (mm)	Z (mm)	Harvard-Oxford cortical and subcortical atlas	SUIT
8.19	-59.0	-11.0	-2.0	Left Frontal Pole: 23.91, Right Frontal Pole: 46.61, Right Insular Cortex: 3.29, Right Middle Frontal Gyrus: 5.71, Left Frontal Orbital Cortex: 3.48	
8.19	59.0	-11.0	-2.0	Right Inferior Frontal Gyrus, pars opercularis: 36.35, Left Precentral Gyrus: 35.24, Left Temporal Pole: 4.69, Right Temporal Pole: 4.60, Left Superior Temporal Gyrus, anterior division: 5.53, Left Superior Temporal Gyrus, posterior division: 4.69, Right Frontal Orbital Cortex: 5.29, Right Frontal Opercular Cortex: 3.11	
8.08	44.0	-64.0	-30.0	Left Precentral Gyrus: 5.79	Left_I_IV: 4.22, Right_I_IV: 4.86, Left_V: 4.70, Right_V: 6.99, Right_VI: 15.13, Right_CrusI: 22.82, Right_Dentate: 3.06
7.94	-6.0	16.0	44.0	Left Frontal Pole: 20.17, Right Frontal Pole: 42.75, Right Inferior Frontal Gyrus, pars opercularis: 11.84, Left Precentral Gyrus: 23.61, Left Juxtapositional Lobule Cortex (formerly Supplementary Motor Cortex): 4.63, Left Paracingulate Gyrus: 10.32, Right Paracingulate Gyrus: 8.41, Left Cingulate Gyrus, anterior division: 10.44, Right Cingulate Gyrus, anterior division: 8.78	
7.65	35.0	-64.0	-53.0		Right_CrusI: 6.37, Right_CrusII: 43.90, Right_VIIb: 24.32, Right_VIIIa: 18.57

**Appendix 5** : All patients, Language (positive z-score) and Calculation (negative z-score) activation z-maps from Localizer task : activation clusters peak z-score, position in MNI space, and cluster overlap on Harvard-Oxford Atlas (Cortical and subcortical) and SUIT Atlas, as a percentage of cluster volume. ROIs were included if overlap represented more than 3% of the cluster volume.

z-score	X (mm)	Y (mm)	Z (mm)	Harvard-Oxford cortical and subcortical atlas	SUIT
8,06	57.0	-9.0	0.0	Right Inferior Frontal Gyrus, pars opercularis: 18.52, Left Precentral Gyrus: 79.68, Right Middle Temporal Gyrus, posterior division: 4.55, Right Middle Temporal Gyrus, temporooccipital part: 3.40, Right Supramarginal Gyrus, posterior division: 4.42, Right Angular Gyrus: 5.44, Right Central Opercular Cortex: 5.63, Right Parietal Opercular Cortex: 5.27, Right Planum Polare: 3.83, Right Planum Temporale: 4.24	
5,71	54.0	-31.0	27.0	Right Inferior Frontal Gyrus, pars opercularis: 50.00, Left Precentral Gyrus: 50.00, Right Supramarginal Gyrus, anterior division: 50.00, Right Parietal Opercular Cortex: 50.00	
5,70	24.0	-12.0	-16.0	Right Inferior Frontal Gyrus, pars opercularis: 10.69, Left Precentral Gyrus: 42.98, Left Superior Temporal Gyrus, posterior division: 22.02, Right Superior Temporal Gyrus, posterior division: 23.40, Right Inferior Temporal Gyrus, posterior division: 10.27, Right Parahippocampal Gyrus, anterior division: 8.84, Right Temporal Fusiform Cortex, anterior division: 5.04, Right Temporal Fusiform Cortex, posterior division: 12.68	
5,50	50.0	26.0	-12.0	Left Precentral Gyrus: 100.00, Right Frontal Orbital Cortex: 33.33	
7,03	-46.0	-19.0	7.0	Left Frontal Pole: 8.79, Right Frontal Pole: 88.27, Left Postcentral Gyrus: 3.35, Left Frontal Orbital Cortex: 8.19, Left Central Opercular Cortex: 10.36, Left Parietal Opercular Cortex: 3.02, Left Planum Polare: 5.62, Left Heschl's Gyrus (includes H1 and H2): 5.49, Left Planum Temporale: 4.73	
6,95	-22.0	-44.0	15.0	Left Frontal Pole: 73.59, Left Insular Cortex: 25.73	
6,78	27.0	-47.0	70.0	Left Frontal Pole: 5.09, Right Frontal Pole: 42.55, Right Inferior Frontal Gyrus, pars opercularis: 9.85, Left Precentral Gyrus: 25.95, Left Postcentral Gyrus: 19.01, Right Postcentral Gyrus: 9.50, Left Superior Parietal Lobule: 3.13, Right Superior Parietal Lobule: 5.72, Left Precuneus Cortex: 9.77, Right Precuneus Cortex: 3.81	
6,78	-44.0	-30.0	14.0	Left Frontal Pole: 40.54, Right Frontal Pole: 59.32, Left Supramarginal Gyrus, posterior division: 3.83, Left Angular Gyrus: 13.86, Left Lateral Occipital Cortex, superior division: 4.68, Left Parietal Opercular Cortex: 23.03, Left Planum Temporale: 16.52	
5,27	0.0	7.0	15.0	Left Frontal Pole: 11.51, Right Frontal Pole: 22.56, Left Insular Cortex: 16.33, Right Inferior Frontal Gyrus, pars opercularis: 4.89, Left Precentral Gyrus: 27.00, Right Precentral Gyrus: 11.16, Left Subcallosal Cortex: 17.79, Right Subcallosal Cortex: 24.87	
4,93	-4.0	57.0	-12.0	Left Frontal Pole: 8.80, Right Frontal Pole: 47.94, Right Inferior Frontal Gyrus, pars opercularis: 3.53, Left Precentral Gyrus: 39.43, Left Frontal Medial Cortex: 15.41, Right Frontal Medial Cortex: 16.37	

<b>z-score</b>	<b>X (mm)</b>	<b>Y (mm)</b>	<b>Z (mm)</b>	<b>Harvard-Oxford cortical and subcortical atlas</b>	<b>SUIT</b>
4,91	-43.0	-19.0	-29.0	Left Frontal Pole: 13.69, Right Frontal Pole: 61.92, Left Inferior Frontal Gyrus, pars triangularis: 14.15, Right Inferior Frontal Gyrus, pars triangularis: 9.05, Left Inferior Temporal Gyrus, posterior division: 12.80, Left Temporal Fusiform Cortex, anterior division: 8.39, Left Temporal Fusiform Cortex, posterior division: 27.19	
3,78	-27.0	-34.0	-20.0	Right Frontal Pole: 100.00, Left Parahippocampal Gyrus, posterior division: 83.33, Left Temporal Fusiform Cortex, posterior division: 16.67	
-6,14	-54.0	-62.0	-13.0	Right Frontal Pole: 99.67, Left Middle Temporal Gyrus, temporooccipital part: 4.56, Left Inferior Temporal Gyrus, temporooccipital part: 60.09, Left Lateral Occipital Cortex, inferior division: 30.51	
-5,90	-42.0	-65.0	-20.0	Right Frontal Pole: 27.35, Left Temporal Occipital Fusiform Cortex: 11.54, Left Occipital Fusiform Gyrus: 8.11	Left_VI: 33.66, Left_CrusI: 42.75

**Appendix 6** : All patients, Atypical language patients were shifted : “Left” correspond to language dominant hemisphere, “Right” to non-dominant hemisphere

Language (positive z-score) and Calculation (negative z-score) activation z-maps from Localizer task : activation clusters peak z-score, position in MNI space, and cluster overlap on Harvard-Oxford Atlas (Cortical and subcortical) and SUI Atlas, as a percentage of cluster volume. ROIs were included if overlap represented more than 3% of the cluster volume.

<b>z-score</b>	<b>X (mm)</b>	<b>Y (mm)</b>	<b>Z (mm)</b>	<b>Harvard-Oxford cortical and subcortical atlas</b>	<b>SUIT</b>
8.93	-61.0	-8.0	0.0	Left Frontal Pole: 20.02, Right Frontal Pole: 71.15, Left Frontal Orbital Cortex: 4.33, Left Central Opercular Cortex: 6.23, Left Parietal Opercular Cortex: 5.82, Left Planum Polare: 3.40, Left Heschl's Gyrus (includes H1 and H2): 3.24, Left Planum Temporale: 5.34	
6.4	-60.0	-50.0	10.0	Left Frontal Pole: 9.67, Right Frontal Pole: 88.55, Left Middle Temporal Gyrus, temporooccipital part: 17.20, Left Supramarginal Gyrus, posterior division: 22.39, Left Angular Gyrus: 29.76, Left Lateral Occipital Cortex, superior division: 8.10	
6.34	-52.0	24.0	-11.0	Right Frontal Pole: 100.00	
6.15	-41.0	-11.0	-41.0	Left Frontal Pole: 19.81, Right Frontal Pole: 79.43, Left Inferior Temporal Gyrus, anterior division: 6.76, Left Inferior Temporal Gyrus, posterior division: 21.05, Left Temporal Fusiform Cortex, anterior division: 12.30, Left Temporal Fusiform Cortex, posterior division: 30.52	
7.38	22.0	-45.0	17.0	Right Inferior Frontal Gyrus, pars opercularis: 60.79, Right Precentral Gyrus: 39.05	
6.65	47.0	-16.0	2.0	Right Inferior Frontal Gyrus, pars opercularis: 24.40, Left Precentral Gyrus: 74.58, Right Postcentral Gyrus: 3.26, Right Supramarginal Gyrus, anterior division: 3.35, Right Central Opercular Cortex: 8.06, Right Parietal Opercular Cortex: 12.56, Right Planum Polare: 6.30, Right Heschl's Gyrus (includes H1 and H2): 7.12, Right Planum Temporale: 10.20	
5.08	46.0	9.0	-17.0	Left Precentral Gyrus: 98.71	
6.24	21.0	-50.0	71.0	Right Frontal Pole: 10.70, Left Precentral Gyrus: 79.67, Left Postcentral Gyrus: 5.45, Right Postcentral Gyrus: 24.96, Right Superior Parietal Lobule: 31.19, Right Precuneus Cortex: 8.84	
6.13	-23.0	-46.0	73.0	Right Frontal Pole: 91.21, Left Postcentral Gyrus: 55.22, Left Superior Parietal Lobule: 17.11	
5.94	4.0	-39.0	-10.0	Right Middle Frontal Gyrus: 23.33, Left Precentral Gyrus: 11.69, Right Precuneus Cortex: 3.37	Left_I_IV: 5.70, Right_I_IV: 17.40
5.27	0.0	7.0	15.0	Left Frontal Pole: 9.68, Left Insular Cortex: 46.77, Right Precentral Gyrus: 43.55	
5.06	0.0	18.0	0.0	Left Frontal Pole: 55.71, Left Insular Cortex: 5.71, Left Precentral Gyrus: 38.57, Left Subcallosal Cortex: 20.00, Right Subcallosal Cortex: 30.00	
-6.58	-20.0	16.0	1.0	Left Frontal Pole: 55.85, Left Superior Frontal Gyrus: 10.45, Right Superior Frontal Gyrus: 33.70	
-6.43	-30.0	-77.0	36.0	Left Frontal Pole: 10.28, Right Frontal Pole: 89.72, Left Superior Parietal Lobule: 9.77, Left Lateral Occipital Cortex, superior division: 89.66	
-6.34	-55.0	-51.0	-17.0	Right Frontal Pole: 100.00, Left Inferior Temporal Gyrus, temporooccipital part: 100.00	
-6.24	-48.0	-40.0	48.0	Right Frontal Pole: 99.70, Left Postcentral Gyrus: 6.20, Left Superior Parietal Lobule: 20.28, Left Supramarginal Gyrus, anterior division: 30.95, Left Supramarginal Gyrus, posterior division: 34.48	

**Appendix 7** : All patients, Right hand (positive z-score) and Hand (negative z-score) motor activation z-maps from Localizer task : activation clusters peak z-score, position in MNI space, and cluster overlap on Harvard-Oxford Atlas (Cortical and subcortical) and SUIT Atlas, as a percentage of cluster volume. ROIs were included if overlap represented more than 3% of the cluster volume.

<b>z-score</b>	<b>X (mm)</b>	<b>Y (mm)</b>	<b>Z (mm)</b>	<b>Harvard-Oxford cortical and subcortical atlas</b>	<b>SUIT</b>
6.56	-17.0	-52.0	-23.0	Right Frontal Pole: 10.59, Left Lingual Gyrus: 4.00, Left Temporal Occipital Fusiform Cortex: 4.10	Left_I_IV: 7.40, Left_V: 44.29, Left_VI: 32.19
6.56	38.0	-29.0	56.0	Right Inferior Frontal Gyrus, pars opercularis: 11.50, Left Precentral Gyrus: 85.01, Right Postcentral Gyrus: 43.29, Right Superior Parietal Lobule: 9.41	
5.76	6.0	-18.0	56.0	Right Inferior Frontal Gyrus, pars opercularis: 41.81, Left Precentral Gyrus: 58.19, Right Postcentral Gyrus: 3.22, Right Juxtapositional Lobule Cortex (formerly Supplementary Motor Cortex): 24.42	
6.37	16.0	-22.0	6.0	Right Inferior Frontal Gyrus, pars opercularis: 7.58, Left Temporal Pole: 92.42	
6.01	38.0	-21.0	15.0	Right Inferior Frontal Gyrus, pars opercularis: 15.86, Left Precentral Gyrus: 57.84, Left Superior Temporal Gyrus, anterior division: 26.25, Right Central Opercular Cortex: 5.88, Right Parietal Opercular Cortex: 21.02, Right Heschl's Gyrus (includes H1 and H2): 7.30	
-7.51	23.0	-48.0	-24.0	Left Precentral Gyrus: 16.74, Right Lingual Gyrus: 6.84, Right Temporal Occipital Fusiform Cortex: 7.54	Right_I_IV: 5.23, Right_V: 26.93, Right_VI: 29.97, Right_Dentate: 3.95
-5.75	16.0	-65.0	-50.0		Right_VIIb: 12.90, Right_VIIIa: 46.05, Right_VIIIb: 29.21, Right_IX: 3.55
-6.95	-18.0	-22.0	4.0	Left Frontal Pole: 21.47, Right Insular Cortex: 78.30	
-6.76	-34.0	-21.0	68.0	Left Frontal Pole: 14.03, Right Frontal Pole: 82.75, Left Postcentral Gyrus: 48.40, Left Superior Parietal Lobule: 7.53	
-6.19	-14.0	-58.0	41.0	Left Frontal Pole: 48.76, Right Frontal Pole: 51.24, Left Precuneous Cortex: 74.85	
-5.89	58.0	-11.0	-3.0	Right Inferior Frontal Gyrus, pars opercularis: 41.17, Left Precentral Gyrus: 58.83, Right Planum Temporale: 16.49	
-5.84	-27.0	-9.0	-10.0	Left Frontal Pole: 58.59, Right Superior Frontal Gyrus: 13.46, Right Inferior Frontal Gyrus, pars triangularis: 26.09	
-5.58	-8.0	-31.0	51.0	Left Frontal Pole: 34.06, Right Frontal Pole: 65.94	

**Appendix 8** : All patients, Atypical language patients were shifted : “Left” correspond to language dominant hemisphere, “Right” to non-dominant hemisphere

Right hand (positive z-score) and Hand (negative z-score) motor activation z-maps from Localizer task : activation clusters peak z-score, position in MNI space, and cluster overlap on Harvard-Oxford Atlas (Cortical and subcortical) and SUI Atlas, as a percentage of cluster volume. ROIs were included if overlap represented more than 3% of the cluster volume

<b>z-score</b>	<b>X (mm)</b>	<b>Y (mm)</b>	<b>Z (mm)</b>	<b>Harvard-Oxford cortical and subcortical</b>	<b>SUIT</b>
-5.98	-61.0	-19.0	5.0	Left Frontal Pole: 8.80, Right Frontal Pole: 90.08, Left Supramarginal Gyrus, posterior division: 6.65, Left Central Opercular Cortex: 3.73, Left Heschl's Gyrus (includes H1 and H2): 7.78, Left Planum Temporale: 23.48	No region
-4.96	-11.0	-59.0	39.0	Left Frontal Pole: 51.81, Right Frontal Pole: 48.19, Left Precuneous Cortex: 89.96	No region
-4.93	11.0	-54.0	42.0	Right Inferior Frontal Gyrus, pars opercularis: 28.44, Left Precentral Gyrus: 71.56, Right Precuneous Cortex: 91.42	No region

**Appendix 9** : All patients, Audio (positive z-score) and Video (negative z-score) activation z-maps from Localizer task : activation clusters peak z-score, position in MNI space, and cluster overlap on Harvard-Oxford Atlas (Cortical and subcortical) and SUIT Atlas, as a percentage of cluster volume. ROIs were included if overlap represented more than 3% of the cluster volume

z-score	X (mm)	Y (mm)	Z (mm)	Harvard-Oxford cortical and subcortical atlas	SUIT
8.2	53.0	-8.0	2.0	Right Inferior Frontal Gyrus, pars opercularis: 28.39, Left Precentral Gyrus: 67.23, Right Precentral Gyrus: 3.44, Right Middle Temporal Gyrus, posterior division: 3.78, Right Precuneous Cortex: 4.66, Right Cuneal Cortex: 3.62, Right Central Opercular Cortex: 6.44, Right Parietal Opercular Cortex: 4.58, Right Planum Polare: 3.37, Right Planum Temporale: 3.69	
7.9	-1.0	-41.0	-8.0	Right Frontal Pole: 9.66, Right Insular Cortex: 4.47, Right Middle Frontal Gyrus: 11.80, Left Precentral Gyrus: 12.67, Left Temporal Pole: 3.90, Left Superior Temporal Gyrus, posterior division: 3.36, Right Lingual Gyrus: 5.93	Left_I_IV: 4.44, Right_I_IV: 7.22, Right_V: 7.02
7.6	-45.0	-10.0	1.0	Left Frontal Pole: 20.55, Right Frontal Pole: 68.45, Left Insular Cortex: 3.06, Left Precentral Gyrus: 5.63, Left Postcentral Gyrus: 4.91, Left Precuneous Cortex: 11.37, Right Precuneous Cortex: 3.23, Left Central Opercular Cortex: 6.43, Left Parietal Opercular Cortex: 4.01, Left Planum Temporale: 3.70	
7.38	45.0	-1.0	-12.0	Right Inferior Frontal Gyrus, pars opercularis: 36.09, Left Precentral Gyrus: 63.91, Right Planum Polare: 33.14	
5.71	8.0	32.0	5.0	Right Frontal Pole: 29.60, Right Inferior Frontal Gyrus, pars opercularis: 27.17, Left Precentral Gyrus: 40.90, Left Cingulate Gyrus, anterior division: 31.11, Right Cingulate Gyrus, anterior division: 48.30	
5.04	-6.0	-18.0	47.0	Left Frontal Pole: 6.54, Right Frontal Pole: 80.75, Left Precentral Gyrus: 12.71, Left Juxtapositional Lobule Cortex (formerly Supplementary Motor Cortex): 24.01, Left Cingulate Gyrus, anterior division: 24.32, Right Cingulate Gyrus, anterior division: 5.04, Left Cingulate Gyrus, posterior division: 13.57	
4.68	-1.0	60.0	14.0	Right Frontal Pole: 49.41, Left Precentral Gyrus: 42.15, Left Paracingulate Gyrus: 4.37	
-9.06	32.0	-91.0	-2.0	Right Inferior Frontal Gyrus, pars opercularis: 15.92, Left Precentral Gyrus: 74.21, Right Lateral Occipital Cortex, superior division: 16.67, Right Lateral Occipital Cortex, inferior division: 27.29, Right Occipital Fusiform Gyrus: 6.92, Right Occipital Pole: 25.36	
-8.04	44.0	-60.0	-15.0	Right Inferior Frontal Gyrus, pars opercularis: 22.07, Left Precentral Gyrus: 71.68, Right Middle Temporal Gyrus, temporooccipital part: 3.20, Right Inferior Temporal Gyrus, temporooccipital part: 19.26, Right Lateral Occipital Cortex, inferior division: 20.03, Right Temporal Fusiform Cortex, posterior division: 8.35, Right Temporal Occipital Fusiform Cortex: 16.74, Right Occipital Fusiform Gyrus: 5.34	

<b>z-score</b>	<b>X (mm)</b>	<b>Y (mm)</b>	<b>Z (mm)</b>	<b>Harvard-Oxford cortical and subcortical atlas</b>	<b>SUIT</b>
-6.0	32.0	-58.0	55.0	Right Inferior Frontal Gyrus, pars opercularis: 23.43, Left Precentral Gyrus: 75.40, Right Superior Parietal Lobule: 23.90, Right Lateral Occipital Cortex, superior division: 61.53	
-9.02	-27.0	-94.0	-6.0	Left Frontal Pole: 17.84, Right Frontal Pole: 77.99, Left Lateral Occipital Cortex, superior division: 7.91, Left Lateral Occipital Cortex, inferior division: 39.58, Left Occipital Fusiform Gyrus: 6.75, Left Occipital Pole: 26.67	Left_CrusI: 3.30
-7.75	-49.0	-59.0	-11.0	Left Frontal Pole: 22.67, Right Frontal Pole: 71.32, Left Middle Temporal Gyrus, temporooccipital part: 5.96, Left Inferior Temporal Gyrus, temporooccipital part: 25.08, Left Lateral Occipital Cortex, inferior division: 12.18, Left Temporal Fusiform Cortex, posterior division: 6.85, Left Temporal Occipital Fusiform Cortex: 13.17, Left Occipital Fusiform Gyrus: 3.43	Left_CrusI: 5.55
-6.24	-35.0	-54.0	50.0	Left Frontal Pole: 25.85, Right Frontal Pole: 74.13, Left Superior Parietal Lobule: 25.48, Left Lateral Occipital Cortex, superior division: 61.80	
-5.9	-6.0	-78.0	-41.0		Left_CrusII: 45.16, Left_VIIb: 54.84

# Communications and Publications

## Published article

Postic, P. Y., Leprince, Y., Brosset, S., Drutel, L., Peyric, E., Ben Abdallah, I., ... & Hertz-Pannier, L. (2024). Brain growth until adolescence after a neonatal focal injury: sex related differences beyond lesion effect. *Frontiers in Neuroscience*, 18, 1405381.

## Posters presented in conferences

### 2022

- Brain growth dynamics in childhood and adolescence after a neonatal stroke: a longitudinal MRI study (**OHBM, Glasgow, Scotland**)
- Devenir adolescent après un AVC Néonatal. La plasticité cérébrale à long terme dépend-elle du sexe ? *Adolescence after neonatal stroke. Does long-term brain plasticity depend on sex ?* (**SFRMBM, Paris, France**)

### 2023

- Contralesional Brain Growth Dynamics in Childhood and Adolescence after an Unilateral Neonatal Stroke : A Longitudinal MRI Study. Does sex affect brain recovery? (**NeuroFrance, Lyon, France**)

### 2024

- Croissance cérébrale à long terme après une lésion focale néonatale : Y a t il un effet du sexe ? *Long-term brain growth after neonatal focal lesion: Is there a sex difference ?* (**SFNP, Rennes, France**)
- Morphometry Longitudinal Study until Adolescence of Brain Growth after early lesion : Sex matters (**OHBM, Seoul, Korea**)

## Formations

- CENIR Courses : MRI protocol design, image processing for anatomical, functional and diffusion MRI. Machine Learning and Deep learning (2 weeks, 2022, CENIR)
- OHBM 2022 Educational courses (1 day, 2022, OHBM)
- Methodological training: Pre-processing in fMRI and diffusion MRI, Registration techniques (~10 sessions, 2h each 2022, NeuroSpin)
- Workshop on image processing in functional MRI (2 days, February 2023, NeuroSpin)
- MOOC Improve your statistical inferences (2 weeks, september 2022 Eindhoven University of Technology)
- Training in multivariate analysis (5 days, 2023, Inserm)
- Research Ethics and Integrity (1 week, 2023, Université de Lyon)
- Mtrix Workshop (1 week, September 2023)